UNIVERSITY OF SÃO PAULO
ESCOLA POLITÉCNICA

Rafael Nogueira Nakashima

Modelling, simulation and optimization of biogas conversion routes integrated with fuel cell technology

São Paulo
May 29, 2022

RAFAEL NOGUEIRA NAKASHIMA

Modelling, simulation and optimization of biogas conversion routes integrated with fuel cell technology

Revised version

Manuscript presented to the Graduate Program in Mechanical Engineering at the Escola Politécnica of the University of São Paulo, as a partial requirement to obtain the degree of Doctor in Science.

Concentration area: Fluids and Energy

supervised by
Prof. Dr. Silvio de Oliveira Junior

São Paulo
May 29, 2022

This copy was revised and corrected based on the original manuscript, under the sole responsibility of the author with the autorization of his PhD advisor.

São Paulo, May 29, 2022.

Author: _____

PhD advisor: _____

INDEX CARD

Nogueira Nakashima, Rafael

Modelling, simulation and optimization of biogas conversion routes integrated with fuel cell technology / R. Nogueira Nakashima – revised version – São Paulo, 2022.

226 p.

Thesis (PhD) - Escola Politécnica of the University of São Paulo. Department of Mechanical Engineering.

1.biogas 2.fuel cell 3.hydrogen 4.exergy 5.optimization

I.University of São Paulo. Escola Politécnica. Department of Mechanical Engineering II.t.

To my beloved parents, Maria Elena and Claudio

Acknowledgements

This thesis would not be possible without the supervision of Prof. Dr. Silvio de Oliveira, who helped me to overcome the challenges of this work. The dedication of Prof. Silvio towards his work and his students can only be match by his joyfulness.

I owe all my accomplishments to the generosity of my parents, Maria Elena and Claudio, and this PhD thesis is not an exception. I am blessed to be their child.

The emotional support and happiness that Elaine provided to me were essential to keep me motivated on the most difficult moments of these last years. Everything becomes simpler when you are beside the person you love.

Along this research, I had the privilege to met incredible people and learn from their experiences and thoughts. I would like to thank Daniel Floréz-Orrego for sharing his knowledge with me in a number of occasions. My sincere thanks to Tuong-Van Nguyen for our long discussions about life, work and food. Thanks for the wonderful colleagues that I met at the University of São Paulo: Ali, Amauri, Beethoven, Bruno, Diego, Fernanda, Fernando, Italo, Izabela, Gabriel, Meire, Rodrigo, Ronaldo and others.

I would like to thank Prof. Julio Silva, Prof. Fernando Sacomano, Prof. Jose Antonio Perrella Balistieri and Prof. Antonio Garrido Gallego for their helpful suggestions to this thesis. In addition, my gratitude towards Pablo Ortiz, Prof. Hector Velasquez and Prof. Silvia Nebra for their company and support in the ECOS 2019. Thanks to Prof. Jaime Ortiz, Prof. Guenther Krieger, Prof. Flávio Fiorelli, Prof. Ernani Volpe and Prof. Antonio Pacífico who help me in the PAE activities. I would also like to acknowledge all professors of the University of São Paulo and IPEN that I had the privilege to learn from.

My sincere gratitude to Marisa and Regianne who always help me when I needed.

I also acknowledge CAPES for the financial support given to this research.

And God for everything.

Abstract

Biogas is a promising renewable and distributed source of energy derived from the anaerobic treatment of organic residues. Different production routes using biogas have been proposed in the literature, such as power and heat cogeneration, biomethane or hydrogen production. However, few studies have evaluated the technical, economic and environmental performance of these production routes in the Brazilian context. In addition, although biogas can provide substantial benefits for the environment, its application may be restricted to large industrial facilities due to the lack of efficient conversion systems at small facilities. An interesting technology alternative for biogas conversion is the use of high temperature fuel cells, such as solid oxide fuel cells (SOFC), due to their high efficiency and modularity. However, the influence of operational parameters in the optimization of revenues, efficiency and environmental impact has been seldom studied for these novel polygeneration systems. Thus, this thesis aims to develop a systematic framework to design, evaluate and optimize biogas production and conversion systems, with a modern approach to modelling and optimization. The research discuss and compare the technical, economic and environmental performance of different biogas conversion routes (electricity, methane and hydrogen) based on the principles of exergoeconomic analysis. Next, different designs for fuel cell systems working with biogas to produce electricity and hydrogen optimized for exergy efficiency and net present value or electricity costs. The results indicate that hydrogen production using biogas is the most profitable production route and its efficiency/economic return can be improved by integrating this process with fuel cells. Moreover, the distributed generation of electricity using fuel cells requires further reductions in equipment costs to be economically viable at competitive interest return ratios.

Keywords: biogas, fuel cell, hydrogen, exergy, optimization.

Nomenclature

Greek letters

α : transfer coefficient (-)

β : exergy coefficient (-)

ϵ : porosity (-)

η : overpotential (V) or efficiency (-)

γ : exergy factor (-) or linear constant (-)

λ : percent of theoretical air (%)

μ : reaction constant (1/h)

ν : stoichiometric coefficient (-)

ρ : gas-liquid transfer rate (kgO_2/m^3.d or kmol/m^3.d)

σ : conductivity (1/Ω.m)

τ : tortuosity (-)

Symbols

A : area (m^2)

B : exergy (kJ/kg)

$\dot{B}$: exergy transfer rate (kW)

b : specific exergy (J/mol or kJ/kg)

C : heat capacity (kW/kg.K) or total year costs (USD)

$\bar{C}$: cold utility set

c : surface concentration (mol/m^2) or specific costs (USD/kWh, kWh/kWh or gCO_2/kWh)

c_p : specific heat capacity at constant pressure (J/mol.K)

$\bar{c}$: Average unit exergy costs (kJ/kJ or gCO_2/kJ)

COD : chemical oxygen demand (kgO_2/m^3)

D : depreciation in a year (USD)

D_{ij} : binary diffusivity (m^2/s)

$D_{ij,eff}$: effective binary diffusivity (m^2/s)

D_{iM} : Knudsen diffusivity (m^2/s)

D_v : diffusion volumes (-)

E : voltage (V)

E_{act} : activation energy (J/mol)

F : Faraday constant (s.A/mol) or cost factor (-)

f : load factor or cost factor (-)

$f_{usd/eur}$: USD/EUR exchange ratio (USD/EUR)

FU : fuel utilization efficiency (-)

G : Gibbs free energy (kJ/kg)

g : gravity (m/s^2)

H : enthalpy (kJ/kg)

$\dot{H}$: enthalpy transfer rate (kW)

h : specific enthalpy (kJ/kg) or electrode height position (m)

HHV: higher heating value (kWh/kg)

HRT : hydraulic retention time (d)

I : inhibition factor (-)

J_i : molar flux (mol/m^2.s)

j : current density (A/m^2)

K_{eq} : equilibrium constant (-)

K_s : half velocity constant (kgO_2/m^3 or kmol/m^3)

K_h : gas-liquid equilibrium constant (mol/m^3.bar)

k_La : gas-liquid transfer coefficient (1/d)

LHV : lower heating value (kJ/kg)

LCOE: levelized cost of electricity (USD/kWh)

LCOP: levelized cost of product (USD/kg or USD/kWh)

$\dot{m}$: mass flow rate (kg/s or kg/h)

M_{co2} : carbon dioxide emissions (gCO_2/s)

M_i : molar weight (g/mol)

M_{ij} : molar weight factor (g/mol)

MY : methane yield ($Nm^3/CH_4.kg_{COD}$)

N: total number

NPV: net present value (USD)

n : number/quantity

$\dot{n}$: molar flow rate (mol/s)

P : pressure (Pa or bar)

Q : heat transfer rate (kW)

R : gas constant (kJ/kg.K) or cascade heat transfer rate (kW)

r : reaction rate (kgO_2/m^3.d or kmol/m^3.d)

r_p : mean pore radius (m)

S : soluble concentration (kgO_2/m^3) or total sales in a year (USD)

T : temperature (K) or total taxes in a year (USD)

TPC: total plant costs (USD)

TOC: total overnight cost (USD)

t : time (h or d)

ThOD : theoretical chemical oxygen demand (gO_2/mol or kgO_2/m^3)

U: overall heat transfer coefficient (W/m^2.K)

V : volume (m^3)

v : velocity (m/s)

$\dot{V}$: volumetric flow rate (m^3/d)

VS : volatile solids concentration (kg/m^3)

W: power (W) or weight (lb)

WACC: weighted average cost of capital (-)

X : bacteria (solids) concentration (kgO_2/m^3)

x : molar fraction (-)

$\dot{W}$: work (kW)

y : binary variable or activity coefficient (-)

Z : concentration (kmol/m^3 or kgO_2/m^3) or temperature factor

z: mass fraction or relative height (m)

Superscript and subscript

0 : reference

act : activation

B : biofuel for the utility system

C : chemicals or Consumption

cat: catalyst

cell: fuel cell (total)

ch : chemical

CO2 : Carbon dioxide emissions

conc : concentration

d : distribution stage

dest : destroyed

e : electrons or end-use stage

epcc: engineering procurement and construction cost

elec: electricity

ex : exergy

exp : exported

F : fuel

f : final

fg : condensation/evaporation

ger : generated

i : counter "i"

in : imported or inlet

j : counter "j"

k : temperature interval "k" or kinetic

K : last temperature interval

l : subsystem

ln: logarithmic mean

M : last hot utility

m : hot utility "m"

min : minimal

N : last cold utility

n : cold utility "n" or year "n"

nr : non-renewable

$O\&M$: operation and management

ohm : ohmic

op : operation

oxy: hydrogen oxidation

owner: owner costs

P : biofuel to market or product

p : potential or process

ph : physical

process: process contingency

project: project contingency

q : item "q"

r : reaction

S : soluble or service

s : source, sulfur or supply stage

smr : steam methane reforming

T : total

t : target or transformation stage

ut : utility

X : insoluble

w : water or work

wgs : water-gas shift

Contents

1 Introduction

The anaerobic digestion of organic substances produces a gaseous mixture of methane, carbon dioxide and impurities (e.g., H_2S, siloxanes, water) called biogas. This alternative energy source supplies 1.7% of the world's renewable energy in 2018, with a growing trend of 11.5% per year [1]. In addition, the current energy supplied by anaerobic digestion represents only 6.1% of the total energy that could be generated from organic wastes [2]. Thus, biogas has a unexplored potential that could increase energy supply and reduce greenhouse gas (GHG) emissions by treating the organic fraction of solid wastes and wastewater. The production and usage of biogas could improve the overall efficiency of different economic sectors by offering new products derived from methane (e.g., hydrogen and natural gas substitute).

Biogas is a flexible source of renewable energy that can provide electricity continuously, store energy or supply methane for several purposes. Although there are different options to produce methane (e.g., gasification and methanation), anaerobic digestion is the leading technology for renewable methane generation in the present moment [2]. Thus, biogas has special features that complements other energy sources (renewable and fossil derived) and could be used to solve modern problems in the energy sector.

Biogas has difficult obstacles to surpass in order to attain its full potential. Since biogas can be produced from multiple sources for different purposes, each scenario presents some particularities. For instance, a successful case for a company or country may not be reproducible in a different environment if not carefully examined. Analogously, equipment for natural gas applications and traditional waste management may not be optimized for biogas systems, energy integration and distributed generation. Thus, a large potential for renewable energy may remain as non-viable opportunities without the development of novel systems for biogas production and usage.

Lastly, as any other renewable energy source, biogas also generates specialized jobs and opens new opportunities for entrepreneurship that create positive social impacts, such as those proposed by the circular economy.

1.1 The development of biogas in Brazil

A recent report indicates that electricity is the main end-use of biogas in Brazil (73%), followed by heat (8%), biomethane (19%) and mechanical energy (0.1%)[3]. Figures 1.1 and 1.2 show the historical data for biogas production and installed capacity of power generation according to data published by CIBIOGÁS [4] and the Brazilian Electricity Regulatory Agency (ANEEL) [5], respectively. Biogas production has been exponentially rising since 2015 (approx. 23% p.a.) and reached an installed capacity of 270 MW (electricity) in 2020.

Figure 1.1: Yearly biogas production in Brazil from 2003 to 2020

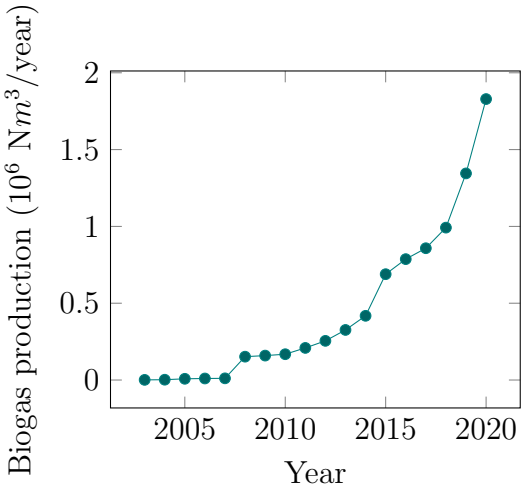

Source: [4]

Figure 1.2: Installed capacity of power generation using biogas by year and feedstock

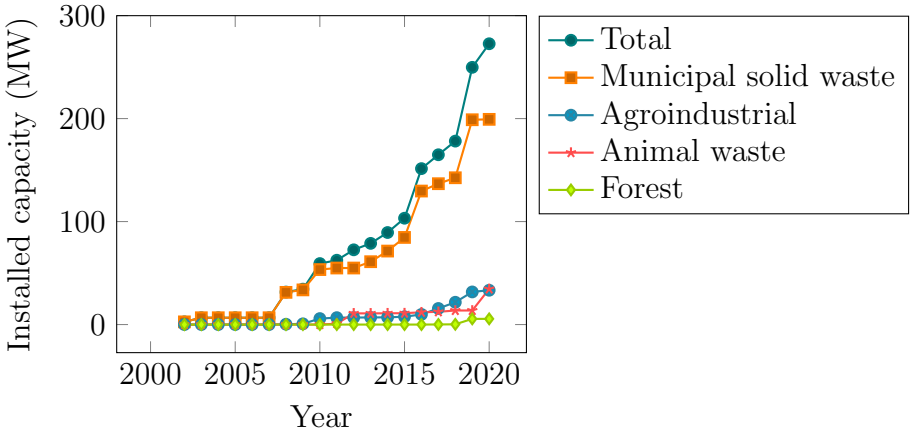

Source: [5]

It can be observed that the municipal solid waste is responsible for the majority of power generation capacity. This can be explained by the relatively low costs of produc-

ing biogas in landfills [2] and the establishment of the clean development mechanism by the United Nations. Thus, landfills can achieve lower electricity costs since they receive financial compensation to dispose solid wastes and to avoid methane emissions. In addition, landfills receive huge amounts of organic matter regularly and, therefore, rarely have problems with fluctuations in biogas production.

The distributed generation using biogas has been growing exponentially since a 2015 update in the net-metering program [6, 7], as it can be observed in Fig. 1.3. This new regulation permits a reduction in the electricity bill of energy producers (<5 MW) in proportion to the amount of power they provided to the grid. Since the electricity prices have been rising in the last few years, as illustrated in Fig. 1.4 [8], the distributed generation has become more attractive regarding economic aspects.

Figure 1.3: Installed capacity of power generation using biogas by year and type

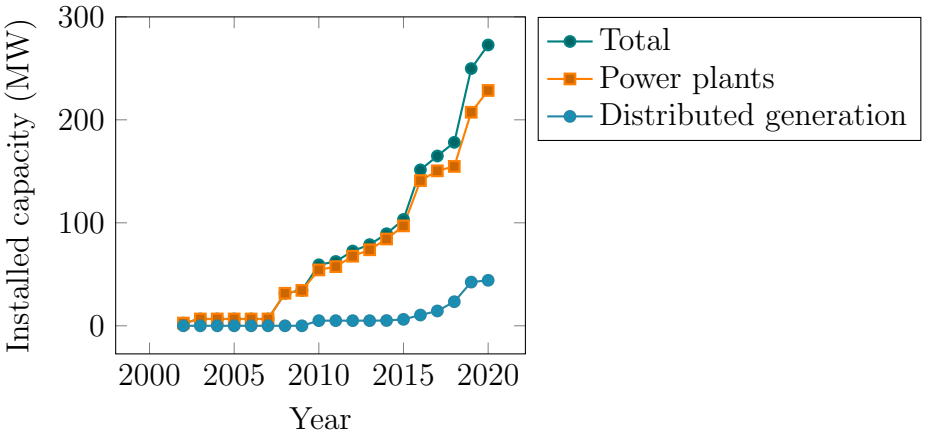

Source: [5]

Figure 1.4: Average electricity prices in Brazil from 2012 to 2020

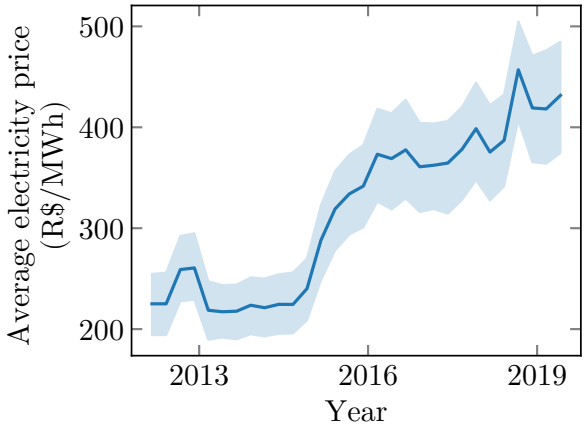

Source: [8]

The open data of ANEEL [5], illustrated in Fig. 1.5, also shows that the majority of

biogas projects have an installed capacity between 50 and 100 kW. This pattern could be assigned to two main factors: the distribution of organic residues and the net-metering system. Although a smaller unit may incur in higher specific prices due to the economy of scale [2], feedstock may only be available at limited quantities or at low concentrations. Moreover, even if there is potential for large biogas production, the financial compensation in the net-metering system is restricted by the electricity consumption of the producer. Thus, investing in a large unit may only be viable for dedicated power plants, which requires large capital investments and may have lower economic returns (electricity prices are more competitive). On the other hand, there is a lack of efficient options for power generation below 50 kW using conventional technologies (e.g., internal combustion engines or micro turbines). For instance, Figure 1.6 shows the efficiency of internal combustion engines and micro-turbines by installed capacity for comparison.

Figure 1.5: Power generation units using biogas by installed capacity, feedstock source and type

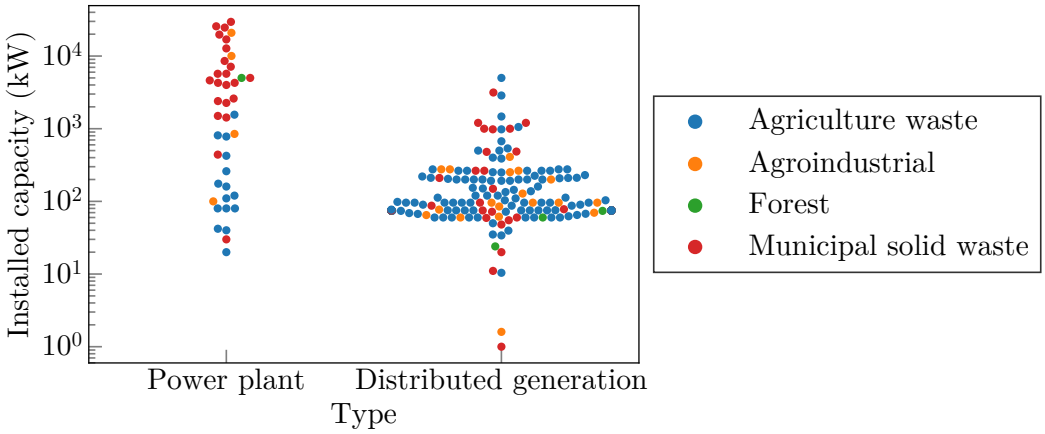

Source: [5]

Although the majority of biogas plants are small (<100 kW), as shown in Fig. 1.5, the main fraction of power generation can be attributed to large units (>5 MNm^3/year) [3]. Figures 1.7 and 1.8 also depict this distribution according to data reported by CIBIOGÁS [3].

1.1.1 The potential of biogas production in Brazil

The Brazilian Energy Research Office (EPE) estimates that the conversion of organic wastes from agriculture, livestock and cities in Brazil could provide approximately 75.7 million toe of energy in 2019 [14]. This represents a potential of 25.1 GW of electricity, which is approximately 80 times higher than the current scenario shown in Fig.1.3. Figure 1.9 illustrates the assessment of biogas potential by source and shows that the most

Figure 1.6: Efficiency of internal combustion engines (ICE) and micro-turbines

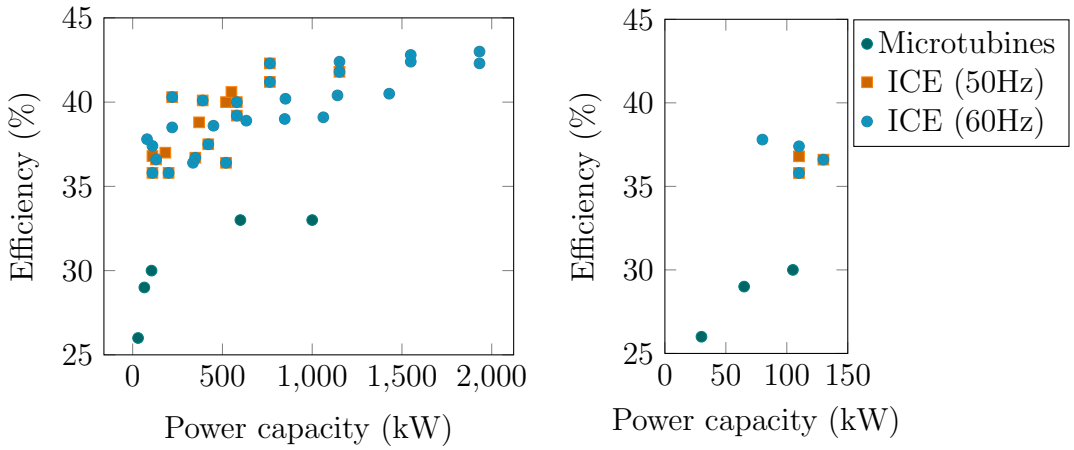

Source: [9, 10, 11, 12, 13]

Figure 1.7: Distribution of total biogas production and production units grouped by scale

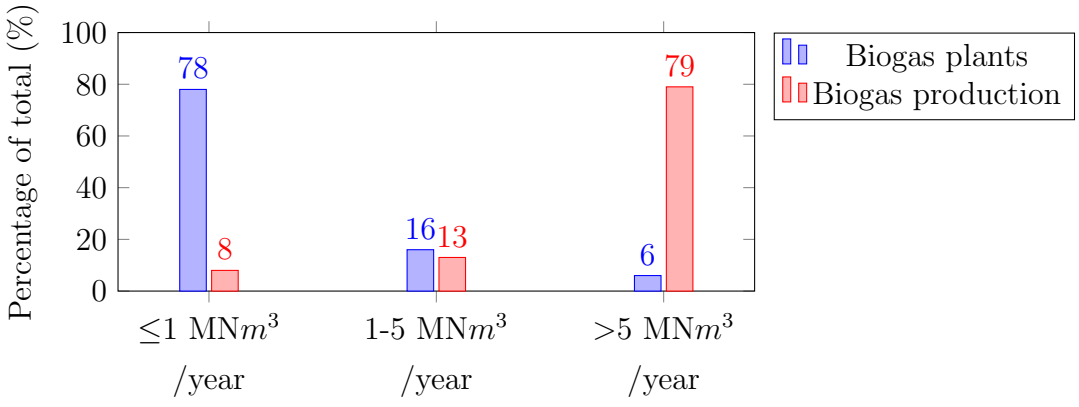

Source: [3]

Figure 1.8: Distribution of total biogas production and production units grouped by end-use

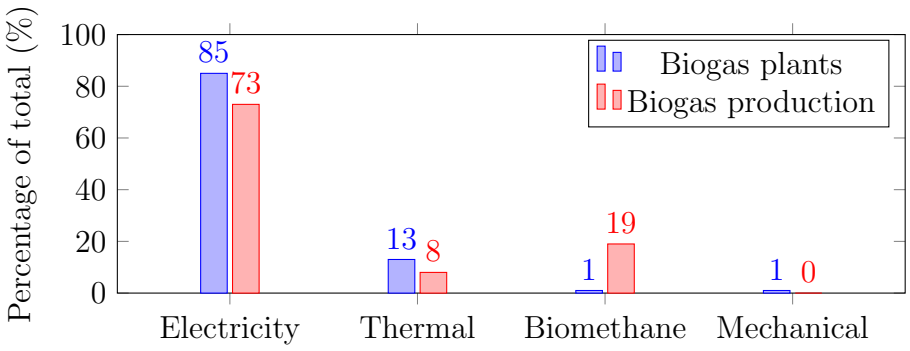

Source: [3]

promising feedstocks are wastes from maize, cattle livestock, sugarcane and municipal solid waste.

Figure 1.9: Biogas potential using wastes from agriculture, livestock and cities

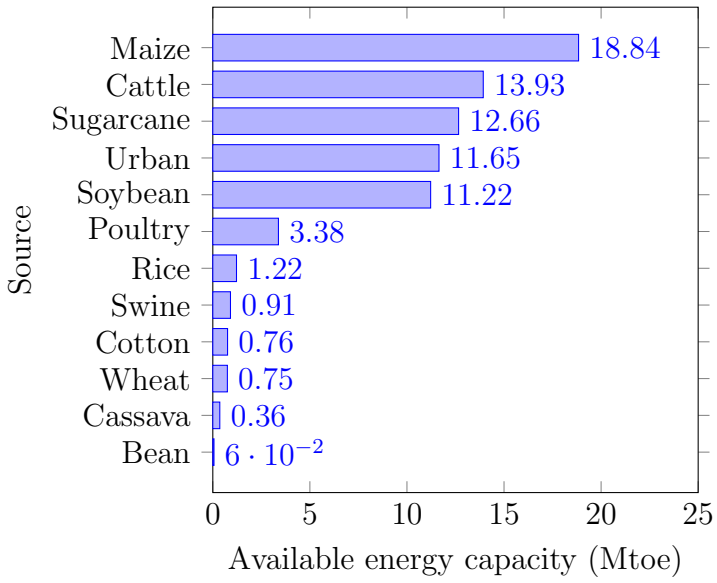

Source: [14]

It is important to highlight that the major sources of organic wastes in Fig. 1.9 do not correspond with the main feedstock used for electricity generation of Fig. 1.2. There is a number of reasons which could explain such contrast between potential and installed capacity. For instance, the seasonality of annual crops may affect the quantity of wastes available along the year and large storage capacities may be necessary to maintain constant operation of biogas plants. In addition, the predominant model of agriculture and cattle farming in Brazil uses extensive areas of land, which difficult the collection of wastes for energy purposes. These characteristics, seasonality and dispersion, may increase the costs and financial risks of using agriculture and livestock wastes, which diminishes the investment interest in these areas. Organic wastes can also be used for other purposes such as animal feeding and land fertilizer, which may be more economic attractive end-use. In addition, in several agriculture applications, it is usual to dispose crop wastes in the cultivated land to recover a portion of the macro-nutrients taken from the land by the crops. Thus, the total amount of crop wastes available for biogas production may be restricted by the balance of soil nutrients.

Data reported by CIBIOGÁS [4] indicate that agriculture wastes are the main feedstock for the majority of biogas production units, as it is shown in Fig. 1.10. However, their share in the total volume of biogas produced is much smaller than those generated by urban wastes and domestic wastewater.

Figure 1.10: Distribution of biogas plants and production per feedstock source

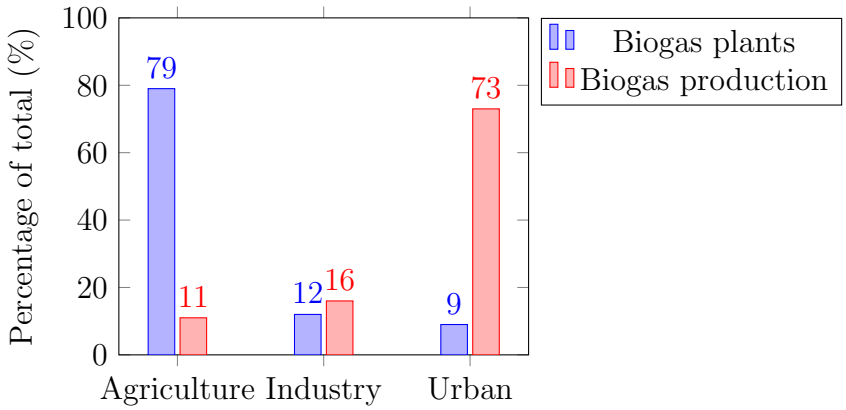

Source: [4]

1.1.2 Future prospects for biogas in Brazil

The National Energy Plan 2050 [15] foresees that biogas will be responsible for the majority of technological development in the bioenergy sector in the following decades, as illustrated in Fig. 1.11. Since biogas development in Brazil has strong correlations with public policies, it is fair to assume that government influence can drive future trends. In recent years, the major novelty in the Brazilian national police for renewable energy is the RenovaBio program, which compensates biofuel producers with decarbonization credits (CBIOs). The biofuel producer receives credits based on the quantity of energy supplied and a fuel score according to a life-cycle analysis.

Figure 1.11: Future technological developments related to biomass energy

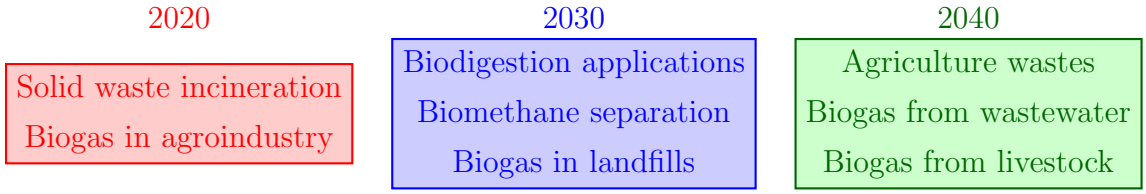

Source: [15]

In this system, biomethane production using biogas can attain one of the highest scores of energy-environmental efficiency (NEEA), as it is shown in Fig. 1.12. The score aims to estimate the emissions avoided compared with fossil fuels consumption, therefore biofuels with higher scores receive more credits. The high performance of biomethane can be explained by the low GHG emissions of biogas production and usage in comparison with diesel and natural gas. In 2020, only 8 biogas plants (1% of the total number of biogas plants) have reported to produce biomethane as their main product, which is estimated to represent 19% of the total biogas production in Brazil [3]. According to the Brazilian

Ministry of Science, Technology, Innovation and Communication (MCTIC), the development of biofuel production from biogas requires the development and optimization of technologies and industrial processes [16].

Recently the Brazilian government approved a new legislation for the natural gas market (PL 4476/20), which aims to increase flexibility and competitiveness in the sector [17]. According to the Brazilian Biogas Association (ABIOGÁS), the possible benefits for the natural gas commercialization would also be applicable to the biomethane derived from biogas [18]. Thus, it is possible that these changes could indirectly promote new business focused on commercializing biomethane for the grid or the industry.

Figure 1.12: Box plot of energy-environmental efficiency (NEEA)for biofuel producers and importers for each biofuel

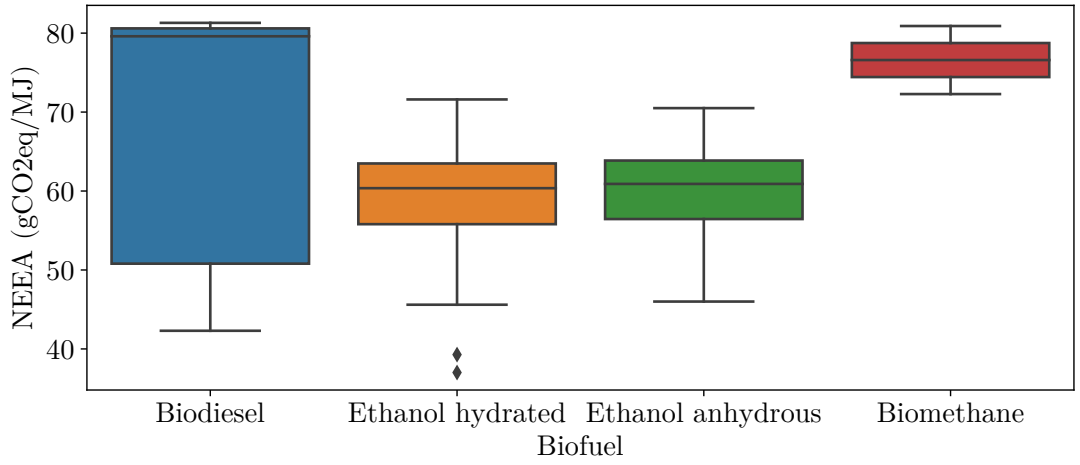

Source: [19]

1.1.3 Major criticisms of biogas

The total energy that could be produced from biogas is usually assessed to be much lower than other biomass sources. For instance, the installed capacity for electricity generation from biomass in Brazil in 2021 is approximately 15.7 GW, in which biogas power plants represent less than 2% [20]. A similar argument could be made for biofuel production, in which one may argue that only a small fraction of the current consumption could be replaced using biogas derivatives. For instance, the International Agency of Energy estimates that the total biogas potential could supply 20% of the global natural gas consumption [2]. However, a recent study of EPE [14] indicates that the energy potential of biogas in Brazil is approximately 75.7 Mtoe, more than double the internal energy offer of natural gas in 2019 (35.9 Mtoe) [21]. It is important to highlight that these studies only consider the biogas derived from wastes and not energy crops (e.g., maize, sugarcane,

wood), which are currently the major sources of biomass energy.

This observation leads to a recurring problem in biogas literature: the uncertainties of biogas production and potential. Since data of composition and biodegradability may be unknown or widely variable, the estimation of biogas potential usually relies on average conversion factors or generalized assumptions. Biogas production is very sensitive to the constitution of organic waste and operational parameters, therefore it is very common to find differences between predictions and experimental values.

Lastly, it is important to highlight that biogas production is not the only option to reuse organic wastes. In fact, the production of animal rations and organic fertilizers competes with biogas production for some feedstocks with excellent qualities. For example, poultry litter is used as nitrogen source for organic fertilizers despite having a high potential for methane production. Another example is the use of distillers grains, which are byproducts of ethanol production in biofuel plants and brewers, as animal ration. Thus, although biogas production could benefit from using certain organic wastes, this practice could affect established practices on agriculture and industry. A similar criticism can be made for using energy crops for biogas production. This could greatly increase the potential of this energy source and solve several operational problems (e.g., reliability, feedstock supply), but requires fertile land that could be used for other practices.

1.2 Hydrogen market expectations

Hydrogen gas has been promoted as a global energy vector in the last decades, a future scenario often described as the hydrogen economy. Recently, research interest in hydrogen has been resurged due to concerns about grid stability and carbon emissions from different sectors (e.g., iron and steel, chemicals, transportation) [22]. For instance, the surplus electricity produced from renewable sources could be stored as hydrogen and reused on demand or as fuel for transportation sectors in which electrification may be inefficient (e.g., ships, trucks and airplanes). Today, hydrogen is mostly produced from natural gas for ammonia production and oil refining. Since biogas is the leading source of renewable methane in the world, anaerobic digestion can contribute for green hydrogen production with minor changes to existing infrastructure and technology.

The hydrogen transition from chemical input to energy vector will require the development of efficient systems of fuel cells and electrolyzers. These technologies can also be used in biogas plants to increase efficiency of power generation, especially at small scales, produce hydrogen or increase methane production by using methanation. For example, hydrogen can be used to convert carbon dioxide into methane using chemical or biological catalysts [23]. Thus, research advances in these technologies could promote new

opportunities for biogas plants increase their efficiency and economic revenues.

1.3 Objectives

Biogas has an enormous potential for distributed energy production and technological development to be explored in the near future. The development of biogas systems can increase the sustainability, efficiency and economic profitability of agriculture, industry and wastewater treatment. Today, landfills are responsible for the majority of biogas production in Brazil, while the distributed generation at small scales (< 100 kW) is the most common type of biogas plant. However, the lack of efficient conversion systems at micro-scale (< 50 kW) combined with the seasonality and distributed nature of organic residues may be significant barriers for new biogas businesses. On the other hand, recent public policies supporting renewable methane and the development of hydrogen technologies may promote new opportunities for biofuel production and efficient electricity generation using biogas.

Based on the current scenario, the research of efficient systems for biogas conversion into power and biofuels on small and distributed scales will play an important role to overcome technological challenges. One promising option is the use of fuel cell systems fueled with biogas, since they are able to achieve higher efficiencies at small scales and produce hydrogen as a byproduct. For instance, the co-production of electricity, heat, methane or hydrogen may increase the efficiency of biogas conversion and end-use, while providing by-products for different markets. Thus, the general objective of this thesis is to develop a systematic framework to simulate and optimize different configurations of biogas systems for electricity and biofuel production. In specific, this research will focus on fuel cell systems to achieve high power conversion efficiencies and flexible hydrogen production, as well as, conventional biomethane production using CO_2 separation. In this way, it is intended to analyze and propose optimal designs in the technical, economic and environmental perspectives.

1.3.1 Specific objectives

- Develop a thermodynamic model (mass, energy and entropy) of power plants using fuel cells working with biogas, embracing different configurations, feedstock and products.

- Analyze the economic and environmental costs of the possible systems, as well as the relationship between these parameters and the efficiency of the thermodynamic processes involved.

- Build the framework to link optimization algorithms with the studied problems, in order to determine optimal relationships between the selected thermodynamic, economic and environmental parameters.
- Evaluate how uncertainties in the biogas production and in the economic scenario could influence design choices and optimal operation.

1.4 Outline

This thesis is organized into four major parts: introduction & objectives, theoretical background & methods, analysis & results and conclusions. Figure 1.13 depicts a graphical outline of this thesis. The following chapters 2 to 4 present the theoretical background of the processes and methods that are studied in this thesis. They provide an introduction to the subjects of biogas (chapter 2), methane reforming, fuel cells (chapter 3) and process design and analysis (chapter 4). Next, chapters 5 to 7 discuss the major novelties of this research compared with the established literature. These analysis can be divided into two minor categories: macro analysis (chapter 5) and system level analysis (chapters 6 and 7). The first group is more focused on the comparison of different production routes, while the second group is dedicated to design and optimize fuel cells systems working with biogas. Finally, chapter 8 summarizes the main results of this thesis and chapter 9 discuss the main conclusions and achievements of this research work and includes suggestions for future works in this research area.

Figure 1.13: Graphical outline of this thesis

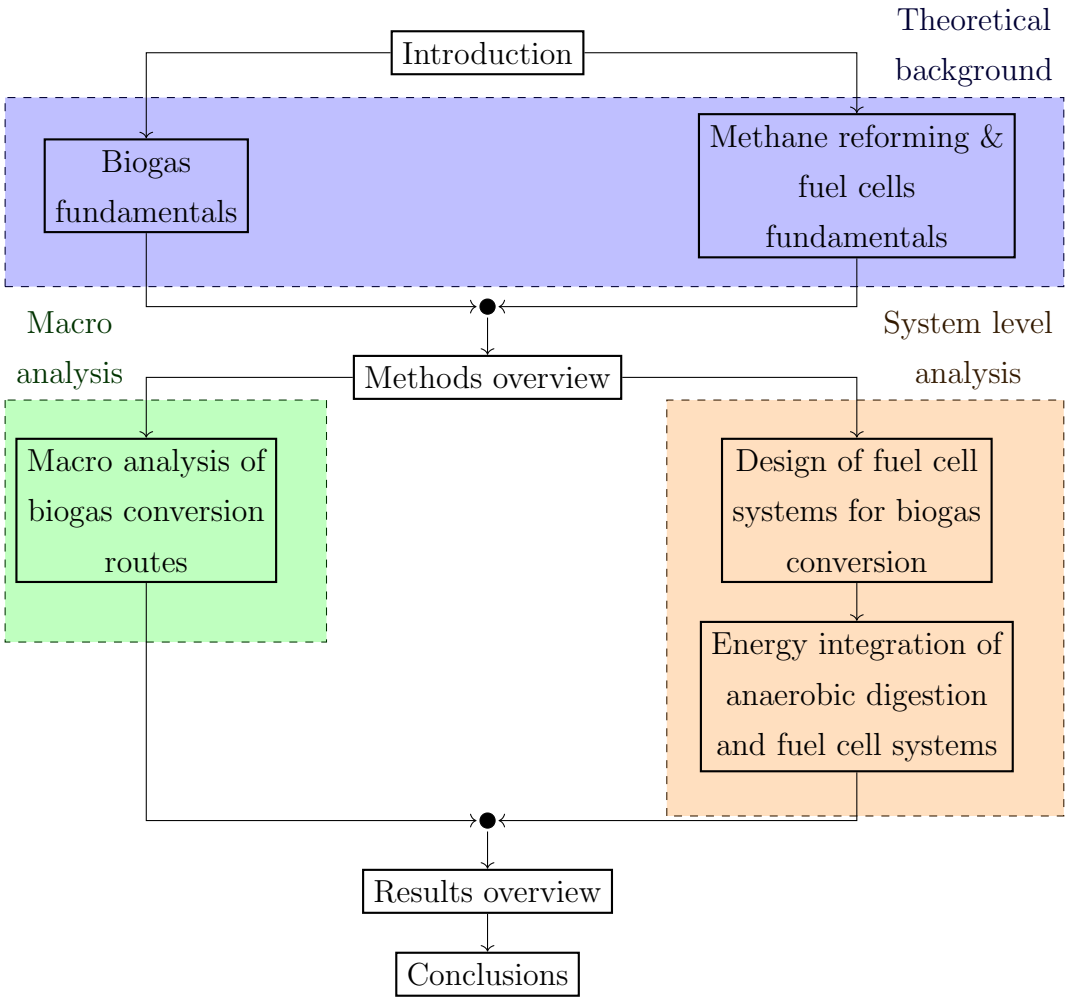

2 Biogas fundamentals

Biomass conversion by anaerobic digestion is a promising alternative to provide renewable energy with relatively low energy consumption. Besides the potential to upgrade organic residues, this process can also reduce greenhouse gas emissions in waste management and produce an alternative fertilizer from the digestate. In general, the main challenges of biomass digestion projects are the low energy density of organic wastes and the economic viability of biogas production. Moreover, in the small and distributed production scale, the efficiency of conventional cogeneration systems may be still significantly limited. Thus, the development of techniques to improve productivity and economic return of products derived from biogas are essential to increase the renewable energy offer from biomass digestion. In view of these remarkable advantages, this chapter focuses on a critical review of the biomass digestion and biogas conversion technologies, as well as their underlying theoretical principles.

2.1 Overview

In this thesis, a facility that produces biogas and converts it to electricity and/or biofuels is called a biogas plant. The conventional design of these units can be divided into five major processes, as shown in Fig. 2.1.

Figure 2.1: Processes in a conventional biogas plant

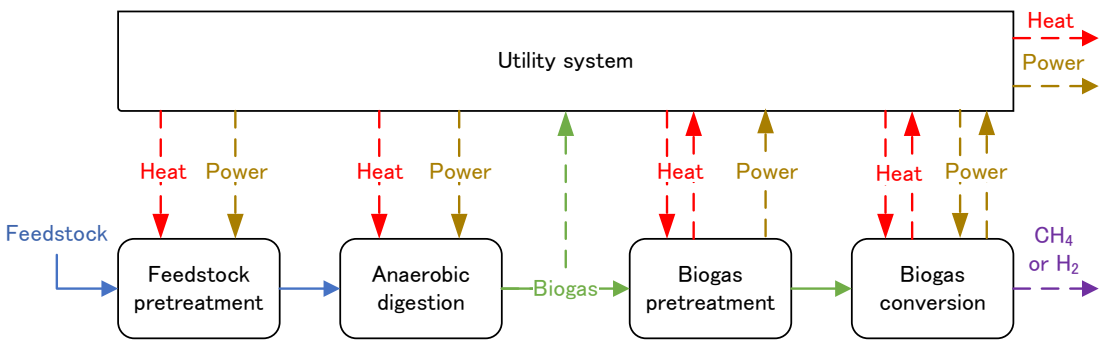

Source: Author

The feedstock pretreatment prepares the organic residues to be more easily converted into biogas. For instance, depending on the local legislations and waste source, it is necessary to disinfect, grind, correct the pH or dilute the feedstock. Next, chemical reactors partially convert organic substances into biogas through anaerobic digestion. This process also produces more bacteria and reduces the organic load of wastewaters and residues. Since biogas naturally contains impurities that could damage or reduce the efficiency of downstream equipment, separation processes are used to remove H_2O, H_2S, siloxanes, among others substances. Finally, biogas is converted into other products such as heat, electricity and biofuels, while a portion of biogas energy may be recovered to meet certain demands of the internal process in the biogas plant.

It is important to highlight that the organic feedstock properties (e.g., temperature, pH, solids concentration) and biogas composition may significantly alter the plant design.

2.2 Anaerobic digestion

Biogas is a gaseous mixture of methane, carbon dioxide and other contaminants (e.g., water, hydrogen sulfide, siloxanes, ammonia and air) produced by the anaerobic digestion of organic material. This process naturally occurs in the absence of oxygen and consists in the degradation of organic material catalyzed by different bacteria groups. As described in Fig. 2.2, anaerobic digestion can be divided into five major conversion steps: hydrolysis, acidogenesis, acetogenesis, methanogenesis and sulfate reduction.

Figure 2.2: A simplified diagram of anaerobic digestion

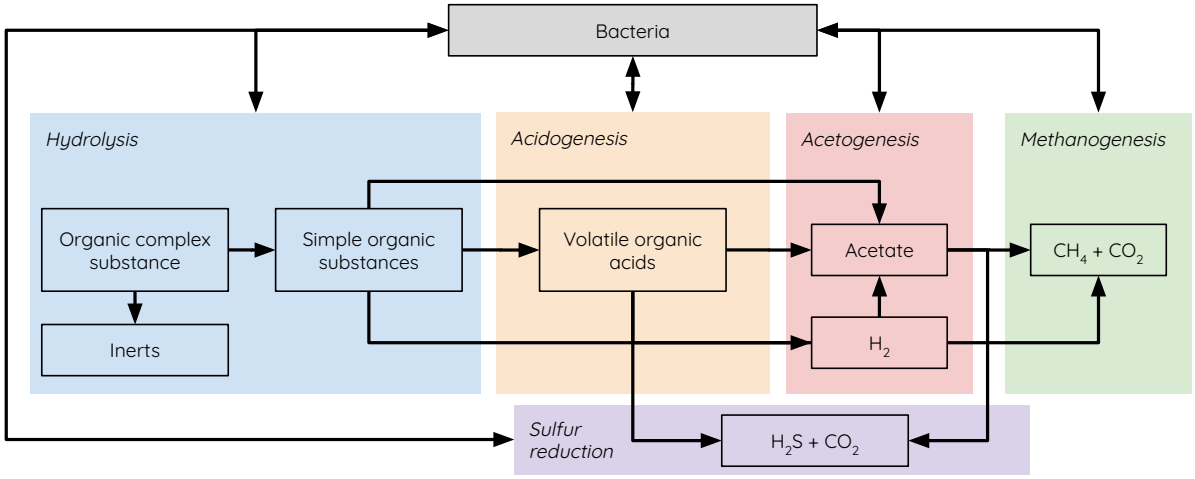

Source: Author

Solid biomass is a complex organic material that can be converted into simple organic components (e.g., sugars, long-chain fatty acids and amino acids) by hydrolysis. This

process is catalyzed by exoenzymes produced by bacteria and may achieve different degrees of conversion depending on the substrate. For instance, lignocellulose and lignin are examples of recalcitrant organic material in anaerobic digestion reactors due to their strong molecular bonds [24]. Next, the acidogenesis bacteria converts the dissolved organic molecules into short chained acids (e.g., acetic, propionic and butyric acids), carbonate and hydrogen.

Acetate, hydrogen and carbonate are produced from these intermediary organic substances in a process called acetogenesis. These products are the main substrates for methanogenesis, the process of methane synthesis. The acetogenesis and methanogenesis bacteria groups are strongly connected by the hydrogen concentration. For example, if the methanogenesis process is disturbed, hydrogen concentration increases and inhibits the acetogenesis bacteria, which causes an accumulation of organic acids [25]. On the other hand, sulfur reduction is a process that competes with methanogenesis for substrates to produce hydrogen sulfide (H_2S). Hydrogen sulfide can decrease the biogas production, while the high concentration of sulfur can inhibit other bacteria groups [26]. This alternative conversion step is especially important for industrial wastewater, which can contain high concentrations of sulfur components.

In sum, anaerobic digestion converts biomass into biogas, intermediary organic components (e.g., organic acids, sugars, amino acids, long-chain fatty acids and inert) and bacteria biomass. Moreover, this process reduces the concentration of organic pollutants (e.g., chemical and biological oxygen demand) and can neutralize the pH of the effluent. However, anaerobic digestion depends on the symbiotic interaction between different bacteria groups, which may be disturbed by the environment, i.e. operating conditions of the diverse components of the biogas plant. Anaerobic reactors are usually designed to enhance the methanogenesis process, since it develops a key role in hydrogen equilibrium and are quite sensitive to environmental changes [27].

2.2.1 Environmental requirements

Anaerobic digestion has certain requirements to develop and sustain an operation at stable conditions. These conditions are directly related with the growth and death of the bacteria groups previously mentioned. As the name of the process implies, there should be an absence of oxygen to avoid the death of anaerobic organisms. Although some bacteria present in anaerobic digestion may be facultative anaerobes, the process can not be developed with significant concentrations of oxygen.

The bacteria growth and death rate are dependent on the reactor temperature. Since this relationship may vary for each species, the anaerobic digestion has three different temperature ranges with optimal growth conditions: psychrophilic (4-15 °C), mesophilic

(20-40 °C) and thermophilic (45-70 °C) [25]. In theory, the higher temperature ranges provide higher bacteria growth rates and, consequently, higher rates of biogas and sludge production. However, the operation at higher temperatures leads to higher energy consumption and less stability, since there are fewer bacteria species that can withstand high temperatures [27]. Thus, the mesophilic temperature range is the usual operation condition for anaerobic digestion reactors.

Bacteria biomass is composed of several chemical elements, thus it is expected that these elements are required as nutrients to their growth. In general, important nutrients are carbon, nitrogen, phosphor, sulfur, potassium, calcium and magnesium. The proportion of recommended nutrients varies depending on the source, since the composition of bacteria varies and experiments are subjected to uncertainties. As an example for the main nutrients, a mass ratio of 500-1000 C : 15-20 N : 5 P : 3 S is considered sufficient for anaerobic digestion [28].

The pH influences the bacteria cell homeostasis and the dissociation equilibrium of acids and bases, which directly and indirectly affect the anaerobic digestion. For instance, hydrolysis and acidogenesis bacteria are more active in relatively low pH (5-6), while methanogenesis bacteria develop strictly in pH close to neutral (7) [27]. Thus, in practice, the pH in anaerobic reactors is controlled to be maintained at neutral with a chemical supplement (e.g., CaO, CaOH, NaOH), or by recycling the effluent. In this last scenario, the anaerobic digestion increases the bicarbonate (HCO_3^-) concentration by decomposing organic material [26].

The majority of toxic inhibitions in anaerobic digestion are associated with acids or bases and, thus, are indirectly related with the pH. The main examples are undissociated acids (e.g., acetic, butyric and propionic acids), dissociated hydrogen sulfide (HS^-) and ammonia (NH_3). The concentration equilibrium of these substances is highly dependent on the pH value, thus a small variation in pH can lead to significant changes in the anaerobic digestion. Other reported toxic materials are heavy metals (e.g., lead, cadmium, copper, zinc) and complex substances found in wastes from specific areas, such as disinfectants, antibiotics and pesticides.

2.2.2 Modelling methods

From the energy perspective, the methane production per unit of organic material, methane yield (MY), is the most important variable in anaerobic digestion since it is directly proportional to power or biofuel production. Thus, it is important to determine the theoretical limits of biomass conversion based on its general characteristics to design and evaluate biogas production plants.

In wastewater treatment, the total solids are all substances derived from wastewater

after water removal (dried wastewater). These solids can be classified depending on if they can be filtered (suspended or dissolved) or ignited at 500 °C (volatile or fixed). Since there is no simple test to verify if a solid has organic components, it is usual to assume that the solids that can be ignited at 500 °C, the volatile solids (VS), are organic substances [29]. Thus, these classifications are directly linked with the availability of organic material for anaerobic digestion.

Another approach to the classification of wastewater quality is the concentration of oxygen demand, which is the quantity of oxygen necessary to oxidize the wastewater under certain conditions. There are two types of oxygen demand measurements: chemical (COD) and biological (BOD). The first uses potassium dichromate ($K_2Cr_2O_7$), while the second uses microorganisms to oxidize the wastewater. In general, COD values are higher than BOD because potassium dichromate can oxidize complex organic material that microorganisms would take a long time to convert. Thus, COD is an indirect measurement of the total organic concentration, while BOD represents the easily digestible fraction of biomass present in wastewater. Moreover, based on the definition of COD, it is also possible to derive a theoretical oxygen demand (ThOD) for a generic organic substance ($C_cH_hO_oN_nS_s$), as described in the Eqs. (2.1) and (2.2) [30].

$$C_cH_hO_oN_nS_s + \left(c + \frac{h}{4} - \frac{o}{2} - \frac{3n}{4} + 1.5s\right) O_2 \rightarrow cCO_2 + \left(\frac{h}{2} - \frac{3n}{2} - s\right) H_2O + nNH_3 + sH_2SO_4 \quad (2.1)$$

$$ThOD\left[\frac{gO_2}{mol_{substrate}}\right] = 32\left(c + \frac{h}{4} - \frac{o}{2} - \frac{3n}{4} + 1.5s\right) \quad (2.2)$$

The chemical oxygen demand (COD) is the theoretical basis for most anaerobic digestion models, since it is commonly agreed that COD is conservative for ideal anaerobic processes. This assumption allows us to determine the theoretical limit of conversion of biomass to methane, since methane (CH_4) ideally would correspond to 64 g of O_2/mol of CH_4. Thus, by converting the units with the ideal gas law, the maximum methane yield is approximately 0.35 Nm^3/kg of COD. It is also possible to extend the analysis to common organic substances in order to evaluate the theoretical yield of different groups. For instance, Figure 2.3 shows the specific methane yield (Nm^3 of CH_4/kg of biomass) per carbon fraction (kg of C/kg of biomass) of the major organic substances present in anaerobic digestion. The overall trend shows that organic matter with high concentration of carbon has a higher specific methane yield.

It is important to highlight that, especially for anaerobic digestion, biomass is often available at high moisture content or significantly diluted. Thus, the maximum specific

Figure 2.3: Theoretical results of specific methane yield per carbon fraction

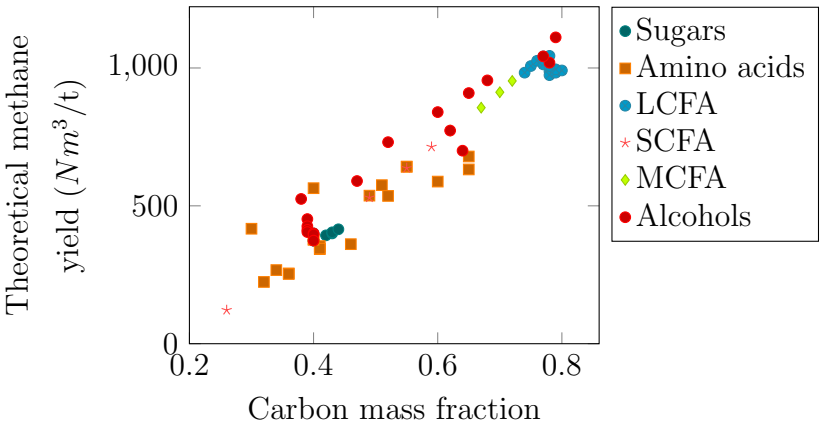

Source: Author

methane production can be significantly lower in total mass basis depending on the humidity, as it can be observed in Fig. 2.4. In this figure, the average values of theoretical methane yields reported in Fig. 2.3 for sugars, amino acids and long chain fatty acids are assumed. These results are in accordance with values reported by Jende, et al. [31] for methane yields of carbohydrates, proteins and fats. In addition, as it can be deduced from Fig. 2.2, COD can not be totally converted into methane, since at least a portion of the organic material has to be converted into bacteria biomass and intermediary compounds (e.g., acids, sugar, amino acids). Moreover, a significant fraction of organic matter in anaerobic reactors has a slow conversion or is difficult to hydrolyze (e.g., cellulose, hemicellulose, lignin). Thus, the actual biogas production of a certain feedstock is only a fraction of its theoretical methane yield.

Figure 2.4: Effect of the humidity in the maximum specific methane production

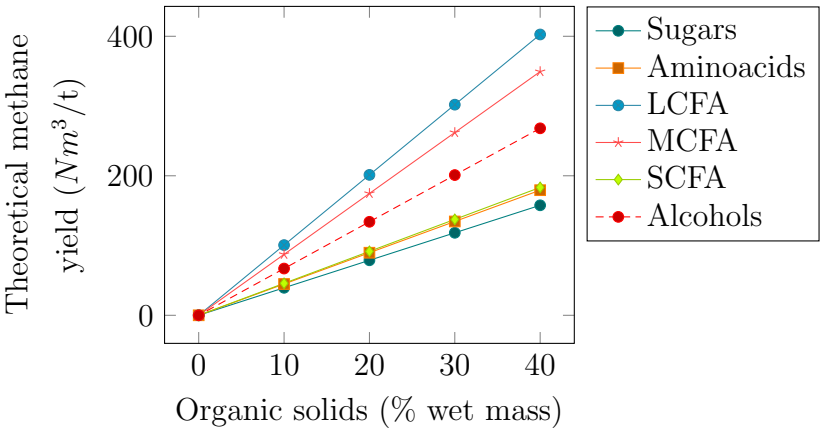

Source: Author

Feedstock supply and production scale

A feedstock can be classified by its origin (e.g., industrial, agriculture, etc.), by its properties (e.g., percentage of solids, concentration of organic compounds) or by its productivity (e.g., methane or biogas yield). In theory, any organic substance or mixture could be used to produce biogas via anaerobic digestion under the suitable conditions. In practice, the organic wastes from agriculture, livestock, industries and cities are the main sources of feedstock for anaerobic digestion. These options are usually available free of charge or with negative costs (e.g., waste disposal in landfills) and their conversion may incur into other benefits or revenues (e.g., energy, fertilizer, irrigation).

Differently from fossil fuel resources, biomass is a seasonal product and wastes have a variable production and quality. Uncontrolled changes in quality and quantity of organic material are not ideal for operation of anaerobic reactors. These uncertainties could lead to reductions on methane production, frequent start-ups and partial load inefficiencies [32].

In order to overcome this issue and to achieve a constant supply of feedstock, it is common to use materials from different sources (co-digestion) and, if possible, with high specific methane production (e.g., energy crops and industrial wastes). Besides the reduction of uncertainties, this practice can also enhance nutrient proportions (C:N:P:S) and increase the reactor specific production (Nm^3 of CH_4/m^3 of reactor) providing higher economic return.

Table 2.1 shows the biogas and methane yield for different feedstock used in anaerobic digestion. It is important to notice that the reported values of methane yield for a feedstock type may vary due to the concentration of water or organic solids (volatile solids). For instance, the methane yields presented in Table 2.1 are relatively lower than most theoretical values presented in Fig. 2.3. The main reason for these differences is the high humidity of these feedstock, as previously exemplified in Fig. 2.4. Other losses can be traced back to the organic fraction in total solids and the production of intermediary substances in anaerobic digestion (e.g., bacteria, volatile acids). Moreover, the experimental conditions for each reference source may not be equal, thus average values of methane yield should be always verified.

Since most feedstock have a low specific production of methane, a significant amount of wastes is necessary to achieve high biogas production rates. Thus, in general, biogas plants rely on different feedstock sources (e.g., co-digestion and centralized plants) to achieve high and stable energy production.

Table 2.1: Average methane yield of some common feedstock

Feedstock	Organic solids (% wet mass)	Average CH_4 yield (Nm^3/kg_{os})	(Nm^3/t_{wet})	Sources
Cattle slurry	6.3-8.0	0.15-0.21	9.6-16.8	[33, 27, 34, 35]
Poultry manure	16.0-30.0	0.28-0.31	48.0-91.6	[33, 27, 36]
Pig slurry	2.9-6.0	0.25-0.35	9.9-15.0	[33, 27, 36]
Maize silage	31.4-32.2	0.25-0.34	80.8-106.6	[27, 31]
Municipal solid waste	19.3-36.1	0.19-0.33	63.2-68.6	[31, 37]

Influence of operational variables in methane production

As it may be expected, the production rate of methane is directly related with the amount of biomass available for anaerobic digestion. Thus, the concentration of organic substances and their residence time are important variables in the operation of anaerobic reactors. The first parameter is usually given by the concentration of volatile solids (g of volatile solids/m^3) or the chemical oxygen demand (kg of O_2/m^3), while the second one is represented by the hydraulic retention time (HRT). The hydraulic retention time (HRT), Eq. (2.3), is the ratio of the reactor volume ($V_{reactor}$) per volumetric flow rate of wastes entering the reactor ($\dot{V}_{in}$).

$$HRT = \frac{V_{reactor}}{\dot{V}_{in}} \tag{2.3}$$

Although higher production rates of methane can be achieved with higher influent flow rate, the specific methane yield tends to decrease at low HRT. Figures 2.5 and 2.6 illustrates the influence of HRT and COD in the methane production per organic load (methane yield, $Nm^3/\mathrm{kgO_2}$) and per reactor volume (volumetric yield, $Nm^3/(\mathrm{d}.m^3_{reactor})$). As it can be observed, high HRT values can produce more methane from a fixed feedstock source, but this limits the volumetric flow rate of influent and reduces the volumetric yield. On the other hand, higher COD concentrations favors both methane and volumetric yields.

Bacteria have a limited rate of conversion of biomass that is proportional to their concentration, which has a maximum value depending on the reactor design [38]. Therefore, for high flow rates, the existing bacteria may not be sufficient to convert all degradable organic substances. This can also occur for sudden increases in the feedstock concentration, which may lead to a disturbance in the equilibrium of acidogenesis and methanogenesis. In drastic situations, the biogas production can be diminished and a reconditioning time may be necessary.

Thus, since the reaction rates are proportional to the concentration of bacteria, some anaerobic reactors with continuous operation are designed for maximum retention of bac-

Figure 2.5: Influence of HRT and COD on methane yield (MY) for vinasse anaerobic digestion at 35 °C, 1.01 bar, pH 7.0 and 0.05 gSO_4^{2-}/gO_2

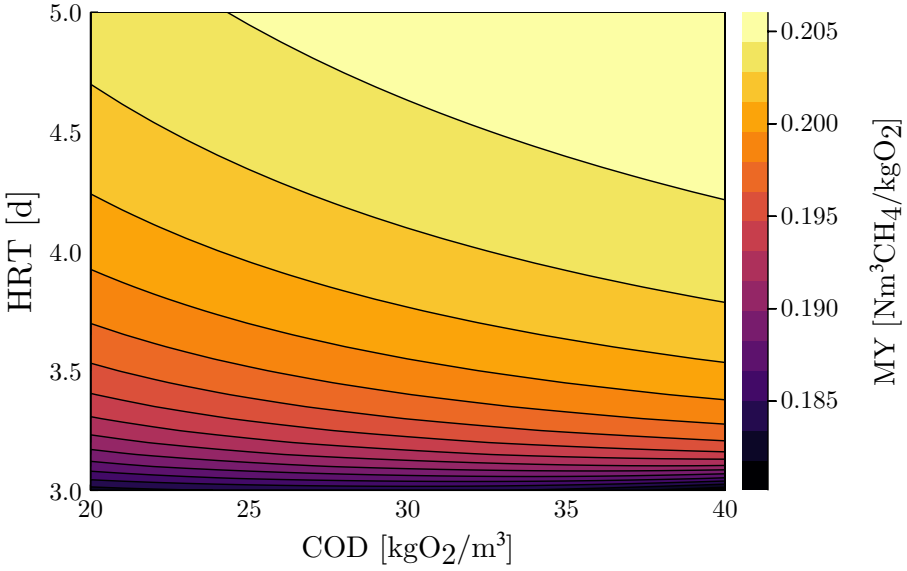

Source: Author

Figure 2.6: Influence of HRT and COD on volumetric yield (VY) for vinasse anaerobic digestion at 35 °C, 1.01 bar, pH 7.0 and 0.05 gSO_4^{2-}/gO_2

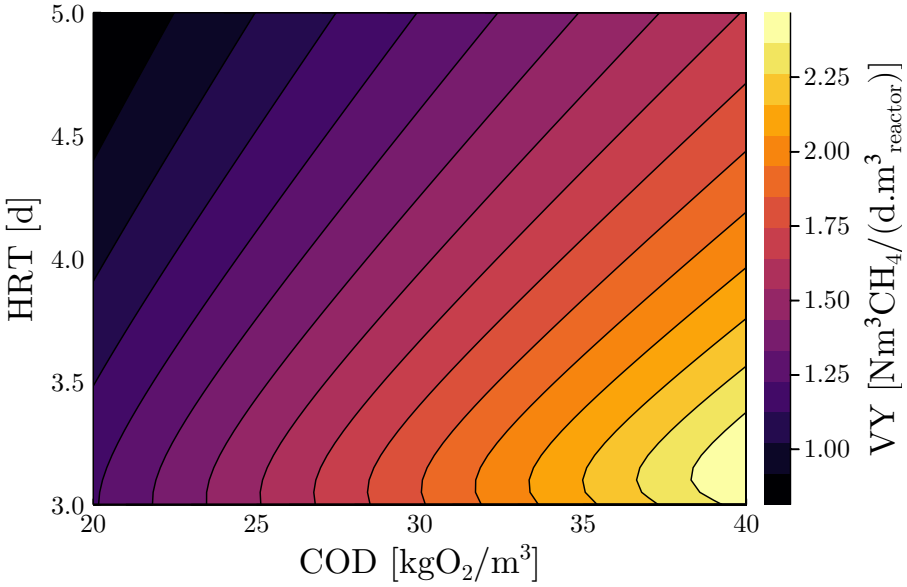

Source: Author

teria biomass (e.g. UASB). The simplest approach to model the rate of a reaction catalyzed by bacteria is to use the Monod equation, as described in Eq. (2.4). The Monod equation estimates the reaction rate of a reaction catalyzed by bacteria (r) based on a constant reaction rate (μ), a half velocity constant (K_s) and the concentrations of bacteria (Z^x) and substrate (Z^s). The effect of bacteria biomass concentration (Z^X) is illustrated

in Fig. 2.7 using the Monod equation, Eq. (2.4), and data reported by Rosen and Jeppsson [39] ($\mu = 8\ d^{-1}$ and $K_S = 0.15$ kgCOD.m^{-3}). It is important to notice that an increase in solids retention may lead to a reduction in the reactor useful volume and, consequently, reduce the hydraulic retention time. Thus, the concentration of bacteria biomass can not provide an unlimited increase in the reaction rate, as the Figure 2.7 may suggest.

Figure 2.7: Reaction rate of acetate conversion for different concentrations of bacteria (Z^X) (Eq. 2.4)

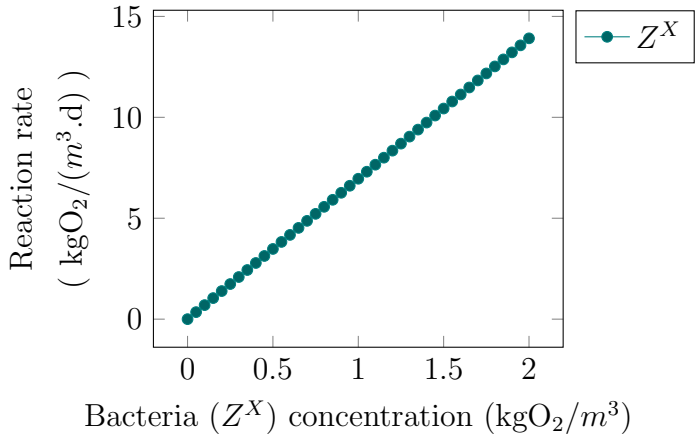

Source: Author based on values reported by [39]

$$r = \mu \frac{Z^S}{K_s + Z^S} Z^X \tag{2.4}$$

Another design choice for anaerobic reactors related with the kinetics of anaerobic digestion is the temperature (T). For instance, high temperatures have higher rates of conversion for chemical, biological and physical processes (as it can be demonstrated by the Arrhenius equation). However, the bacteria are quite sensitive to temperature changes and have narrow intervals with high growth rate. Figure 2.8 illustrates the results from a mathematical model, Eq. (2.5), validated by Zwietering, et al. [40] for Lactobacillus plantarum. As previously mentioned, this pattern can be explained by the competitiveness between bacteria growth and decay; growth is the dominant behavior for relatively lower temperatures, while bacteria decay is dominant at high temperatures.

$$\mu = 0.041\,(T - 277)^2\left(1 - e^{0.161(T-317)}\right) \tag{2.5}$$

Thus, the reactor thermal insulation and heat management directly impacts the production rate of biogas. Higher temperatures are able to increase the productivity of biogas production and reduce the specific costs of the reactor, but it also requires more energy for its operation. Thus, in most cases the mesophilic temperature range (20-40 °C) is employed in commercial applications.

Figure 2.8: Example of temperature influence in the bacteria growth (Eq. 2.5)

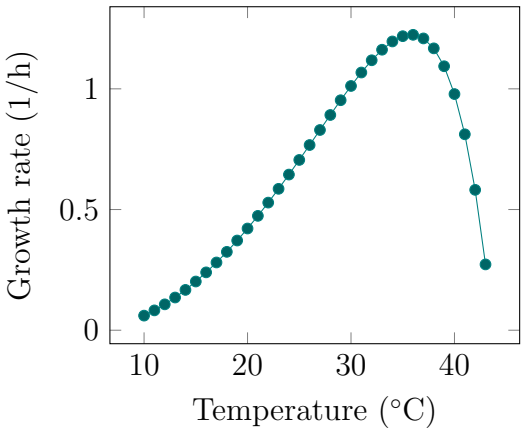

Source: Author

Modelling anaerobic reactors

Anaerobic digestion is a relatively difficult process to model due to the variability of organic feedstock and the several reactions involved in the process. The simplest approach, Eq. (2.6), is to assume an average methane yield (MY), as presented in Table 2.1, and estimate the methane production ($\dot{V}_{CH_4}$) as linearly proportional to the flow rate of wastes ($\dot{V}_{in}$) and its concentration (Z^s) [27]. This type of model can be used to grossly estimate the minimum amount of organic feedstock required for an specific methane production. However, since the average methane yields reported in literature may significantly vary according to the source, the methane production may be imprecise.

$$\dot{V}_{CH_4} = \dot{V}_{in} Z^S MY \tag{2.6}$$

A generic approach to model anaerobic digestion can be obtained based on the COD (COD_{in}) and theoretical maximum methane yield ($MY_{max} = 0.35\ Nm^3$/kg of O_2), as shown in Eq. (2.7). In practical applications, only a fraction of the total COD present in wastewater is converted into methane, therefore values obtained from Eq. (2.7) can only determine an upper limit for methane production ($V_{CH_4,max}$). Figure 2.9 illustrates an example of COD balance for anaerobic digestion. The methane production calculated from Eq. (2.7) can be partially corrected by considering the efficiency of COD removal (η_{COD}), described by Eqs. (2.8) to (2.9). However, it is important to highlight that the difference between the influent and effluent COD concentrations (COD_{in} and COD_{out}, respectively) may not reflect the actual COD removed from the wastewater, because organic substances can accumulate (and/or decay) in the anaerobic reactor (e.g. solids

retention).

$$\dot{V}_{CH_4,max} = \dot{V}_{in} COD_{in} MY_{max} \tag{2.7}$$

Figure 2.9: COD balance for anaerobic digestion of vinasse (COD = 40 gO_2/m^3 and 0.05 $gSO_4{}^{2-}/gO_2$) at 35 °C, 1.01 bar, pH 7.0 and HRT= 5 d

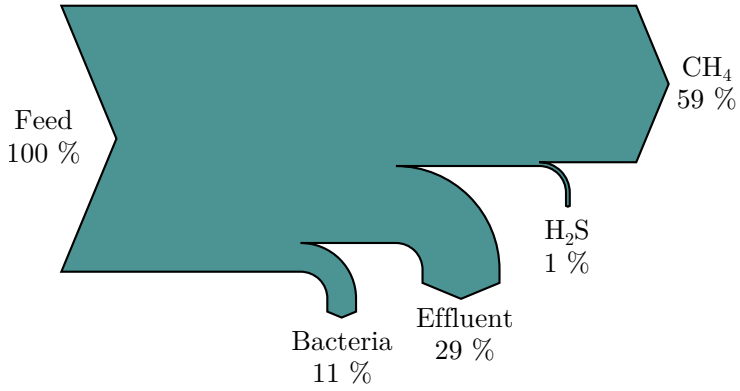

Source: [41]

$$MY = MY_{max} \eta_{COD} \tag{2.8}$$

$$\eta_{COD} = \left(\frac{COD_{in} - COD_{out}}{COD_{in}} \right) \tag{2.9}$$

Equations (2.7) to (2.9) are very useful because their variables are widely reported in the literature. However, the design and control of anaerobic digestion reactors often requires more information about the effect of the reactor dimensions and operational variables in the mass balance. In these cases it is possible to use a generic kinetic model to describe anaerobic digestion. The most widely accepted model is the Anaerobic Digestion Model N°1 (ADM1), which consists of 19 reactions (hydrolysis, acidogenesis, acetogenesis and methanogenesis) and 32 main variables [25]. Equations (2.10) to (2.13) exemplify the use of the ADM1 to model a perfectly mixed reactor, as illustrated in Figure 2.10, assuming liquid-gas phase equilibrium. Differently from conventional reactors, the balances and stoichiometric coefficients of ADM1 are written in COD basis for organic substances and the reaction rate is described by an Monod equation. In addition, inhibitions from pH, NH_3 and organic acids influence the reaction rate. Figure 2.11 illustrates the ADM1 results of methane production for the anaerobic digestion of sugarcane vinasse, a wastewater from ethanol distillation.

$$\frac{dZ_i}{dt} = (Z_{in,i} - Z_{liq,i}) \frac{\dot{V}_{liq}}{V_{liq}} - Z_{gas,i} \frac{\dot{V}_{gas}}{V_{gas}} + \sum_j \nu_{i,j} r_j \tag{2.10}$$

Figure 2.10: ADM1 model assuming perfectly mixed reactor

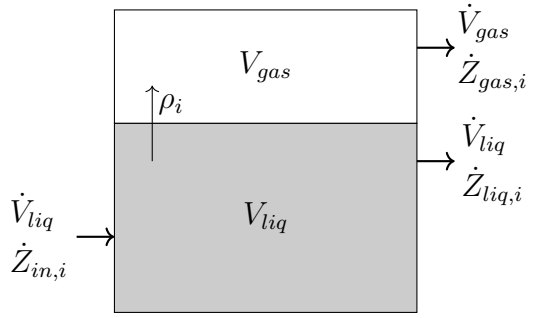

$$\dot{V}_{gas} = \frac{RTV_{liq}}{P - P_{H_2O}} \left(\frac{\rho_{H_2}}{16} + \frac{\rho_{CH_4}}{64} + \rho_{CO_2} \right) \tag{2.11}$$

$$\rho_i = k_L a \left(Z_i - K_{H,i} Z_{gas,i} RT \right) \text{ for i } \in \{H_2, CH_4, CO_2\} \tag{2.12}$$

$$r_j = \begin{cases} \mu_j Z_j^X & \text{for j } \in \text{ hydrolysis, decay and disintegration} \\ \mu_j \frac{Z_j^S}{K_{S,j} + Z_j^S} Z_j^X I_j & \text{otherwise (acid., acet. and methanogenesis)} \end{cases} \tag{2.13}$$

In which,

$Z_{in,i}$, $Z_{liq,i}$ and $Z_{gas,i}$: concentration of substance "i" in inlet, liquid outlet and gas outlet [kg of O_2/m^3 or kmol/m^3];

V_{liq} and V_{gas}: volume of the liquid and gas phases in the reactor [m^3];

$\nu_{i,j}$: calibrated coefficient for substance "i" and reaction "j" [-];

R: universal gas constant, 8.3145 [J/mol.K];

P and P_{H_2O}: total pressure and partial pressure of water [bar];

$k_L a$: coefficient of gas-liquid transfer (1/d);

$K_{H,i}$: Henry's law equilibrium constant for substance "i" in water (kmol/m^3.bar);

I_j: inhibition factor for reaction "j" [25].

The ADM1 can model the dynamic response of anaerobic digestion to feedstock variations, such as changes in flow rate, concentration, pH or temperature. Moreover, the composition of biogas and effluent can be estimated in detail (e.g., composition and concentration). However, this model approach requires calibration for each waste/wastewater, since there are a large number of model parameters. Calibrated model parameters and data to validate models may not be widely available in the literature.

Figure 2.11: Comparison between ADM1 and experimental results

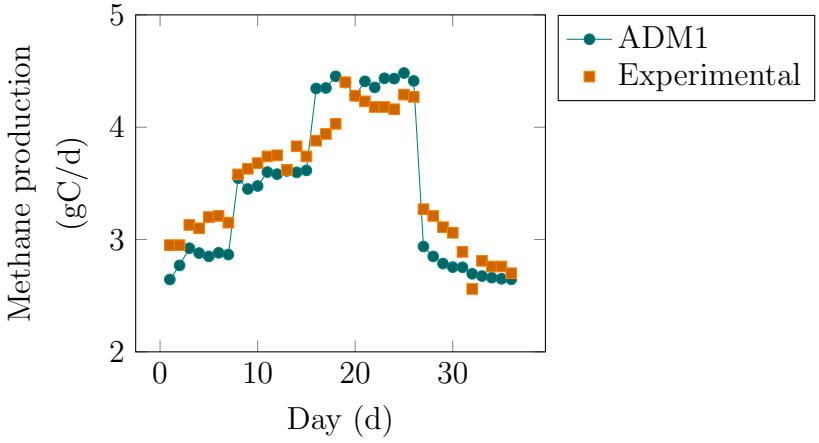

Source: [26, 41]

2.2.3 Process improvements

The most simple and effective optimization technique for methane production using anaerobic digestion is to control the quality of the feedstock. As it was exemplified in the previous sections, the feedstock composition determines the maximum methane production and its humidity is inversely proportional to the reactor productivity. For instance, increasing the concentration of organic substances or feedstock pretreatment can greatly improve the methane production of an anaerobic reactor, as previously shown in Fig. 2.4. In addition, maintaining a specific ratio of macronutrients (e.g., C, N, S, P) and avoiding inhibitory substances (e.g. NH_4^+, SO_4^{-2}, organic acids) or operational parameters (e.g., too low or too high temperature) are essential to maximize bacteria growth and, consequently, the reaction rate.

If the quality of the feedstock can not be improved, the anaerobic reactor size can be optimized to reduce methane production costs. High hydraulic retention times can improve the efficiency of methane conversion, but at a certain point this benefit is outweighed by the reactor costs, as in many other equipment. Figure 2.12 illustrates the impact of the hydraulic retention time in the electricity costs and exergy efficiency of a biogas plant, derived from the results of an ADM1 model [42]. As it can be observed, the minimal specific costs are close to the inflexion point in the methane yield, since after this point the changes in MY are relatively small. In practice, anaerobic reactors are usually oversized to favor stability of methane conversion, since feedstock quality or quantity can vary over time.

Another improvement opportunity is to recover or repurpose the effluent derived from anaerobic digestion, called digestate. Anaerobic digestion can not convert complex organic molecules which may represent a significant portion of the wastewater exergy. For

Figure 2.12: Effect of hydraulic retention time and concentration in methane specific cost

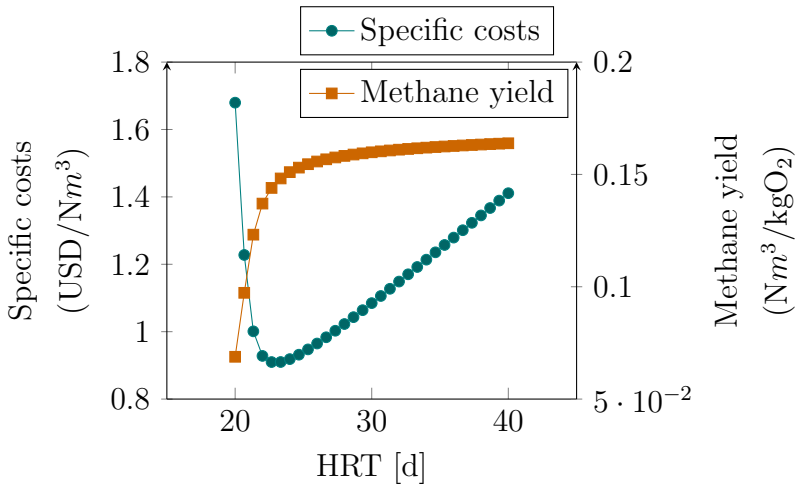

Source: [42]

example, Figure 2.13 shows the results observed by Nogueira Nakashima et al. [43] for the exergy balance of anaerobic digestion. In order to avoid losses, the anaerobic digestion can be operated in stages and the solid portion of the digestate can be separated and recycled.

Figure 2.13: Exergy balance for anaerobic digestion of vinasse (sugarcane ethanol wastewater)

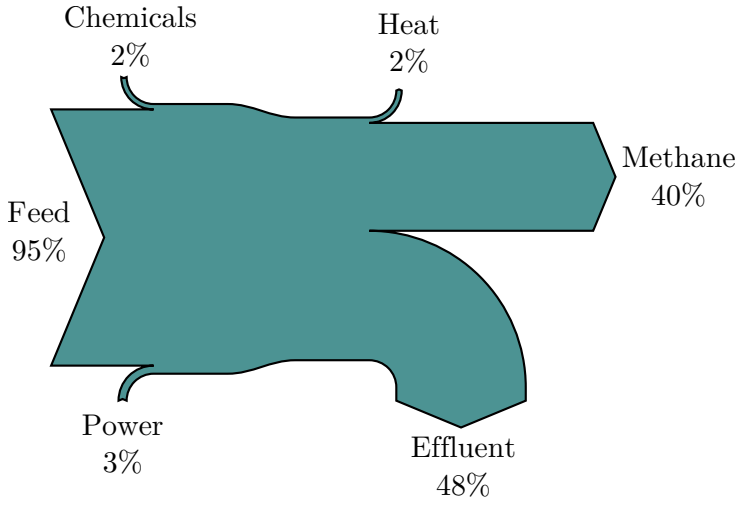

Source: [43]

Lastly, anaerobic digestion can also be integrated with other processes to improve heat management. In general, anaerobic digestion requires energy to operate at mild temperatures which has to be supplied from another process. Heat is usually supplied by the power conversion process through cogeneration, but other integrations with separation, hydrogen production or heat pumps are also possible [42]. Another type of process integration

is the inhibition of sulfur reduction by injecting small doses of oxygen in anaerobic digestion. This effectively reduces the production of H_2S and acts as a gross desulfurization process inside the anaerobic reactor [27].

2.2.4 Commercial process examples

There are several designs for anaerobic reactors with commercial application, which can be conveniently summarized in terms of some key characteristics [38]. These features are related to some characteristics of the feedstock (solids concentration and feeding frequency), the velocity of anaerobic digestion reactions (temperature, mixing and bacteria biomass retention) and the number of stages/phases of the process. An ideal process would be able to continuously convert a feedstock with high concentration of solids at elevated flow rates with high efficiency and stability. In practice, the anaerobic reactor design is strongly dependent on the solids concentration in the feedstock. Table 2.2 and Figure 2.14 show a brief summary and the schematics of the main characteristics of three very common anaerobic reactors: the continuously stirred tank reactor (CSTR), the upflow anaerobic sludge blanket (UASB) and the anaerobic lagoons.

Table 2.2: Main features of selected anaerobic reactors

Type	Total solids content % wet mass	Hydraulic retention time (days)	Relative costs
Upflow anaerobic sludge blanket (UASB)	<3%	0.1-5	+++
Continuous stirred tank reactor (CSTR)	3-20%	15-180	++
Anaerobic lagoons	0.5-5%	30-200	+

Source: [38, 31, 44]

2.3 Biogas conversion systems

Once produced, biogas can be converted into heat, power or energy carriers, such as methane and hydrogen. For each transformation route, the biogas composition has to comply with the technical and legislation limits. Figure 2.16 shows some possible scenarios for biogas conversion systems and required auxiliary processes. The optimal choice

Figure 2.14: Schematics of selected anaerobic reactors

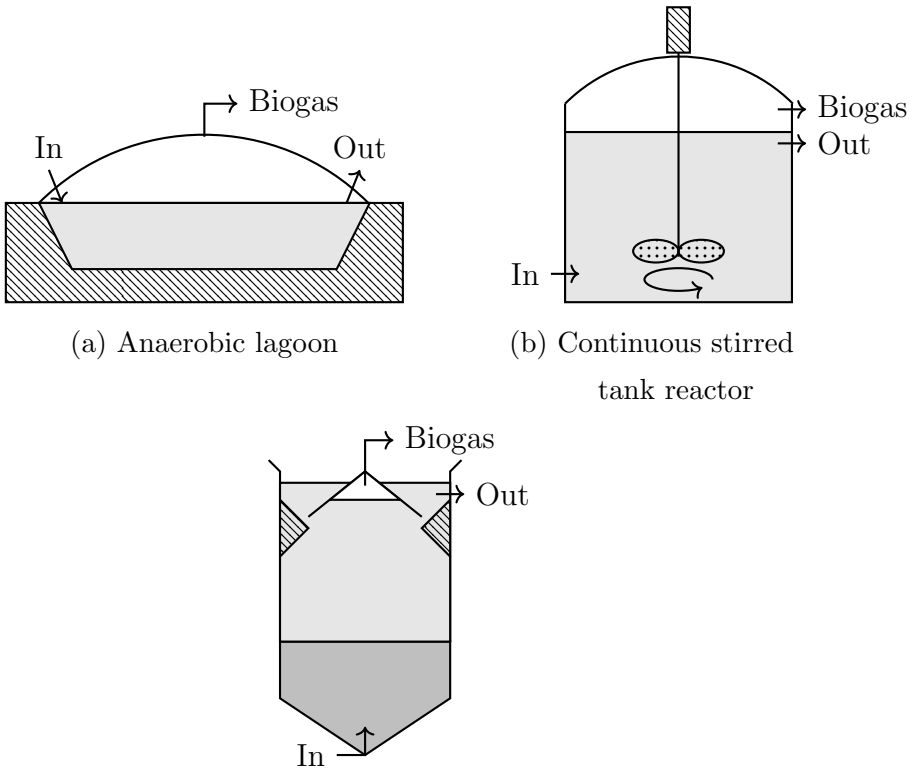

(a) Anaerobic lagoon

(b) Continuous stirred tank reactor

(c) Upflow anaerobic sludge blanket

Source: Author

of purification and conversion technologies is dependent on several factors related with biogas production (e.g., quantity, quality, variation). Moreover, cost, efficiency and environmental impact are likely to be conflicting objectives in the design optimization [43, 45].

Figure 2.16: Main conversion options for biogas

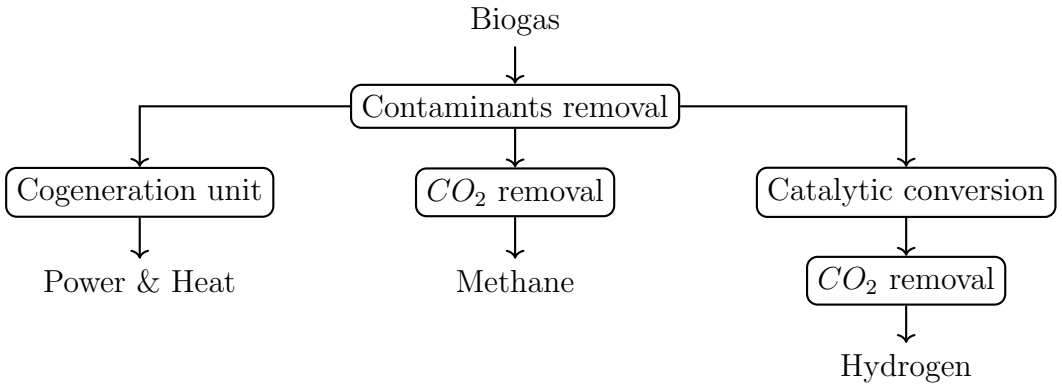

Source: Author

It is also important to highlight that, depending on the application, other energy sources

may be available (e.g., biomass, solar) or it may be required to provide energy for an auxiliary process (e.g., concentration, sanitation, refrigeration) [46]. In this way, there are several design solutions for biogas conversion and their optimization is an ongoing research topic. Nevertheless, there are some common features and limitations for most designs which are discussed in the following topics.

2.3.1 Biogas pretreatment

Since some substances may reduce the operational lifetime and efficiency of certain equipment, biogas requires a pretreatment process to reduce their concentration. The main impurities removed in this step are water, hydrogen sulfide and siloxanes. Other less common examples of harmful substances are ammonia, chlorofluorocarbons (CFCs) and volatile organic compounds (VOCs). Air and carbon dioxide can also be considered as impurities, but their removal is not strictly necessary in most cases, since their presence mainly affects the equipment efficiency. As it can be observed in Table 2.3, the inlet concentration of these impurities varies with the feedstock source. Moreover, higher operational temperatures can increase water and VOCs concentration in biogas, since the gas-liquid equilibrium pressure is directly proportional to temperature.

Table 2.3: Biogas concentration ranges for different feedstock sources

Feedstock	Landfill gas	Sewage	Agriculture	Industrial
CO_2 (mol%)	15-40	20-35	25-55	35-45
H_2O (mol%)	-	sat.	sat.	sat.
N_2 (mol%)	0-50	3.4	0-5	trace
O_2 (mol%)	0-10	0.5	0-2	trace
H_2S (mol%)	0-1	0-8	0.01-30	10-45
Siloxanes (mg/m^3)	0-50	0-5	trace	-
Ammonia (mg/m^3)	0-5	trace	0-2.5	-
CFCs (mg/m^3)	0-800	0	20-1000	-
Source	[47]	[28]	[28]	[48]

The selection of an adequate pretreatment technology depends on the average loading rate (concentration x biogas flow rate) of the impurity and the target outlet concentration. For instance, regenerative processes (e.g., physical and chemical absorption) are highly recommended for high loading rates of impurities to reduce operational costs with chemical inputs [48]. In the same line of reasoning, it is also common to combine two technologies, one for gross removal and another for fine removal, to achieve low concentrations of a certain impurity [47]. In general, the standard solution for biogas pretreatment is a

sequence of refrigeration and adsorption (activated carbon) processes [49]. An absorption separation system can be introduced in cases with high loading rate of impurities, such as industrial wastewaters, to reduce operational costs.

2.3.2 Cogeneration of heat and power

The cogeneration of heat and power (CHP) is the most common option for biogas conversion for energy purposes in Brazil [3]. The technologies available for CHP are not different from those applied for natural gas, but the equipment is adapted to operate with a safe level of carbon dioxide and contaminants (e.g., H_2S and siloxanes) . Among the main options for CHP, which are described in Table 2.4, the internal combustion engines (ICEs) and microturbines are the most consolidated technologies in biogas power plants. The first is able to reach relatively high efficiencies for power generation, while the second is more flexible for heat cogeneration and higher tolerance of sulfur concentration in the fuel [50].

Table 2.4: Summary of the main technologies for CHP from biogas

Characteristic	Gas engine	Micro-turbine	Fuel cells
Power range (kW)	80-2000	30-1000	100-3000
Power efficiency (%)	36-43	26-36	42-47
Equipment cost (USD_{2015}/kW)	938[a]	1455[b]	3200-6500[c]
Installation cost (USD_{2015}/kW)	662[a]	1069[b]	1500-1700[c]
Fixed operation and maintenance cost (USD/kW.y)	20.00[a]	18.22[b]	332.00[d]
Variable operation and maintenance cost (USD/kWh)	0.011[a]	0.014[b]	0.045[d]

[a] based on a commercial system of 300 kW; [b] based on a commercial system of 250 kW; [c] assumed 2500 USD/kW higher cost to operate on biogas than on hydrogen; [d] based on a commercial system of 200 kW;

Source: [51, 52, 9, 10, 11, 12, 13]

ICEs and microturbines are commercially available in a wide variety of sizes and their power generation efficiency tends to be higher for larger power generation units, as illustrated in Fig. 1.6. Furthermore, as many industrial equipment, microturbines and

ICEs also tend to have a lower specific cost ($ per installed kW) for larger units due to the economy of scale. However, the biomass readily available might not be sufficient to achieve the biogas production necessary for power generation at large scales. Thus, several opportunities for power generation from agriculture and domestic wastes may not be fully exploited due to their relatively small scale of biogas production. For instance, while the power generation capacity of microturbines can be relatively small, the total amount of fuel consumption is similar to gas engines because the efficiency is quite low. In addition, the low efficiency also diminishes the expected economic return from power generation.

In this context, fuel cells are foreseen as an interesting alternative for power generation due to its high efficiency and modular framework. Fuel cell systems can be dimensioned to specific biogas production flow rates, which maximizes the system availability and reduces fuel losses that otherwise would required to be flared. These advantages, modularity and high efficiency, could allow expand the number of distributed generation plants to lower installed capacities (<100 kW) and increase the economic return of biogas production. However, the capital cost of fuel cell systems is still substantially higher than conventional options, as it can be observed in Table 2.4. The reduction of production costs of fuel cells is an ongoing research target alongside with the increase of operating lifetime (since catalysts losses their activity with time). For instance, the 2020 technical targets of the US Department of Energy for fuel cells working with biogas is 1400 USD/kW [52], which are very close to costs for gas engines and micro-turbines. In addition, the effective use of fuel cells for biogas conversion will require significant research efforts to optimize fuel processing units and the energy integration of the co-generated heat.

Heat management for anaerobic digestion

Heat represents the majority of the energy available in CHP systems, therefore the proper utilization of this resource is crucial to achieve technical viability. Since anaerobic digestion is usually performed at temperatures above the environmental conditions, heat is necessary to maintain operational conditions. Fortunately, heat is required to keep devices at low temperatures (35-55 °C) allowing an easy integration of the waste heat from the CHP system. The reactor heat loss is dependent on its design (dimensions and materials), operational and environmental temperatures [29]. Thus, day-night cycles and climate seasons create a variable heat demand for anaerobic digestion that has to be well managed to avoid disturbances in the bacteria growth. Otherwise, a failure in the heat management could lead to a cascade effect by producing sub-optimal temperature conditions and, consequently, reducing biogas production and available heat. In rare cases, such as industrial wastewater, the effluent may be at high temperatures and only require

cooling for continuous operation [46].

It is important to highlight that, if heat has to be directed for anaerobic digestion to sustain a constant operation condition, in reality, only a portion of the available heat in CHP systems is a possible exportable product (e.g., for distributed heating, steam). Moreover, this fraction is higher for affluent wastes with high concentration of organic substances, since a higher specific production of methane (m^3CH_4 $/m^3$ of waste) can be achieved (as previously shown in Figure 2.4). Based on these factors, a higher concentration of degradable substances in the influent waste leads to more available heat and, consequently, to a more profitable biogas plant.

Energy integration with waste treatment

Apart from steam generation for distributed heating or other industrial processes, the cogenerated heat can also be used to improve the waste treatment. For example, heat can be used to reduce the water concentration of the effluent and sludge in order to reduce transportation costs of these residues [46]. Dried sludge can also be used as a biomass resource to provide extra heat or syngas, by using pyrolysis or gasification techniques [29]. Another option is to use steam in the pre-treatment of waste influent, increasing the hydrolysis rate and, consequently, the biogas production [27]. In this way, these practices can substantially increase the energy efficiency of the biogas plant and reduce the environmental impact of its byproducts (e.g., sludge, digestate). However, the systems can become quite complex and difficult to operate.

2.3.3 CO_2 separation

It is possible to produce a natural gas substitute from biogas, often called biomethane, by simply removing the CO_2 and other impurities. This process can achieve significantly high energy efficiencies ($> 90\%$) since it avoids methane combustion, one of the major sources of irreversibilities in CHP systems [43]. Although natural gas has a lower value specific value (\$/kWh) compared with electricity, the high efficiency of CO_2 separation makes this production route financially attractive. Biomethane also can be used as biofuel for transportation and a diesel fuel substitute, allowing to reduce fossil fuel dependency in the production chain of biofuels [45]. The composition requirements for biomethane may change depending on the local legislation, as it can be observed in Table 2.5 for the Brazilian context.

Differently from other renewable alternatives for natural gas, biomethane production does not rely on catalysts or chemical reactors such as methanation, gasification and pyrolysis. Furthermore, most purification processes have relatively low energy demands,

Table 2.5: Biomethane composition requirements in Brazil

		Region		
Characteristics	unit	North	Northeast	Other
Higher heating value	MJ/m^3	34-38.4	35-43	35-43
Wobbe index	MJ/m^3	40.5-45	46.5-53.5	46.5-53.5
CH_4 (min)	% mol	90	90	90
O_2 (max)	% mol	0.8	0.8	0.8
CO_2 (max)	% mol	3	3	3
CO_2+O_2+N_2 (max)	% mol	10	10	10
H_2S (max)	mg/m^3	10	10	10
S (max)	mg/m^3	70	70	70
H_2O dew point (max)	°C	-39	-39	-45
HC dew point (max)	°C	15	15	0

Source: [53]

which varies for each technology as it can be seen in Table 2.6 and 2.7. The design choice for biogas purification depends on several factors, such as production size, cost, contaminants tolerance, methane concentration and methane loss.

Table 2.6: Overview of the main CO_2 removal processes: scale, purity and losses

Technology	Scale (Nm^3_{biogas}/h)	Methane purity (vol. %)	Methane loss (%)
Pressure swing adsorption	>100	83 - 99	1.5 - 10
Water scrubber	250 - 660	96 - 99	0.5 - 2
Physical absorption	>100	93 - 99	1 - 4
Chemical absorption	>100	97 - 99	0.1
Membrane	>130	78 - 99	1 - 15
Cryogenic	161 - 600	>97	0.1 - 2

Source: [54, 55, 56]

The purification systems costs are heavily influenced by the production size of the biogas plant [55], therefore, biomethane production is generally considered only for large biogas production scales. Moreover, the operational costs can be diminished for biogas plants next to a natural gas infrastructure, by avoiding excessive transportation and storage costs. Although all available technologies are relatively efficient, the amount of methane lost slightly varies for each process and, therefore, the final biomethane production can

Table 2.7: Overview of the main CO_2 removal processes: demands and losses

Technology	Power demand (kWh/Nm^{3*})	Heat demand (kWh/Nm^{3*})	Capital cost (USD/kWh)	Operational costs (USD/kWh)
Pressure swing adsorption	0.16 - 0.35	0	332 - 1080	0.01-0.03
Water scrubber	0.20 - 0.30	0	761 - 950	-
Physical absorption	0.23 - 0.33	0.1 - 0.15	332 - 1260	0.01
Chemical absorption	0.06 - 0.17	0.4 - 0.8	343 - 569	0.01 - 0.02
Membrane	0.18 - 0.35	0	376 - 685	0.01 - 0.02
Cryogenic	0.18 - 0.25	0	512 - 1248	0.05 - 0.07

*Biogas flow rate

Source: [54, 55, 56]

be higher for certain options. It is important to highlight that some purification processes may require an additional step to achieve the natural gas specifications. For instance, biomethane requires a dehumidifier after the CO_2 removal in a water scrubber.

2.3.4 Hydrogen production

Molecular hydrogen is an important chemical input for the industrial sector that mainly relies on natural gas for its production. Moreover, this substance is a promising energy vector, since it has a high energy density (per mass) and could be produced from several substances that contain hydrogen atoms. Although there are several alternatives for hydrogen production, the main renewable options available are based on water electrolysis and biomass conversion. Since water electrolysis may only be justifiable as a form of energy storage for solar and wind energy, due to energy losses in hydrogen transformation and the carbon footprint of electricity, biomass conversion has a strategic advantage in this market field.

Hydrogen gas can be produced from biogas without requiring an upstream CO_2 removal process. In fact, carbon dioxide is a methane reforming agent and, therefore, its presence can be beneficial for the chemical reactions. Furthermore, hydrogen could also be produced in the solid oxide fuel cells operating with biogas, providing a valuable by-product [57]. Thus, biogas could potentially be an important source of renewable hydrogen, reducing CO_2 emissions and increasing operational revenues of anaerobic digestion plants [45]. However, the system would still require a downstream CO_2 removal process and, depending on the hydrogen molar fraction, the separation process may not achieve a high

efficiency.

3 Methane reforming and fuel cells fundamentals

The use of renewable energy sources for hydrogen production is an alternative to increase the efficiency of power generation and decarbonize the production of some important chemical products (e.g., methanol, ammonia, synthetic natural gas). Today, methane reforming is the main process for hydrogen production, which is mainly used in refineries and in ammonia production. However, in order to efficiently use hydrogen for power and heat cogeneration, the study and development of fuel cell systems is indispensable. Among the different types of fuel cells available, solid oxide fuel cells stand out by their high efficiency, fuel flexibility and cogeneration possibilities allowed by their high operational temperature. Thus, this chapter presents a brief introduction about the process of hydrogen production by methane reforming and the basics of fuel cell systems, with emphasis on solid oxide fuel cells.

3.1 Methane reforming

The methane reforming processes are classified based on the main reactants involved. Table 3.1 shows the usual name given for each reform process according to the main reacting species. The main products of methane reforming are hydrogen (H_2), carbon monoxide (CO) and carbon dioxide (CO_2). The gas produced in methane reforming, the synthesis gas (syngas), may also include water ($H_2O_{(v)}$) as well as the excess oxygen (O_2) and inert nitrogen gas (N_2), if air is supplied to reforming.

The main goal in methane reforming is to achieve a high conversion ratio of CH_4 and a high concentration of H_2 using the minimal amount of energy. Different conditions may be desirable for applications different from hydrogen production (e.g., ammonia or methanol production). The main design limitations for the process are related to the deactivation of catalysts (e.g., provoked by contaminations, soot formation or catalysts sintering) and the reactor cost, which is connected to the reaction rates and yields. Thus, as it may be expected, commercial applications of methane reforming tend to make design choices which would favor the aforementioned specifications under these constraints.

Table 3.1: Types of reforming processes and main reacting species

	Species			
Type	CH_4	CO_2	H_2O	O_2
Dry	X	X	-	-
Steam	X	X	X	-
Partial oxidation	X	X	-	X
Autothermal (Oxidative steam)	X	X	X	X

Source: Author

3.1.1 Chemical reactions

There is not an unique way to convey the reactions of methane reforming. One possible way is shown in the reactions R 3.1 to R 3.4.

$$CH_4 + H_2O_{(v)} \rightleftharpoons CO + 3\,H_2 \tag{R 3.1}$$

$$CO + H_2O_{(v)} \rightleftharpoons CO_2 + H_2 \tag{R 3.2}$$

$$CH_4 + 2\,O_2 \rightleftharpoons CO_2 + 2\,H_2O_{(v)} \tag{R 3.3}$$

$$2\,CO \rightleftharpoons CO_2 + C_{(s)} \tag{R 3.4}$$

Two or more of these reactions can be combined to represent a particular chemical process. For example, the dry reform reaction can be obtained by combining the steam reform (R 3.1 and water gas shift (R 3.2) reactions:

$$CH_4 + CO_2 \rightleftharpoons 2\,CO + 2\,H_2 \tag{R 3.5}$$

In addition, the partial oxidation reform can be described by combining the reactions R 3.1, R 3.2 and R 3.3:

$$CH_4 + \frac{1}{2}\,O_2 \rightleftharpoons CO + 2\,H_2 \tag{R 3.6}$$

Lastly, at high temperatures, methane decomposition into hydrogen and carbon (R 3.7) may be more predominant than the Boudouard reaction (R 3.4):

$$CH_4 \rightleftharpoons C_{(s)} + 2\,H_2 \tag{R 3.7}$$

Thus, the reactions (R 3.1-R 3.4) can be used to model the equilibrium composition of any reforming type shown in Table 3.1. The usual conditions of temperature and pressure for the reactions (R 3.1) to (R 3.4) are presented in Table 3.2.

Table 3.2: General technical conditions for methane reforming reactions

Reaction	ID	Starting temperature (°C)	End temperature (°C)	Reaction pressure (MPa)	ΔH_r (kJ/mol)
Steam methane reforming	R 3.1	500	870	2.0	234.66
Water gas shift (Low temperature)	R 3.2	220	250	2.0	-37.19
Water gas shift (High temperature)	R 3.2	350	420	2.0	-36.48
Methane oxidation	R 3.3	300	1400	0.1	-646.83
Boudouard reaction	R 3.4	-	-	-	-172.54
Methane decomposition	R 3.7	-	-	-	74.9

Source: [58]

In practical applications, steam methane reforming is the most common technique to produce hydrogen at large scales, since the theoretical yield of hydrogen per methane is the highest (4 H_2/CH_4). However, this reaction is highly endothermic (as shown in Table 3.2) and, therefore, requires the consumption of heat at high temperatures. In general, this energy is mostly supplied by the combustion of gases purged in the hydrogen purification. Nevertheless, this option requires an effective energy integration with other processes to avoid excessive consumptions of fuel in the reformer.

Partial oxidation uses low concentrations of oxygen to produce hydrogen in an exothermic reaction (as shown in Table 3.2). Some advantages of this process are: a simplified heat management, higher resistance to contaminants (e.g., sulfur and olefins), higher concentration of CO and the reduced dependency of catalysts [58]. However, the theoretical yield of hydrogen production is quite low (2 H_2/CH_4) and, therefore, partial oxidation is usually less attractive than steam reforming for hydrogen production. Moreover, the available heat energy has to be integrated with other processes to avoid excessive losses, since the reforming is exothermic, and the hydrogen purification process may be more complex [59]. For instance, if air is used as a reforming agent, nitrogen gas (N_2) can not be simply separated from the synthesis gas as steam can be by phase separation. In general, nitrogen is separated prior to the reforming in an air separation unit, which

increases the energy consumption in auxiliary processes.

A possible in between solution is the oxidative steam reforming, also called autothermal reforming, in which steam and oxygen are used as main reforming agents. In this process, the methane partial oxidation is able to supply energy for the steam reforming reaction to ideally achieve a thermoneutral global reaction. In practice, this point of operation is difficult to attain due to a number of uncertainties (e.g., heat losses, reaction kinetics, fuel composition) and the usual approach is to achieve an exothermic global reaction by providing an excess of oxygen (relative to the partial oxidation reaction) [58].

Lastly, another option is the dry reforming of methane, in which carbon dioxide could be used as the main reforming agent. This process can achieve high yield of hydrogen production with a low consumption of water, which could greatly benefit the energy balance of the overall process. However, the chemical equilibrium of a mixture of CH_4-CO_2 highly tends for soot formation in practical temperatures and reasonable concentrations of CO_2. This undesirable side product can rapidly deactivate catalysts and shorten the reformer lifetime, which turns the overall idea impractical. Several researchers have been trying to develop new catalysts which could resist soot formation, but commercial applications are scarce [60]. Some possible options for practical applications of dry reforming would be to include a carbon dioxide recycle or other reforming agents to reduce the possibility of soot formation. However, apart from cases in which carbon dioxide is already present in the fuel (e.g., biogas) the benefits provided by the insertion of carbon dioxide may not overcome disadvantages in hydrogen purification.

3.1.2 Catalysts contaminants

The methane steam reforming reactions require catalysts, often made of nickel oxides, to achieve practical conversion levels and manageable operational conditions [60]. Ideally, catalysts are required to have a high specific area, low pressure drop and high mechanical resistance, especially at high temperatures [58].

Catalysts efficiency can be negatively affected by excessive temperatures and contaminants. High temperatures can reduce the active area of the catalyst by causing the sintering of the material. On the other hand, catalysts contaminants can be derived from the feedstock, such as sulfur, olefins, halogen compounds and heavy metals, or produced during the reforming reactions, as in the case of soot. Among these contaminants, sulfur concentration and soot formation are the most reported sources of catalyst deactivation in hydrogen production using natural gas. For instance, concentrations as low as 0.1 ppm can form a deactivating layer in steam reforming reactors [58].

The contaminants derived from the feedstock are separated or eliminated prior to the reforming reactions, similarly as done for other energy conversion purposes (e.g., adsorp-

tion and absorption separation). For example, since methane reforming has a very strict limit for sulfur concentration, natural gas is reacted with hydrogen to convert S to H_2S, which is removed by reacting with zinc oxide at 350-400 °C to form zinc sulfide [60]. On the other hand, changing operational temperature and reactants composition are the main design choices to avoid soot formation in methane reforming. In general, chemical equilibrium estimates are used to define operational regions in which carbon formation is unlikely to occur [61]. For instance, Figure 3.1 illustrates the influence of temperature in the equilibrium constant of the two important reactions of soot formation. It can be observed that the usual temperature range of steam reforming, 500-870°C (Table 3.2), is also the less favorable range for soot formation.

Figure 3.1: $ln(K^0_{eq})$ for carbon formation reactions

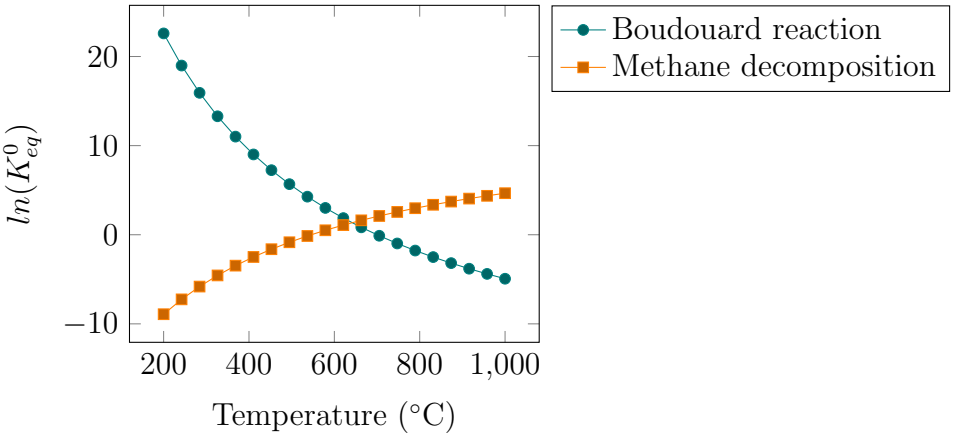

Source: Author

3.1.3 Chemical equilibrium

The design choices for methane reforming can be better understood by analyzing the equilibrium and kinetics of the involved reactions (R 3.1-R 3.4). The synthesis gas from commercial reformers and water shift reactors usually corresponds to the estimates from chemical equilibrium with a slight deviation in the equilibrium temperature (usually 5 to 20 K lower than the final temperature) [58]. Thus, the chemical equilibrium of R 3.1-R 3.4 can be used to derive insights about the influence of operational conditions in the efficiency of methane reforming.

Figure 3.2 shows the natural logarithm of the equilibrium constant at the reference pressure (100 kPa) for different methane reforming reactions and temperature. It can be observed that steam methane and dry reforming is more favorable ($ln(K_{eq}) > 1$) at high temperatures (above 650-670 °C) while water gas shift has an opposite trend. On the other hand, the partial oxidation is a highly active reaction for the temperature range of

200-1000 °C.

Figure 3.2: $ln(K^0_{eq})$ for methane reforming reactions

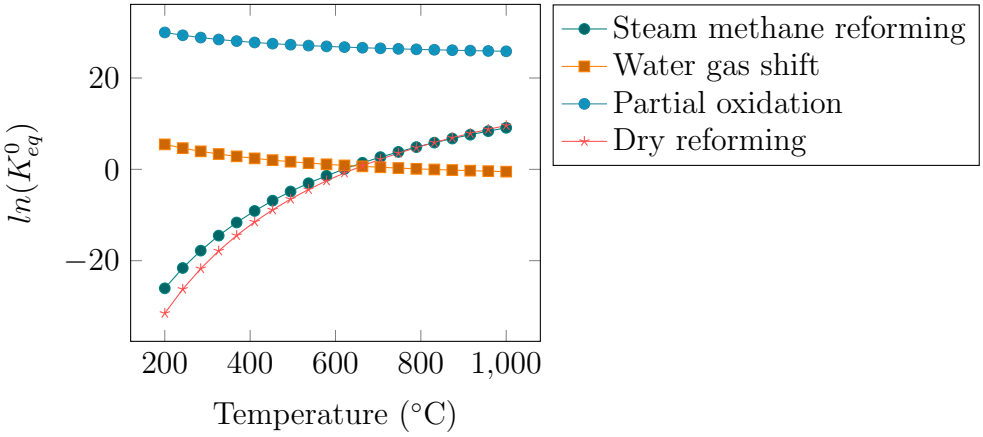

Source: Author

As it can be deduced from the chemical equilibrium condition (Eq. 3.1), the hydrogen concentration is affected by the equilibrium constant ($K_r|_{T,P_0}$), the molar concentration of other species (x_j and x_i) and operational pressure (P), depending on the stoichiometric coefficients (ν_i and ν_j). In general, the process is divided into at least two steps with different temperature levels to optimize the hydrogen production from methane. High pressures affect negatively the hydrogen production, since the majority of reforming equations increases the number of moles in the mixture. However, most commercial plants operate at high pressures (1.5 to 3 MPa) due to synergies with hydrogen purification and storage, as well as increments in the reaction rate, which decreases the rector volume and leads to lower costs of production [60]. For instance, a pressure swing adsorption separation requires syngas at high pressures and compressing the fuel upstream requires less energy than compressing syngas, since the molar flow rate of the former is lower.

$$K_r|_{T,P_0} = \frac{\Pi_j^k x_j^{\nu_j}}{\Pi_i^k x_i^{\nu_i}} \left(\frac{P}{P_0}\right)^{\sum_j \nu_j - \sum_i \nu_i} \tag{3.1}$$

Another important variable that can be deduced from Eq. (3.1) is the water concentration, since it affects the equilibrium of steam methane reforming and it is required for water gas shift reaction. Moreover, by reducing the concentration of carbon monoxide, steam can also reduce the formation of soot. For example, Figure 3.3 depicts the minimal steam to carbon ratio for steam reforming considering only graphite form of carbon. Since whisker carbon can also be formed during the steam reforming, the actual minimal ratio of steam to carbon are slightly higher than those of Figure 3.3 [62]. Thus, methane reforming usually operates with steam to carbon ratios far superior than stoichiometric values (e.g., 2.5 to 6 in molar basis) [58]. The downside of high concentrations of wa-

ter is the increase in energy required to preheat the reactants and to sustain the steam reforming reactions, which can reduce the overall efficiency of the system.

Figure 3.3: Minimal steam to carbon ratio to avoid carbon (graphite) formation

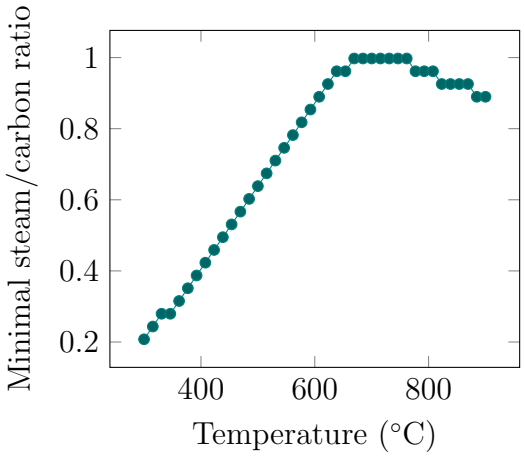

Source: Author

3.1.4 Commercial production systems

In general, as previously mentioned, hydrogen is obtained by converting natural gas using steam methane reforming. Figure 3.4 shows an example of a commercial scale plant for hydrogen production, which can be divided into four major steps: desulfurization, reforming, conditioning and hydrogen separation. In general, the overall process is able to produce 2.25-2.5 moles of H_2 per mole of CH_4 [58, 63].

Figure 3.4: Hydrogen production plant using steam reforming

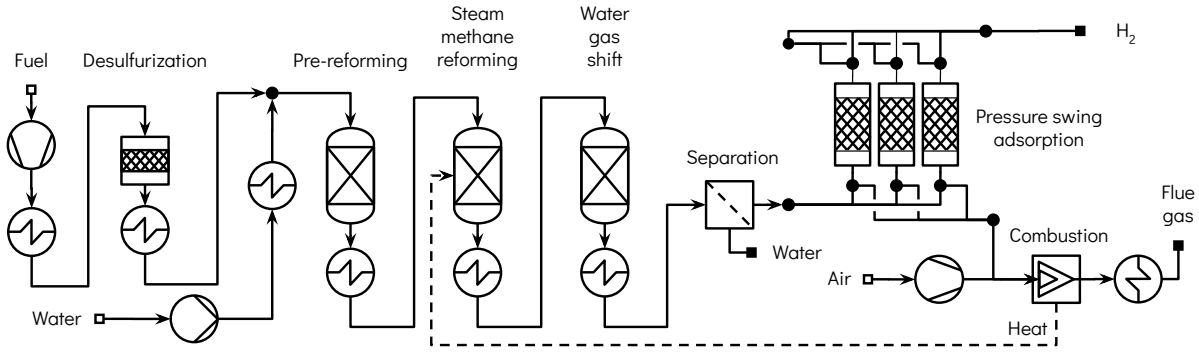

Source: [58, 64]

In the desulfurization process, sulfur components are removed by reacting it with zinc oxide at 350-400 °C to form zinc sulfide and avoid catalyst poisoning ($<$ 0.1 ppm of sulfur) [60]. In cases in which sulfur is bounded with organic molecules, a pre-step of

hydrogenation (reacting with hydrogen gas) can be performed to convert organic derived sulfur into hydrogen sulfide, which can be separated in the zinc oxide beds. Next, steam is added to natural gas according to the concentration of carbon (e.g., 2 to 6 molar ratio of steam to carbon) and the reforming process occurs in two steps: a pre-reforming and the main reformer [58]. Pre-reforming consists in a reforming process at relatively low temperatures (below 700 °C) and generally without external heat supply, which allows the selective conversion of higher hydrocarbons and, thus, reduces the chances of soot formation and abrupt temperature differences in the main reformer. Moreover, the absence of higher hydrocarbons also reduces the risk of steam cracking (which occurs in steam-natural gas mixtures above 550 °C), allowing the reactants mixture to be preheated to higher temperatures (e.g., 650 °C) [60].

The main reformer usually consists in several rows of tubes impregnated with catalysts that receive heat from the combustion of purge gases from hydrogen separation. The syngas mixture leaves the reformer at high temperatures and with composition close to the chemical equilibrium for 5-20 °C below the actual temperature [58]. Since the concentration of carbon monoxide in syngas is high, which is undesirable for hydrogen production, the mixture is conditioned using the water gas shift reaction. The current standard process uses only one reactor at relatively high temperatures for this reaction (350-450 °C) without heat supply, but older designs also use a second reactor at lower temperature levels (220-250 °C) [58]. Finally, after these processes, the water vapor is condensed and hydrogen is separated using a pressure swing adsorption system. This process is largely employed because it can achieve high purities of hydrogen and benefits from the high pressure of hydrogen, which is usually required for its end-use. Hydrogen recovery efficiency is usually between 72-78% for PSA systems, but this value can vary depending on the initial concentration of hydrogen and the pressure difference [65].

3.2 Fuel cell systems

A fuel cell is an equipment able to convert chemical energy into electrical energy in a continuous and direct way by consuming a certain fuel (usually hydrogen). The reduction of conversion steps allows fuel cells to achieve higher efficiencies than traditional engines, while the fuel supply enables continuous operation, differently from batteries.

A fuel cell is mainly composed of two electrodes with catalyst deposits, one electrolyte and some interconnections as illustrated in the Fig. 3.5. The fuel and oxygen are physically separated and react in certain regions where electrodes, catalyst and electrolyte are connected, the triple phase region. This process generates an electrical potential difference, which causes ions to pass through the electrolyte from one electrode to another,

while electrons are forced to move by the interconnections generating an electrical current. Since the voltage provided by a single cell is insufficient to drive an equipment (< 1V), several cells are arranged in series (a stack) using interconnectors to deliver high voltage differences. In this way, the fuel cell is able to supply electrical power in an efficient process.

Figure 3.5: Components of a single planar cell with solid electrolyte

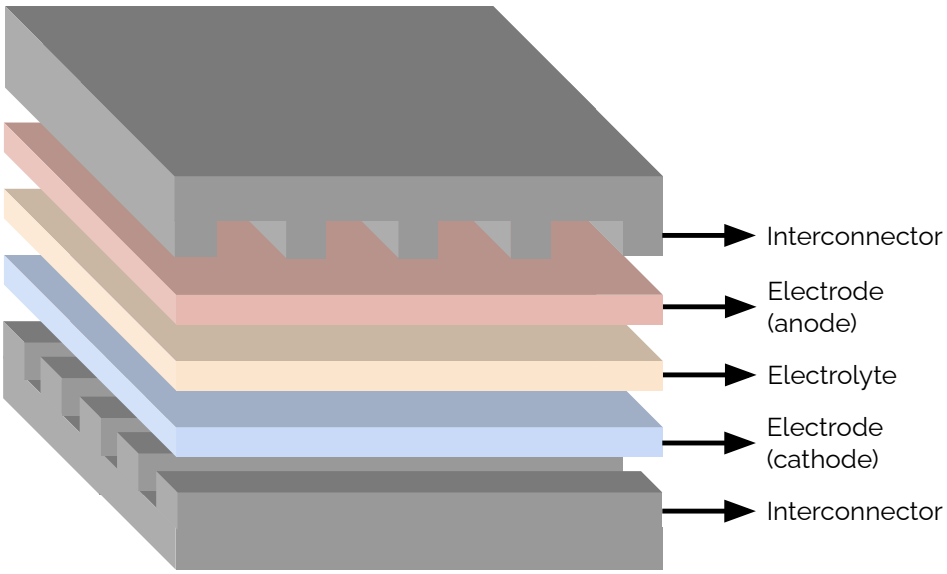

Source: [66, 67]

The maximum electrical efficiency of a fuel cell ($\eta_{FC,max}$) can be estimated by the Gibbs free energy of reaction ($\Delta G_r\big|_{T,P}$) and the enthalpy of reaction ($\Delta H_r\big|_{T,P}$), as described in Eq. (3.2) and illustrated in Fig. 3.6. As it can be observed, the efficiency of fuel cells are far superior than Carnot engines for relatively low temperatures and this theoretical advantage decreases at high temperatures. In practice the electrical efficiency is determined indirectly by measuring the voltage provided by a fuel cell (E) at certain current densities (j), since these parameters are related with the specific power (w) delivered by the cell (Eq. 3.3).

$$\eta_{FC,max} = \frac{\Delta G_r\big|_{T,P}}{\Delta H_r\big|_{T,P}} \tag{3.2}$$

$$w = Ej \tag{3.3}$$

The ideal voltage provided by a hydrogen fuel cell (E^0) can also be estimated by the Gibbs free energy of reaction ($\Delta G_r\big|_{T,P}$) and Faraday constant (F) by Eq. (3.4). However, in real applications, the voltage provided by a fuel cell is dependent on the current density, as illustrated in Fig. 3.7, since this variable is related with the rate of reactions occurring

Figure 3.6: Ideal efficiency of fuel cells vs. Carnot efficiency for different temperatures

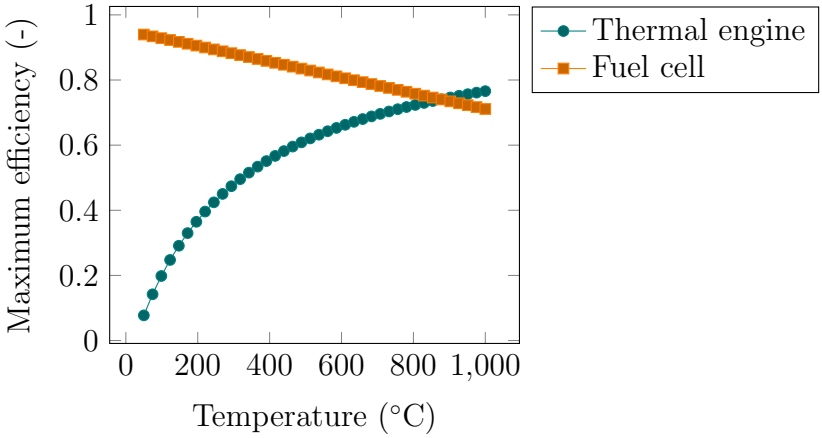

Source: Author

in the electrodes (charge and ion transfer rate). It is common to categorize the effects of current density in three types (overvoltages): activation, ohmic and concentration.

$$E^0 = \frac{\Delta G_r|_{T,P}}{2F} \tag{3.4}$$

Figure 3.7: Experimental voltage and power density of a PEM fuel cell (80°C, 1 atm, 20% wt. Pt/C)

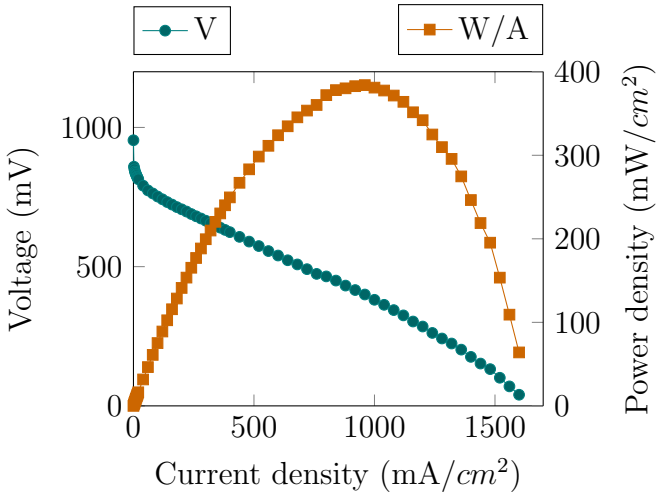

Source: Author

The activation overvoltage (η_{act}) describes the voltage losses due to the activation energy of the reactions occurring in each electrode. This irreversibility is predominant for low current densities and it is related with the effectiveness of catalysts and the reaction mechanism. The activation overvoltage can be described by the Butler-Volmer equation (Eq. 3.5), which can be simplified for special cases as described in Eq. (3.6) [66]. Different

representations of the Butler-Volmer equation have been reported by a number of authors, since the values can alter depending on the materials and reactions involved [68].

$$j = j_0^0 \left[\frac{c_r}{c_r^0} \exp\left(\alpha \frac{2F}{RT} \eta_{act} \right) - \frac{c_p}{c_p^0} \exp\left((\alpha - 1) \frac{2F}{RT} \eta_{act} \right) \right] \tag{3.5}$$

Where,

j_0^0: exchange current density at a "standard concentration" [A/m^2];

c_r and c_p: actual surface concentration of reactants and products [mol/m^2];

c_r^0 and c_p^0: reference surface concentration of reactants and products [mol/m^2];

α and η_{act}: transfer coefficient [-] and activation overpotential [V].

$$j \approx \begin{cases} j_0 \frac{2F}{RT} \eta_{act} & \text{for j } << j_0 \\ j_0 \exp\left(\alpha \frac{2F}{RT} \eta_{act} \right) & \text{for j } >> j_0 \end{cases} \tag{3.6}$$

Next, the ohmic overvoltage (η_{ohm}) comprises the heat produced by the charge transfer in the electrolyte and interconnectors, which can be estimated by the Ohm's laws as described in Eq. (3.7). The resistance (R) can be estimated from the conductivity (σ) and thickness (l) of the materials or experimentally measured, Eq. (3.8), while the active area of the cell (A) is usually known from manufacturing.

$$\eta_{ohm} = (jA)R \tag{3.7}$$

$$R = \frac{l}{\sigma} \tag{3.8}$$

The concentration overpotential (η_{conc}) is related with the lower concentration of reactants in the triple phase region, where the reaction actually happens, compared with inlet streams. These differences arise from the mass transfer (convection in feeding channels and diffusion in electrodes) and reactant consumption across the fuel cell. For instance, at high current densities, the consumption of reactants demanded by the fuel cell can surpass the mass transfer rate and cause the "starvation" of the cell, halting the operation. The concentration of reactants impact on the Gibbs free energy of reaction (often called Nernstian effects) and the exchange current density in the Butler-Volmer equation, thus altering the activation overvoltage. The concentration overvoltage can be estimated by analyzing the mass transfer of reactants in the fuel cell or by observing the limit current density (j_L), as described in Eq. (3.9) [66].

$$\eta_{conc} = \frac{RT}{2F} \left(1 + \frac{1}{\alpha} \right) ln \left(\frac{j_L}{j_L - j} \right) \tag{3.9}$$

Thus, the operational voltage of a fuel cell can be estimated based on the theoretical maximum and accounting for activation, ohmic and concentration losses, as exemplified in Eq. (3.10). In practice, other types of minor losses could also occur, such as parasitic losses from fuel cross-over, unwanted side-reactions and failures in electric insulation [66, 67]. Moreover, catalyst efficiency also reduces with operational time, which impacts negatively in the overvoltage losses.

$$E = E_0 - \eta_{act} - \eta_{ohm} - \eta_{conc} \tag{3.10}$$

It is important to highlight that a high operational voltage is not sufficient to guarantee that the operation of a fuel cell is efficient, since only a portion of the fuel may be converted. In fuel cell systems it is common to use the fuel utilization efficiency (FU), as shown in Eq. (3.11), to describe the amount of fuel converted in the fuel cell ($\dot{n}_{fuel,consumed}$) compared with the total fuel available ($\dot{n}_{fuel,total}$) [69]. As it can be observed, this parameter is related with the size of the fuel cell (surface area) and operational parameters (e.g., current and fuel flow rate). A low fuel utilization efficiency may lead to great losses of unconverted fuel, while high values may reduce the concentration of H_2/CO and, consequently, reduce the conversion efficiency (concentration overvoltage). In general, for systems focused in producing electricity, it is advantageous to work with high fuel utilization efficiencies (e.g., 0.8 to 0.9).

$$FU = \frac{\dot{n}_{fuel,consumed}}{\dot{n}_{fuel,total}} \tag{3.11}$$

3.2.1 Fuel cell types and applications

There are several types of fuel cells which are usually divided by their range of operational temperature and by their electrolyte. The main types of fuel cells and their characteristics are shown in Table 3.3. As it can be seen in Table 3.3, the reactions promoted in each electrode and the ion exchanged through the electrolyte vary according to the type of fuel cell. Moreover, fuel cells operating at lower temperature levels can only operate with hydrogen (and in special cases, liquid alcohols), while high temperature fuel cells can use syngas derived from different hydrocarbon sources. Today, the most prominent fuel cells in the market are based on solid electrolytes, such as the proton exchange membrane fuel cell (PEMFC) and the solid oxide fuel cell (SOFC). The use of a solid electrolyte enables fuel cells to have simpler designs and operation, while achieving a high degree of reliability.

The PEMFC works at low temperatures and with pure hydrogen using noble catalysts (Pt) for transportation or portable equipment. This fuel cell was envisioned as an alter-

Table 3.3: Main characteristics of selected fuel cell types

Characteristic	Alkaline	Proton exchange membrane	Phosphoric acid	Molten carbonate	Solid oxide
Temperature	60-90 °C	50-90 °C	160-220 °C	620-660 °C	800-1000 °C
Fuel	H_2(pure)	H_2	H_2	CO and H_2	CO and H_2
Oxidant	O_2(pure)	Air/O_2(pure)	Air	Air	Air
Contaminants	CO, CO_2 and H_2O	S and CO (>10 ppm)	S (>0.5% and CO (>50 ppm)	S (>0.5 ppm)	S(>1.0 ppm)
Ion exchange	OH^-	H^+	H^+	$CO_3{}^{2-}$	O^{2-}
Internal reforming	No	No	No	Yes	Yes
Heat cogeneration	No	No	Yes	Yes	Yes
Electrolyte*	KOH_{aq} in a SiC matrix	Nafion	$H_3PO_{4(aq)}$	$Li_2CO_{3(l)}$ and $K_2CO_{3(l)}$ in a LiO-AlO2 matrix	Yttria-stabilized zirconia $ZrO_2(Y_2O_3)$
Electrodes*	Ni/C or Pt/C	Pt/C	Pt/C	Ni (anode) and NiO (cathode)	Ni-YSZ cermet (anode) and $SrLaMnO_3$ (cathode)
Interconnector*	Ni	Steel	C	Ni-Cr alloy	Cr alloys or cermet

Source: Adapted from [70, 66, 67]

native for internal combustion engines on utilitarian vehicles, since it could reduce local emissions and fuel consumption, but its adoption has been quite small compared with electric batteries. The lack of a dedicated hydrogen infrastructure, concerns with environmental sustainability and the high price of noble catalysts are significant barriers for

widespread adoption. On the other hand, SOFC are high temperature fuel cells dedicated for combined heat and power generation (CHP) that can use hydrogen or hydrocarbons (e.g. natural gas or biogas) as fuel. The high operating temperatures allows the use of ceramic materials as electrodes and electrolyte, enhances the contaminants tolerances and creates synergies with fuel reforming and cogeneration. However, conversion systems based on SOFCs are significantly more complex and require more auxiliary equipment and temperature resistant materials for interconnectors and sealing components.

Although SOFCs seem to address the major drawbacks of PEMFCs by working with less expensive materials and flexible options of fuel, their adoption also has been limited. Traditional CHP solutions, such as combined cycle power plants or diesel engines, can be highly efficient (40-50%) at large scale with lower investment costs, which undermines the potential advantages of fuel cells. Thus, SOFCs have been targeting problems in which conventional technologies are infeasible or inefficient, such as the micro-CHP market for domestic households and distributed power generation.

Recently fuel cells interest have resurged with the possibility of large scale production of hydrogen from renewable power for energy storage purposes [22]. In the long run this could provide sustainable and affordable fuel for CHP and heavy transportation (e.g., aviation, maritime and cargo) that would require efficient fuel cell systems. Moreover, the possibility of operating reversible fuel cells, which could act as electrolyzers for energy storage or fuel cells for energy supply, could lead to an increased adoption of this technology to promote smart grids. In summary, the expectations for the future of fuel cells systems are certainly lower than previous waves of enthusiasm, but the development path today seems clearer and attainable in a few years.

3.2.2 Solid oxide fuel cell systems

As previously mentioned, solid oxide fuel cells are strong competitors for micro-CHP due to their high efficiency compared with other established options. Figure 3.8 illustrates the main parts of a simple SOFC system and their interconnections.

The solid oxide fuel cells usually work with hydrocarbon mixtures such as natural gas or biogas, which require a purification step to remove possible contaminants (e.g., sulfur and siloxanes). Then, the fuel needs to be reformed into hydrogen and carbon monoxide to be converted into electricity in the fuel cell stack. This reforming process requires a reforming agent which can be supplied from the environment (e.g., air or water) or by recycling a portion of the exhaust gases from the fuel cell (which may contain water and carbon dioxide). Moreover, the reforming process demands a lot of heat energy at high temperatures (500-800 °C) which may be provided externally, indirectly or directly by the fuel cell.

Figure 3.8: Simplified flowsheet of a SOFC system

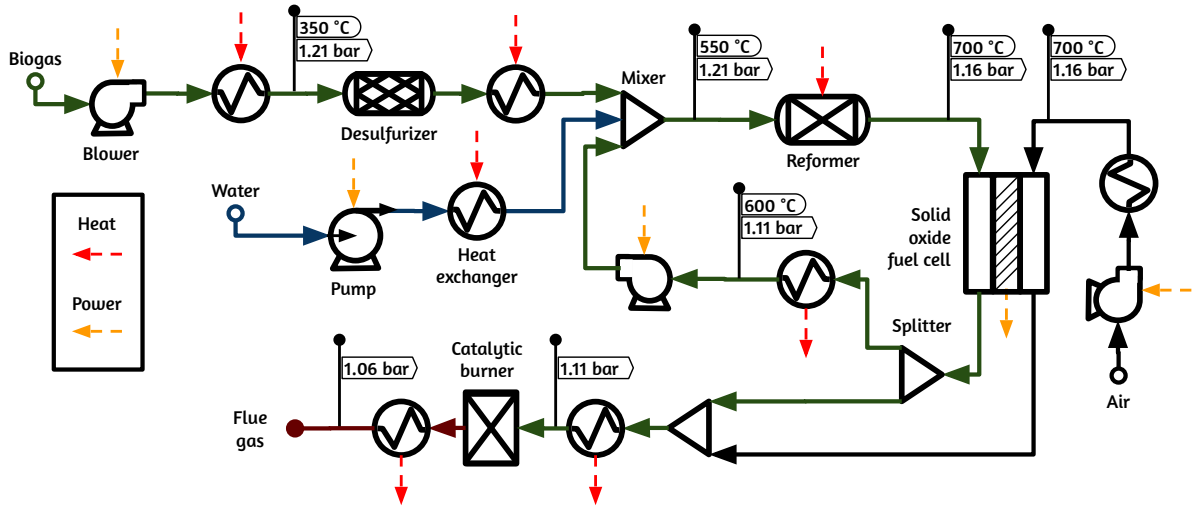

Source: [71]

A reforming process which operates externally to the fuel cell resembles the methane reforming for hydrogen production. The indirect option is to physically connect the fuel reformer with the fuel cell, allowing heat transfer between the two components. On the other hand, in the direct reforming the fuel oxidation and methane reforming occurs simultaneously in the fuel cell stack. The design choice of fuel reforming impacts on the number of equipment and the hydrogen concentration in the fuel cell stack. Today, the most advantageous option seems to use anode gas recycle and internal reforming (with a pre-reforming stage) to supply fuel for the fuel cell [72].

The unconverted portion of fuel is usually reacted with a portion of the depleted air to supply energy for other processes (e.g., reactants preheating or reforming) through heat. Since this process is highly irreversible and can impact negatively in the overall efficiency, different options have been proposed in several studies. The most common alternative is to recycle a portion of the anode exhaust gases to increase the fuel use ratio and facilitate the reforming process [72]. Other options include combining the fuel cell system with a gas turbine cycle or with a hydrogen purification unit [57, 73].

It is important to highlight that, apart from these main components illustrated in Fig. 3.8, a fuel cell system also requires an inverter and a control system. Although these equipment may have a limited influence in the system efficiency, the overall cost of a fuel cell can be greatly influenced by them [67].

4 Methods overview

The development of new processes for energy conversion requires the conception and evaluation of different design options in order to choose the best arrangement of variables (e.g., technologies, dimensions and operational variables) for a certain objective (e.g., economic, technical or environmental) respecting technical specifications.

Thus, several guidelines have been proposed to complete this task for specific types of processes, mostly based on heuristic knowledge. The main drawback of this approach is the need of human experience and conceptualization to design and optimize solutions, which significantly hinders the possibilities to apply mathematical optimization. On the other hand, computer algorithms can automate a number of important choices in process design, such as those regarding the heat exchanger network and utilities consumption. The use of these algorithms allows the engineer/researcher to focus only in the modelling aspects of the core process (e.g., chemical reactions, purification, pressure changes, etc.), while the plant design can be partly automated based on an optimization problem. In this chapter, the fundamentals of pinch technology, exergy method, economic analysis and optimization are presented. In this thesis, pinch technology and exergy analysis are the main techniques employed to design and evaluate energy conversion processes, therefore this chapter presents some fundamental concepts of these two methods.

4.1 Pinch technology

The design of efficient heat exchanger networks can reduce the excessive consumption of energy resources to produce power and biofuels. However, this design can be complex and counter-intuitive for systems with several flow streams. Thus, different methods have been developed to assist the design of heat exchanger networks, among which the pinch technology is one of the most referenced one [74].

In brief, the pinch technology method simplifies the heat network into a linear programming problem (LP) in order to determine the minimal energy requirement for the analyzed system. In general, pinch analysis is used to compare the minimal energy requirement with the energy consumption and utility system cost of existing designs. However, the principles of pinch analysis can also be used to size utility systems and process units in

order to maximize operating revenues. In addition, pinch analysis can also be used to derive possible heat networks following certain constrains (e.g., minimal number of units) and heuristic guidelines.

4.1.1 Minimal energy requirement

In a pinch problem, streams are the material flows that may be heated (cold streams) or cooled (hot streams) from its source temperature ($T_{s,i}$) to a target one ($T_{t,i}$). This temperature change is associated with a heat transfer ($\dot{Q}_i$) or a mean heat capacity is assumed (C_i). An important distinction of the pinch technology is that energy transfer is assumed as linearly proportional to temperature, as denoted in Eq. (4.1).

$$\dot{Q}_i = C_i \left(T_{t,i} - T_{s,i}\right) \tag{4.1}$$

If a heat transfer process can not be approximated by a linear function of temperature, a general workaround is to break it into multiple linear functions. For heat transfer processes with phase transitions ($\Delta T = 0$), it is usual to assume a small temperature difference (e.g., $T^s - T^t = 1$ K) to artificially create a function with temperature. For instance, the heating of water at 1 bar from 25 °C to 150 °C can not be represented by a single linear function since the process includes a phase transition, as depicted in Figure 4.12. However, it is possible to approximate the overall process as three subsequent transitions: 1) from 25 °C to saturated liquid, 2) from saturated liquid to saturated vapor, 3) from saturated vapor to 150 °C.

Figure 4.1: Temperature x Enthalpy diagram for heating water at 1 bar from 25 °C to 150 °C

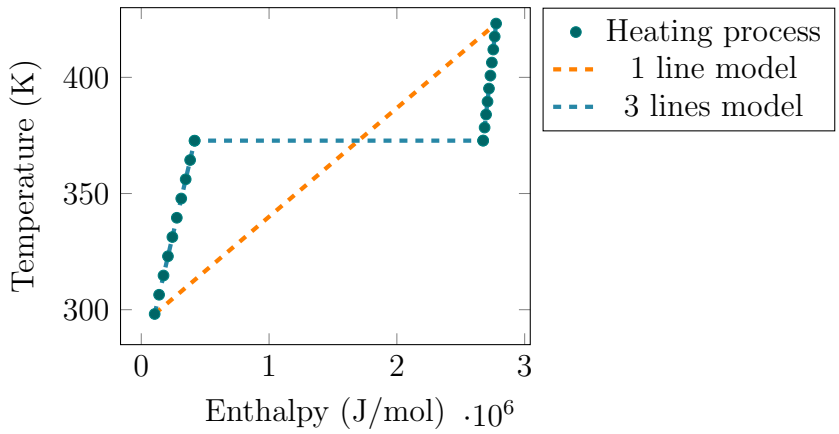

Source: Author

Similarly, the utility systems are also modelled as streams with a specific heat capacity (c_m^{ut}), target and source temperature ($T_{t,m}$ and $T_{s,m}$), Eq. (4.2). In this case, the energy

transferred ($\dot{Q}_m^{ut}$) or the mass flow rate ($\dot{m}_m$) is a variable to be optimized in the problem.

$$\dot{Q}_m^{ut} = \dot{m}_m^{ut} c_m^{ut} \left| T_{t,m} - T_{s,m} \right| \tag{4.2}$$

Another important parameter is the minimal temperature difference for heat exchange (ΔT_{min}), which may be assumed as equal for all streams (global). This parameter is usually a heuristic value based on previous designs of similar projects, but it may also be the result of an optimization study or technical constraint.

For instance, Figure 4.2 illustrates the influence of the logarithmic temperature difference (ΔT_{ln}) in the heat exchanger area (A) assuming an average coefficient of heat transfer (U), as described by Eq. (4.3). The value of ΔT_{min} has a similar effect in the heat exchanger area, an increment in this parameter tends to decrease the cost of heat exchangers. On the other hand, higher values of ΔT_{min} also reduce the amount of heat that can be exchanged between two streams, which may lead to higher consumption of utility systems (operating costs). As an example, Figure 4.3 illustrates the effect of the ΔT_{min} in the amount of heat transferred from a hot gas (200 kW, from 200 °C to 120 °C) to evaporate water (200 kW, at 100 °C). It can be observed that if minimal temperature difference is <20 °C the two streams can meet their cooling and heating demands, otherwise other streams/utilities will be required to design a working heat exchanger network.

Figure 4.2: Influence of the logarithmic temperature difference in the heat exchanger area (U = 1.1 kW/m^2.K, Q = 10 kW)

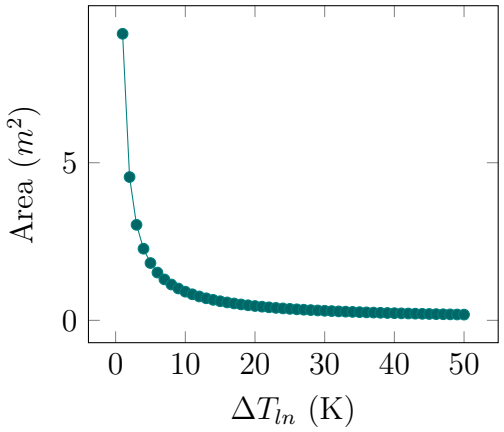

Source: Author

$$\dot{Q} = (UA)\Delta T_{ln} \tag{4.3}$$

Since heat can only be transferred from a higher temperature level to a lower one according to the second law of thermodynamics, the pinch method introduces the concept of heat cascade. In this model, the temperature range of heat transfer is divided into

Figure 4.3: Influence of ΔT_{min} in the heat transfer of two streams

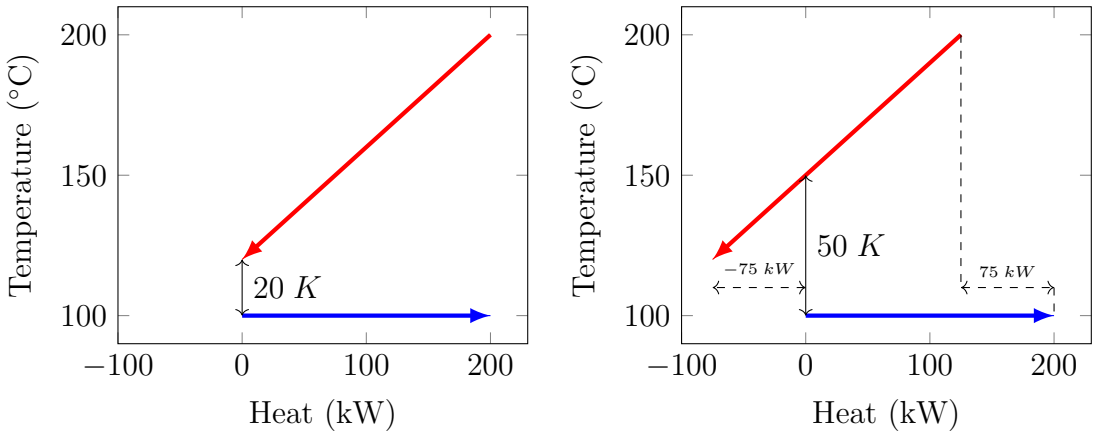

a)$\Delta T_{min} = 20\ K$ b)$\Delta T_{min} = 50\ K$

Source: Author

multiple intervals that are shifted proportionally to the ΔT_{min} and the stream type. This ensures that a hot stream can always transfer heat to a cold stream at a same temperature interval or below it. The specific method to determine the temperature intervals and the shift temperature ($T_{shifted}$) varies. For instance, the method proposed by Grimes [75] consists in the following steps:

1. Reduce the temperature of hot streams and utility systems by the minimal temperature difference for heat exchange.

$$T^{hot}_{shifted} = T^{hot} - \Delta T_{min}$$

$$T^{cold}_{shifted} = T^{cold}$$

2. List all temperature sources from all streams and utilities in decreasing order.

3. Create the temperature intervals from pairs of subsequent temperatures from the aforementioned list.

Figure 4.4 depicts the heat cascade for the examples in Figure 4.3 following the methods proposed by Grimes [75]. As it can observed, the heat cascade separate the streams into intervals where heat can be exchanged between: 1) hot stream in an interval “k” and any cold stream from an interval below it; or 2) a cold and hot stream from the same interval. Thus, the heat cascade allows to easily identify the heat transfers that are technically feasible under the constraint of minimal temperature difference. It is important to notice that the temperature target temperature for the cold stream in Fig. 4.4 is modelled as 101 °C in order to determine the heat cascade.

Figure 4.4: Heat cascade for examples in Figure 4.3

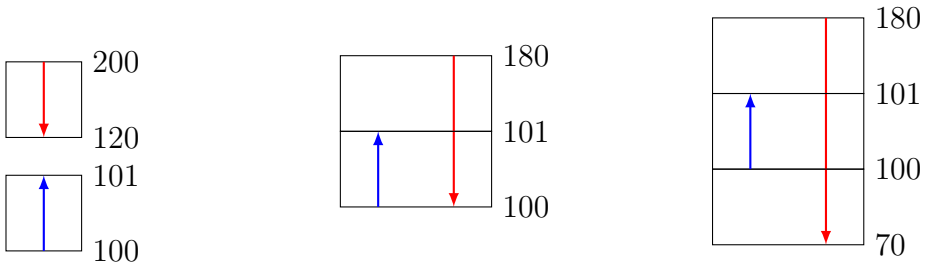

(a) Real temperatures

(b) Heat cascade $\Delta T_{min} = 20\ K$

(c) Heat cascade $\Delta T_{min} = 50\ K$

Source: Author

Each temperature interval of the heat cascade can be examined as a virtual thermodynamic system subjected to the principle of energy conservation, as depicted in Figure 4.5. in which R is the residual heat load from a temperature interval. Thus, the optimization problem to determine the minimal energy requirement can be described as the Eq. (4.4), subjected to the constraints of energy conservation, Eq. (4.5), and variable limits, Eqs. (4.6)-(4.9) [76]. Equation (4.9) derives from the fact that there is no temperature interval above the first one and the all heat demands should be fulfilled by the last temperature interval.

Figure 4.5: Virtual thermodynamic system of a temperature interval of the heat cascade

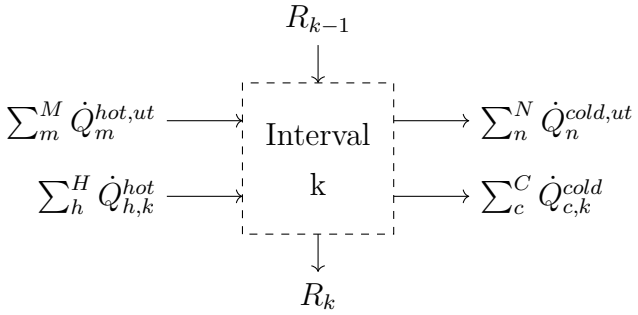

Source: [76]

$$\min_{\dot{m}_m^{hot,ut}, \dot{m}_n^{cold,ut}} \sum_m^M \sum_k^K \dot{Q}_{m,k}^{hot,ut} + \sum_n^N \sum_k^K \dot{Q}_{n,k}^{cold,ut} \tag{4.4}$$

Subjected to,

$$R_k - R_{k-1} - \sum_m^M \dot{Q}_{m,k}^{hot,ut} + \sum_n^N \dot{Q}_{n,k}^{cold,ut} = \sum_h^H \dot{Q}_{h,k}^{hot} - \sum_c^C \dot{Q}_{c,k}^{cold} \tag{4.5}$$

$$\dot{Q}_{m,k}^{hot,ut}, \dot{Q}_{n,k}^{cold,ut} \geq 0 \tag{4.6}$$

$$\dot{Q}_{h,k}^{hot}, \dot{Q}_{c,k}^{cold} \geq 0 \tag{4.7}$$

$$R_0 = R_K = 0 \tag{4.8}$$

$$R_k \geq 0 \tag{4.9}$$

Where,

$\dot{Q}_{m,k}^{hot,ut}$ and $\dot{Q}_{n.k}^{cold,ut}$: heat transfer rate from hot and cold utilities ("m" and "n") at temperature interval "k" [W];

$\dot{Q}_{h,k}^{hot}$ and $\dot{Q}_{c,k}^{cold}$: heat transfer rate from hot and cold streams ("h" and "c") at temperature interval "k" [W];

R_k: residual heat load from the temperature interval "k" [W].

As previously mentioned, Equation (4.4) can be rewritten in a cost basis by multiplying the energy consumption by their respective specific costs (c_m) as denoted in Eq. (4.10). The minimal energy requirement does not guarantee a design with maximum efficiency or minimal cost since it only minimizes the utilities consumption in energy basis. Specific costs can be used to change the objective function from energy basis to an exergy basis or economical basis in order to maximize efficiency or minimize costs, if necessary.

$$\min_{\dot{m}_m^{hot,ut}, \dot{m}_n^{cold,ut}} \sum_{m}^{M} c_m^{hot,ut} \dot{Q}_m^{hot,ut} + \sum_{n}^{N} c_n^{cold,ut} \dot{Q}_n^{cold,ut} \tag{4.10}$$

Determining $\dot{Q}_k$

The minimization of energy requirement demands the determination of the heat transfer available at each temperature interval ($\dot{Q}_k^{ut}$ e $\dot{Q}_k$), as denoted in Eq. (4.5). One may argue that this process is straightforward and, therefore, may be omitted from the explanation of the optimization problem. However, since this process is fundamental to the development of computer algorithms and this problem is rarely explained in literature, a brief exposition of a possible solution seems relevant.

For every temperature interval, it is necessary to determine if a specific stream or utility exchanges heat or not. The simplest way is to verify the if a stream or utility does not exchange heat at a particular temperature interval defined by pair of high and low

temperatures (T_k^{high} and T_k^{low}). This happens when both target and source temperatures (T_s and T_t) are mutually below or above the temperature interval. This condition can be expressed with logical operators as denoted in Eq. (4.11).

$$\left[(T_t \geq T_k^{high}) \wedge (T_s \geq T_k^{high})\right] \vee \left[(T_t \leq T_k^{low}) \wedge (T_s \leq T_k^{low})\right] \tag{4.11}$$

If the expression in Eq. (4.11) is false, than the stream or utility has some energy transfer at that particular temperature interval. In this case, there are four possibilities to how the stream/utility crosses the temperature interval, as depicted in Fig. 4.6, which determines the high and low temperatures of a stream "i" inside an interval "k" ($T_{i,k}^{high}$ and $T_{i,k}^{low}$). Equations 4.12-4.13 summarize the possibilities and how this affects the heat load.

Figure 4.6: Four possible interactions between streams and a temperature interval "k"

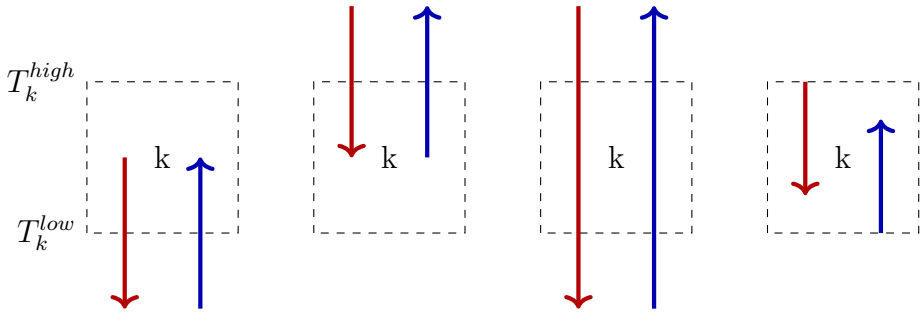

Source : Author

$$\dot{Q}_{k,i} = C_i(T_{i,k}^{high} - T_{i,k}^{low}) \tag{4.12}$$

$$T_{i,k}^{high} = \begin{cases} min(T_{s,i}, T_k^{high}) & \text{if it is hot stream/utility} \\ min(T_{t,i}, T_k^{high}) & \text{if it is cold stream/utility} \end{cases} \tag{4.13}$$

$$T_{i,k}^{low} = \begin{cases} max(T_{t,i}, T_k^{low}) & \text{if it is hot stream/utility} \\ max(T_{s,i}, T_k^{low}) & \text{if it is cold stream/utility} \end{cases} \tag{4.14}$$

4.1.2 Sizing utilities and process units

The mathematical framework presented in the previous subsection can be extended to determine the optimal size of utility and process units. This can be achieved by modelling these units as linear systems composed of streams (resources, products, heat and power) which share a common sizing factor. For instance, a simple gas burner can be modelled as two cold streams with a variable mass flow rate of fuel ($\dot{m}_{fuel}$), as described in Eq. (4.15)

for data presented in Table 4.1. In addition, power (W) and CO_2 emissions ($\dot{m}_{CO2}$) can also be assumed as linearly proportional to the mass flow rate of fuel (Eqs. 4.16 and 4.17)

Table 4.1: Streams of a simple gas burner

Description	w [kJ/kg_{fuel}]	c [kJ/kg.K]	T_s [°C]	T_t [°C]	γ_{CO2} [kg_{CO2}/kg_{fuel}]
Heating (radiation)	-	28.0	1001	1000	-
Heating (convection)	-	18.9	1000	160	-
Blower	28.2	-	-	-	-
Flue gases emission	-	-	-	-	2.74

$$\dot{Q}_i^{hot,burner} = \dot{m}_{fuel} c_i (T_{s,i} - T_{t,i}) \tag{4.15}$$

$$\dot{W}_i^{burner} = \dot{m}_{fuel} w \tag{4.16}$$

$$\dot{m}_{CO_2}^{burner} = \dot{m}_{fuel} \gamma_{CO_2}^{burner} \tag{4.17}$$

In some particular cases, the choice of the utility system can affect the process layout and alter the heat cascade. For example, Figure 4.7 illustrates a problem in which a finite biomass resource should be converted into hydrogen using gasification. The heat demands of the process plant should be supplied internally by the combustion of biomass or syngas. Since the amount of biomass available is constant, the choice of the furnace fuel can impact on the size of the gasification and/or hydrogen production units and, consequently, affects the heat cascade. Thus, the optimal solution that maximizes the production of hydrogen requires the design of the process layout and utility system together.

One possible solution for this type of problem is to separate the process plant into units that can be scaled linearly with the mass flow rate of the main resource [77]. This process is analogous to the definition of utility systems described previously, however in this case an additional linear constraint is needed to represent the mass balance of resources. Equations (4.18) to (4.21) exemplify this type of constraint for the problem illustrated in Figure 4.7. It is important to notice that the mass flow rate of products is proportional to the mass flow rate of resources by a certain factor (γ), since the system is assumed linear (Eq. 4.21). Once again, these additional linear constraints can be included in pinch

Figure 4.7: Example problem of a hydrogen production from biomass

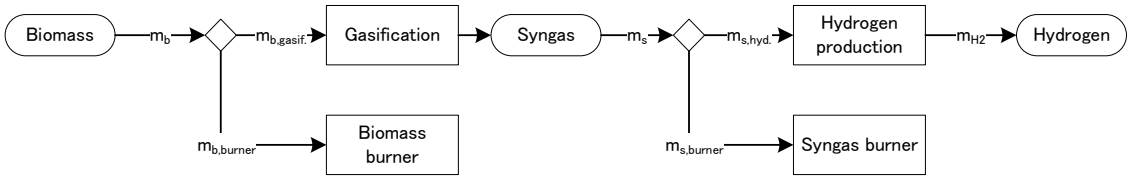

Source: Author

problem to determine the optimal sizes of the utility and process units (according to the mass flow rate of resources)

$$\dot{m}_{b,gasif.} + \dot{m}_{b,burner} = \dot{m}_b \tag{4.18}$$

$$\dot{m}_{s,hyd.} + \dot{m}_{b,burner} = \dot{m}_s \tag{4.19}$$

$$\dot{m}_s = \gamma_{gasif}\dot{m}_{b,gasif.} \tag{4.20}$$

$$\dot{m}_{H_2} = \gamma_{hyd.}\dot{m}_{s,hyd.} \tag{4.21}$$

In a general form, one can rewrite the heat cascade constraint derived from pinch principles (Eqs. 4.22 to 4.28) in order to include linear systems instead of just streams. As it can be observed, each linear system is associated with a scale factor (f^{ω}) that may represent the consumption of a certain resource.

$$R_k - R_{k-1} + \sum_{\omega_u}^{\Omega_u} f^{\omega_u}\dot{Q}_{k,0}^{\omega_u} = \sum_{\omega_p}^{\Omega_p} f^{\omega_p}\dot{Q}_{k,0}^{\omega_p} \tag{4.22}$$

$$\dot{Q}_{k,0}^{\omega_u} = \sum_{m}^{M_{\omega_u}} \dot{Q}_{m,k}^{cold,\omega_u} - \sum_{n}^{N_{\omega_u}} \dot{Q}_{n,k}^{hot,\omega_u} \tag{4.23}$$

$$\dot{Q}_{k,0}^{\omega_p} = \sum_{h}^{H_{\omega_p}} \dot{Q}_{h,k}^{hot,\omega_p} - \sum_{c}^{C_{\omega_p}} \dot{Q}_{c,k}^{cold,\omega_p} \tag{4.24}$$

$$\dot{Q}_{m,k}^{hot,\omega_u}, \dot{Q}_{n,k}^{cold,\omega_u} \geq 0 \tag{4.25}$$

$$\dot{Q}_{h,k}^{hot,\omega_p}, \dot{Q}_{c,k}^{cold,\omega_p} \geq 0 \tag{4.26}$$

$$R_0 = R_K = 0 \tag{4.27}$$

$$R_k \geq 0 \tag{4.28}$$

In which,

$\dot{Q}_{m,k}^{hot,\omega_u}$ and $\dot{Q}_{n.k}^{cold,\omega_u}$: reference heat transfer rate from hot and cold utilities ("m" and "n") at temperature interval "k" [W];

$\dot{Q}_{h,k}^{hot,\omega_p}$ and $\dot{Q}_{c,k}^{cold,\omega_p}$: reference heat transfer rate from hot and cold streams ("h" and "c") at temperature interval "k" [W];

$\dot{Q}_{k,0}^{\omega_u}$ and $\dot{Q}_{k,0}^{\omega_p}$: reference net heat transfer rate at temperature interval "k" for utility ω_u and process ω_p units [W];

R_k: residual heat load from the temperature interval "k" [W].

Each time that a resource and/or product is distributed along different processes and/or utilities a new linear constraint associated is created due to the principle of mass conservation. This type of constraint can be represented as exemplified in Equation (4.29). In addition, the mass flow rate of products is assumed to be linearly proportional to the mass flow rate of a resource ($\dot{m}_r^{\omega_i}$) or to a reference value ($\dot{m}_{p,0}^{\omega_i}$), as described by Eqs. (4.30) and (4.31). It is important to highlight that, if a resource is finite or a specific amount of products should be attained, an extra linear constraint needs to be included in the problem (e.g., $\sum_o^O f^{\omega_o}\dot{m}_o = cte.$). Common examples of these type of constraints are when biomass available is finite or when the overall system should not import power from the grid.

$$\sum_i^I f^{\omega_i}\dot{m}_i^{\omega_i} = \sum_o^O f^{\omega_o}\dot{m}_o^{\omega_o} \tag{4.29}$$

$$\dot{m}_p^{\omega_i} = \gamma_{p,r}^{\omega_i}\dot{m}_r^{\omega_i} \tag{4.30}$$

$$\dot{m}_p^{\omega_i} = f^{\omega_i}\dot{m}_{p,0}^{\omega_i} \tag{4.31}$$

In most cases, the objective function of this modified pinch problem can be described as the operating revenues. In other words, the difference between the costs of products and resources, as exemplified in Eq. (4.32).

$$\min_{f^{\omega_u}, f^{\omega_p}} \sum_r^R (c_r\dot{m}_r)_{resource} - \sum_p^P (c_p\dot{m}_p)_{product} \tag{4.32}$$

4.1.3 Minimal number of heat exchanger units

The minimal energy requirement does not provide the complete design of a heat exchange network. This process can be complicated and full of technical restrictions, such as cost, location, materials, etc. Thus, the ideal heat exchanger network is usually unattainable by automated procedures such as computer algorithms and math optimization. On the other hand, it is possible to determine optimal solutions for simplified versions of this complex problem. Among the different approaches is the minimization of heat transfer units, which aims to provide a workable solution with reduced costs by minimizing the number of equipment necessary in the network [74, 76]. Since the cost of a large equipment may be lower than two (or more) smaller equipment due to the economy of scale, this design approach may indirectly produce a heat exchanger network closer to the minimal cost.

The minimization of heat exchanger units uses the information given by the minimal energy requirement (MER) to produce an optimal solution. It is important to notice that the residual heat will be zero at a pinch point by definition. Moreover, if there is no heat transfer between two temperature intervals, then it is possible to separate the heat cascade into two independent subsystems.

The theoretical minimal number of heat exchangers for each closed subsystem (n_{min}) can be derived by the graph theory [74] as denoted by Eq. (4.33). In which the $n_{streams}$ is the number of streams and s is the number of separate components, which is usually equals one. Therefore, the minimal number of heat exchanger units is somewhat known, the problem itself is to determine which stream pairs that exchange heat.

$$n_{min} = n_{streams} - s \tag{4.33}$$

In order determine where the units will be placed, it is necessary to include a binary variable for each stream pair at each subsystem "l" ($y_{i,j,l}$), as expressed in Eq. (4.34). Thus, the objective function can be written as denoted in Eq. (4.35).

$$y_{i,j,l} = \begin{cases} 1 & \text{unit between i and j streams at subset l} \\ 0 & \text{no unit between i and j streams at subset l} \end{cases} \tag{4.34}$$

$$minimize \sum_{l} \sum_{i} \sum_{j} y_{i,j,l} \tag{4.35}$$

As in the minimal energy requirement, the major constraint to this optimization is the energy balance, but, differently from the previous case, the energy balance will be applied to each stream individually. Since there is not practical differentiation between streams and utilities in this problem, it is possible to create a new set of variables which

include streams and utilities for hots and cold types ($\bar{H}$ and $\bar{C}$). In addition, the heat transfered between each pair of streams at each temperature interval (k) can be described as "k" matrices of hot x cold streams ($\dot{Q}_{i,j,k}$). Thus, for hot streams/utilities, the energy balance can be described as presented in Eq. (4.36). The energy provided by a superior temperature interval ($R_{i,k-1}$) plus the energy available at the specific temperature interval ($\dot{Q}^{hot}_{i,k}$) should be equal to the energy provided for the cold streams ($\sum_j \dot{Q}_{i,j,k}$) plus the energy transferred for the inferior temperature interval ($R_{i,k}$). Figure 4.8 depicts the energy balance for a hot stream "i" at a particular temperature interval "k", as expressed in Eq. (4.36).

$$R_{i,k} + \sum_j \dot{Q}_{i,j,k} = \dot{Q}^{hot}_{i,k} + R_{i,k-1} \quad \forall i \in \bar{H}, k \in K \tag{4.36}$$

Figure 4.8: Energy balance of hot stream "i" at a temperature interval "k"

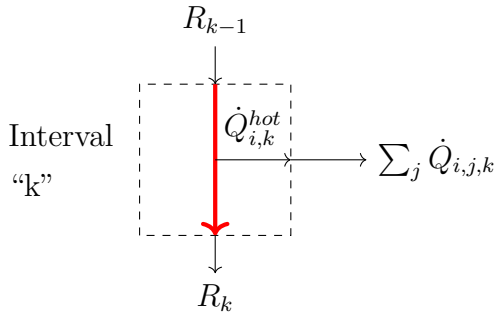

Source: Author

For cold streams, the sum of energy transferred for the cold stream $\sum_j Q_{i,j,k}$ should be equal to the energy required in the specific temperature interval $Q^{cold}_{j,k}$, as denoted in Eq. (4.37) and Figure 4.9. In addition, since the hot stream can not provide more energy than it has or that the cold stream can receive ($\dot{Q}^{max}_{i,j,l}$), this restriction should be included as Eq. (4.38)-(4.39) [78].

$$\sum_j \dot{Q}_{i,j,k} = \dot{Q}^{cold}_{j,k} \quad \forall j \in \bar{C}, k \in K \tag{4.37}$$

$$\sum_{k \in l} \dot{Q}_{i,j,k} \leq y_{i,j,l} \dot{Q}^{max}_{i,j,l} \quad \forall l \in L, \forall i \in \bar{H}, \forall j \in \bar{C} \tag{4.38}$$

$$\dot{Q}^{max}_{i,j,l} = min\left(\sum_{k \in l} \dot{Q}^{hot}_{i,k}, \sum_{k \in l} \dot{Q}^{cold}_{j,k}\right) \quad \forall l \in L \tag{4.39}$$

As previously discussed, R_k and R_{k-i} will be null at certain conditions, such as in the first or last temperature interval of each subsystem l of L. All variables are real positive numbers, except for the binary coefficient y.

Figure 4.9: Energy balance of cold stream "i" at a temperature interval "k"

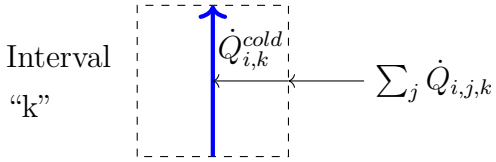

Source: Author

4.2 Exergy method

Exergy can be defined as "the work required to produce a material to its specific state from materials common in the environment in a reversible way, heat being exchanged only with the environment at temperature T_0" [79, 80]. Since this definition imposes a hypothetical reversible process, exergy can also be understood as the work obtained in a reversible process from a material at a specific state to the common materials in the environment, in which heat and mass are only exchanged with the environment at the reference temperature.

4.2.1 Evaluating exergy of a material stream

In general, for the processes studied in this thesis, it is usual to exclude nuclear, magnetic, electrical and interfacial effects in the calculation of exergy. Thus, the exergy of a certain stream ($\dot{B}$) may be expressed as a sum of kinetic ($\dot{B}^k$), potential ($\dot{B}^P$), physical ($\dot{B}^{ph}$) and chemical ($\dot{B}^{ch}$) components, as denoted in Eq. (4.40). Figure 4.10 depicts a diagram of the exergy components of a material at a specific state.

$$\dot{B} = \dot{B}^k + \dot{B}^p + \dot{B}^{ph} + \dot{B}^{ch} \tag{4.40}$$

Since kinetic and potential energies can be entirely converted into work in a reversible way, the kinetic and potential exergies are equal to the kinetic and potential energies, as shown in Eqs. (4.41) and (4.42) for a material point. The contribution of these exergy components for the total exergy is negligible for most chemical processes.

$$\dot{B}^k = \frac{\dot{m}v^2}{2} \tag{4.41}$$

$$\dot{B}^p = \dot{m}gz \tag{4.42}$$

Where,

g: gravitational acceleration, 9.81 [m/s^2];

v and z: velocity [m/s] and height relative to reference [m].

Figure 4.10: Exergy components of a material

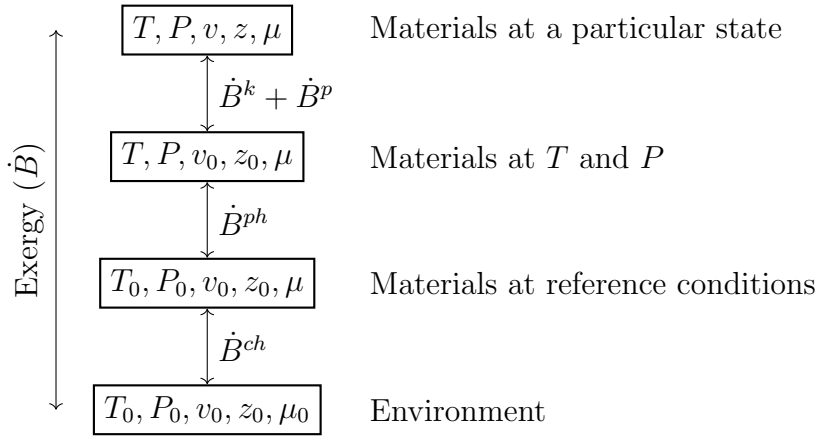

Source: Author

Physical exergy represents the work obtained in a reversible process from the material state (T,P) to the environment temperature and pressure (T_0,P_0), in which heat and mass can only be exchanged with the environment at reference temperature (T_0). The physical exergy of a stream can be determined using the energy and entropy balances for a reversible process, as denoted in Eq. (4.43) for a generic system.

$$\dot{B}^{ph} = \dot{H} - \dot{H}_0 - T_0(\dot{S} - \dot{S}_0) \tag{4.43}$$

In which,

$\dot{H}$ and $\dot{H}_0$: state and reference enthalpies flow rate [W];

$\dot{S}$ and $\dot{S}_0$: state and reference entropies flow rate [W/K].

Chemical exergy represents the work required in a reversible process to produce a material at the environmental temperature and pressure from the materials common in the environment, heat transfered only with the environment at T_0. Therefore, the chemical exergy requires the definition of a reference environment (species and concentrations) from which the exergy calculations will be based. The most widely accepted model of reference environment is the one proposed by Szargut, Morris and Steward (1987) [80] from which several tables of chemical exergy for pure substances are based. In general, these tabulated values compiled by key references [81, 82] are widely accepted in the scientific community to estimate the total exergy of a certain stream.

In special cases, the specific chemical exergy (b_i^{ch}) of a pure substance can be indirectly determined by analyzing a reversible reaction with other materials of known chemical exergy, as described in Eqs. (4.44)-(4.45) [83]. However, this method requires reliable

information about the substance composition and specific gibbs free energy ($g_i\big|_{T_0,P_0}$), which may not be available for biomass and other complex materials.

$$b^{ch} = -\Delta G_r\big|_{T_0,P_0} - \left[\sum_i \nu_i b_i^{ch}\right]_{co-reactants} + \left[\sum_j \nu_j b_j^{ch}\right]_{products} \tag{4.44}$$

$$\Delta G_r\big|_{T_0,P_0} = \left[\sum_j \nu_j g_j\big|_{T_0,P_0}\right]_{products} - \left[\sum_k \nu_k g_k\big|_{T_0,P_0}\right]_{reactants} \tag{4.45}$$

Another common method to estimate the chemical exergy is by using correlations with the elemental composition and lower heating value (LHV). Equations (4.46)-(4.47) exemplifies a method to estimate the chemical exergy of wood biomass (humid) [80].

$$b_{wood}^{ch} = \beta_{dry}\left(LHV_{humid} + h_{fg}^0 z_{water}\right) + (b_s^{ch} - LHV_s)z_s + b_{ash}^{ch} z_{ash} + b_w^{ch} z_w \tag{4.46}$$

$$\beta_{dry} = \frac{1.044 + 0.2160(\frac{z_{h2}}{z_c}) - 0.2499(\frac{z_{o2}}{z_c})\left[1 + 0.7884(\frac{z_{h2}}{z_c})\right] + 0.0493(\frac{z_{n2}}{z_c})}{1 - 0.3035(\frac{z_{o2}}{z_c})} \tag{4.47}$$

$$\frac{z_{o2}}{z_c} \leq 2.67 \tag{4.48}$$

Where,

LHV_{humid} and LHV_s: net heating value of humid biomass and sulfur [kJ/kg];

h_{fg}^0: specific enthalpy of water evaporation [kJ/kg];

z_{water}, z_s, z_{ash} and z_w: mass fractions of water, sulfur, ash and water;

z_{h2}, z_c and z_{n2}: mass fractions of H_2, C and N_2;

b_{wood}^{ch}, b_s^{ch}, b_{ash}^{ch} and b_w^{ch}: specific chemical exergy of wood, sulfur, ash and water [kJ/kg].

Lastly, the specific chemical exergy of a mixture can be calculated by using the Eq. (4.49) [83]. This equation can be derived from the reversible work required to compress each substance of a mixture from its partial pressure to the environmental reference P_0 [82].

$$b^{ch} = \sum_i b_i^{ch} + RT_0 \sum_i x_i \ln(y_i x_i) \tag{4.49}$$

Where,

b_i^{ch}: specific chemical exergy of substance "i" [J/mol];

y_i: activity coefficient [-];

x_i and R: molar fraction [-] and universal gas constant [J/mol.K].

Exergy method applied to anaerobic digestion

As previously discussed, the methane and biogas yield may be used to determine the potential for energy conversion of wastewater and organic residues. However, this assessment usually relies on experimental data and its connection with energy analysis may not be straightforward. For instance, a COD balance may convey the necessary information to analyze the treatment performance in an anaerobic reactor, but not so much for its impact on power generation.

In this context, it is convenient to express the processes of wastewater treatment and biogas conversion using a unique basis, such as exergy. Nonetheless, determining the chemical exergy of organic substances is a challenging task due to its variable composition. Moreover, the concentration of organic substances in wastewaters may be too small to obtain detailed information, such as elemental composition or concentration of components. Thus, researchers have been using indirect methods to correlate the chemical exergy of organic substances with the concentration of carbon or COD [84, 46]. These correlations have different shapes depending on the substances that it uses as basis.

A more general solution for this problem can be obtained by analyzing the correlation between the specific chemical exergy of organic groups, which were reported by Szargut [81], and their theoretical chemical oxygen demand. Figure 4.11 shows the correlation between these two variables using data from Szargut [81] and Eq. 4.50. In this chart, the organic groups with nitrogen are separated from others with carbon, oxygen, hydrogen and sulfur, since their correlation is quite different. Based on these results, it is reasonable to assume a linear correlation between specific chemical exergy and ThOD if the concentration of "organic nitrogen" is relatively low. It is important to notice that, differently from previous analysis [84, 46], the comparison shown in Figure 4.11 uses group contributions instead of substances, therefore the chemical exergy can be negative in some cases [81].

$$b^{ch} = 14.36 \cdot 10^3 \cdot ThOD \tag{4.50}$$

In which,

b^{ch}: Specific chemical exergy [J/mol]

ThOD: Theoretical chemical oxygen demand [gO_2/mol]

Figure 4.11: Correlation between ThOD and specific chemical exergy for organic groups

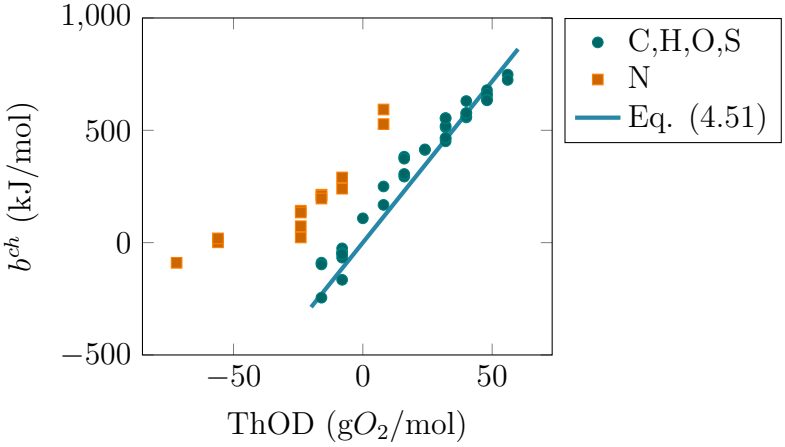

Source: Author

It is possible to estimate the chemical exergy of the wastewater using the Eq. (4.50) and assuming that the molar concentration of water is quite close to an unit ($x_{water} \rightarrow 1$). In this case, the chemical exergy of the wastewater mixture can be reduced to Eq. (4.51), since the term $xln(x)$ tends to zero for $x \rightarrow 1$ (water) and $x \rightarrow 0$ (other substances). Although a different correlation using quadratic polynomials or independent coefficients may reduce correlation error in Fig. 4.11, they can not be extended to Eq. (4.51) in the same manner as Eq. (4.50) [41]. Equation (4.51) provides a reasonable estimate for the chemical exergy of wastewater which is practical, since the necessary information is easily available, but should be used with caution. If detailed information about the wastewater is available, traditional methods for evaluating chemical exergy should be preferred.

$$\dot{B}^{ch}_{wastewater} \approx \dot{n}_{water} b^{ch}_{water} + \dot{V}(14.36 \cdot 10^3 \cdot COD_{total}) \cdot 10^3 + \sum_i \dot{n}_i b^{ch}_{i,inorganic} \qquad (4.51)$$

Where,

$\dot{B}^{ch}_{wastewater}$: chemical exergy flow rate of wastewater $[W]$;

$\dot{V}$: volumetric flow rate $[m^3/s]$;

COD_{total}: total chemical oxygen demand $[gO_2/l]$;

$\dot{n}_i$: molar flow rate of substance "i" [mol/s].

Figure 4.12 (left) exemplifies the accuracy of results from Eq. (4.51) assuming a flow rate of 1L/s of an ideal solution of water and acetic acid at different concentrations. As it can be observed, the results obtained from Eq. (4.51) are quite close to those obtained from the traditional method, but diverge for concentrations higher than 100 gO_2/l. On

the other hand, as it can be seen in Figure 4.12 (right), huge errors are obtained if the chemical exergy of the organic substance is neglected. Thus, the Eq. (4.51) may be used to estimate the exergy of wastewaters with COD concentrations below 100 gO_2/l and low nitrogen concentration in organic components.

Figure 4.12: Comparison of exergy rate results

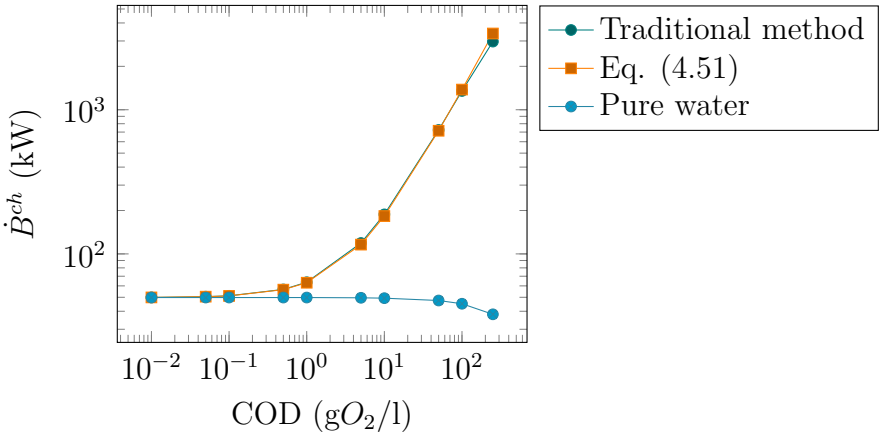

Source: Author

4.2.2 Exergy balance

Besides the value associated with material streams, exergy can also be transferred by heat or work. By definition, exergy associated with work ($\dot{B}_w$) and work ($\dot{W}$) are numerically equal, as denoted in Eq. (4.52), since one can be entirely converted into another (e.g., elevation of a weight). On the other hand, according to the second law of thermodynamics, the energy transfer associated with heat can only be partially converted into work and, consequently, exergy. Thus, the exergy transfer associated with a heat transfer ($\dot{B}_q$) can be calculated using Eq. (4.53), which can be derived from the energy and entropy balances of a reversible heat engine.

$$\dot{B}_w = \dot{W} \tag{4.52}$$

$$\dot{B}_q = \int \left(1 - \frac{T_0}{T}\right) d\dot{Q} \tag{4.53}$$

The exergy balance for an open system can be described as in Eq. (4.54). It is important to highlight that exergy is not a conservative quantity and, therefore, a sink variable called exergy destruction ($\dot{B}_{dest}$) is required to express the exergy balance as an equation. Exergy destruction is directly proportional to the entropy generation ($\dot{S}_{ger}$), as denoted by Eq. (4.55), and it can be understood as a measurement of the work potential lost due to

irreversible processes in the analyzed system. Therefore, this parameter can be used to pinpoint the equipment that incorporate the main inefficiencies of an overall system.

$$\frac{dB}{dt} = \sum \dot{B}_{o,out} - \sum \dot{B}_{i,in} + \dot{W} - \sum_{q} \left[\int \left(1 - \frac{T_0}{T_q} \right) d\dot{Q}_q \right] + \dot{B}_{dest} \tag{4.54}$$

$$\dot{B}_{dest} = T_0 \dot{S}_{ger} \tag{4.55}$$

Another important parameter in exergy analysis is the efficiency, which may have an specific definition for a particular process/equipment. A general definition of efficiency (η), often called "rational efficiency", is the ratio of exergy outputs by exergy inputs as shown in Eq. (4.56). However, this definition may not provide a meaningful parameter to evaluate and compare a particular process/equipment with others that share similarities. This discussion appears in a number of publications and several guidelines have been proposed to define efficiencies [85, 86].

$$\eta = \frac{\sum \text{exergy outputs}}{\sum \text{exergy inputs}} = 1 - \frac{B_{dest}}{\sum \text{exergy inputs}} \tag{4.56}$$

4.2.3 Exergy based costs

In the analysis of an industrial unit it is usual to express the costs (c) of a particular product in a certain basis. For instance, electricity costs are generally reported as USD/kWh, while hydrogen costs are presented as USD/kg or USD/kWh. Likewise, exergy can also be used as a common basis for electricity, heat, products and fuels. Equation (4.57) exemplifies a cost balance using exergy as a common basis, assuming that the equipment costs can be levelized ($C_{equipment}$) [83].

$$\sum_{i} c_i \dot{B}_{i,in} + \dot{C}_{equipment} = \sum_{o} c_o \dot{B}_{o,out} \tag{4.57}$$

As it may be deduced from Eq. (4.57), the exergy based costs are indeterminate for a system with multiple products, assuming that the costs of all inputs and equipment are known. There are two major guidelines to solve this problem: (i) assume that one or more output share the same costs that an input (ii) assume that the costs of one or more outputs are equal. These guidelines may be referenced as extraction and equality methods, respectively [87, 83]. In addition, the cost of outlet streams may be defined as zero if it can be considered as process loss. A complete explanation of the rationale of these assumptions can be consulted in Refs. [87, 83, 85].

In Equation (4.57), cost refers as the monetary value paid to produce/acquire a particular stream, work or heat. However, it is also possible to rewrite this equation defining cost

as the amount of emissions or exergy consumed to produce/acquire a particular material, work or heat [88, 89]. An advantage of this method is the possibility to encapsulate and reuse results of a particular production route in the form of cost. The results of exergy and emission costs of work, heat and chemical products can be used to evaluate the costs of other products.

4.3 Economic analysis

Investment costs can be estimated using correlations between equipment costs and its main characteristics (e.g., mass flow rate, size, temperature, pressure, etc.). Equation (4.58) describes a simple correlation between purchased equipment costs (PEC) and a specific characteristic dimension (S) based on reference values (PEC_0 and S_0). In general, the correlation presented in Eq. (4.58) is not linear ($\alpha \neq 1$) since the specific costs of an equipment tend to be lower for larger equipment (economy of scale). Moreover, the correlations are only valid for a specific time frame (usually a year) and, therefore, extrapolations for other periods have to consider the effects of economic inflation. The simplest approach is to use inflation indexes such as the Chemical Engineering Plant Cost Index (CEPCI)[90], as exemplified in Eq. (4.59).

$$PEC = PEC_0 \left(\frac{S}{S_0} \right)^{\alpha} \tag{4.58}$$

$$PEC_y = PEC_{y0} \left(\frac{CEPCI_y}{CEPCI_{y0}} \right) \tag{4.59}$$

In which,

PEC_y and PEC_{y0}: estimated equipment cost for year "y" and reference year "y0" [USD];

$CEPCI_y$ and $CEPCI_{y0}$: Chemical Engineering Plant Cost Index for year "y" and reference year "y0" [-].

The purchased cost of equipment is only a fraction of the total overnight cost (TOC) required to build and run a new facility. Additional investment costs can be attributed to installation, engineering procurement, construction labor and contingencies. Since these values are difficult to estimate for the preliminary design of production plants, usually the total investment costs is estimated using average cost factors (f_i). Equation (4.60) exemplifies the estimation of the total overnight costs based on the equipment costs and

average costs factors.

$$TOC = \left(\sum_i PEC_i \right) f_{install} f_{epcc} f_{process} f_{project} f_{owner} \tag{4.60}$$

Besides evaluating the investment costs, the economic analysis needs to estimate the revenues considering taxes and include the effects of time in the cash flow (CF_n). One of the most common methods to evaluate the economic rentability of a project is to calculate its net present value (NPV). Equation (4.61) shows the mathematical definition of net present value. This method allows to compare the future income of a certain project over a certain number of year (n) with its present investment cost based on an appropriated interest ratio (WACC). If a project has a positive NPV the investment can be considered as profitable, otherwise the project would not be able to attain a minimal interest return ratio. In addition, two different project can be compared based on their net present values, since the one with higher NPV is able to acquire more value for an investor.

$$NPV = \sum_n \frac{CF_n}{(1 + WACC)^n} \tag{4.61}$$

Another type of economic analysis is to estimate the levelized cost of a certain product such as electricity or a biofuel. For instance, Equation (4.62) shows the mathematical equation used to determine the levelized cost of electricity (LCOE) of a power plant. The calculation of the levelized cost is simpler than the NPV because it does not require to estimate the income cash flows, only yearly costs (C_n). This value is very useful to compare results among different production routes of a certain product (e.g., electricity, hydrogen or methane) since these values are widely reported in the literature.

$$LCOE = \frac{\sum_n C_n (1 + WACC)^{-n}}{\sum_n W_{net} (1 + WACC)^{-n}} \tag{4.62}$$

4.4 Optimization

In most problems, efficiency and profitability are conflicting objectives [85]. For instance, a larger heat exchanger would be more effective to transfer heat between two streams, but it would also cost more. Thus optimizing a production plant solely based on efficiency or costs may not provide a good understanding on the trade-offs between technical and economic benefits. A more complete optimization can be achieved using a multi-objective optimization algorithm, such as the Non-dominated Sorting Genetic Algorithm II (NSGA-II)[91]. In this method, multiple objective functions can be optimized simultaneously based on the principles of natural selection, in which a random population of process conditions is "evolved" along a predefined number of generations. Figure 4.13 illustrates

the optimization overview employed in some the analysis of this thesis, while Fig. 4.14 exemplifies the type of results of this method.

Figure 4.13: Overview of the optimization process

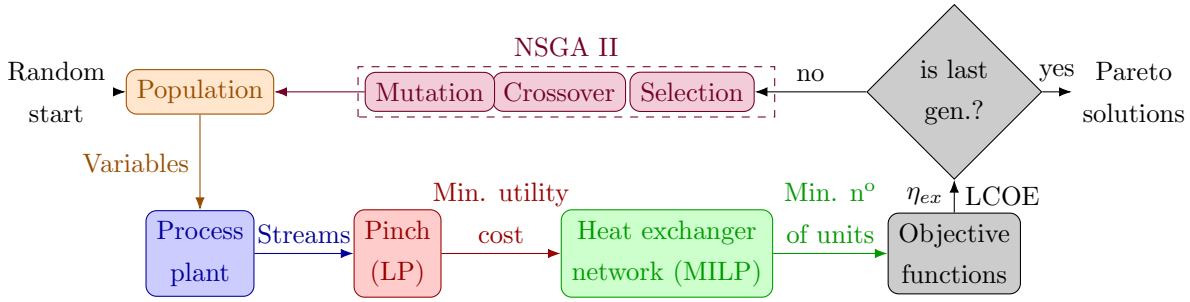

Source: [42]

Figure 4.14: Example of Pareto frontier results

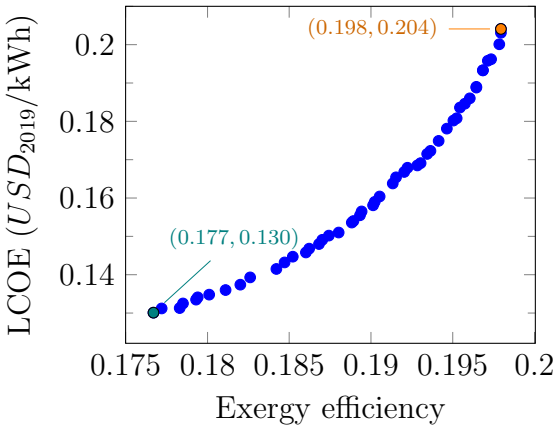

Source: [42]

At each generation, pairs of individuals (e.g., set of operating conditions or design choices) are selected based on a ranking system to create offsprings, which inherit features from the original pair ("parents"). These offsprings are randomly modified to increase the diversity of the population of solutions, a process called "mutation". At the end of a generation the best and more diverse individuals from the previous population ("parents") and its offsprings are selected to form a new population and continue the cycle.

The NSGA-II is extremely versatile and can be used to optimize two or more objective functions (e.g., exergy efficiency and NPV) for a production plant. The results of the optimization can be illustrated as a Pareto frontier, as depicted in Figure 4.14, which describes the limit where no further improvement of an objective function is possible for a fixed value of another objective function.

The main disadvantage of this method is the computational time required to find optimal solutions. Since each generation requires the simulation of all population of process

designs, the optimization process can require a significant amount of time for a complex process model.

5 Macro analysis of biogas conversion routes

Biomass residues can be converted into electricity and biofuels in order to increase the efficiency and revenues of biorefinery plants, but this requires the integration of different energy intensive processes. In other words, the requirements of work and heat from additional waste/fuel conversion processes should be internally supplied whenever possible in order to minimize the operational costs of these technologies.

Currently, anaerobic digestion and gasification are the main alternatives to convert organic residues into biofuels and electricity. However, few studies have explored the energy integration possibilities between these technologies and compared different production pathways. In addition, the technical and environmental competitiveness of products derived from biomass wastes have rarely being compared against their non-renewable counterparts.

Thus, in this chapter, different process layouts combining anaerobic digestion and gasification are proposed to produce methane, hydrogen or electricity from sugarcane wastes (bagasse and vinasse). The energy integration of these designs are optimized using a mixed integer linear optimization problem (MILP) based on the principles of pinch technology, which aims to maximize the operational revenues. Moreover, a comparative assessment between the total (c_T) and non-renewable (c_{NR}) unit exergy costs and specific CO_2 emissions (c_{CO2}) of the electricity, methane and hydrogen produced from sugarcane vinasse and bagasse is presented and compared with the conventional (fossil fuel-based) supply chains.

Among the waste upgrade alternatives considered in this analysis, methane production is able to maximize the exergy flow rate of products in the transformation stage (52.4-58.6 MW), since it requires fewer resources and separation steps compared with the other alternatives. On the other hand, the co-production of hydrogen and electricity can substantially increase the transportation service in the end-use stage (51.7-52.1%) and the operational revenues (2706-2889 EUR/h). These results indicate that methane production is the most efficient production route (biomass to fuels), but hydrogen and electricity achieve better performance indicators (technical, economic and environmental) when the

analysis includes the end-use of biofuels and electricity (biomass to transportation service).

The exergy destruction in the proposed designs can be mainly attributed to vinasse disposal, since a significant fraction of its organic wastes are inert to anaerobic digestion. Other important sources of irreversibilities are the bagasse gasifier and utility systems, due to the irreversible reactions occurring in these processes (e.g. combustion). In addition, the non-renewable unit exergy costs and specific CO_2 emissions for the transportation service in all cases analyzed are 3.1 to 4.7 times lower compared with conventional fossil fuels (i.e., diesel, gasoline, natural gas and hydrogen).

5.1 Context

The transportation sector is responsible for a significant portion of energy consumption and greenhouse gas emissions in the world. In 2016, this economic sector produced a quarter of emissions (8 GtCO_2) in the world, a number that has been steadily increasing in the last years [92]. In Brazil, for instance, the transportation sector already accounts for 45.8% of carbon dioxide emissions and 32.7% of the energy demand of the country [93]. An alternative to improve the sustainability of this sector is the gradual replacement of fossil fuels by biofuels and electricity. The expansion of these energy resources is expected to reduce or eliminate the CO_2 emissions derived from fossil fuel combustion. However, these improvements in the end-use stage may be offset by inefficiencies in upstream processes (e.g., supply, transformation, distribution) and their dependence on resources derived from non-renewable energy sources [94].

In the recent years, biofuels represented almost 70% of renewable energy production in the world [95] and biomass was responsible for 25.5% of Brazilian domestic energy supply [96]. This contribution could be further increased if biorefinery wastes were converted into valuable energy products. In this way, the energy consumption and greenhouse gas emissions of biomass processing plants could be reduced alongside with the waste disposal cost and their environmental impact. In Brazil, the production of biofuels and electricity from sugarcane wastes may be a promising source of renewable energy, since this biomass resource is responsible for 17% of the domestic energy supply in the country [93]. Traditionally, bagasse biomass is used to provide combined heat and power to the sugarcane mill, whereas vinasse is generally used as an alternative fertilizer in sugarcane crops [97]. However, these practices are still fairly inefficient and can be replaced by improved energy conversion processes [98, 99].

In this context, gasification and anaerobic digestion are prominent research topics among the available technological routes for waste to energy conversion [100]. Accord-

ingly, these technologies could lead to higher production yields [101] and reduced the size of treatment plants [102]. Aside from the potential improvements for the existing ethanol production framework, this alternative would not require another biomass source or the expansion of the cultivation area, while the amount of wastes discarded in the environment could be significantly reduced [46]. For example, Palacios-Bereche et al. [101] observed a substantial increase in exergy efficiency with the addition of the enzymatic hydrolysis of sugarcane bagasse and anaerobic digestion of effluents to the traditional sugarcane distillery. Moreover, Silva Neto et al. [103] demonstrated that biogas production could increase the amount of renewable energy produced from sugarcane and potentially reduce CO_2 emissions by replacing natural gas or diesel.

Previous studies have already investigated the use of lignocellulosic biomass for synthetic natural gas [104], hydrogen and electricity production [105]. These studies highlight the importance of energy integration to attain highly efficient plant designs. However, the impact of the upstream processes in the efficiency and carbon footprint of products derived from industrial wastes has been rarely studied. The usual approach is to consider the wastes as fully renewable resources, a hypothesis that can underestimate the fossil fuel dependency of biofuel production. On the other hand, the effect of the end-use efficiency of biofuels in the overall efficiency and carbon dioxide emissions was also seldom analyzed. For instance, Piekarczyk et al. [106] investigated the influence of the cumulative consumption in the production route of several biofuels. It was observed that the energy source (e.g., biomass, coal, electricity) used in the utility systems has a strong impact in the efficiency and thermo-ecological indicators for biofuels. Flórez-Orrego et al. [107] proposed an exergoeconomy methodology to evaluate the unit exergy costs (total and non-renewable) and specific CO_2 emissions of different fuels. Their findings indicate that biofuels, such as ethanol and biodiesel, require relatively more resources (in exergy basis) than their fossil-derived correspondents, but the major portion of these energy inputs can be considered as renewable. Moreover, in a next study, Flórez-Orrego et al. [108] estimated that only a small percentage of the exergy available in fuels (5-34%) is actually converted into transportation service.

These literature gaps in conjunction can promote misleading conclusions in the comparison of conversion routes from wastes to biofuels and electricity. Thus, this chapter presents a thermodynamic evaluation of possible processes combining anaerobic digestion and gasification to capitalize sugarcane vinasse and residual bagasse by using a systematic approach of energy integration and exergy analysis. In order to fulfill gaps in current literature, the biomass supply, transformation, fuel distribution and the end-use are also included in this analysis to promote different perspectives for the same problem. Moreover, the exergoeconomic methodology proposed by Flórez-Orrego et al. [107] is employed to

examine the possible improvements in environmental indicators compared with petroleum derived fuels.

5.2 Process description

In Brazil, sugarcane is usually processed in mills annexed with an ethanol distillery to produce sugar, ethanol and electricity as depicted in Figure 5.1. The main by-products of this conventional design are the surplus bagasse and a wastewater derived from the ethanol distillation called vinasse. The first is sold to other industries as an alternative fuel, while the second is dispersed in sugarcane fields to provide mineral supplementation for new crops. Although these are well-established designs and practices, they certainly undermine the potential of bagasse and vinasse, which could be used to produce more biofuels and/or electricity.

Figure 5.1: Conventional scenario for sugarcane ethanol industry

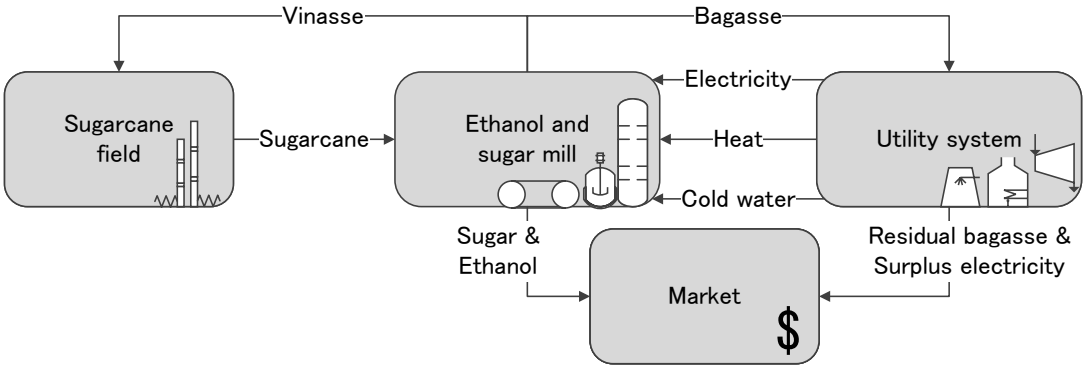

Source: Author

Figure 5.2 illustrates the scenario investigated in this research work, a revamp design in which vinasse and surplus bagasse are converted into biofuels and electricity in a separated waste upgrade plant (WUP). The waste upgrade plant aims to reduce losses in waste disposal and add commercial value to sugarcane residues, but requires the design of a integrated system with unknown connections.

The sugar and ethanol production plant (SEP) consumes bagasse in the utility system to match its energy demands, while the waste upgrade plant (WUP) uses either bagasse, purified syngas or vinasse-derived biomethane as fuels. Both production plants, SEP and WUP, have independent utility systems that internally provide electricity and heat by using a Rankine cycle with an extensive waste heat recovery system. The waste upgrade plant can be divided into four sub units which are combined to produce three different products from vinasse and bagasse are considered: electricity, methane and hydrogen. In

Figure 5.2: Waste upgrade scenario for sugarcane ethanol industry

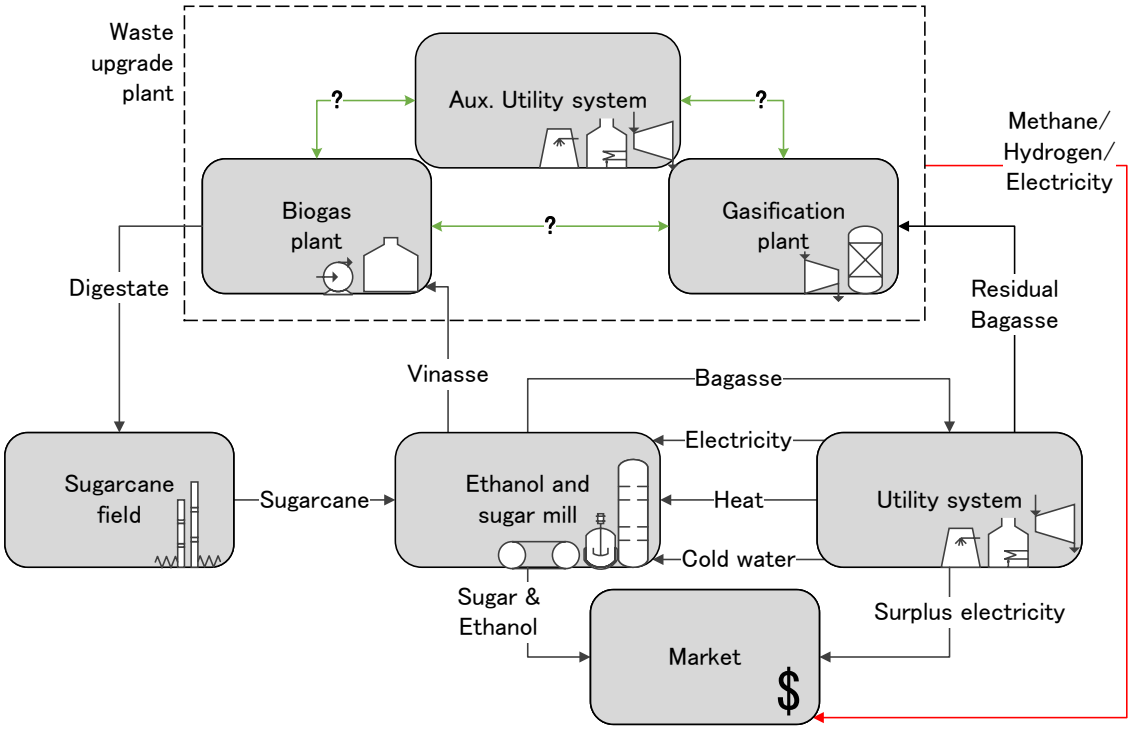

Source: Author

addition, the surplus electricity produced in SEP may be used to partially supply the demand of the WUP.

Table 5.1 summarizes the different scenarios analyzed in this study: a conventional scenario, as shown in Figure 5.3 (a), and other five cases for different configurations of the waste upgrade concept, illustrated in Figure 5.3 (b).

Table 5.1: Summary of proposed cases for biofuels and electricity production

	Case					
Parameter	Base	E	M1	M2	H1	H2
Sugar and ethanol plant						
Sugar production	Yes	Yes	Yes	Yes	Yes	Yes
Ethanol production	Yes	Yes	Yes	Yes	Yes	Yes
Surplus electricity production	Yes	Yes	Yes	Yes	Yes	Yes
Waste upgrade plant						
Gaseous biofuel produced	-	No	CH_4	CH_4	H_2	H_2
Surplus electricity production	-	Yes	Yes	Yes	Yes	Yes
Surplus electricity from SEP to WUP	-	No	No	Yes	No	Yes

Source: [45]

Figure 5.3: Overview of biofuel and electricity production scenarios: (a) Base case (b) Waste upgrade concept

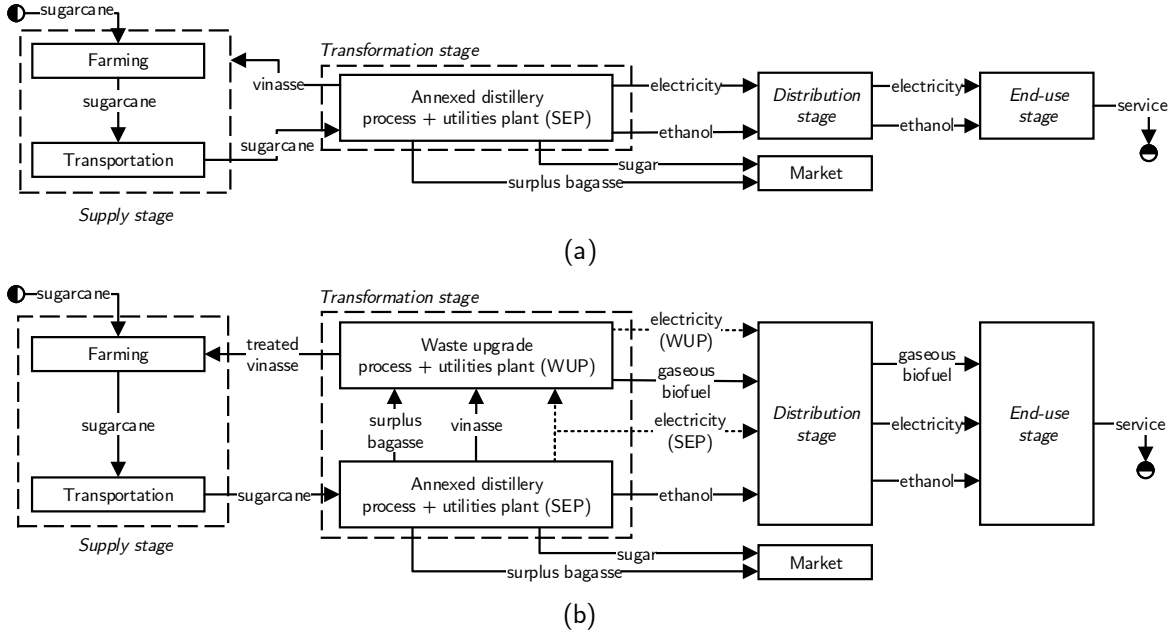

Source: [45]

5.2.1 Sugar and ethanol process plant

The main processes of a conventional sugar and ethanol process plant in Brazil are illustrated in Figure 5.4. Once sugarcane is harvested and transported to the mill, the feedstock has to be cleaned and sliced in preparation for the extraction process. Sugarcane juice and fibers (bagasse) are separated in milling rolls with the addition of water to increase the sucrose extraction. After extraction, sugarcane juice is subjected to a sequence of treatment and concentration processes (e.g. filtration, clarification, evaporation), while bagasse is stored and used as fuel to produce steam and electricity. In order to produce sugar, the sucrose in the concentrated juice has to be crystallized, separated and dried. On the other hand, ethanol is produced by the fermentation of a mixture of juice, molasses (by-product of sugar production) and syrup (concentrated juice). The resulting products of fermentation are separated by a distillation process, forming the hydrated ethanol and a wastewater called vinasse. In general, vinasse is an undesired by-product which is repurposed in the irrigation of sugarcane fields (fertirrigation).

The main parameters of the annexed distillery considered in this study are shown in Table 5.2 and a detailed description of these processes is provided in Refs. [107, 109].

Figure 5.4: Simplified flowsheet of an sugar and ethanol production plant

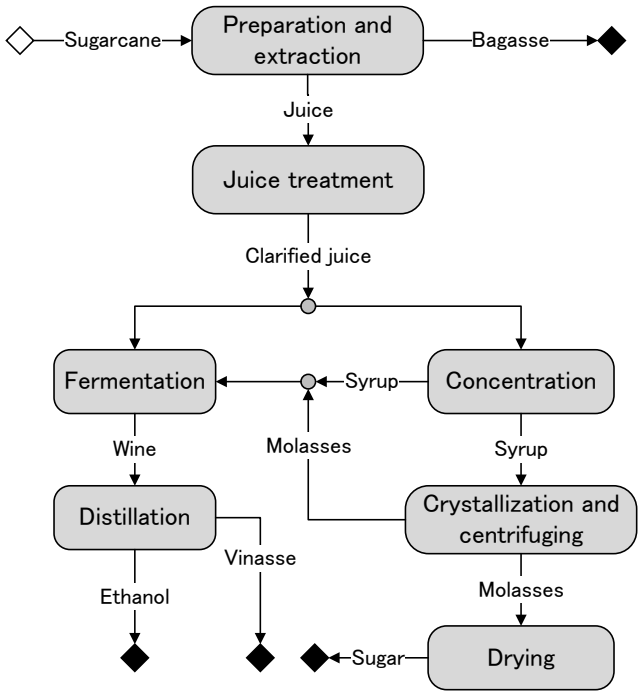

Source: Author

Table 5.2: Key parameters of the annexed distillery

Parameter	Value
Sugarcane milling rate	500 t/h
Sugar production rate	64.8 kg/$t_{sugarcane}$
Hydrated ethanol production rate	40 l/$t_{sugarcane}$
Surplus electricity	8.45 kWh/$t_{sugarcane}$
Surplus bagasse	53.28 kg/$t_{sugarcane}$
Vinasse production rate	552 l/$t_{sugarcane}$

Source: [107, 109, 45]

5.2.2 Vinasse conversion: biomethane and hydrogen production units

The vinasse separated in the ethanol distillation column is at temperatures higher than ambient (60 °C) and presents a low pH (3.75-5) [96], which are not ideal environmental conditions for anaerobic bacteria cultures. Thus, vinasse must be first cooled down and mixed with a recycled digestor effluent (15:1 effluent to influent flow ratio) [110] for temperature and pH correction, as illustrated in Figure 5.5. Mesophilic anaerobic digestion (35 °C) is conducted in an upflow anaerobic sludge blanket (UASB) reactor, as widely practiced in vinasse treatment plants [111]. The treated vinasse is temporarily stored

in lagoons to be distributed to sugarcane crops (fertirrigation) by means of channels, diesel-fueled pumps or special trucks. On the other hand, biogas is desulfurized using a cold sodium hydroxide solution (10g NaOH/L; 15 °C) in order to avoid corrosion in downstream equipment. The caustic solution flow rate is adjusted to guarantee a maximum output H_2S concentration (200 ppmv). The remaining biogas impurities, mainly CO_2 and H_2O, are physically absorbed by using a Selexol process to achieve commercial specifications. This technology consists of a high pressure column absorber (30 bar, 25 °C) using a mixture of dimethyl ethers of polyethylene glycol (DEPG). The rich solution is partially regenerated by releasing the CO_2 gas at lower pressures (1 bar) and higher temperatures (60 °C). The purged gas may still contain a portion of methane and, thus, it has to be burned to avoid environmental damages.

Figure 5.5: Flowsheet of biomethane production from vinasse

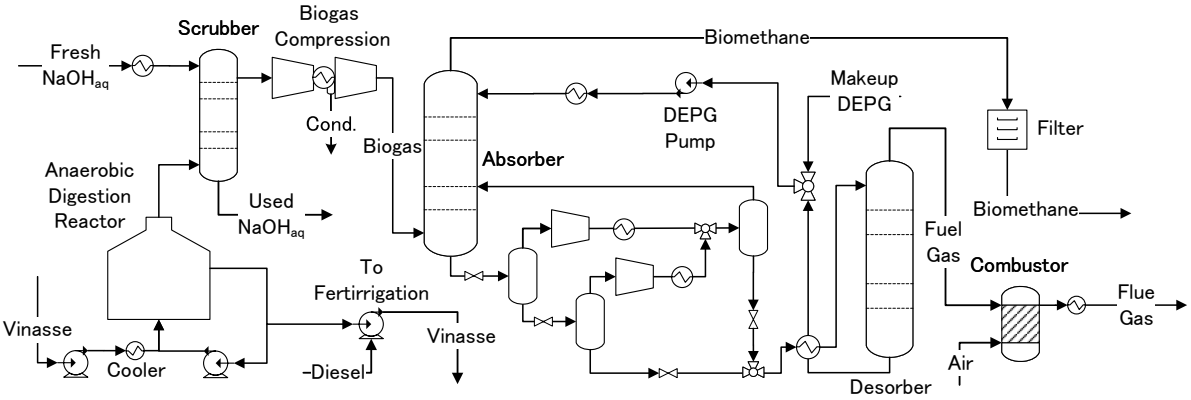

Source: [43]

In the hydrogen via vinasse unit, Figure 5.6, biomethane is depressurized (20 bar) to enhance the production of a H_2 and CO rich mixture by using steam reforming process. The highly endothermic steam reforming reaction requires a large heat duty above 700 °C. To avoid excessive formation of carbon that could affect the performance and lifetime of catalyst, the molar steam to methane ratio is set as 3 [112]. Two sequential high (390 °C) and a low (212 °C) temperature shift reactors are used to increase hydrogen concentration through the water-shift exothermic reaction. In this step, the hydrogen rich mixture is intercooled by using a heat recovery system in order to control the maximum attainable reaction temperature [113]. The additional CO_2 produced is removed by using physical absorption and a pressure swing adsorption (PSA) system. At last, purified hydrogen is compressed (200 bar) with intercooling for commercialization.

Figure 5.6: Flowsheet of hydrogen production from biomethane

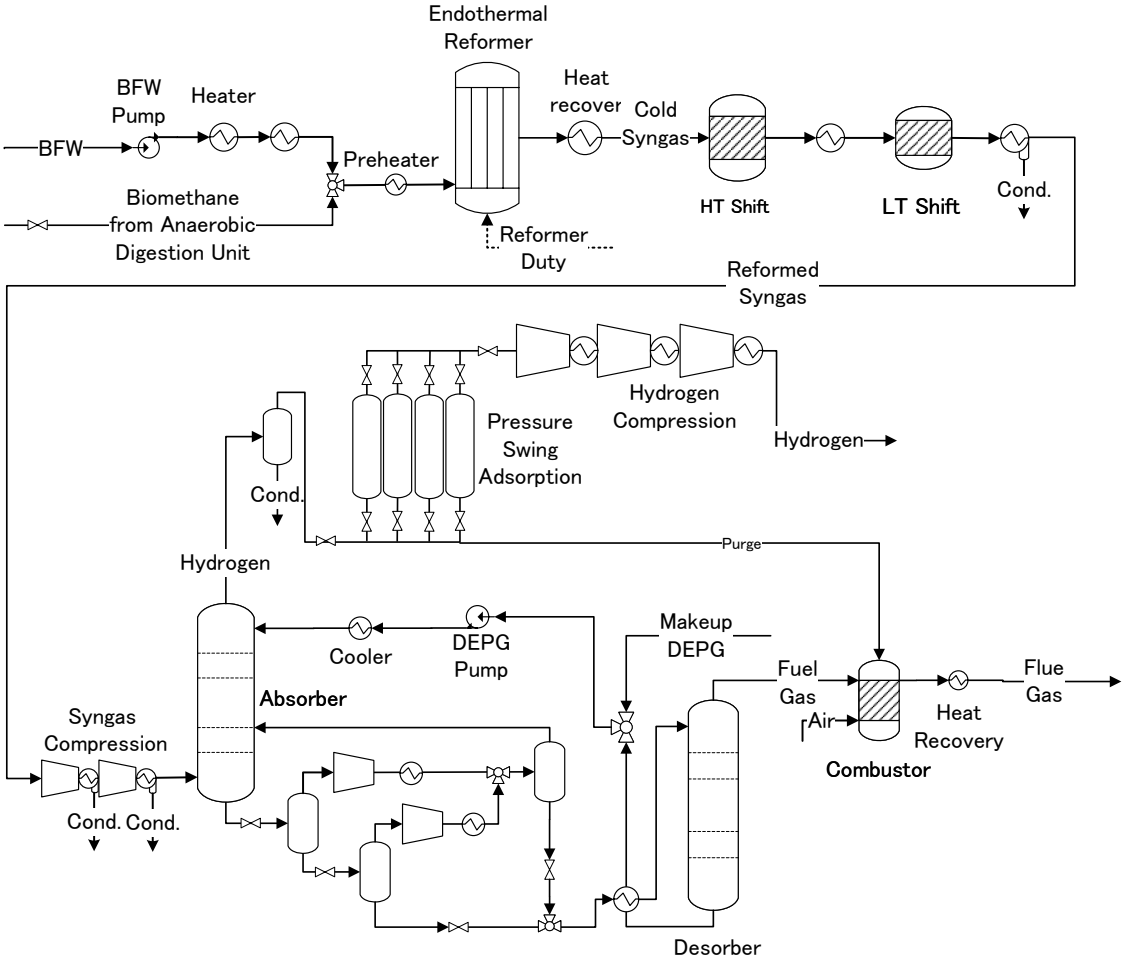

Source: [43]

5.2.3 Bagasse conversion: gasification, biomethane and hydrogen production units

Figure 5.7 shows the gasification process and the water gas shift sub-unit assumed in this study. The bagasse as-received from the sugarcane mill has a large moisture content (50%) which must be reduced to less than 10% in a rotary dryer that consumes power and heat provided by the utility systems as well as recovers heat from the gasifier flue gas [114]. Bagasse is also chipped in an energy intensive process that may require between 1-3% of the total energy embodied (lower heating value basis) in the consumed biomass [115]. The bagasse ultimate composition is set as 46.70% C, 6.02% H, 44.95% O, 0.17% N, 0.02% S and 2.14% ash, whereas proximate analysis is considered as 50% moisture (as-received), 14.32% fixed carbon, 83.54% volatile substances, and ash in balance [116]. The Battelle Columbus Laboratory (BCL) indirect gasifier at atmospheric pressure avoids

the dilution with nitrogen of the syngas produced, as the combustion and gasification processes occur in a separate double column system (Figure 5.7) [117]. Steam is used as the gasification medium (steam-to-biomass mass ratio 0.75), whereas the combustion with air of a fraction of the char produced in the bagasse pyrolysis step supplies the heat required by the endothermic drying, pyrolysis and gasification reactions.

Figure 5.7: Flowsheet of sugarcane bagasse gasification

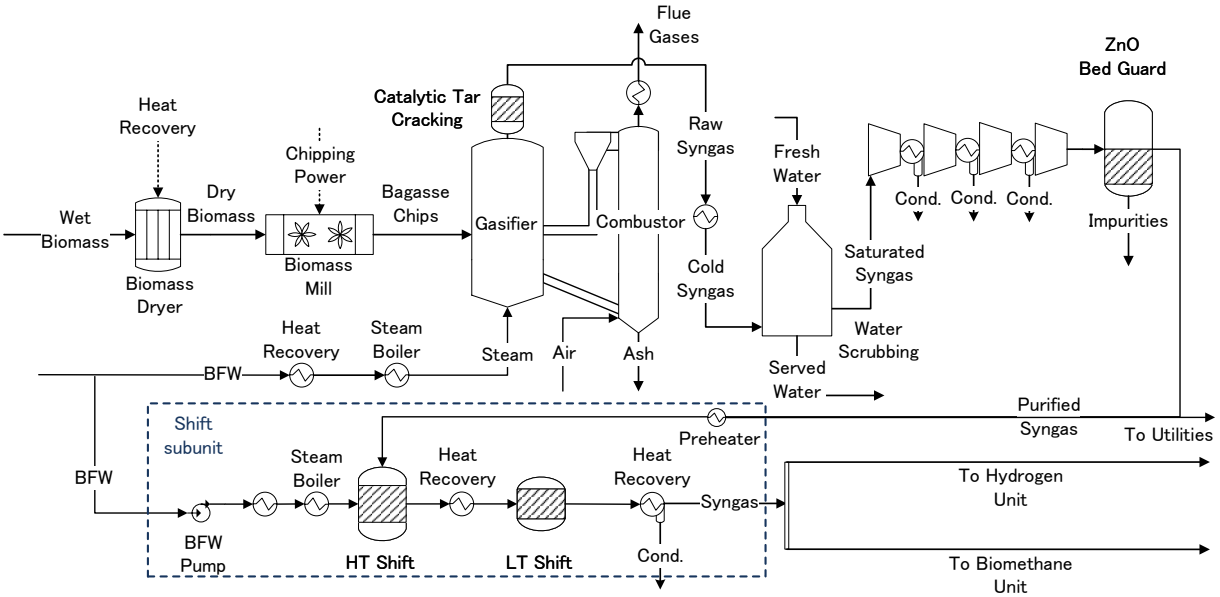

Source: [43]

After the syngas produced leaves the gasifier, a thermal catalytic cracking of the tar produced is performed. The syngas is cooled down to 400 °C, scrubbed with water, in order to remove the impurities that may affect the downstream equipment, and then it is compressed to 30 bar. At this point, the purified syngas can be converted to either hydrogen-rich syngas or electricity and heat. As it still contains high levels of CO, a water gas shift conversion (analogous to that described for the hydrogen production via vinasse) helps increasing the hydrogen content simultaneously producing more CO_2. On the other hand, this is not necessary for the sake of power production and it would represent an additional source of steam demand and irreversibility. The production of pure hydrogen by using biomass gasification, Figure 5.8, shares some similar processes with biomethane conversion in the vinasse route, namely, Selexol and PSA purification steps and multistage hydrogen compression.

When methane production is intended, a portion of CO_2 is removed from syngas to obtain the desired proportion of hydrogen per carbon necessary in methanation. This process, illustrated in Figure 5.9, consists in the conversion of hydrogen, CO and CO_2 into methane and water in three sequential reactor beds [118, 119]. The methanation reactions

Figure 5.8: Flowsheet of hydrogen production from syngas

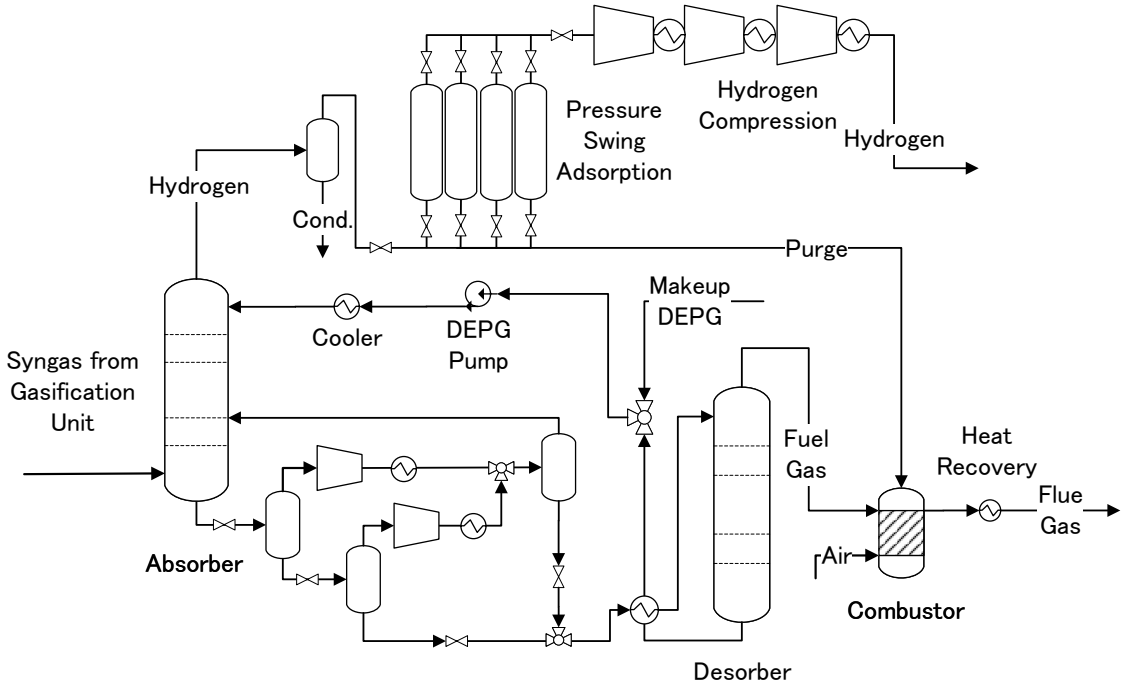

Source: [43]

are exothermic and, therefore, an interbed heat recovery system is required to avoid the fast catalyst deterioration. For instance, the first methanator bed uses a recycle stream combined with intercooling in order to maintain the maximum temperature below 700 °C. As a result, the gas mixture produced has a high methane concentration ($\geq$97%), which is sent to a temperature swing adsoption system to reduce its humidity to commercial standards.

5.3 Modelling details

Due to the intricate relationship in terms of energy and mass transfer between material streams and unitary operations, different computational frameworks are used in order to properly model the mass, energy and entropy balances of the studied processes. Figure 5.10 shows a visual summary of the software used to model each part of the scenarios proposed in this study. For instance, the sugar and ethanol process plant (SEP) is modelled in the Engineering Equation Solver (EES) [120], while the model for the waste upgrade plant is developed in Aspen Plus [121]. In order to model the biogas production and composition, the Anaerobic Digestion Model N°1 (ADM1), with sulfur reduction reac-

Figure 5.9: Flowsheet of methane production from syngas

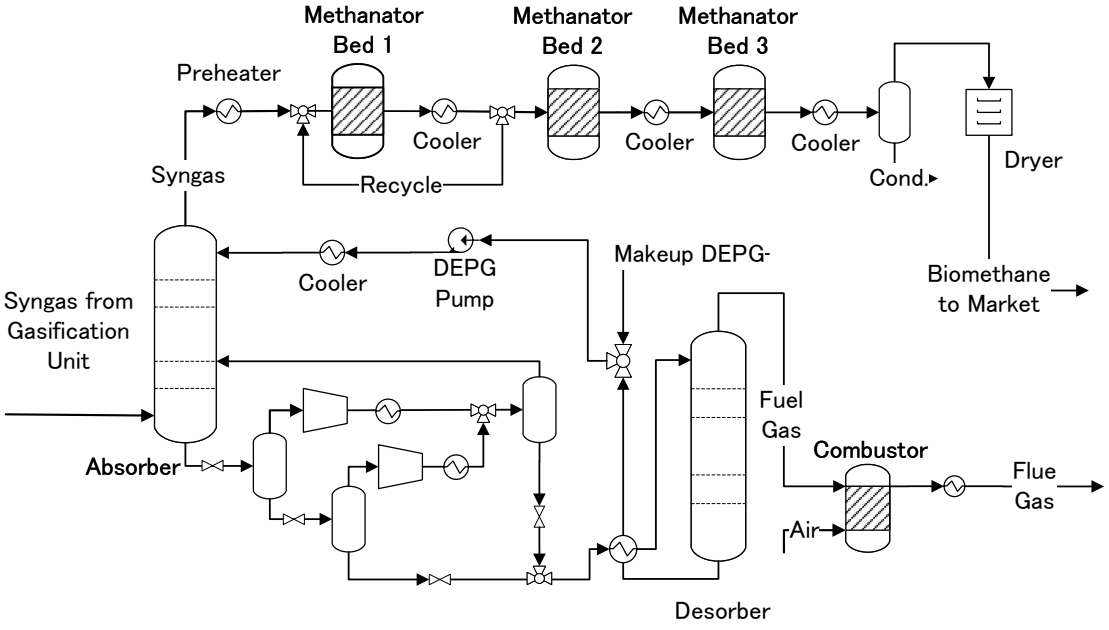

Source: [43]

tions and calibrated parameters for vinasse digestion [25, 122], is solved in Matlab [123] and the results linked with Aspen Plus via Microsoft Excel [46]. On the other hand, the utility systems for the waste upgrade process plant are designed based on the Equation Oriented (EO) approach in the OSMOSE Lua platform [124], aiming to minimize the energy requirements and operating cost of the plant.

The results are analyzed following the exergoeconomy methodology proposed by Flórez-Orrego et al. [107], which consists of an adaptation of the available exergy costing methods [125, 87, 126] to allocate the total and non-renewable cumulative exergy consumption and specific CO_2 emissions of fuels, chemicals and electricity. This methodology allows to easily pinpoint connections between the quality of the energy conversion and the environmental impact in industrial processes. The software EES and Microsoft Excel are employed in order to determine the unit exergy costs and the results for the exergy indicators (e.g., efficiency, exergy destroyed).

5.3.1 Process modelling

Sugarcane composition is assumed as 70% water, 14.5% sucrose, 13.5% fiber and 2% other solids in mass basis, while bagasse is considered as containing 50% water and 50% fiber [109]. In addition, bagasse composition is set by using an ultimate composition (46.70% C, 44.95% O, 6.02% H, 2.14% ash, 0.17%N and 0.02%S) and a proximate analysis

Figure 5.10: Graphic summary of the software employed in this study

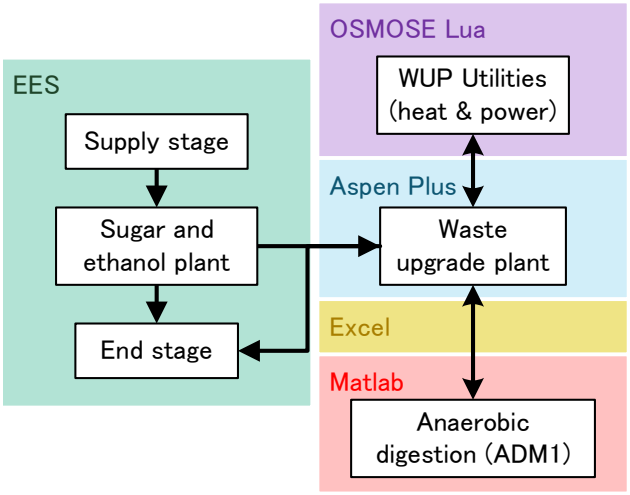

Source: Author

concentration (83.54% volatile, 14.32% fixed carbon and ash in balance) [116]. On the other hand, vinasse is approximated by a mixture of water, inorganic substances (e.g., KOH, KCl, NH_3, among others) and organic material with average concentrations, as proposed by Nogueira Nakashima and Oliveira Junior [46]. The vinasse temperature, chemical organic demand and sulfate concentrations are assumed as 75 °C, 36 gO_2/l and 0.05 gSO_4^{2-}/gO_2, respectively.

The thermodynamic properties of the mixtures are determined by using different correlations depending on their suitability. The sucrose-water solutions properties are estimated based on the methodology described by Nebra and Fernandez Parra [127]. The composition of vinasse has been estimated based on the experimental observations of Barrera et al. [110] with general components (e.g., sugars, lipids, inert, etc.) modelled as commonly observed chemical substances (e.g., glucose, linoleic acid, lignin, etc.) using the Non-Random Two-Liquid activity model (NRTL) [46]. Meanwhile, since the biogas desulfurization involves electrolytic reactions, the adaptation of the NRTL model for electrolytes (ELEC-NRTL) is used to estimate properties of caustic solutions. On the other hand, the Perturbed-Chain Statistical Associating Fluid Theory is used to model the absorption via Selexol solvent (DEPG) [128]. For other unit operations, which mainly involve gaseous substances (i.e., gasification, methanation, flare, etc.), the Peng-Robinson EOS with Boston-Mathias modifications is used to derive their thermophysical properties [121].

The anaerobic reactor was modelled as a continuous ideally stirred-tank reactor using the Anaerobic Digestion Model N°1 (ADM1) [25], a generic kinetic model for anaerobic

digestion, with modifications and parameters adapted for sugarcane ethanol vinasse [122]. Moreover, the inlet vinasse temperature was calculated considering the reactor heat loss, estimated by using average heat transfer coefficients [129] and a constant process temperature (35 °C). The vinasse disposal process (fertirrigation) is modelled as a black-box process with an average diesel consumption of 0.19 $l/m^3_{vinasse}$ to transport the effluent to the sugarcane fields, based on observations from Macedo et al. [130]. In the desulfurization unit, the process mass balance is estimated using a rate-based model and a set of chemical reactions involving electrochemical and gas-liquid interactions [131, 132].

Gasification is modelled as composed of sequential drying, pyrolysis, reduction and combustion processes. In order to estimate the actual yield rates of hydrogen, CO, CO_2, methane, tar, char and water in the pyrolysis reaction step, empirical correlations reported in the literature as a function of temperature were used [133]. The tar and methane produced, typically underestimated via the non-stoichiometric equilibrium methods, is adjusted with a set of approach-to-equilibrium temperatures to reflect the actual syngas composition of the gasifier [134]. Thermodynamic equilibrium is also used for modelling the steam reforming (with temperature approach correction), water shift and methanation reactors and flare combustor. Moreover, a 150% theoretical air is assumed in the combustion of the purification purge gas.

Table 5.3 summarizes the main processes parameters assumed for the waste upgrade plant (WUP). Pumps and compressors were modelled based on fixed isentropic efficiencies of, respectively, 60% and 80%. Pressure swing adsorption is simplified as a black-box model assuming a hydrogen recovery efficiency of 80% mol, based on previous works [112]. As a simplification, the adsorption systems consumptions are assumed too small regarding the overall system and the temperature swing adsorption was assumed as lossless.

The non-renewable consumption, direct specific CO_2 emissions and conversion efficiencies reported by Flórez-Orrego et al.[108, 135], shown in Tables 5.4, 5.5 and 5.6, are used to determine the unit exergy costs in the cultivation, transportation, distribution and end-use stages.

5.3.2 Energy integration and operating cost minimization

The energy integration analysis is performed by using the OSMOSE Lua platform developed by the IPESE group at EPFL, Switzerland [124]. This tool allows to determine the most suitable utility systems and their operating conditions, that satisfy the minimum energy requirement (MER) with the lowest resources consumption and optimal operating cost (water consumption, vinasse and bagasse). This computational framework manages the data transfer with the Aspen Plus software and builds the mixed integer linear programming (MILP) problem described in the Eqs. (5.1) to (5.5) that minimizes

Table 5.3: Main parameters assumed for the waste upgrade plant

Parameter	Value
Gasification	
Pressure	1 bar
Steam to biomass ratio	0.75 (mass)
Anaerobic digestion	
Temperature	35 °C
Effluent recycle	15:1
H_2S removal	
Temperature and pressure	15 °C / 1 bar
H_2S concentration	$\leq$ 200 ppmv
CO_2 removal	
Temperature and pressure	25 °C / 30-35 bar
CO_2 final concentration	5%
Biomethane steam reforming	
Temperature and pressure	25 °C / 15 bar
Steam/carbon ratio	3 (molar)
Water gas shift	
Pressure (for biomethane conversion)	15 bar
Pressure (for syngas conversion)	30 bar
Inlet temperature (fist/second reactor)	390 / 212 °C
Methanation	
Inlet temperatures (first/second/third reactor)	300 / 300 / 250 °C
Pressure	35 bar
$(H_2 - CO_2)/(CO + CO_2)$ inlet ratio	3
PSA and compression	
Hydrogen concentration	99%
Hydrogen export pressure	200 bar

Source: [45]

the operating cost of the chemical plant [136] while satisfying the constraints of the MER problem. In other words, the optimization problem consists of finding the load factor (f^i) of each utility unit that minimizes the operational cost function (objective function) given by Eq. (5.1).

$$\min_{f^i, y^i} \left[(\dot{B}^{ch}c)_{vinasse} + (\dot{B}^{ch}c)_{bagasse} + \sum_i (f\dot{V}c)^i_{water} - \sum_i (f\dot{B}^{ch}c)^i_{product} \right] \tag{5.1}$$

Table 5.4: Non-renewable consumption and direct CO_2 emissions in sugarcane supply stage

Ratio per fuel	Sugarcane (fuel)
Natural gas	
consumption ($J_{natural\,gas}/kJ_{cane}$)	15.05
CO_2 emission (gCO_2/MJ_{cane})	2.93
Diesel	
consumption (J_{diesel}/kJ_{cane})	34.19
CO_2 emission (gCO_2/MJ_{cane})	0.85

Source: [108, 135, 45]

Table 5.5: Non-renewable consumption and direct CO_2 emissions in the distribution stage

	Fuel		
Ratio per fuel	Hydrated ethanol	Biomethane	H_2
Natural gas			
consumption ($J_{natural\,gas}/kJ_{fuel}$)	-	30.0	-
CO_2 emission (gCO_2/MJ_{fuel})	-	1.695	-
Diesel			
consumption (J_{diesel}/kJ_{fuel})	24.5	-	-
CO_2 emission (gCO_2/MJ_{fuel})	0.445	-	-
Electricity			
consumption (J_{power}/kJ_{fuel})	-	15.5	35.7
CO_2 emission (gCO_2/MJ_{fuel})	-	0	0

Source: [108, 135, 45]

Table 5.6: Exergy efficiencies for each fuel conversion technology

Fuel	Exergy efficiency
Hydrated ethanol	8.69%
Biomethane	6.06%
Hydrogen	15.79%
Electricity	34.02%

Source: [108, 135, 45]

Subject to the following constrains:

$$\sum_{i}^{\Omega} f^i \dot{Q}_k^i + R_{k+1} - R_k = 0 \quad \forall k = 1...K \tag{5.2}$$

$$\sum_{i}^{\Omega} f^i \dot{W}^i + \dot{W}_{in} - \dot{W}_{exp} = 0 \tag{5.3}$$

$$f^i_{min} y^i \leq f^i \leq f^i_{max} y^i \quad \forall i = 1...\Omega \tag{5.4}$$

$$R_1 = 0,\ R_{K+1} = 0,\ R_k \geq 0 \tag{5.5}$$

Where, $\dot{B}^{ch}$ and c stands, respectively, for the chemical exergy flow rate and cost of the feedstock consumed or prices of marketable fuels and electricity produced; while $\dot{V}_i$ and t_{op} are the amount of water consumed by unit "i" and the operational time. Furthermore, Q and R are, respectively, the heat transfer rate and cascade heat transfer rate; and Ω is the number of different units in the set of utility systems.

Additional equations for the mass and energy balances on each stream layer (water, feedstock, fuels, electricity), along with the equations for modelling each one of the different energy technologies, are also included in the optimization problem. The optimal utility set is determined by calculating the integer variables (y^i) associated to the existence or absence of a given utility unit and the corresponding continuous load factor (f^i) of the selected utility systems. Representative Brazilian market costs for water (3.03 EUR/m^3), vinasse (0.0006 EUR/kWh), and bagasse (0.0056 EUR/kWh) consumed, as well as the selling prices of hydrogen (0.072 EUR/kWh), biomethane (0.032 EUR/kWh) and electricity (0.06 EUR/kWh) produced are taken from literature [136, 137, 138].

5.3.3 Exergy analysis

The potential and kinetic exergy were neglected in the evaluation of the total exergy flow rate of the streams. The chemical exergy is estimated based on the values and procedures proposed by Szargut, Morris and Steward [80] for most mixture flows. However, specific procedures are used to calculate the chemical exergy of sugarcane, bagasse and vinasse. For instance, sugarcane chemical exergy is estimated based on the mass weighted average of the chemical exergy of its components, i.e. sucrose, fiber and water. Bagasse chemical exergy is determined based on its lower heating value, estimated by using the correlations of Channiwala and Parikh [139], and the $\frac{b^{ch}}{LHV}$ ratio is calculated in terms of its atomic composition [80]. Furthermore, the specific chemical exergy of diesel fuel was considered as 44.85 MJ/kg [108].

Vinasse chemical exergy is estimated based on its theoretical chemical organic demand (ThOD) concentration, as proposed Nakashima and Oliveira Junior [98] based on early studies of Tai, Matsushide and Goda [84]. Assuming that ThOD and experimental chemical organic demand (COD) are approximately equal, the chemical exergy of vinasse or-

ganic material ($b^{ch}_{\text{org. vinasse}}$) can be estimated based on the reported COD concentrations according to Eq. (5.6).

$$b^{ch}_{\text{org. vinasse}} \left[\frac{kJ}{mol}\right] = 14.56 \cdot ThOD \left[\frac{gO_2}{mol}\right] \tag{5.6}$$

It is important to highlight that, in this analysis, all the irreversibility generated via the heat exchanger network and the power generation systems is allocated to the utility systems. This simplifies the exergy analysis, since the heating or cooling exergy requirements ($\dot{B}_{Qi}$ and $\dot{B}_{Qo}$) can be easily calculated based on the knowledge of the exergy balance of each process equipment (e.g., heat exchangers, endothermic reactors, etc.). Otherwise, a detailed design of the utility system would be necessary in the first stages of the overall plant design.

Unit exergy cost and specific CO_2 emissions

As previously mentioned, the unit exergy costs and specific CO_2 emissions are used to evaluate the thermodynamic performance (cumulative exergy consumption) and the environmental impact of the industrial processes, as proposed by [107]. This approach aims to calculate the total and non-renewable exergy costs (c_T and c_{NR} in kJ/kJ) and specific CO_2 emissions (c_{CO2} in gCO_2/MJ) of the fuels and electricity production and consumption, i.e. encompassing from the supply stage (sugarcane farming and transportation) up to its end-use (service in transportation sector). It is important to highlight that only the CO_2 emissions derived from non-renewable sources are considered in the net CO_2 emissions balance. Thus, the carbon dioxide produced through the reactions involving biomass feedstock (e.g., combustion, fermentation, gasification) are not accounted for the specific CO_2 emissions.

Figure 5.11 illustrates the methodology proposed by Flórez-Orrego et al. [107] applied for the sugarcane conversion, considering the stages of supply, transformation, distribution and end-use. In the supply stage, the unit exergy costs associated with materials consumed in biomass cultivation and transportation steps ($c^i_{C,s}$) are added to the initial sugarcane costs ($c_{F,t}$) proportionally to the exergy ratio of consumption to fuel ($\dot{B}_{C,s}/\dot{B}_{F,s}$). Thus, the balances for the total (c_T), non-renewable (c_{NR}) unit exergy costs and specific CO_2 (c_{CO2}) emissions for the supply stage can be described as in Eqs. (5.7), (5.8) and (5.9), respectively. As it may be observed in Eq. (5.9), an additional term ($\dot{M}_{co2}$) is introduced in the CO_2 balance to include the emissions generated by the combustion of non-renewable fuels in the stage.

$$c_{T,F,t} = c_{T,F,s} + \sum_i \left[\frac{\dot{B}^i_{C,s}}{\dot{B}_{F,s}} c^i_{T,C,s}\right] \tag{5.7}$$

Figure 5.11: Scheme of the methodology used in the allocation of the unit exergy costs and specific CO_2 emissions

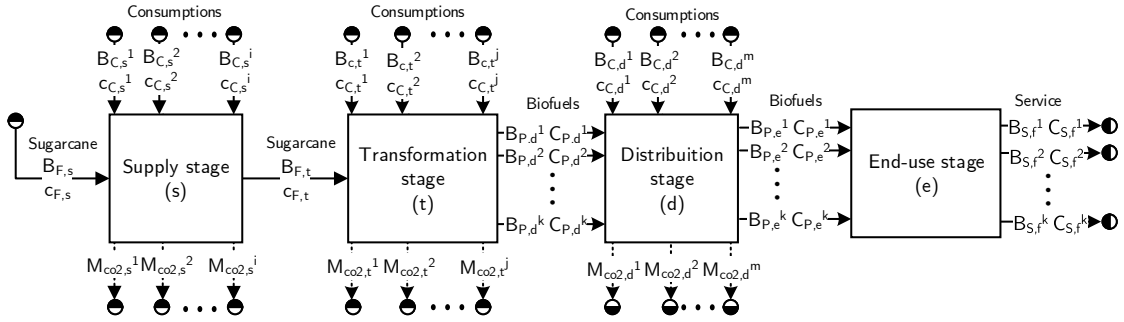

Source: [45]

$$c_{NR,F,t} = c_{NR,F,s} + \sum_i \left[\frac{\dot{B}^i_{C,s}}{\dot{B}_{F,s}} c^i_{NR,C,s} \right] \tag{5.8}$$

$$c_{co2,F,t} = c_{co2,F,s} + \sum_i \left[\frac{\dot{B}^i_{C,s}}{\dot{B}_{F,s}} c^i_{co2,C,s} + \frac{\dot{M}^i_{co2,s}}{\dot{B}_{F,s}} \right] \tag{5.9}$$

The transformation stage comprises the processes necessary to convert sugarcane into sugar, electricity and biofuels, as illustrated in Figures 9.1, 9.2 and 9.3. Since the processes may have multiple products, the exergy unit costs are allocated following the criteria recommended by the thermoeconomy methodologies (i.e., equality, extraction) [125, 87]. The general balance for unit exergy costs (total and non-renewable) and specific CO_2 emissions are shown in Eqs. (5.10), (5.11) and (5.12).

$$c_{T,F,t}\dot{B}_{F,t} + \sum_j (c^j_{T,C,t}\dot{B}^j_{C,t}) = \sum_k (c^k_{T,P,d}\dot{B}^k_{P,d}) \tag{5.10}$$

$$c_{NR,F,t}\dot{B}_{F,t} + \sum_j (c^j_{NR,C,t}\dot{B}_{C,t}) = \sum_k (c^k_{NR,P,d}\dot{B}^k_{P,d}) \tag{5.11}$$

$$c_{co2,F,t}\dot{B}_{F,t} + \sum_j (c^j_{co2,C,t}\dot{B}_{C,t} + \dot{M}^j_{co2,t}) = \sum_k (c^k_{co2,P,d}\dot{B}^k_{P,d}) \tag{5.12}$$

Next, the distribution stage considers the consumption of non-renewable resources to transport the biofuels from the process plant to the vehicles fuel tank, as shown in Table 5.5. Since this stage is analogous to the supply stage, the cost balance equations are similar to Eqs. (5.7), (5.8) and (5.9), except for the fact that the main substance consumed corresponds to products (vehicle fuels), instead of raw materials.

At last, the end-use stage comprises the conversion of biofuels into transportation services. Since the transportation exergy efficiency (η_{ex}) varies for each technology, the exergy costs balances are evaluated separately for each biofuel as in Eqs. (5.13), (5.14) and (5.15).

$$c^k_{T,f} = \frac{c^k_{T,e}}{\eta^k_{ex}} \tag{5.13}$$

$$c^k_{NR,f} = \frac{c^k_{NR,e}}{\eta^k_{ex}} \tag{5.14}$$

$$c^k_{co2,f} = \frac{c^k_{co2,e}}{\eta^k_{ex}} \tag{5.15}$$

In order to compare the performance of different biorefinery configurations, a mean average of the total and non-renewable unit exergy costs and specific CO_2 emissions for the transportation service can be determined as described in Eqs. (5.16), (5.17) and (5.18).

$$\bar{c}_T = \frac{\sum_k c^k_{T,f} B^k_{S,f}}{\sum_k B^k_{S,f}} \tag{5.16}$$

$$\bar{c}_{NR} = \frac{\sum_k c^k_{NR,f} B^k_{S,f}}{\sum_k B^k_{S,f}} \tag{5.17}$$

$$\bar{c}_{co2} = \frac{\sum_k c^k_{co2,f} B^k_{S,f}}{\sum_k B^k_{S,f}} \tag{5.18}$$

5.4 Results and discussion

Figure 5.12 shows the exergy consumption and production breakdown for each one of the units in the waste upgrade plant. It is noteworthy that the gasification unit analysis was separated into two parts, since the water gas shift process is only used for the production of biofuels. As it can be observed, the larger fraction of exergy consumption (98-76%) is related with biomass chemical exergy (vinasse, bagasse, methane and syngas) and the two highest production of irreversibilities (27% and 58%) are present in the primary units. In the biomethane via vinasse unit, the vinasse high concentration of organic material inert to anaerobic digestion represents a substantial exergy loss (50% of discarted vinasse). Furthermore, water, minerals and sludge present in the discated vinasse were not considered as products in this analysis, which could substantially increase the unit exergy efficiency (18% points). As for the gasification unit, a significant part of the exergy of the biomass has to be internally consumed in syngas production, which significantly reduces the produced gas.

Figure 5.12: Exergy consumption and production breakdown for each chemical process unit

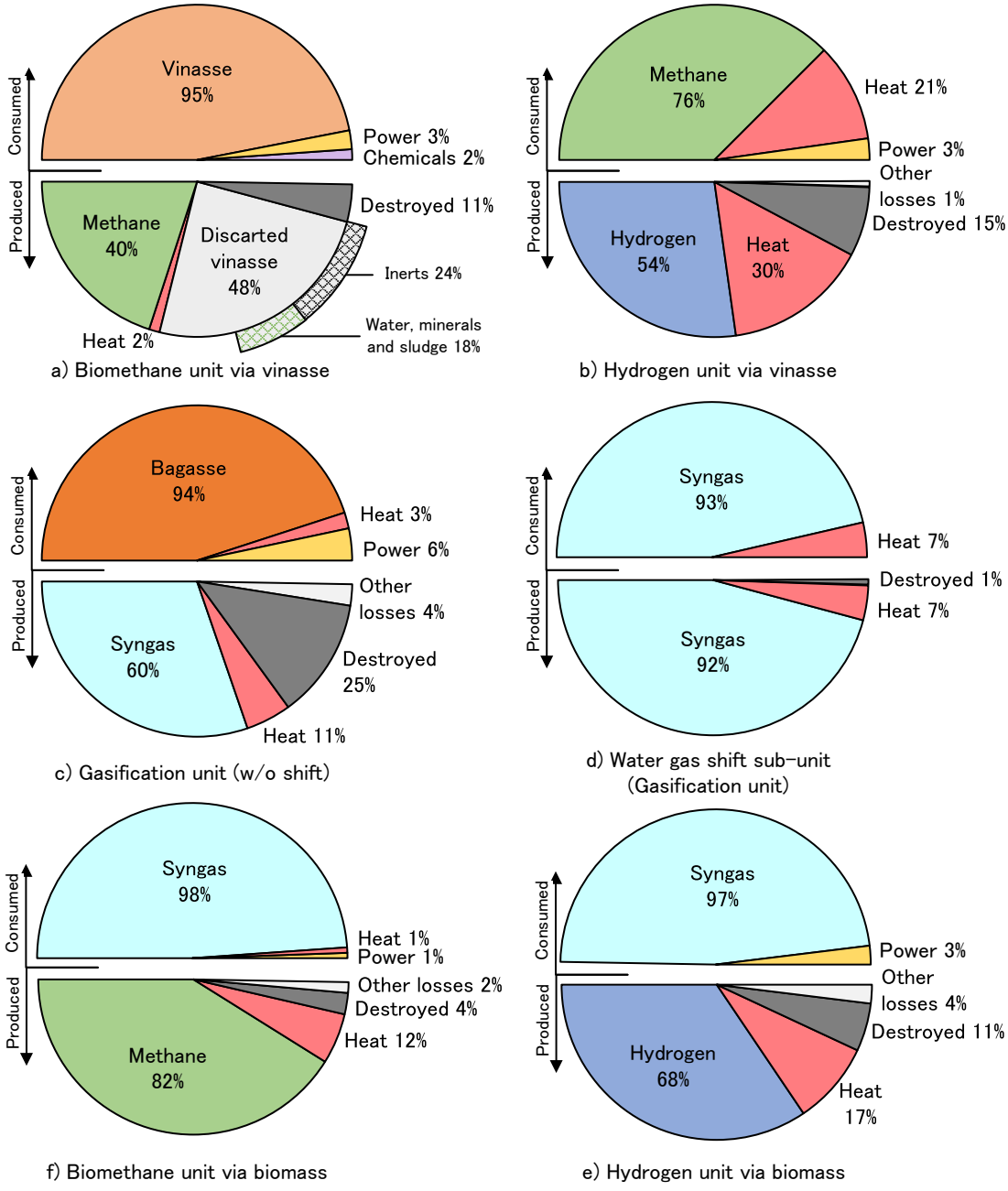

Source: [43]

The biomass-derived biomethane and hydrogen units attained the two highest exergy efficiencies, 94% and 85%, respectively. The high efficiency of the biomass biomethane unit efficiency can be attributed to lower requirements for CO_2 separation (since a portion of CO_2 is converted in the methanator), and the absence of the adsorption process. As for the hydrogen via biomass unit, there are few sources of irreversibilities, mainly related

with purge gas from purification processes and its subsequent combustion (flare), since the unit mainly consists of purification processes with low exergy consumption.

In the process units analyzed, heat appears as the second largest exergy consumption and an important side-product, especially in those with highly endothermic (gasification and steam reform) or exothermic (combustion, water gas shift and methanation) reactions. Thus, the heat recovery system efficiency can have a major impact in the overall production system efficiency. For example, although the hydrogen production units from either biogas or biomass have similar exergy efficiencies (84% and 85%, respectively), the former is much more dependent of heat at high temperatures compared with the latter. In other words, were it not for a rational use of the available waste heat, the exergy efficiency of the overall system could be compromised. Finally, in this analysis, electricity appears as a small exergy expense (1-3%) in comparison to others exergy consumption sources.

Table 5.7 summarizes the main results for each case described in Table 5.1, showing the production remarks, utilities consumption, estimated operational revenue and total transportation service available (in exergy basis). It is important to note that, some results for the SEP remain constant for all scenarios, such as sugar and ethanol production, since the design for this plant is not varied in the analysis. Thus, the conversion strategy chosen for the available residues only affects other products. For instance, the use of vinasse and surplus bagasse in case E can substantially increase the power generation compared with the base case (+13.5 MW or +320%). In fact, the electricity production could be further increased with the use of high pressure boilers or by including sugarcane straw as supplementary fuel [140, 141, 142].

The waste heat recovery system of the WUP can not provide heat and power to all processes in cases M1 and H1. Among the available energy resources for the utility systems, syngas and bagasse are the alternatives that promote the most competitive revenues, mainly due to their reduced production costs (lower cumulative energy consumption) compared with biomethane. The optimal choice between syngas and surplus bagasse is not straightforward and depends on the profile of energy demand of the chemical plant, fuel conversion efficiency and market prices [43].

Table 5.8 shows the ratio of fuel, heat and power consumed per product for each route. In the methane production case, for example, each kW of methane requires 1.23 kW of syngas or 1 kW of vinasse-derived biomethane. Thus, it is coherent to avoid biomethane combustion in order to maximize operating revenues, since more methane can be produced from biomethane compared with syngas. However, this may change according to the efficiency of the utility system and the exergy consumptions of the chemical process unit, as it can be seen for the hydrogen production case with a Rankine cycle based utility system. Although vinasse-derived biomethane could produce slightly more hydrogen, this

Table 5.7: Summary of the main consumption and production remarks per case

	Cases					
Parameter	Base	E	M1	M2	H1	H2
Main products						
Sugar (kg/s)	9	9	9	9	9	9
Hydrated ethanol (m^3/h)	20	20	20	20	20	20
Electricity (kW)	4,225	17,766	4,225	2,499	4,225	2,193
Surplus bagasse (kg/s)	7.4	-	-	-	0.11	-
Biomethane (kg/s)	-	-	0.997	1.115	-	-
Hydrogen (kg/s)	-	-	-	-	0.326	0.363
SEP utility consumption						
Bagasse (kg/s)	30.8	30.8	30.8	30.8	30.8	30.8
WUP feedstock consumption						
Bagasse (kg/s)	7.40	7.40	7.40	7.40	6.39	7.40
Vinasse (m^3/h)	276	276	276	276	276	276
WUP utility consumption						
Bagasse (kg/s)	-	-	-	-	0.89	-
Biomethane (kg/s)	-	0.369	-	-	-	-
Syngas (kg/s)	-	3.34	0.53	-	-	-
Operational revenue from waste upgrade (EUR/h)	-	401	1,278	1,378	2,706	2,889
Transportation service (MW)	12.24	16.84	15.41	15.20	18.62	18.57

Source: [45]

would require substantially more power and heat than by using syngas (see Table 5.8). Thus, even if there is a gain on product per fuel yield by prioritizing the vinasse route for hydrogen production, there is also a penalty related to the increased consumption of fuel in the utility system.

The surplus electricity produced in the SEP (4.2 MW) could be partially used in the WUP, as proposed in cases M2 and H2, promoting an increase in the biofuel production rate (11-12%) compared to the cases M1 and H1, respectively. This trade-off between products occurs due to the difference of fuel consumption in the WUP utility system for each case.

Table 5.7 also shows that the operational revenues, i.e. the difference between consumption and products market costs (Eq. (5.1)), is not directly related with the total service exergy available to the end-user. For instance, the cases in which biomethane is produced from the sugarcane residues (cases M1 and M2) offer significantly more revenues (219-

Table 5.8: Ratio of exergy consumption per product for each biofuel production units

Consumption ratio	Production route			
	Methane		Hydrogen	
	from biomethane (vinasse)	from syngas	from biomethane (vinasse)	from syngas
Fuel/product	1 $\frac{kW_{CH_4}}{kW_{CH_4}}$	1.23 $\frac{kW_{syngas}}{kW_{CH_4}}$	1.42 $\frac{kW_{CH_4}}{kW_{H_2}}$	1.43 $\frac{kW_{syngas}}{kW_{H_2}}$
Heat/product	0 $\frac{kW}{kW_{CH_4}}$	0.11 $\frac{kW}{kW_{CH_4}}$	0.38 $\frac{kW}{kW_{H_2}}$	0.12 $\frac{kW}{kW_{H_2}}$
Power/product	0 $\frac{kW}{kW_{CH_4}}$	0.01 $\frac{kW}{kW_{CH_4}}$	0.06 $\frac{kW}{kW_{H_2}}$	0.04 $\frac{kW}{kW_{H_2}}$

Source: [43]

244%) compared with the electricity production scenario (case E). However, since electric vehicles have a higher efficiency compared to those fueled by compressed natural gas, the total end-use service in case E is 9-10% higher than cases M1 and M2. Thus, a conflict of interests between biofuel producers and end-users can be foreseen in some scenarios. A possible alternative is the promotion of biofuels with a high market value and conversion efficiency, such as hydrogen, as proposed in cases H1 and H2. In these scenarios, high operational revenues and transportation service can be achieved. Thus, the co-production of electricity and hydrogen seems the best strategy among those proposed in this study.

5.4.1 Exergy analysis results

The exergy flow rate of products from the transformation stage in each case is shown in Figure 5.13. The results indicate that sugar and ethanol (hydrated and secondary) represent the major fraction of products in exergy basis for all cases (78.9-94.1%). Moreover, the residual bagasse exportation allows the base case to achieve the highest exergy flow rate of products (364.4 MW) due to the high chemical exergy associated with this energy resource. However, it is important to highlight that the residual bagasse has a limited application in the market (e.g., steam production and cogeneration systems) and may be subjected to other transformation processes. For instance, in the other cases which include a waste upgrade plant, the several irreversibilities in the conversion of residual bagasse into biofuels and electricity reduces the amount of exergy flow rate available as product. In theory, the conversion of organic substances in vinasse could outweigh this inefficiencies, but their exergy flow rate is relatively low compared with bagasse. This result is rarely seen in literature because residual bagasse is often not considered as a product or it is used to produce surplus electricity [141, 142, 101].

The production of biomethane is the alternative which delivers more exergy as fuels to

Figure 5.13: Exergy flow rate of the products of the transformation stage

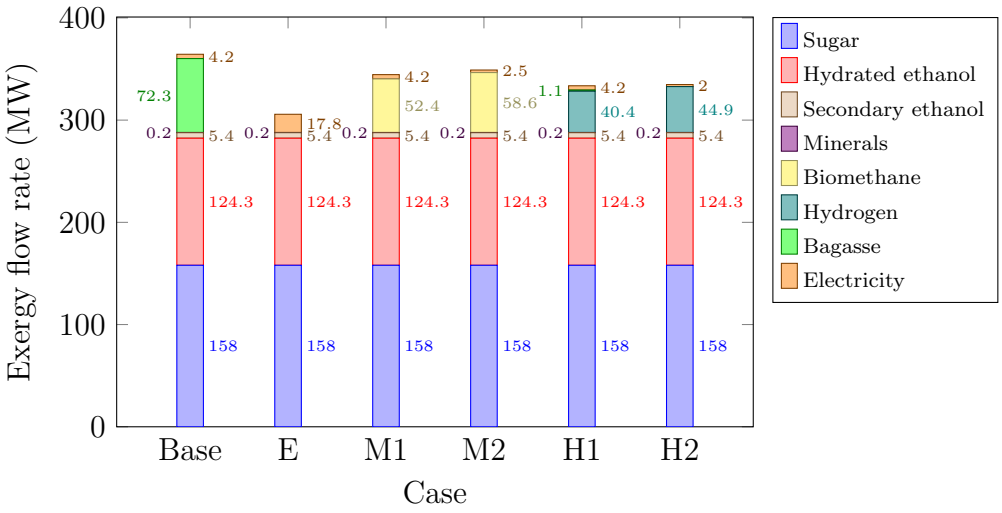

Source: [45]

the transportation sector (cases M1 and M2, 52.4 and 58.6 MW respectively), followed by hydrogen (cases H1 and H2, 43.3 and 47.8 MW respectively) and electricity (case E, 17.8 MW). The reason for the higher productivity of methane conversion is mainly attributed to the reduced number of processes involving chemical reactions (e.g., combustion, reform, water gas shift), which are key sources of irreversibilities. A similar result was also published by Piekarczyk et al. [106] in a study evaluating different routes of biofuel production (methanol, hydrogen, methane and Fischer-Tropsch fuels), which reinforce the competitive efficiency of methane production. The cases in which the WUP is able to use the surplus electricity of the SEP (M2 and H2) slightly increased (0.4-1.3%) the amount of products flow rate in exergy basis. This trade-off is a consequence of the reduction of fuel consumption in the utility systems for the WUP, as previously shown in Table 5.7.

The distribution of the exergy destruction rate among the different processes in the SEP and WUP is shown in Figure 5.14. As it can be seen, the SEP utility system is responsible for most of the exergy destruction share, since it relies on the bagasse combustion to deliver the required heat and power demands of sugar and ethanol units. Certainly, since the SEP system is not subject to optimization in the case studies, it may be possible to reduce its irreversibilities by using a optimized heat recovery system or more efficient power generation cycles [140]. In general, the processes in the SEP are responsible for the majority of the exergy destruction in the overall system, since the exergy flow rate of its streams are higher than the WUP streams. For instance, the fermentation, washing and milling processes are responsible for 6.0% to 10.0% of the overall exergy destruction. These processes are widely reported as sources of irreversibilities in sugar and ethanol plants [107, 101, 109, 143].

Figure 5.14: Exergy destruction rate from supply to transformation stage

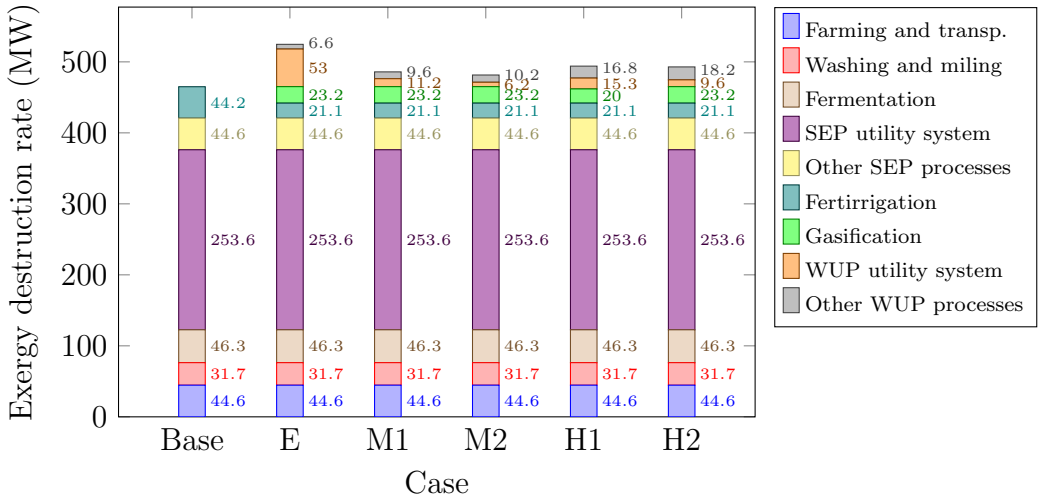

Source: [45]

A significant portion of exergy destruction (4.0-9.5%) occurs in the fertirrigation process, since the exergy of the non-converted organic substances in vinasse is discarded to the environment. In fact, a great portion of the vinasse exergy is actually attributable to organic substances of difficult conversion in anaerobic digestion (e.g., lignin). Nevertheless, the exergy destruction in fertirrigation can be substantially reduced (52.3%) through the vinasse anaerobic digestion in WUP. Other units with high exergy destruction shares are the WUP utility system, mainly due to the fuel consumption, and the gasification system, which also includes highly irreversible reactions and substantial bagasse consumption to maintain the reactor conditions. It is also noticeable that, in the biomethane and hydrogen production cases (M1, M2, H1 and H2), the WUP utility system destroys less exergy due to its lower fuel consumption compared with the standalone electricity generation case. Figure 5.14 also shows that the waste upgrade process does not necessarily reduce the overall exergy destruction, since it consumes/transforms the residual bagasse that otherwise would be sold to the market.

Improvements in the exergy efficiency of the waste upgrade plant can be foreseen for anaerobic digestion and gasification processes. For instance, the reuse of vinasse water or the exploitation of vinasse organic inerts (e.g., concentration and combustion) could significantly reduce the exergy destruction in fertirrigation. As for gasification, a significant part of the exergy of the biomass has to be internally consumed in syngas production, which significantly reduces the amount of gas produced. Higher gasification pressures may lead to reduced power consumption and, consequently, lower exergy destruction in the utility system. Other possibility is to increase the efficiency of the separation processes to reduce the amount of purged gas and increase biofuel production.

The gasification and the anaerobic digestion processes also present the high power consumption compared to other processes in the waste upgrade plant. Gasification and biomethane via vinasse units include energy intensive processes required for biomass pre-treatment (chipping and vinasse recirculation) as well as several compression steps, due to the close-to-atmospheric operating conditions. Higher gasification pressures may lead to reduced power consumption, provided that pressurized biomass injection does not offset the advantages of pressurized gasification. On the other hand, vinasse recirculation and biogas compression also consume large amounts of power. The reduction of electricity consumption in these processes can lead to a smaller utility system and lower internal fuel consumption, increasing the overall exergy efficiency and revenues.

5.4.2 Unit exergy costs and specific CO_2 emissions

The unit exergy costs and specific CO_2 emissions of biofuels and electricity at the end of the transformation stage for each case are presented in Figure 5.15. A detailed description of the exergy flow rate, unit exergy costs and specific CO_2 emissions for the waste upgrade cases can be consulted in the Appendix A.

The total unit exergy costs for ethanol presented in Figure 5.15 are close to values reported previously by Palacios-Bereche et al. [101] (2.04-2.39 kJ/kJ) and Flórez-Orrego et al. [107] (3.06 kJ/kJ). As it may be expected, ethanol is the biofuel that presents the lowest unit exergy costs and specific CO_2 emission since its production comprises of less energy conversion processes. The ethanol unit exergy costs and specific CO_2 emissions for cases with a waste upgrade plant (E, M1, M2, H1 and H2) are reduced in 6-7%, since a portion of the exergy costs and specific CO_2 emissions is now allocated to biogas due to the anaerobic digestion of vinasse. Thus, this process reduces the unit exergy costs and specific CO_2 emissions of vinasse sent for fertirrigation and, consequently, decreases the exergy consumption in sugarcane farming.

According to Figure 5.15, the unit exergy costs and specific CO_2 emissions for electricity generation have the highest values and variances. This can be explained by the close dependency between the efficiency of electricity generation and the profile of energy demand of the chemical process plant. For instance, the sole production of electricity causes a significant increase in the unit exergy costs and specific CO_2 emissions due to the higher quantity of fuel consumed in the utility systems. However, although the exergy indicators are better for the co-production of biofuels due to the waste heat recovery system, the amount of electricity exported to the market is quite lower (41-48%) compared with the base case, as shown previously in Table 5.7. Therefore, the extent of the electricity generated (amount) and its exergy indicators (performance) may be conflicting objectives in the optimization of the electricity production for some biorefinery configu-

Figure 5.15: Unit exergy costs and specific CO_2 emissions of the main products of the transformation stage for each case study

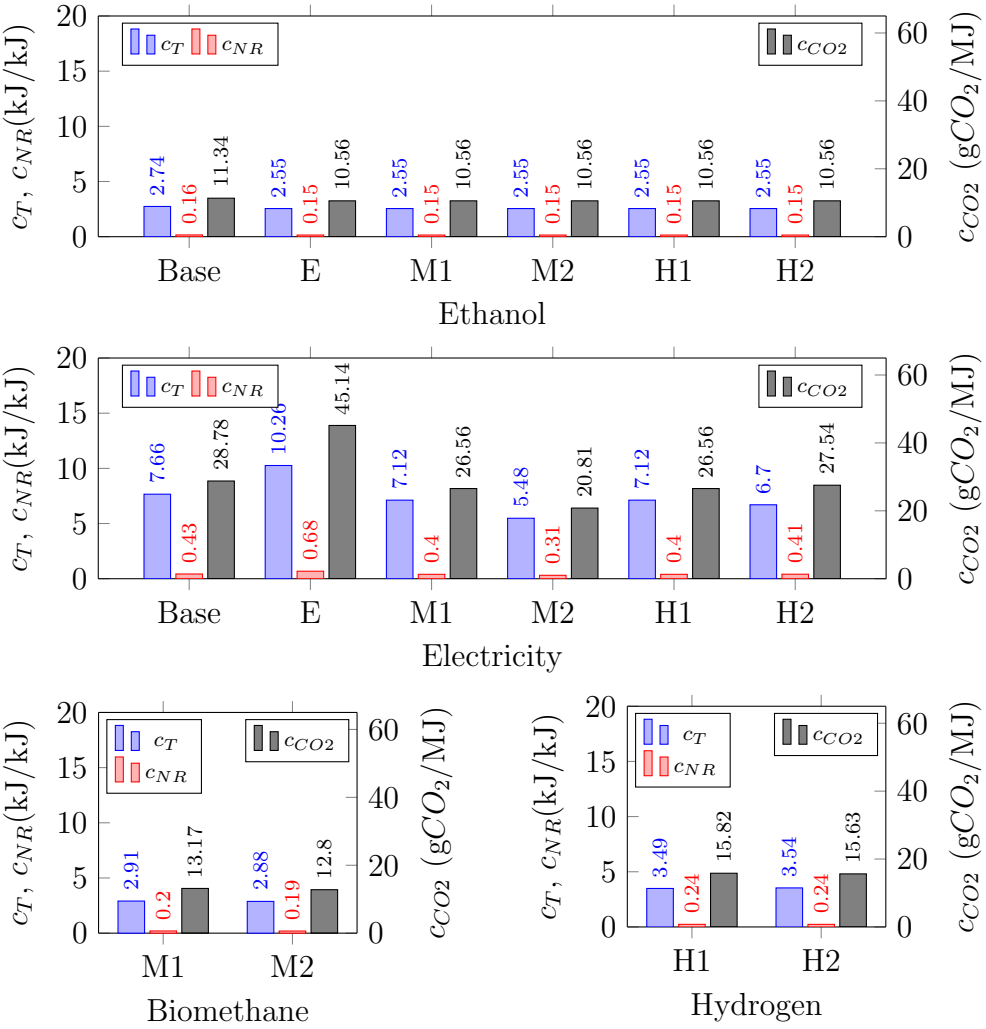

Source: [45]

rations. These results denote that optimal solutions for decarbonization and reduction of fossil fuel consumption in the transportation service are not strictly related with higher shares of electricity production from biomass or wastes.

Figure 5.15 also reveals that methane is the waste-derived product that has the lowest unit exergy costs and specific CO_2 emissions in the transformation stage, due to its higher production yield (as presented in Figure 5.13). It is also worthy to notice that the share of non-renewable unit exergy cost out of the total unit exergy cost for all fuels derived from sugarcane is almost negligible, especially when compared with the results for petroleum-derived fuels ($c_{NR}/c_T > 99\%$) [107]. Furthermore, the results for the non-renewable unit exergy costs are in agreement with the thermo-ecology costs reported by Piekarcyk et al. [106] for hydrogen and synthetic natural gas production from lignocellulosic biomass (0.232 kJ/kJ and 0.135 kJ/kJ, respectively, for the best scenario).

The unit exergy costs and specific CO_2 emissions for the end-use stage are presented in Figure 5.16, while data for fossil fuel alternatives in the Brazilian context, as reported by Flórez-Orrego et al. [108], is reproduced in Table 5.9 for the sake of comparison. The results denote that biofuels and electricity have a significantly low non-renewable consumption and CO_2 emissions compared with petroleum derivatives, despite the higher total unit exergy costs. For instance, biomethane and hydrogen have 3.1-4.7 times lower non-renewable unit exergy costs and specific CO_2 emissions compared with their fossil correspondents, but their total unit exergy costs are 1.7 times higher. Furthermore, electricity is the fuel option with the lowest value of these indicators, followed by hydrogen and ethanol, differently from that observed in Figure 5.15 for the transformation stage. Thus, the performance of electric vehicles is able to outweigh inefficiencies in the power generation and overcome the other options presented in this research. Therefore, apart from the cumulative consumption in the transformation stage, the analysis of biofuel production options has to include the efficiency in the end-use stage in order to avoid misleading conclusions.

Table 5.9: Unit exergy costs and specific CO_2 emissions for petroleum derivatives in the Brazilian context

Fuel	c_T [kJ/kJ]	c_{NR} [kJ/kJ]	c_{CO2} [gCO_2/MJ]
Gasoline C	24.71	15.84	1,191.30
Diesel B05	11.00	10.47	728.16
Hydrogen	9.99	9.59	471.79
Natural gas	19.44	18.67	1045.23

Source: [108, 45]

The results for the weighted average of unit exergy costs and specific CO_2 emissions for the transportation service, presented in Figure 5.17, indicate that the best overall performance is achieved by the co-production of electricity and hydrogen in case H1. As previously discussed, this shift in the performance indicators is explained by the difference in the end-use conversion efficiency for the fuels analyzed in this study. In the best case, a reduction of 13-12% in the unit exergy costs and specific CO_2 emissions compared with the base case can be achieved. However, the production of methane as biofuel (cases M1 and M2) causes an increase in the unit exergy costs and specific CO_2 emissions due to the reduced efficiency of compressed natural gas vehicles and the non-renewable consumption in the fuel distribution. In this way, the cases producing biofuel with relative high end-use efficiency, such as electricity and hydrogen, may have better exergy performance in the overall analysis and lower CO_2 emissions.

Figure 5.16: Unit exergy costs and specific CO_2 emissions of the transportation service for each fuel and case study

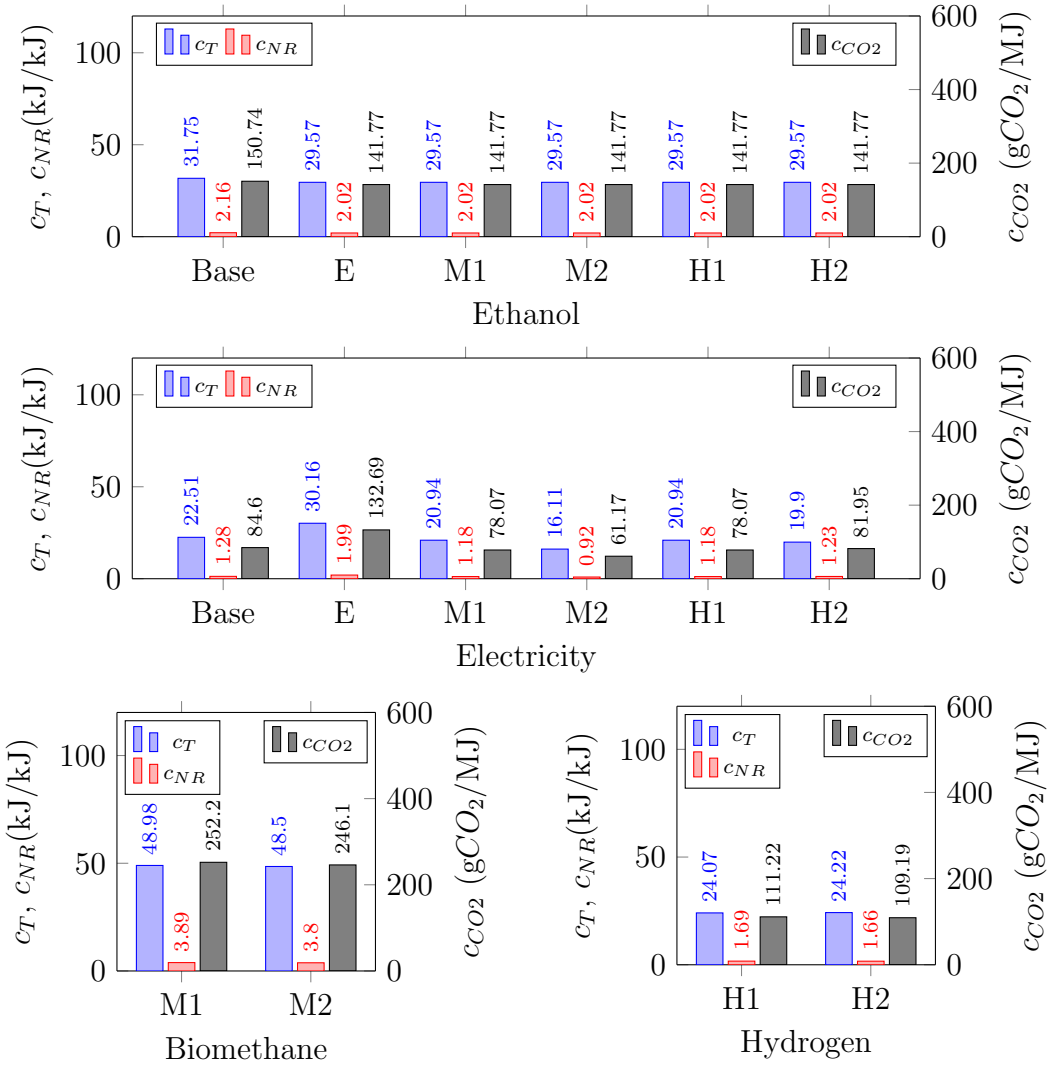

Source: [45]

Figure 5.17: Weighted average unit exergy costs and specific CO_2 emissions for the transportation service

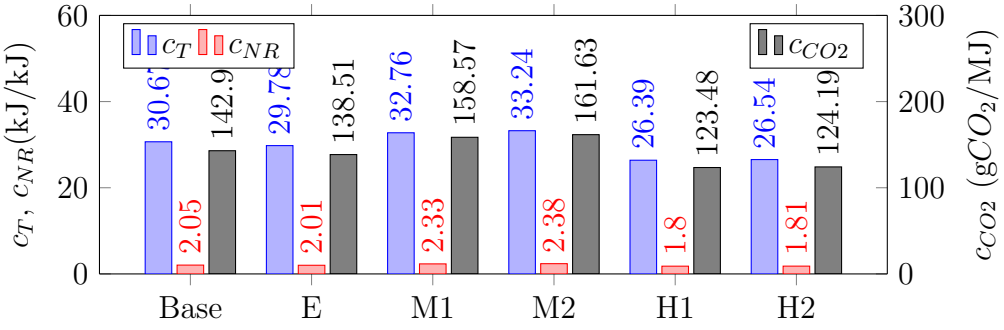

Source: [45]

5.5 Concluding remarks

In this chapter, an analysis of the unit exergy costs and specific CO_2 emissions of the production and end-use of biofuel and electricity from sugarcane industry residues (e.g., vinasse and bagasse) was presented. A base case (consisting in a sugar mill with an annexed distillery) and other five possible production cases, in which the different biofuel products (methane, hydrogen or electricity) are produced from sugarcane residues, were investigated. The utility units for the waste upgrade plant were optimized based on the minimization of production costs and energy requirements.

The results indicate that, in the best scenario, the production of biofuels from sugarcane wastes significantly increases (38-52%) the amount of transportation service compared with the base case. However, the inclusion of a waste upgrade plant does not necessarily decrease the exergy destruction in the transformation stage (37-135% increase), especially if residual bagasse is considered as a byproduct. For the cases in which waste upgrade is employed, the production of methane delivers more products to the market (52.4-58.6 MW) with lower unit exergy costs and specific CO_2 emissions for the transformation stage (20-260% lower than electricity and hydrogen). However, the co-production of hydrogen and electricity may attain better technical and environmental indicators considering the end-use stage (60-322% lower than biomethane) due to their higher efficiency in fuel conversion to transportation service. Furthermore, it is estimated that the hydrogen production offers higher operational revenues (2706-2889 EUR/h), since its market prices are more elevated compared with electricity and methane.

In comparison with petroleum derivatives, the biofuels presented 1.7 times higher total unit exergy costs and 3.1-4.7 times lower non-renewable unit exergy costs and specific CO_2 emissions. Thus, the production and usage of gaseous biofuels generate more irreversibility at the expense of the consumption of mostly renewable exergy sources with a lower indirect carbon footprint. The exergy destruction results indicated that further improvements can be obtained by improving the utility system efficiencies and/or by reducing the energy consumption in various chemical processes (e.g., anaerobic digestion and gasification). Moreover, since anaerobic digestion cannot fully convert the exergy of the vinasse, other processes must be used to reduce losses in wastewater disposal (e.g., concentration, solid separation, etc.).

6 Design of fuel cell systems for biogas conversion

In the previous chapter, the exergoeconomic analysis of biogas conversion routes indicated that the co-production of hydrogen and electricity can minimize costs, emissions and boost operating revenues. Thus, improving the efficiency of biogas conversion into hydrogen and electricity may play a major role in promoting biogas adoption as an renewable energy source. In this context, solid oxide fuel cells (SOFC) have been promoted as an alternative to convert biogas into electricity and heat with high efficiency. However, few studies have considered the use of the anode exhaust gas to co-produce green hydrogen together with electricity and heat, which could increase the performance and profitability of these systems. In other words, the influence of design variables in the optimization of revenues and efficiency has seldom been studied for these novel cogeneration systems.

In order to answer this knowledge gap, this chapter proposes a new approach to model SOFC with direct internal reforming to produce power, hydrogen and heat. In addition, a multi-objective optimization problem using the NSGA-II algorithm is proposed to evaluate optimal solutions for systems producing hydrogen and electricity from biogas. The energy integration is optimized based on the pinch analysis and a mixed-integer linear optimization routine is used to attain an efficient heat recovery system with minimal number of heat exchanger units.

The results indicate that for a SOFC system with hydrogen separation is capable of reaching exergy efficiencies between 57% and 69% depending on the methane content of biogas. Hydrogen separation reduces the amount of fuel that has to be burned, which leads to less destruction of exergy in multiple processes (e.g., mixers, burners and heat exchangers). However, this design change also diminishes the amount of heat delivered by the system, which may negatively affect the energy integration with anaerobic digestion. In addition, major performance improvements can be achieved by optimizing the hydrogen recovery of the pressure swing adsorption and the SOFC operating temperature.

Hydrogen production with a fuel cell downstream is able to achieve the highest exergy efficiencies (65-66%) and a drastic improvement in net present value (1346%) compared with sole power generation. Despite the additional equipment, the investment costs are

estimated to be quite similar (12% increase) to conventional steam reforming systems and the levelized cost of hydrogen is very competitive (2.27 USD/kgH_2).

6.1 Context

In order to promote the decarbonization of energy and transportation sectors, the development and optimization of sustainable solutions is an ongoing research topic. In the last years, several alternatives have been proposed for converting biomass into different products, for example, electricity [46, 144], ethanol [145, 101], methanol [146, 147], ammonia [148, 149], synthetic natural gas [104, 43], among others. The complexity and diversity of the options available for biomass makes it one of the most challenging energy sources in the technical and economic perspectives. The optimal solution for biomass conversion into products may vary for each country and scenario, as well as for each particular type of biomass. In the case of biomass wastes, a promising alternative is to produce electricity and biofuels, such as natural gas and hydrogen. This approach may reduce carbon dioxide emissions derived from waste management, energy production and fuel conversion, creating new economic opportunities based on a sustainable interaction with the environment [45]. In this context, the efficient conversion of biogas derived from the anaerobic digestion of organic wastes is a major opportunity for technological development.

In recent studies, the use of solid oxide fuel cells in biogas conversion systems has been proposed as an efficient solution for renewable power generation. Since fuel cell systems can be complex and expensive, the effect of different design choices has been the subject of discussion in many studies. In general, these studies have focused mainly on systems that work with natural gas. For instance, Palazzi, et al. [150] proposed a methodology to optimize solid oxide fuel cell (SOFC) systems using the principles of energy integration combined with evolutionary algorithms. They observed that an optimized design for a SOFC system is able to achieve energy efficiencies between 34% and 44%. Becker, et al. [57] indicated that a conventional SOFC system could attain higher energy efficiencies (83.5-86.1%) by including a separation step to export hydrogen as a byproduct. More recently, Pérez-Fortes, et al. [151] reported energy efficiencies as high as 81.4% for a SOFC system co-producing hydrogen, electricity and heat under different operating conditions. It is important to highlight that the efficiency values from the aforementioned studies [57, 150, 151] are calculated based on energy. Therefore, they do not take into account the limits derived from the second law of thermodynamics.

The utilization of biogas as a fuel imposes some additional constraints for the design of SOFC systems due to the presence of contaminants and carbon dioxide. For instance, Van Herle, et al. [152] examined different technologies for biogas reforming and operating

variables in order to estimate their impact on the system efficiency. Moreover, Curletti et al. [153] demonstrated several possibilities for biogas-SOFC systems including carbon capture; and determined optimal design parameters using a sophisticated optimization routine. MosayebNezhad, et al. [154] extended the analysis of energy integration to include the energy demands of a wastewater treatment plant. Another remarkable example is the study of Gandiglio et al. [155] which presented promising results for a SOFC plant operating with biogas produced from a wastewater treatment facility

In general, these previous studies have reported energy efficiencies as high as 50% despite the high concentration of carbon dioxide in biogas composition. Thus, despite the relative high investment costs, the economic assessments of biogas-fed SOFC systems indicate a positive net gain which may surpass traditional energy conversion systems (e.g., microturbines, engines, boilers) [156]. Although there are examples of studies evaluating the usage of biogas in fuel cell systems, most mathematical models in use neglect variations of fuel concentration and temperature along the fuel cells. Furthermore, simulations validated for different mixtures of hydrogen, water and carbon dioxide are scarce, despite the high concentration of these components in the reformed biogas. These factors can significantly impact the performance of high temperature fuel cells [67]. In addition, the inclusion of a hydrogen separation step in SOFC systems that work with biogas has rarely been discussed in detail.

Sustainable solutions for hydrogen production have been an ongoing research topic due to its prospects as a future energy carrier. Among the several possible routes for green hydrogen, biogas has also been proposed as an alternative feedstock since it shares similarities with natural gas, from which most hydrogen is produced today. For example, Marcoberardino et al. [157] evaluated the production of green hydrogen from biogas using the steam reforming or autothermal reform combined with a pressure swing adsorption separation. The levelized cost of hydrogen was estimated as 4.2 EUR/kg in the best scenario, a value close to the expected cost for electrolysis derived hydrogen (3.83-4.95 USD/kg) [158]. Since electricity can be a significant operational cost or a valuable product, some researchers have also proposed hybrid solutions using fuel cells to deliver power alongside hydrogen refuelling stations [57, 151]. For instance, Minutillo et al. [159] have estimated a maximum exergy efficiency of 59% for some hybrid systems, a possible 18% increase compared with biogas-fed SOFC systems.

However, there seems to be a lack of studies focused on the economic evaluation of these hybrid systems designs for power and hydrogen production using biogas as feedstock [45]. Although these systems may have higher complexity and investment costs, the additional revenues and relatively lower competitiveness of green hydrogen may overcome the aforementioned downsides [160]. Moreover, since these hybrid systems will certainly

present different characteristics, optimal solutions for their design and operation may still to be determined. Thus, this study aims to provide a new insight by determining optimal solutions for a biogas conversion system using solid oxide fuel cells producing hydrogen and electricity.

6.2 Process description

The proposed system consists of a small centralized plant producing an average of 100 Nm^3/h of biogas [2], assuming that a gas processing unit removed the fuel impurities. Two conventional designs, a solid oxide fuel cell (SOFC) system (Figure 6.1) and a steam methane reforming system (Figure 6.2), are compared with two proposed hybrid solutions, as described in Figure 6.3 and 6.4, for biogas conversion into electricity and hydrogen. As it can be observed, the two hybrid systems mainly differ in the order of each process: power generation and hydrogen separation. In the first arrangement, named as SOFC-H_2, the power conversion is performed first in order to partially substitute the high pressure steam reforming reactor. The SOFC system is designed to use only a fraction of fuel, leaving most of the hydrogen to be separated in the downstream PSA system. On the other hand, the second design named H_2-SOFC uses a conventional steam methane reforming system to produce hydrogen from biogas, while the purge gas from hydrogen separation is partially used for power generation.

Figure 6.1: Flowsheet of the SOFC system

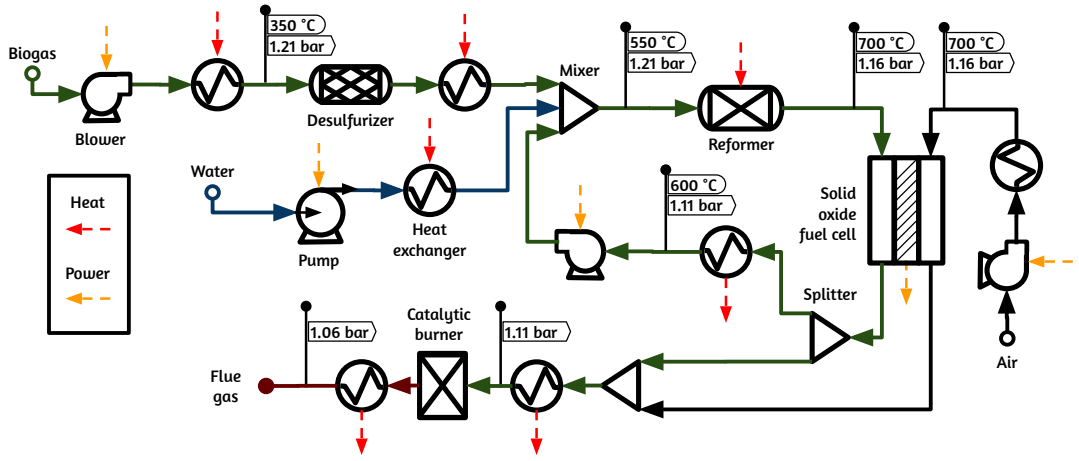

Source: [71]

In all cases, the heat exchanger network is designed by a mixed-integer linear programming problem (MILP), as proposed by Papoulias and Grossmann [76], which minimizes the number of units necessary to attain the minimal energy requirement according to the pinch analysis. Thus, a total of four systems are evaluated in this study, two hybrid sys-

Figure 6.2: Flowsheet of the H_2 system

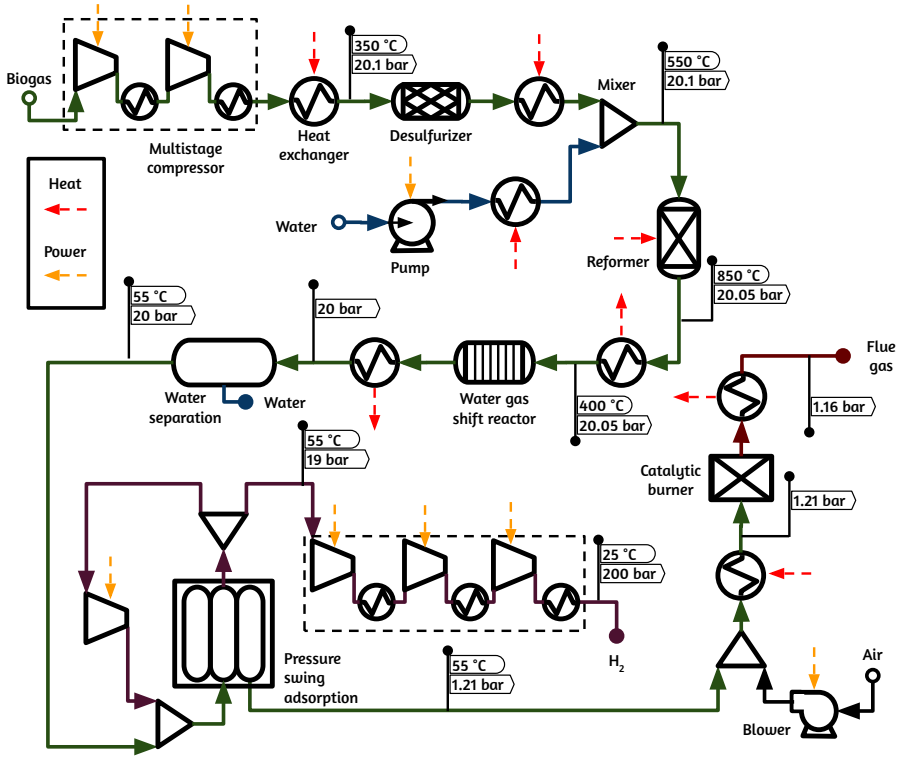

Source: [71]

Figure 6.3: Flowsheet of the SOFC-H_2 system

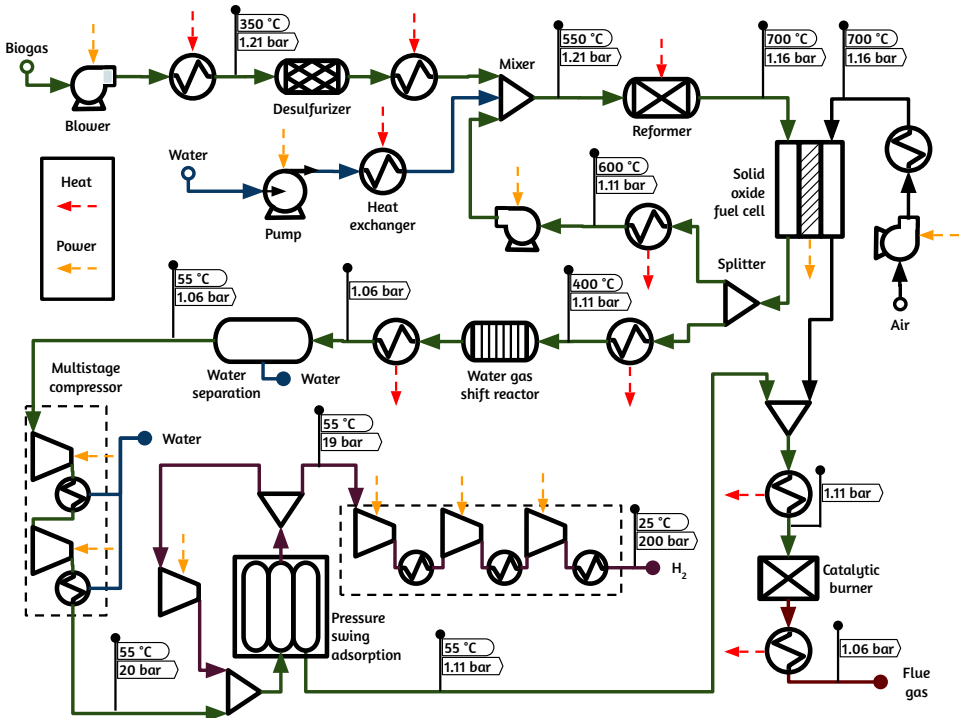

Source: [71]

Figure 6.4: Flowsheet of the H_2-SOFC system

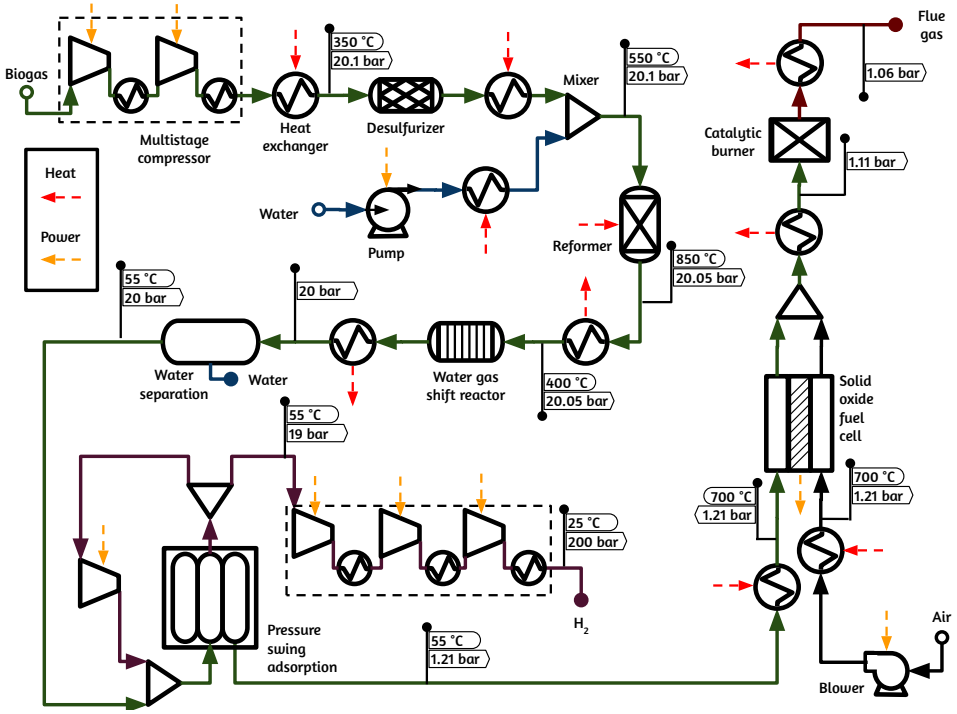

Source: [71]

tems (SOFC-H_2 and H_2-SOFC) and two single systems (SOFC and H_2) for comparison. The modelling assumptions for all systems evaluated in this study are summarized in Table 6.1. The details of the power generation and hydrogen production sections for each system are described in the following subsections.

6.2.1 Power generation sections

In order to increase hydrogen concentration in the fuel cell inlet, biogas may be partially reformed from 550 °C to 700 °C using an external source of heat. This theoretically reduces the reactor size and the minimal steam to carbon ratio compared with adiabatic pre-reformers, since the high temperature favors the reaction rate and inhibits the soot formation [152]. The inflow rate of steam is controlled to attain a minimal ratio of 1.8 mol of steam per mol of carbon in the reformer inlet, since water can also be supplied by the recycle of anode off-gas. Moreover, the outlet gas composition is assumed to be close to the chemical equilibrium, using a fixed value of temperature approach (15 °C below outlet temperature).

The solid oxide fuel cells are assumed to be planar, anode supported and arranged in stacks with co-current flow of fuel and air, a flow pattern which simplifies the model solution. The materials and dimensions are specified based on experimental data published by Jiang and Virkar [161], from which the model was calibrated and validated. A detailed

Table 6.1: Process modelling assumptions

Parameter	Value
Efficiency of pumps and compressors (%)	70
Efficiency of anode recycle compressor (%)	50
Heat loss of SOFC (% fuel LHV)	2
Heat loss of catalytic burner (% fuel LHV)	2
SOFC and reactors pressure drop (kPa)	5
PSA pressure drop (kPa)	100
Steam reforming conversion (% inlet CH_4) - SOFC case	5
Steam reforming conversion (% inlet CH_4) - other cases	Equilibrium
Anode recycle ratio - SOFC	0.5
Anode recycle ratio - other cases	0.0
Water-gas shift conversion (% inlet CO)	Equilibrium
Hydrogen recovery of PSA (% inlet H_2)	75
H_2 inlet concentration for PSA (% molar)	74
Minimal temperature for heat recovery (°C)	T_{cond}+30 °C
Global temperature approach (°C)	20

Source: [71]

description of these assumptions is provided in the following sections. The SOFC is dimensioned based on the design values of current density (j) and fuel utilization efficiency (FU), which varies depending on the system. For instance, in the SOFC case, the FU is kept at a high value range (60-80%) to avoid excessive losses in the catalytic burner. On the other hand, in the SOFC-H_2 system, the fuel utilization efficiency is reduced to avoid low concentration of hydrogen in the downstream separation system.

As previously mentioned, the SOFC also partially converts methane into hydrogen along the anode of the fuel cell, which allows a significant reduction in size of the external reformer. The electricity produced by the fuel cells is converted by a power inverter into AC current with an assumed efficiency of 95%. Moreover, the percent of theoretical air in the fuel cell system is controlled to maintain a maximum temperature difference in the fuel cell stacks (<200 K) and a maximum temperature of 800 °C[152].

6.2.2 Hydrogen production sections

Methane in biogas is converted into hydrogen using the steam reforming reaction, which may be performed at high pressures (H_2 and H_2-SOFC cases) or close to atmospheric pressures (SOFC and SOFC-H_2 cases) depending on the system design. Moreover, the steam

to carbon ratio may also vary for each case in order to attain a good compromise between hydrogen production and energy demand for steam reforming reactions [58]. Anyway, the reformate gas produced by the fuel cell anode or an external reactor contains a significant concentration of carbon monoxide and water. In order to maximize the hydrogen separation efficiency, carbon monoxide is partially converted in a high temperature water gas shift reactor (400-450 °C), which is followed by water separation via condensation. If the dry reformate mixture is not at high pressure levels (20 bar), such as in the SOFC-H_2 case, a multistage compression is carried to allow hydrogen separation using a PSA system.

The pressure swing adsorption system is based on a 4 bed Batta cycle with 75% of hydrogen recovery for high purity hydrogen (99.999% H_2), as reported by Papadias et al. [162] and NREL [163]. Since biogas has a high concentration of carbon dioxide, a portion of pure hydrogen is recycled to attain a minimal inlet concentration of 74% molar [163]. Next, the non-recycled portion of hydrogen is compressed to 200 bar for storage in high pressure vessels, while the purge gas is directed to the fuel cell (H_2-SOFC system) or catalytic burner (H_2 system).

6.3 Modelling details

This research developed a thermodynamic model using the Julia programming language in order to reduce computational time necessary to compute the results. The 'DifferentialEquations.jl' suite [164] was used to solve the ordinary differential equations. The CoolProp library [165], NASA Gleen coefficients [166] and empirical correlations proposed by Fuller, et al. [167, 168, 169] were implemented to determine properties of pure fluids, ideal gas mixtures and binary diffusivity, respectively. The exergy analysis uses the specific chemical exergies published by Szargut [81]. Moreover, the heat exchanger network with a minimal energy requirement is determined by the solution of a linear programming problem [76]. The JuMP modelling language [170] and the GLPK package [171] were employed to solve the optimization problem.

6.3.1 Solid oxide fuel cell model

In short, the model consists of two 1-D differential equations for mass transport (flow channels and porous diffusion) and a set of algebraic equations to estimate the average voltage of the fuel cells. In this study, the methods proposed by Aguiar, et al. [69] for a planar fuel cell with internal reforming are simplified and extended with the diffusion equations proposed by Bao, et al. [172]. Figure 6.5 illustrates the mathematical modelling of the solid oxide fuel cells.

Figure 6.5: Coordinates and boundary conditions for the fuel cell model

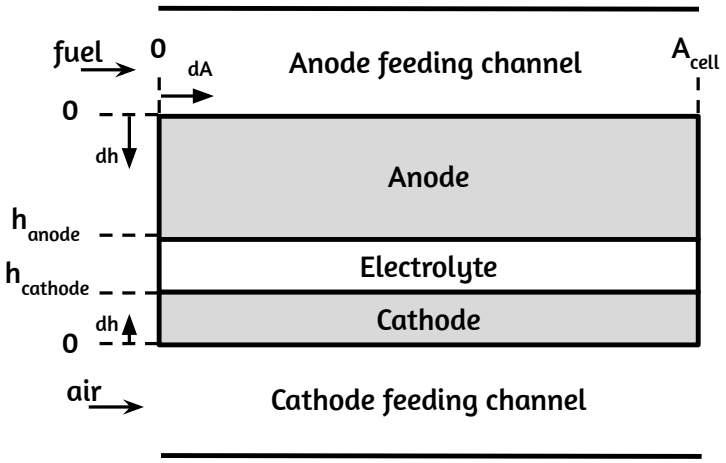

Source: [173]

The differential equation for diffusive transport estimates the molar fraction (x_i) and flux (J_i) of reactants along the porous electrode thickness (coordinate "h"), taking into account the reactions of water gas shift (WGS) and electrochemical oxidation (EOXY). Next, a set of equations estimates a local cell voltage (V) for an average current density (j), which is fixed along the fuel cell stack to avoid numerous iterations. Finally, the differential equation for the feeding channel includes the steam methane reforming (SMR) and calculates the molar flow rate (n) and temperature of reactants (T) along the cell area (coordinate "A"). It is important to highlight that only one type of mass transport is considered to be predominant for each coordinate.

In order to simplify the problem, the diffusion model uses an adapted version of the Stefan-Maxwell diffusion proposed by Bao, et al. [172] and neglects the pressure drop along the porous electrodes. In addition, the carbon monoxide oxidation is neglected as a simplification. Eqs. (6.1) and (6.2) describe the differential equations that determine the molar fractions (x_i) and flux (J_i), respectively. This problem has fixed boundary conditions in the electrode surface (h = 0) for the molar fractions and in the triple phase boundary (h = $h_{electrode}$) for the molar fluxes, as shown respectively in Eqs. (6.3) and (6.4). Furthermore, the bulk concentrations in Eq. (6.3) are estimated based on the molar flow rate ($\dot{n}_i$) in the fuel cell channels.

$$\frac{dx_i}{dh} = \frac{RT}{P} \sum_{j=1, j\neq i}^{n} \frac{x_j J_i - x_j J_i}{D_{ij,eff}} \tag{6.1}$$

$$\frac{dJ_i}{dh} = \nu_{i,wgs} r_{wgs} \tag{6.2}$$

$$x_i\big|_{h=0} = x_{i,bulk} = \frac{\dot{n}_i}{\sum \dot{n}_i} \tag{6.3}$$

$$J_i\big|_{h=h_{electrode}} = \nu_{i,eoxy} r_{eoxy} \tag{6.4}$$

In which,

$$D_{ij,eff} = \frac{\epsilon}{2\tau}\left(\frac{1}{1/D_{ij} + 1/D_{iM}} + \frac{1}{1/D_{ij} + 1/D_{jM}}\right) \tag{6.5}$$

$$D_{ij} = \frac{0.0143 T^{1.75}}{P M_{ij}^{0.5}\left[\left(\sum D_{v,i}\right)^{1/3} + \left(\sum D_{v,j}\right)^{1/3}\right]^2} \tag{6.6}$$

$$M_{ij} = 2\left[\frac{1}{M_i} + \frac{1}{M_j}\right]^{-1} \tag{6.7}$$

$$D_{iM} = \frac{2 r_p}{3}\sqrt{\frac{8RT}{\pi M_i}} \tag{6.8}$$

$$r_{wgs} = 0.0171 exp\left(\frac{-103191}{RT}\right)\left(x_{H_2O} x_{CO} - \frac{x_{H_2} x_{CO_2}}{K_{eq,wgs}}\right) P^2 \tag{6.9}$$

$$K_{eq,wgs} = exp\left(-0.2935 Z^3 + 0.635 Z^2 + 4.1788 Z + 0.3169\right) \tag{6.10}$$

$$Z = \frac{1000}{T} - 1 \tag{6.11}$$

The effective ($D_{ij,eff}$), binary (D_{ij}) and Knudsen (D_{iM}) diffusivities are calculated by using the Eq. (6.5) [172], Eqs. (6.6)-(6.7) [167] and Eq. (6.8) [174], respectively. The values of molecular weight (M [g/mol]) and diffusion volume (D_v) of species reported by Refs. [166] and [169] were assumed in this model. In addition, the Eqs. (6.9)-(6.11) [175] determine the water gas shift reaction rate (r_{wgs}). Table 6.2 shows the cell dimensions assumed in this model, which are based on experiments reported by Jiang and Virkar [161].

The local voltage (V) of the fuel cells is estimated based on the open current voltage (V_0) and overpotential losses (η), as described in Eqs. (6.12)-(6.17). The set of equations suppose that the activation overpotentials (η_{act}) in cathode and anode can be estimated by one Butler-Volmer equation, as represented in Eq. (6.14). Moreover, a linear approximation using the Tafel equation [66] with data reported by Jiang and Virkar [161] calibrates the exchange current density (j_0) value. The ohmic overpotential (η_{ohmic}) is determined using the conductivity (α) and dimensions of the cell anode, cathode and electrolyte [69],

Table 6.2: Cell dimensions

Parameter	Value	Source
Anode thickness (h_{anode})	1.1 mm	[161]
Cathode thickness ($h_{cathode}$)	20 μm	[161]
Electrolyte thickness ($h_{electrolyte}$)	10 μm	[161]
Porosity (ϵ)	0.54	[161]
Tortuosity (τ)	5.4	Fitted
Mean pore radius (r_p)	0.5 μm	[161]

Source: [173]

as shown in Eq. (6.15) and Table 6.3. On the other hand, the concentration overpotential (η_{conc}) is separated into two types, described in Eqs. (6.16) and (6.17), in order to properly account for variations in fuel and air concentrations [66].

$$V = V^0 - \eta_{act} - \eta_{ohmic} - \eta_{conc.act} - \eta_{conc.Nernst} \tag{6.12}$$

In which,

$$V^0 = \frac{G^0_{H_2} + 0.5G^0_{O_2} - G^0_{H_2O}}{2F} \tag{6.13}$$

$$j = j_0 \left(exp\left(\frac{2\alpha F}{RT}\eta_{act}\right) - exp\left(\frac{2(1-\alpha)F}{RT}\eta_{act}\right)\right) \tag{6.14}$$

$$\eta_{ohmic} = j\left(\frac{h_{electrolyte}}{\sigma_{electrolyte}} + \frac{h_{anode}}{\sigma_{anode}} + \frac{h_{cathode}}{\sigma_{cathode}}\right) \tag{6.15}$$

$$\eta_{conc,act} = \frac{RT}{2\alpha F} ln\left(\frac{x_{H_2}\big|_{h=0}}{x_{H_2}\big|_{h=h_{anode}}}\left(\frac{x_{O_2}\big|_{h=0}}{x_{O_2}\big|_{h=h_{cathode}}}\right)^{0.5}\right) \tag{6.16}$$

$$\eta_{conc,Nernst} = \frac{RT}{2F}\left[ln\left(\frac{x_{H_2O}\big|_{h=h_{anode}}}{x_{H_2}\big|_{h=h_{anode}}(x_{O_2}|_{h=h_{cathode}})^{0.5}}\left(\frac{P_0}{P_{cathode}}\right)^{0.5}\right)\right] \tag{6.17}$$

A simple molar balance, as shown in Eq. (6.18), calculates the molar flow rate (n) in the fuel cell channels assuming that there is no significant variation of gas composition along the channel height. The differential equation employs the empirical correlations proposed by Achenbach and Riensche [176] and modified by Aguiar et al. [69] to estimate the reaction rate of steam reforming. In addition, the Eq. (6.18) estimates the reaction rates of the water gas shift and electrochemical reactions based on the molar flux results derived from Eqs. (6.1) and (6.2).

$$\frac{dn_i}{dA} = \nu_{i,smr} r_{smr} + J_i\big|_{h=0} \tag{6.18}$$

Table 6.3: Electrochemical model parameters

Parameter	Value/Function	Source
σ_{anode}	80000 [1/Ω.m]	[69]
$\sigma_{cathode}$	8400 [1/Ω.m]	[69]
$\sigma_{electrolyte}$	33400 $exp\left(-\frac{10300}{T}\right)$ [1/Ω.m]	[69]
j_0	2250 $exp\left(\frac{E_{act}}{R}\left(\frac{1}{1073}-\frac{1}{T}\right)\right)$ [A/m^2]	Fitted
E_{act}	140000 [J/mol]	[69]
α	0.639	Fitted

Source: [173]

Where,

$$r_{smr} = 4.272 \cdot 10^{-2} exp\left(-\frac{82000}{RT}\right) x_{CH_4} \frac{P_{anode}}{10^5} \tag{6.19}$$

A simplified energy balance estimates the temperature of the fuel cells (T), described in Eq. (6.20), assuming that the fuel, air and cell components are in thermal equilibrium for each positions across the coordinate A (length x width x cells x stacks). As it can be observed, this premise greatly reduces the number of thermal properties that have to be evaluated. Eq. (6.20) supposes that the heat losses (Q_{loss}) are proportional to the lower heating value of the consumed fuel, as previously shown in Table 6.1. The boundary conditions for Eqs. (6.18) and (6.20) are the inlet composition and temperature in the fuel cell.

$$\frac{dT}{dA} = \frac{\Delta H_{smr} r_{smr} + \Delta H_{wgs} J_{CO}\big|_{h=0} + \Delta H_{eoxy} \frac{j}{2F} - jV - Q_{loss}/A_{cell}}{\sum n_i c_{p,i}} \tag{6.20}$$

Lastly, the average voltage (V_{avg}) is estimated by integrating the local cell voltage (V) over the cell area (A), as described in Eq. (6.21).

$$\frac{d(V_{avg}A)}{dA} = V \tag{6.21}$$

Model validation

The model was fitted and validated with the experimental data reported by Jiang and Virkar [161] for an anode supported SOFC cell (Ni+YSZ anode, YSZ-SDC electrolyte and LSC+SDC cathode) with 1.1 cm^2 of cathode area. The exchange current density (j_0) and transfer coefficient (α) were fitted based on the activation overpotential by using a linear approximation with the Tafel equation [66] for the experimental results. The calibration of j_0 and α assumes that the difference between the experimental results of voltage and

the model solutions without the Butler-Volmer equation, Eq. (6.17), can be attributed to the activation overpotential.

As it can be observed in Figures 6.6, the simulation results were in agreement with the experimental data. For instance, for a range of 0.1 A/cm^2 to 1 A/cm^2 , the maximum relative error observed were 5.7% and 7.0% for H_2-H_2O and H_2-CO_2 mixtures, respectively. The relative differences are higher for the mixture with 81% CO_2 and current densities above 0.5 A/m^2 due to the effect of concentration losses. These deviations can be mainly attributed to simplifications in the diffusion equation, which could be reduced by extending the Stefan-Maxwell model to a Dusty-gas model [177]. The unified Butler-Volmer equation may also influence the results.

Figure 6.6: Model results and experimental data reported by Jiang and Virkar [161]

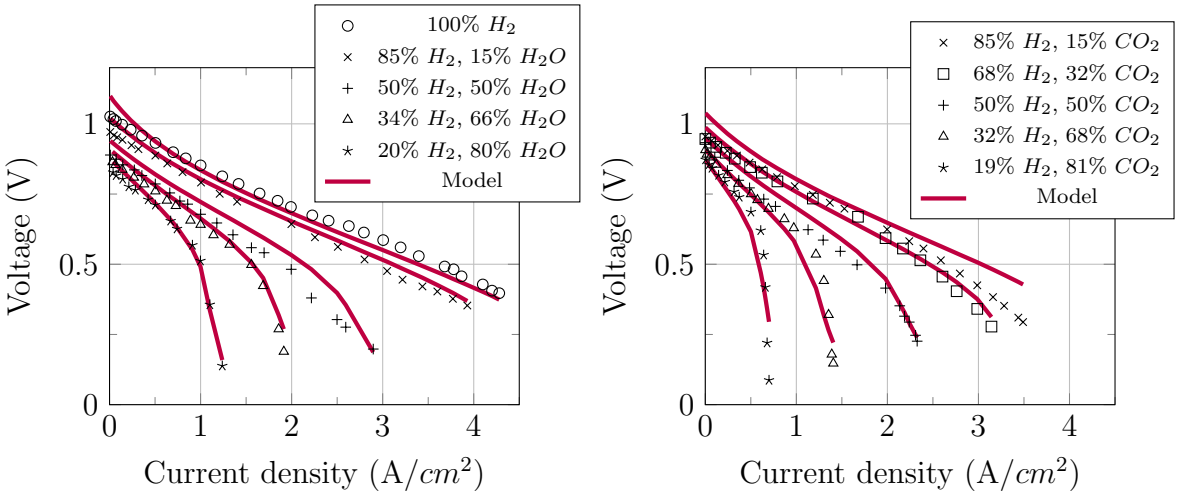

Source: [173]

Lastly, this research also compares the model results against the experimental data reported by Fu, et al. [178], which employed anode supported cells with similar materials arranged in stacks of 8 cells (84 cm^2 each) [161]. Moreover, in the study of Fu, et al. [178], the SOFC stack works with a mixture of pre-reformed methane (28.1% CH_4 , 12.5% H_2 and 59.4% H_2O in molar basis). Table 6.4 shows that the estimated relative error is lower than 5.1% for a current density of 0.3 A/cm^2 using different fuel utilization efficiencies (0.35 and 0.70).

6.3.2 Auxiliary equations

Besides the model equations described in the previous section, the design of the proposed system also requires some auxiliary equations. In this study, the FU is treated as a design variable, while the total area of fuel cells (A_{total}) and percent of theoretical air (λ_{cell}) are

Table 6.4: Comparison between model results and experimental data reported by Fu, et al. [178]

Operational conditions	Experiment [178]	Model	Difference
j = 0.3 A/cm^2			
T = 750 °C	0.82-0.83 V	0.85 V	2.4-3.6%
FU = 0.351			
j = 0.3 A/cm^2			
T = 750 °C	0.79-0.80 V	0.83 V	3.6-4.8%
FU = 0.702			

Source: [173]

determined using the Eqs. (6.22) and (6.23), respectively.

$$FU = \frac{jA_{total}/2F}{\dot{n}_{H_2,inlet} + \dot{n}_{CO,inlet} + 4\dot{n}_{CH_4,inlet}} \tag{6.22}$$

$$\frac{\lambda_{cell}}{100} = \frac{\dot{n}_{air}x_{O_2,air}}{(0.5\dot{n}_{H_2,inlet} + 0.5\dot{n}_{CO,inlet} + 2\dot{n}_{CH_4,inlet})FU} \tag{6.23}$$

6.3.3 Optimization routine

The optimization routine employed in this study consists in three subroutines: a linear optimization to determine the minimal energy requirements [76]; a mixed-integer linear programming problem to provide a heat exchanger network with the minimal number of units [76, 78]; and a multi-objective optimization (NSGA II) to search the operational parameters that maximize efficiency or net present value [91]. The operational parameters optimized in this analysis are shown in Table 6.5, while the relationship between each of these optimization subroutines and the thermodynamic process is illustrated in Fig. 6.7. This procedure is fairly similar to previous methodologies proposed by Marechal et al. [179] and Palazzi et al. [150], but it significantly differs in the approach to estimate the heat exchanger network cost.

In general, the heat exchanger area is roughly estimated based on the composite curves and the minimal number of units, derived from Euler General Network Theorem [180, 181]. This procedure can be improved using the heat rate and stream pairs for each heat exchanger unit, which could be determined by a mixed-integer linear programming problem. Although possible, this method is usually avoided due to the computational time necessary to solve the optimization problem. However, for systems with few number of streams (≤ 15) and modelled entirely in Julia programming language, the computational time necessary to perform this calculation is not a significant bottleneck (≤ 1 s). On the

Table 6.5: Variables in the multi-objective optimization

	Case			
Parameter	H_2-SOFC	H_2	SOFC-H_2	SOFC
Steam/fuel ratio (mol/mol)	1.8-3.0	1.8-3.0	1.8-3.0	1.8-3.0
Percent of theoretical air (%)	120-180	120-180	120-180	250-350
Fuel utilization efficiency	0.1-0.3	-	0.1-0.3	0.6-0.8
Current density (A/cm^2)	0.1-0.3	-	0.1-0.3	0.1-0.3
Burner inlet temperature (°C)	300-400	300-400	350-450	300-400
Population	50	50	50	50
Number of generations	30	30	30	30

Source: [71]

Figure 6.7: Flowchart of the optimization routine

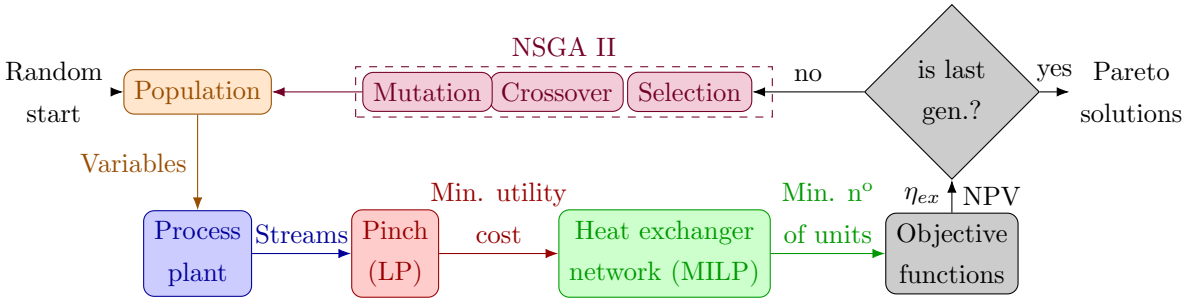

Source: [71]

other hand, it is not a straightforward procedure to estimate the total heat exchanger area from the results of this optimization routine, since the inlet and outlet temperatures for each heat exchanger unit are still to be determined. Thus, a simple method to estimate the total heat exchanger area based on the results of a MILP is proposed in the next subsection.

6.3.4 Heat exchanger area estimation

The solution for the optimization problem of a heat exchanger network with the minimal number of units gives the heat rate exchanged by the stream pairs at certain temperature intervals. According to the definition of the heat cascade, the cold streams can only receive a fixed amount of heat at predetermined intervals, while the hot streams may provide heat from one temperature interval to another below it. As a consequence, the inlet and outlet temperatures for a cold stream "c" ($T^{cold}_{in,c,k}$ and $T^{cold}_{out,c,k}$) are bounded by the temperature interval in which the heat exchange occurs (T^{low}_k, T^{high}_k) or the stream

target/source temperature ($T_{s,c}^{cold}, T_{t,c}^{cold}$), as shown in Eq. 6.24 and 6.25.

$$T_{in,c,k}^{cold} = \begin{cases} T_k^{low} & if\ T_k^{low} > T_{s,c}^{cold} \\ T_{s,c}^{cold} & otherwise \end{cases} \tag{6.24}$$

$$T_{out,c,k}^{cold} = \begin{cases} T_k^{high} & if\ T_k^{high} > T_{t,c}^{cold} \\ T_{t,c}^{cold} & otherwise \end{cases} \tag{6.25}$$

The inlet and outlet temperature for each hot stream "h" at each temperature interval ($T_{in,h,k}^{hot}$ and $T_{out,h,k}^{hot}$) may be determined by the stream heat capacity, as shown in Eq. 6.26 and 6.27. This approach implies a certain configuration of heat exchanger network that may not lead to the minimal heat exchange area, but it is a general workable solution. Once the temperatures for each stream and temperature interval are determined, the heat exchanger area ($A_{h,c,k}$) can be determined by each heat transfer rate ($Q_{h,c,k}$), as demonstrated in Eq. 6.28.

$$T_{in,h,k}^{hot} = \begin{cases} T_{s,h}^{hot} & if\ k = 1 \\ T_{out,h,k-1}^{hot} & otherwise \end{cases} \tag{6.26}$$

$$T_{out,h,k}^{hot} = T_{in,h,k}^{hot} - \frac{1}{C_i^{hot}} \sum_{c}^{C} Q_{h,c,k} \tag{6.27}$$

$$A_{h,c,k} = \frac{Q_{h,c,k}}{U_{h,c} \Delta T_{ln,h,c,k}} \tag{6.28}$$

In this study an average value for the overall heat transfer coefficient ($U_{h,c}$= 50 $W.m^{-2}.K^{-1}$)) is used to simplify the determination of the total heat exchanger area [179]. This could be further improved by estimating the heat exchanger coefficient based on the properties of the stream pairs that exchanges heat.

6.3.5 Economic assessment

The purchase equipment cost (PEC_i) was estimated based on correlations published by different authors which are presented in the Appendix B. In order to account for inflation in the equipment costs, corrections based on the CEPCI cost index were made for every equipment [182]. Next, the total overnight cost (TOC) was estimated based on the total purchase equipment costs (TPC) following the methods suggested by Theis [183] for power plants, as can be seen in the Eq. (6.29) and (6.30). The cost factors and other economic assumptions for the cash flow analysis are presented in Table 6.6.

$$TPC = f_{install} f_{epcc} f_{process} f_{project} \sum_{i} PEC_i \tag{6.29}$$

$$TOC = f_{owner} TPC \tag{6.30}$$

Table 6.6: Economic assumptions

Parameter	Value	Source
Install factor ($f_{install}$)	1.17	[163]
Engineering procurement and construction factor (f_{epcc})	1.175	[183]
Process contingencies factor ($f_{process}$)	1.125	[183]
Project contingencies factor ($f_{project}$)	1.225	[183]
Owner's cost factor (f_{owner})	1.202	[183]
Operation and maintenance factor ($f_{O\&M}$)	0.02	[153]
Effective tax rate (f_{tax})	0.2574	[183]
Weighted average costs of capital (WACC)	$\begin{cases} 0.0654 & \text{if taxes included} \\ 0.0725 & \text{otherwise} \end{cases}$	[183]
Electricity costs (c_{elec})	0.1 USD/kWh	[184]
Biogas costs (c_{biogas})	0.02 USD/kWh	[48, 2]
Hydrogen costs (c_{H_2})	3 USD/kg	Assumed
Process water costs (c_{H_2O})	0.27 USD/m^3	[185]
Cooling water costs (c_{cw})	0.027 USD/m^3	[185]
Operational hours (t_{op})	8000 hours/year	[185]

Source: [71]

The operation and maintenance costs were assumed to be proportional to the total plant cost (2%) [153] and no additional labor costs were included assuming that the proposed system would be an expansion of an existing biogas plant. Additional costs related with utilities were assumed as proportional to the cooling demands using costs reported by Seider et al. [185], while additional fuel consumption was included when the heat recovery system was not able to supply energy internally. The lifetime of catalysts and fuel cell stack were assumed as 5 years [52, 157], while the activated carbon for desulfurization was replaced yearly [186]. The replacement costs ($C_{replace,i,n}$) were assumed to be equal to the costs of the fuel cell stack, catalysts media and desulfurization media as shown in the Appendix B. A linear depreciation model for the first 10 years of operation was assumed for simplicity. Moreover, the replacement costs were also depreciated linearly during their

lifetime. In addition, costs related to startup, land, royalties and working capital (besides inventory capital) are not accounted for in the analysis, as well as any salvage value at the end of the project life. Thus, cash flow for each year can be estimated by using the Eq. (6.31)-(6.42) [185, 153] and assumptions in Table 6.6.

$$CF_n = \begin{cases} TOC & if\ n = 0 \\ S_n - C_n - T_n & otherwise \end{cases} \tag{6.31}$$

Where,

$$S_n = \begin{cases} S_{elec} + S_{H_2} & if\ W_{net} > 0 \\ S_{H_2} & otherwise \end{cases} \tag{6.32}$$

$$S_{elec} = c_{elec} \left(\frac{W_{net}}{10^3} \right) t_{op} \tag{6.33}$$

$$S_{H_2} = c_{H_2} \dot{m}_{H_2} t_{op} \tag{6.34}$$

$$C_n = C_{cons.} + f_{O\&M} TPC + \sum_i C_{replace,i,n} \tag{6.35}$$

$$C_{cons.} = \begin{cases} C_{fuel} + C_{water,net} + C_{utility} & if\ W_{net} > 0 \\ C_{elec} + C_{fuel} + C_{water,net} + C_{utility} & otherwise \end{cases} \tag{6.36}$$

$$C_{fuel} = c_{biogas} \dot{m}_{biogas} HHV_{biogas} t_{op} \tag{6.37}$$

$$C_{water,net} = c_{water} \dot{V}_{water,net} t_{op} \tag{6.38}$$

$$C_{utility} = (c_{cw} \dot{V}_{cw} + c_{biogas} \dot{m}_{extra\ fuel} HHV_{biogas}) t_{op} \tag{6.39}$$

$$C_{elec} = c_{elec} \left(\frac{|\dot{W}_{net}|}{10^3} \right) t_{op} \tag{6.40}$$

$$T_n = \begin{cases} (S_n - C_n - D_n) * f_{tax} & if\ S_n - C_n > 0 \\ 0 & otherwise \end{cases} \tag{6.41}$$

$$D_n = D_{TOC,n} + \sum_i D_{replace,i,n} \tag{6.42}$$

Next, the results for cash flow were used to determine the net present value of the project (NPV, after-taxes), Eq. (6.43), and the levelized costs of each product (LCOP,

pre-taxes), Eq. (6.44) and (6.45). Since in some cases there are two products, the levelized costs were divided between the products proportionally to the exergy of each product. This simplification is used to avoid a detailed thermoeconomic cost model, which would require the solution of a linear system of equations [85, 187]. The levelized costs of products in this study only aims to give a parameter for easy comparison with other studies, while the NPV is used to compare the economic performance of each design.

$$NPV = \sum_{n} \frac{CF_n}{(1 + WACC)^n} \tag{6.43}$$

$$LCOP_i = \frac{\gamma_i \sum_n C_n (1 + WACC)^{-n}}{\sum_n P_i (1 + WACC)^{-n}} \tag{6.44}$$

Where,

$$\gamma_i = \frac{B_{product,i}}{\sum_i B_{product,i}} \tag{6.45}$$

6.3.6 Exergy analysis

As previously mentioned, the heat exchanger network is designed at each simulation based on results of a pinch analysis including all heat transfer units. This solution method allows for design flexibility, but requires an additional assumption to evaluate the exergy destruction distribution. The simplest approach is to evaluate the heat exchanger network as a whole, as described in Eq. (6.46). Thus, by considering the exergy recovered from hot streams as input and the exergy delivered to cold streams as products, the analysis estimates the exergy destruction of all heat exchanger units ($B_{d,HXs}$). This method also assumes that temperature distribution for all heat transfers is linear, as it is considered in the pinch analysis.

$$B_{d,HXs} = \sum_{h}^{H} |Q_h| \left(1 - \frac{T_0}{\Delta T} ln\left(\frac{T_{target}}{T_{source}}\right)\right) - \sum_{c}^{C} |Q_c| \left(1 - \frac{T_0}{\Delta T} ln\left(\frac{T_{target}}{T_{source}}\right)\right) \tag{6.46}$$

The exergy efficiency was employed in this study to provide a technical parameter to compare the system response to different operational parameters. A simple rational definition, as shown in Eq. (6.47), is used to determine the exergy efficiency of the system. Additional power and water consumptions related to the use of utility systems were neglected as a simplification. However, the additional fuel consumption required by the heating utilities were included using a proportional factor derived from a biogas

furnace model.

$$\eta_{ex} = \begin{cases} \dfrac{B_{H_2} + W_{net}}{B_{fuel} + B_{heating} + B_{water,net}} & if\ W_{net} > 0 \\ \dfrac{B_{H_2}}{B_{fuel} + B_{heating} + |W_{net}| + B_{water,net}} & otherwise \end{cases} \tag{6.47}$$

6.4 Results and discussion

Figure 6.8 shows a comparison between the optimization results for each system analyzed in this study. As it can be seen, the H_2 and H_2-SOFC systems are able to attain the highest level of exergy efficiency (63.1-65.6%) and net present value (327.2-402.8 kUSD_{2019}). Furthermore, the SOFC systems are able to achieve a wide range of exergy efficiency (45.4-58.6%) which may achieve economic viability at specific conditions. Although the SOFC-H_2 may not be economic viable (NPV < 0), this design can achieve slightly higher efficiencies (60.2%) compared with the original SOFC system.

Figure 6.8: Multi-objective optimization results

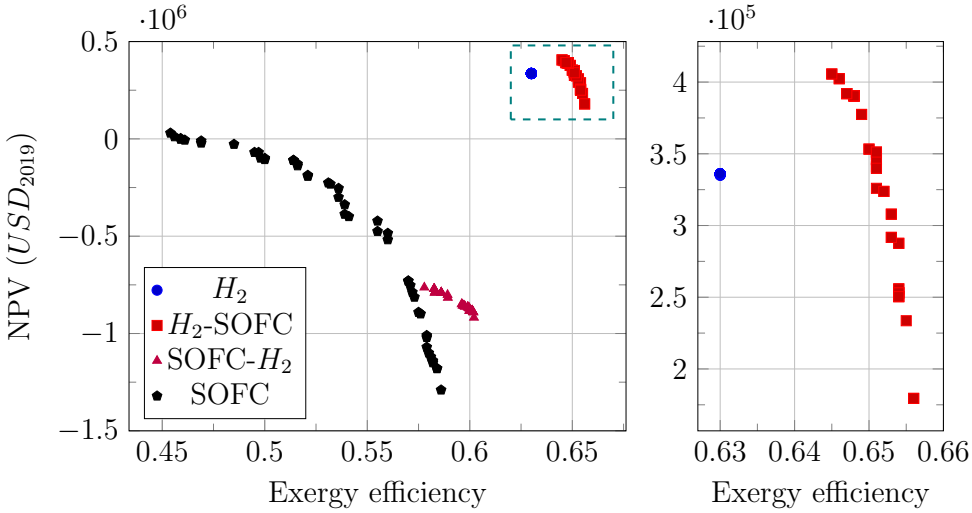

Source: [71]

The optimal variables are significantly different for each design, as it can be observed in Table 6.7, but may not be different for each objective function. For instance, the percent of theoretical air and fuel utilization efficiency of each optimal solution are quite similar for the H_2-SOFC and SOFC-H_2 systems. Thus, in these cases, the trade-off between efficiency and NPV seems to arise from variations in the current density, burner inlet temperature or steam/fuel ratio. In general, a high current density is able to increase the power density of the fuel cell, but decreases the average cell voltage, which directly impacts equipment costs and efficiency [66]. On the other hand, the burner inlet temperature influences the

energy integration by varying the maximum burner temperature, while the steam/fuel ratio alters the hydrogen yield of the steam reformer and shift reactor. Thus, these last two parameters affect the hydrogen production and the heat exchanger network cost, which can significantly change the system efficiency and NPV.

Table 6.7: Optimal variables for each objective function and system design

	H_2	H_2-SOFC		SOFC		SOFC-H_2	
Description	-	η_{ex}	NPV	η_{ex}	NPV	η_{ex}	NPV
Objective functions							
Efficiency (%)	63.0	65.6	64.5	58.6	45.5	60.2	57.8
NPV ($kUSD_{2019}$)	327.2	179.5	402.8	-1293	29.9	-918.3	-763.4
Design variables							
Percent of theoretical air (%)	174	135	135	276	303	121	121
Steam/fuel ratio	2.87	2.25	2.25	1.80	1.84	2.59	2.15
Current density (A/cm^2)	-	0.10	0.29	0.10	0.30	0.19	0.29
Fuel utilization efficiency	-	0.30	0.30	0.80	0.65	0.10	0.10
Burner inlet temperature (°C)	314.8	368.5	368.5	325.4	326.5	431.4	431.4

Source: [71]

The percent of theoretical air controls the flow rate of air and maximum temperature in the catalytic burner, therefore a reduction in this parameter decreases the power consumption and tends to reduce the equipment cost of blowers and heat exchangers. However, the percent of theoretical air is limited by some technical restrictions, such as the maximum temperature difference in the fuel cell ($\Delta T < 200$ K), maximum absolute temperature in the fuel cell (800 °C) or the maximum burner temperature (assumed as 1500 °C). The results for fuel utilization efficiency can be explained by the impact that this parameter has in the power generation and fuel combustion. A high fuel utilization efficiency can reduce fuel losses and increase power generation when hydrogen production is not present, since the heating demand at high temperatures is not significantly high. On the other hand, if hydrogen production is included, the fuel utilization efficiency is limited by the heating demand of the steam reforming in order to avoid additional fuel consumption to match the energy integration. Similarly to the percent of theoretical air, the fuel utilization efficiency may also be restricted by the temperature limits of the fuel cells.

A detailed description of the main technical parameters for the solutions with optimal NPV is presented in Table 6.8. As expected, the hydrogen production and power generation are maximized in the system producing only one product, respectively, H_2 and SOFC designs. The hybrid solutions produce less hydrogen since part of the fuel is also converted into electricity, which the results indicate to lead to higher exergy efficiencies and NPV. In this analysis, the electricity price (0.1 USD/kWh) is higher than the hydrogen costs if compared on an energy basis (approx. 0.09 USD/kWh), therefore power generation may be more financially attractive depending on the conversion efficiency. On the other hand, a hybrid system with different products may offer more possibilities for performance improvement. For instance, in the H_2-SOFC system, the introduction of a fuel cell leads to the possibility to use the purge gas to generate electricity rather than heat, which would be used mainly in the steam reformer. As the methane conversion reaches higher levels, the use of purge gas for heating becomes less attractive compared with power generation and, therefore, the switch can lead to higher efficiencies.

Table 6.8: Main technical results for the optimal NPV solutions

	Optimal NPV case			
Description	H_2	H_2-SOFC	SOFC	SOFC-H_2
Consumptions and products				
Water (m^3/h)	0.08	0.07	0.15	0.10
Cooling water (kW_{heat})	-	11	-	45
Gross power (kW)	-	65	307	46
Net power (kW)	-38	29	285	-34
Hydrogen production (kg/d)	292	263	-	267
Extra fuel (Nm^3/h)	0.04	0.33	-	-
Fuel cell				
Voltage (V per cell)	-	0.80	0.71	0.83
Total cell area (m^2)	-	29	150	20
PSA				
Recycle ratio	0.38	0.44	-	0.43
Investments				
Equipment ($kUSD_{2019}$)	378	424	380	716
TOC ($kUSD_{2019}$)	861	966	866	1632
Levelized cost				
Electricity (USD_{2019}/kWh)	-	0.06	0.09	-
Hydrogen (USD_{2019}/kg)	2.34	2.27	-	3.53

Source: [71]

Table 6.8 also shows promising results for the levelized cost of hydrogen ($\leq$2.3 USD_{2019}/kg) and electricity ($\leq$0.09 USD_{2019}/kWh), excluding the SOFC-H_2 case. For instance, hydrogen production using natural gas and carbon capture technology is expected to cost between 1.5-3 USD/kg [22], while the global average costs of electricity from bioenergy is approximately 0.07 USD/kWh [188]. Thus, the proposed systems may be competitive compared with other technologies and related energy sources.

The levelized costs for hydrogen production in this study are also lower than values previously reported by other researchers for biogas conversion systems. For example, Marcoberardino et al. [157] determined the levelized costs of hydrogen to be between 4.2-7.1 EUR/kg for different reforming technologies and operational conditions. Yao et al. [189] calculated a break-even price of approximate 6 USD/kg for hydrogen derived from biogas. These differences can be explained by different economic assumptions (e.g., cost functions, indirect costs and discount rate), design choices (e.g., reformer temperature and hydrogen pressure) and the lack of an optimization study. Moreover, the hydrogen recovery assumed in this study, which is based on values reported by Papadias et al. [162] and NREL [163], is significantly higher than those calculated by Marcoberardino et al. [157]. On the other hand, Becker et al. [57] reported a hydrogen cost of 1.8 USD/kg for a hybrid system co-producing electricity and hydrogen from natural gas. The use of natural gas and electrochemical hydrogen separation associated with the project scale (1 MW) could explain the significantly lower costs.

The SOFC, PSA and reactors are responsible for most of the purchase equipment cost, as it can be seen in Figure 6.9. In the case of SOFC-H_2, the low pressure in the shift reactor leads to an enormous equipment size, since the reaction rate is quite influenced by the partial pressure of reactants [190]. Moreover, the compression of reformate gas also demands a larger equipment compared with other designs, in which the reactants are compressed prior to steam reforming. On the other hand, the total equipment costs for H_2, H_2-SOFC and SOFC systems are very similar despite the differences in design. In the SOFC system, the cost of steam reforming is significantly reduced by the internal reforming in the fuel cell. However, in order to achieve the high levels of fuel utilization efficiency, the total area of the fuel cell has to be maximized and, therefore, counterbalances the savings in fuel processing. Furthermore, the H_2-SOFC configuration corrects the main drawbacks of the SOFC-H_2 system by placing the fuel cell after the hydrogen separation and, since a large portion of fuel is separated, the fuel cell size can be quite reduced. Thus, despite having a fuel cell as in the SOFC system, the H_2-SOFC option is only 12% more expensive than the original H_2 design. This additional investment can be justified by the increase of 23% in the net present value obtained by the electricity sales, as previously presented in Tables 6.8 and 6.7.

Figure 6.9: Total equipment cost for optimal NPV cases

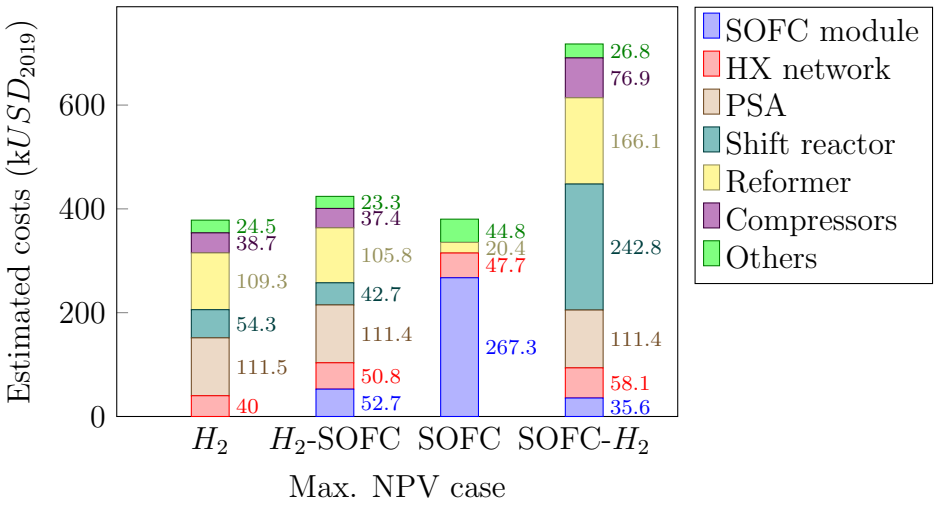

Source: [71]

It is important to highlight that the SOFC-H_2 solution produces less electricity than the H_2-SOFC solution due to the interactions between fuel cell and hydrogen separation. Although an increase in fuel utilization efficiency could boost the power generation in the SOFC-H_2 case, this would reduce the hydrogen concentration in the reformate gas and impact negatively in the hydrogen separation, which requires a minimum of 74% molar concentration of H_2. Thus, a small increase in power generation would lead to a drastic reduction in the hydrogen production because the PSA would need to recycle more hydrogen to attain technical viability. On the other hand, this problem does not occur in the H_2-SOFC system, therefore it can operate with higher fuel utilization efficiencies and increase power generation. However, the use of purge gas for power generation reduces the heat available to supply energy for the steam reformer. Thus, the optimization algorithm tries to find an optimal relationship between power generation and heat supply.

6.4.1 Energy integration results

Figure 6.10 shows the grand composite curves for each scenario derived from the pinch analysis. It can be noticed that the power generation case have a large potential for heat cogeneration (approx. 140 kW), which is greatly reduced with hydrogen co-production (approx. 0-25 kW). This difference can be explained by the reduction of fuel sent to the catalytic burner due to the separation of hydrogen. Since biogas production often requires an energy demand for temperature control, a reduction in the energy available as heat may be undesirable. For example, the heating of anaerobic reactors may require an extra consumption of fuel in order to maintain the biogas productivity [43]. However, the heating demand for anaerobic digestion may not be a concern for industrial wastewater

[46], in which the feedstock may be at elevated temperatures, or landfills. Thus, hydrogen production is an interesting option for these processes, since they are not very dependent on the heating supply from power generation.

Figure 6.10: Grand composite curves for H_2 and H_2-SOFC systems with optimal NPV

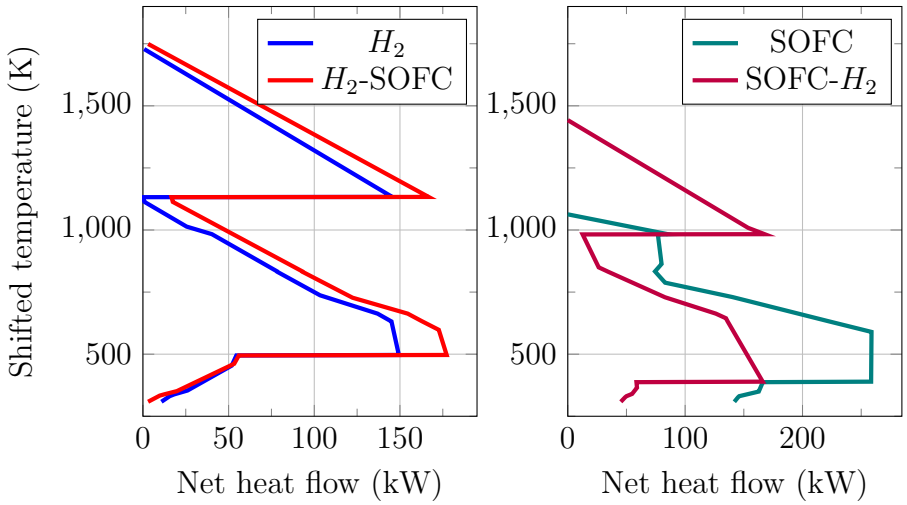

Source: [71]

Figure 6.10 also shows that steam generation and steam methane reforming have a large impact on the available heat for cogeneration. Thus, a reduction in steam consumption may benefit the energy efficiency when heat is a desirable product. However, steam also reduces the formation of soot and promotes the hydrogen generation in methane reforming according to the chemical equilibrium principle; therefore the steam to carbon ratio should be optimized. These trade-offs are very similar to those reported for hydrogen production in steam reforming units [58].

6.4.2 Exergy destroyed assessment

The distribution of exergy destroyed rate for the main process in each system with maximum NPV is presented in Figure 6.11. The catalytic burner and heat exchanger network are the main sources of irreversibilities in all cases, but the systems with hydrogen production are able to avoid these losses by separating part of fuel as hydrogen [160]. The same principle explains the gains in exergy efficiency for the H_2-SOFC compared with the H_2, since the purge gas combustion is partially avoided by converting hydrogen into electricity.

The high exergy destroyed rate in the solid oxide fuel cell is related with the high fuel utilization efficiency and current density for the SOFC system with optimal NPV. This can be greatly improved by reducing the current density, as demonstrated in the multi-objective optimization results in Table 6.7 and Figure 6.8, but leads to an enormous

Figure 6.11: Exergy destroyed rate distribution for optimal NPV cases

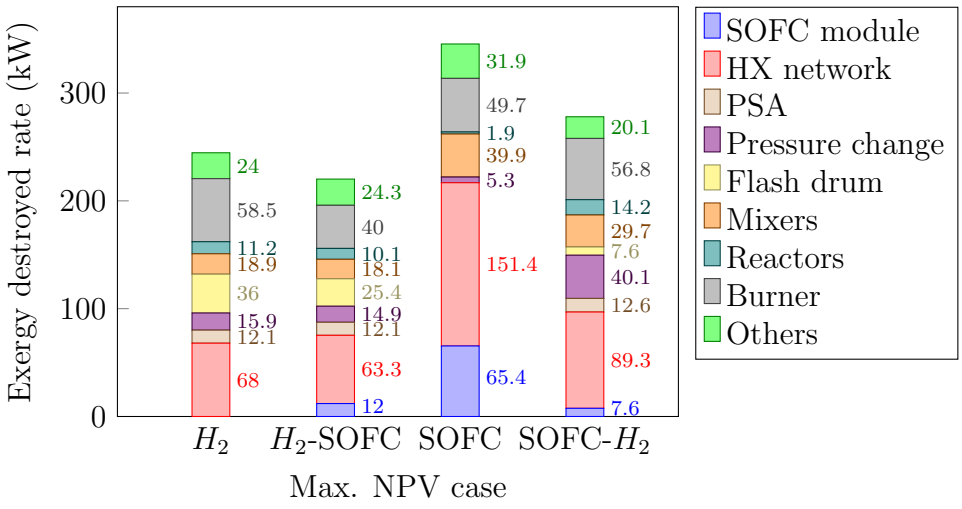

Source: [71]

increase in equipment cost since the power density is drastically reduced. In the SOFC-H_2 and H_2-SOFC cases, the influence of the fuel cell is significantly reduced because only a small fraction of fuel is converted into electricity.

6.4.3 Influence of methane concentration in SOFC and SOFC-H_2 cases

In order to estimate the impact of methane concentration, the cases SOFC and SOFC-H_2 were also simulated using biomethane (assumed as pure methane) and compared with the performance of their respective biogas scenarios. The flow rate of biomethane is adjusted to 60 Nm^3/h to maintain the same amount of energy input as in the biogas scenarios. Table 6.9 shows the main technical results separated by fuel and products. The results indicate that, for these operational conditions, the fuel cells attain similar performances ($< 3\%$ difference) in voltage and power density despite working with different fuels. This can be explained by the similar initial concentrations of hydrogen in the anode inlet, caused by the fixed steam to carbon ratio and the anode off-gas recycle. For instance, the initial molar concentration of hydrogen in the biogas case is approximately 0.12-0.14, while for biomethane the value is between 0.14-0.18. Furthermore, at low current densities, the impact of overpotential losses related to reactants concentration is low, which also can be observed in experimental data reported by Jiang and Virkar [161].

Table 6.10 presents the result for the energy analysis of each proposed scenario. As it can be observed, the net energy gain of hydrogen co-production compared with sole power generation is significantly lower for using biogas (34 kW) instead of biomethane (85 kW). In fact, one may argue that in an extended analysis including the hydrogen final

Table 6.9: Main technical results for base cases

	Biogas		Biomethane	
Description	SOFC	SOFC-H_2	SOFC	SOFC-H_2
Pre-reforming				
T_{outlet} (°C)	465	417	468	395
ΔCH_4 (%)	24	16	15	12
Water consumption (l/h)	121	161	63	97
Inlet O/C ratio	3.29	4.67	2.95	2.95
SOFC				
ΔT (°C)	177	113	200	134
T_{max} (°C)	893	781	889	771
T_{min} (°C)	716	668	688	638
Area (m^2)	158	96	158	96
Voltage (V per cells)	0.75	0.76	0.78	0.76
Power (kW)	338	206	349	208
Power density (W/m^2)	2144	2157	2216	2172
Burner				
T_{max} (°C)	871	1155	966	1176
Water gas shift				
T_{outlet} (°C)		405		413
ΔCO (%)		83		79
PSA				
H_2 initial concentration (molar)		0.52		0.65
Recycle ratio (%)		66		26
Separation effective efficiency (%)		58		63
Products				
Net power (kW)	319	158	333	163
H_2 (kg/d)		139		182

Source: [173]

use (e.g., 50% efficiency) the co-production of hydrogen may reduce the overall efficiency. This dilemma between production and end-use efficiency was discussed in the previous chapter. Thus, these results indicate that the proposed system could be more profitable, given its better efficiency, but may not score as well as conventional SOFC systems in environmental performance.

The results for energy efficiency presented in Table 6.10 are in agreement with previous studies of similar systems. For instance, Fontell, et al. [72] estimated a net electrical

Table 6.10: Energy analysis for base cases

	Biogas		Biomethane	
	SOFC	SOFC-H_2	SOFC	SOFC-H_2
Power balance (kW)				
Biogas compressor	-0.8	-0.8	-0.5	-0.5
Water pump	≈0	≈0	≈0	≈0
Air compressor	-9.9	-7.0	-9.9	-7.0
SOFC + inverter	338.9	206.4	349	207.9
Recycle compressor	-8.4		-5.7	
PSA multistage compressor		-32.6		-26.8
PSA recycle compressor		-0.4		-0.1
H_2 multistage compressor		-7.9		-10.3
Hydrogen energy (kW)		195.2		225.1
Energy efficiency (%)	52.2	57.7	54.5	68.4

Source: [173]

efficiency of 55.9% for a SOFC system designed for natural gas. Peters, et al. [191] reported a net electrical efficiency between 40-50% for a SOFC demonstration unit of 20 kW operating with natural gas. For systems working with biogas, Van Herle, et al. [152] determined an energy efficiency of 48.7%, while Curletti, et al. [153] calculated a value close to 50% (FU = 70%). Dietrich, et al. [192] observed an energy efficiency of 52% for a 1 kW SOFC module operating with a biogas mixture containing 55% of methane (in volume). Moreover, Gandiglio, et al. [155] reported an average energy efficiency of 50-52% for an industrial size SOFC plant that works with biogas. For systems co-producing hydrogen and electricity, results published by Becker, et al. [57] indicated an efficiency of 62- 65%, considering natural gas as fuel and excluding the contribution from heat cogeneration. In addition, Pérez-Fortes, et al. [151] also calculated efficiencies between 53- 67% for a pilot SOFC unit producing hydrogen and electricity using natural gas.

In general, the different values of energy efficiency can be attributed to design choices (e.g., anode recycle, reforming, operational variables), electrode materials and analysis assumptions. For instance, Gandiglio, et al. [155] does not include the power consumption for biogas and air compression in their calculations for energy efficiency, which may induce an overestimate for efficiency. Besides, the mathematical modelling of previous studies does not provide crucial information to evaluate technical restraints of fuel cells, such as minimal fuel concentration and local temperature. For example, Curletti, et al. [153] neglects the effect of fuel consumption along the fuel cells, which may lead to misleading results of performance for high efficiencies of fuel utilization. The present analysis also

shows that, although previous studies have indicated substantial increases in efficiency by co-producing hydrogen [57, 151], these improvements are significantly lower for systems using biogas as fuel. The comparison between the results for biomethane and biogas operation in Table 6.10 demonstrates these differences.

Exergy analysis results

Figure 6.12 shows the values of exergy efficiency for the different scenarios evaluated in this study. As it can be observed, the values are close to those for energy efficiency, since the lower heating value and specific chemical exergy of fuels are similar. Hydrogen production is able to significantly boost the exergy efficiency by avoiding key losses in energy conversion, as illustrated in the exergy destruction breakdown on Figure 6.13.

Figure 6.12: Exergy efficiency for base cases

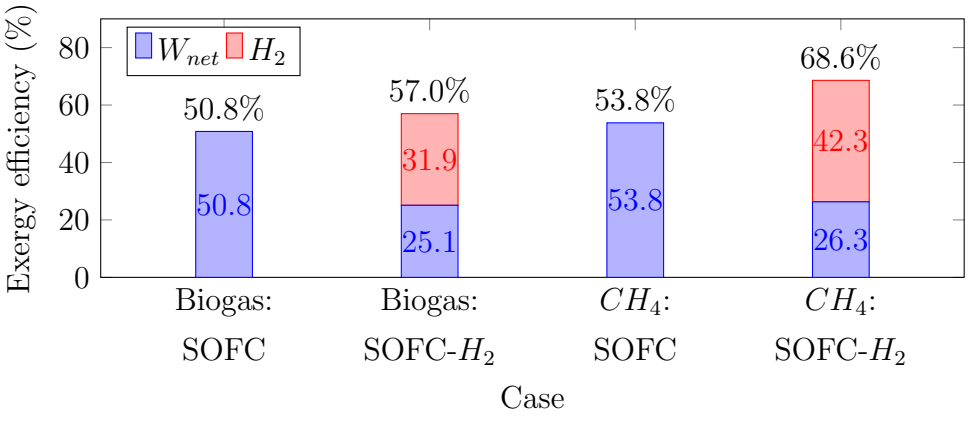

Source: [173]

The exergy destruction assessment indicates that the heat exchanger network is the major source of irreversibility in all scenarios (31-50%). This can be explained by the unexplored potential for heat cogeneration and high temperature differences, as previously shown in the energy integration results. For instance, for hydrogen production cases, the lower amount of fuel converted to heat indirectly reduces the losses in the heat exchanger network. Thus, future improvements can be achieved with heat cogeneration or reductions in fuel combustion promoted by higher separation efficiencies.

Figure 6.13 also shows that the solid oxide fuel cell is a relevant source of exergy destroyed. The activation overpotential, low concentration of hydrogen and power inverter efficiency leads to significant losses which explain this result. Moreover, the exergy destruction for hydrogen co-production cases is relatively high compared with power generation despite the reduction in fuel utilization efficiency. This can be explained by the lower operating temperature, as shown in Table 6.9, which reduces the physical exergy of

Figure 6.13: Exergy destroyed assessment for base cases

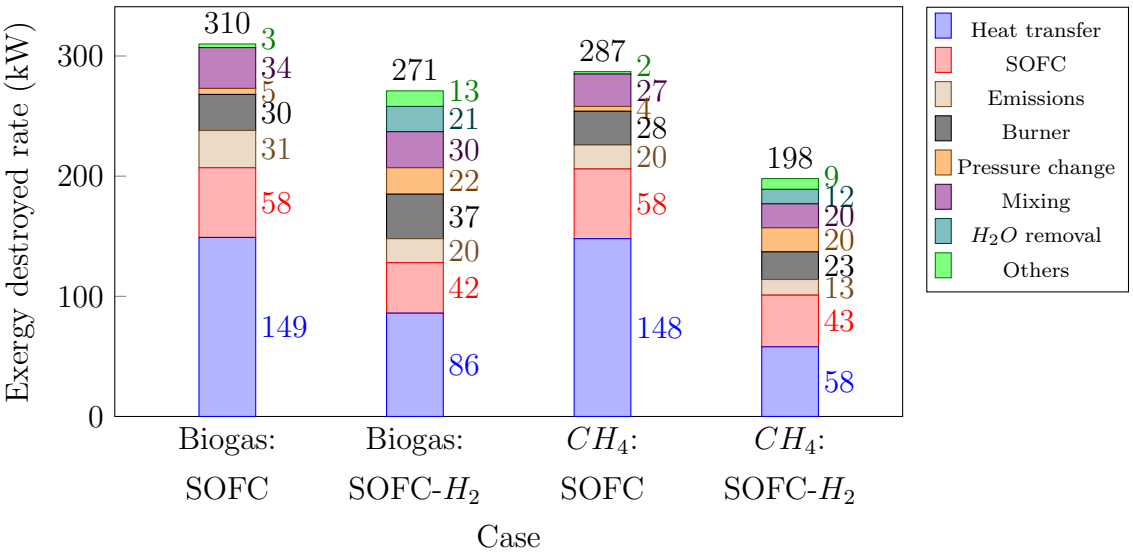

Source: [173]

outlet gases. A simple alternative to increase the efficiency of solid oxide fuel cells is to operate it at higher pressures [67, 66]. However, the additional power consumption for pressurization may overcome the benefits of a higher cell voltage. A proposed alternative is to include a turbine to produce more electricity from the anode exhaust gases, such as in the hybrid configurations of SOFC with gas turbines (SOFC-GT) [73].

These results have minor disagreements with previous studies that investigated the exergy analysis of SOFC systems, mostly for natural gas and hydrogen operation. For instance, Bedringås, et al. [193] reported the fuel preheating as the major source of irreversibilities in SOFC systems, but indicate the after-burner as the second largest source followed by the SOFCs. A similar conclusion can be inferred based on the results of other authors, such as Chan, et al. [194], Gandiglio, et al. [155] and Lee, et al. [195]. These deviations can be explained by the differences in the fuel reforming and control volumes used in the exergy analysis of previous researches compared with the present study. For instance, although the internal reforming can simplify the heat management, it adds more irreversibilities to the SOFCs compared with systems using indirect or external reforming, such as those aforementioned. In addition, the exergy analysis shown in Figure 6.13 separates the irreversibilities of mixing fuel and air from the reaction of both substances. Thus, if both processes were joined into the control volume for the catalytic burner, the exergy destruction of this equipment would be higher.

Other major sources of exergy destruction can be linked with irreversible reactions (Burner) and the mixture of streams with different temperatures or compositions (Mixing). The scenarios with hydrogen production also include significant losses in multistage

compressors (Pressure change), which could be avoided by improving the equipment efficiency or lowering the pressure for hydrogen separation. Furthermore, since the analysis assumes that energy derived from water condensation is unsuitable for heating cold streams, the exergy destruction in the process of water removal is relatively high.

Parametric analysis

Figure 6.14 presents the impact of some key operational parameters in the exergy efficiency of hydrogen and electricity co-production using biogas. It is important to highlight that the range of some variables was limited to avoid technical complications, such as negative pressures, elevated temperatures or external heat demand.

Figure 6.14: Parametric analysis of operational conditions for the co-production of H_2 and electricity using biogas

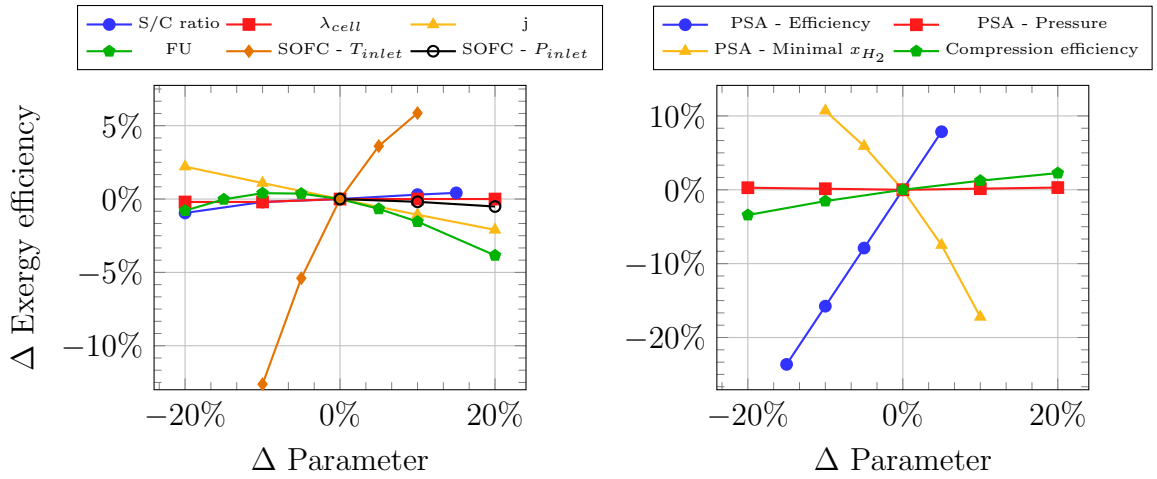

Source: [173]

As it can be observed, the stack temperature has a high influence in the exergy efficiency, since it heavily impacts on the exchange current density, conductivity of materials and open current voltage. Although higher temperatures could lead to significant gains in efficiency, they may require expensive materials for inter-connectors, gaskets and other auxiliary equipment [67, 66]. Thus, technical and economic factors should be considered in the optimization of SOFC design variables [153, 73].

The efficiency of fuel utilization and the current density have a relatively low effect on exergy efficiency (±5% for a ±20% variation). Moreover, changes in the steam to carbon ratio, percent of theoretical air and stack pressure do not significantly alter the exergy efficiency. This may be explained by the multiple effects these parameters have in the system. For instance, a reduction in steam to carbon ratio may decrease the water concentration, but also diminishes the methane reforming yield [196]. The superposition of positive and negative changes may result in a small effect in exergy efficiency.

Lastly, it is clear that the PSA separation efficiency and minimal hydrogen concentration have a huge impact in the proposed system (±10% for a ±10% variation). Thus, a detailed analysis and optimization of hydrogen separation could lead to great improvements and reduce risks related with uncertainties in the system performance [162]. The analysis also points out that variations in the PSA inlet pressure or compressors efficiency may not directly lead to significant gains in performance.

6.5 Concluding remarks

A multi-objective optimization of two different systems combining hydrogen production and power generation using fuel cells for biogas conversion is analyzed and discussed in this chapter. The proposed hybrid solutions are compared with two relatable systems only producing power or hydrogen in order to provide real understanding of the possible improvements. Furthermore, a detailed model of a solid oxide fuel cell, which includes the effects of fuel depletion and temperature variation across the stack, and a procedure to estimate the heat exchanger area from the minimal number of heat exchanger units are employed in this study to enhance the model prediction and cost analysis.

The results indicate that hydrogen production with a downstream fuel cell system is able to achieve the highest net present value (402.8 USD_{2019}) and exergy efficiency (65.6%) among the available options, leading to a levelized cost of 2.27 USD_{2019}/kgH_2 and 0.06 USD_{2019}/kWh for hydrogen and electricity, respectively. The proposed system named H_2-SOFC is able to increase 23% of the NPV compared with sole hydrogen production under the defined economic scenario. Moreover, compared with a traditional SOFC system, the H_2-SOFC can tenfold the NPV (1346%) and promote a 42% increase in exergy efficiency at selected optimal solutions (max. NPV).

The H_2-SOFC system is able to outperform the other solutions by avoiding fuel combustion in the catalytic burner by either separating it as hydrogen or converting it into electricity. This dual possibility leads to the reduction of main exergy losses in key equipment, such as the catalytic burner and heat exchanger network, while utility consumption is minimized thanks to an optimized energy integration system. Thus, the co-production of hydrogen and electricity can be a promising alternative for future biogas plants projects.

The pinch analysis results shows that hydrogen production greatly reduces the heat cogeneration potential, which may be an undesirable feature if biogas production has high energy demand for temperature control. The SOFC temperature, PSA separation efficiency and the minimal concentration of hydrogen at the PSA inlet have huge effects in the exergy efficiency for the SOFC and SOFC-H_2 cases (± 5-10% for a ± 10% variation). The parametric analysis also demonstrated that changes in the current density,

fuel utilization and compression efficiency cause minor effects on the system efficiency (± 5% for a ±20% variation). Thus, the optimization of hydrogen separation and SOFC operation parameters could lead to significant performance improvements and minimize uncertainties in the results.

7 Energy integration of anaerobic digestion and fuel cell systems

Organic wastes derived from agriculture represent a cheap and widely available resource for the production of energy, fertilizers and fuels for several countries. Their conversion using anaerobic digesters into biogas, for instance, is able to reduce pollution from organic waste disposal, produce liquid fertilizer and provide energy for different purposes. Although this technology has been massively adopted in recent years, new projects for biogas production plants still struggle with low productivity and energy efficiency, which limits their economic viability despite numerous benefits. Multiple technologies have been proposed to diminish these problems, however the high costs of such options may overcome their benefits if not carefully designed and optimized.

In this chapter, the energy integration of anaerobic digestion and fuel cells systems is evaluated in detail. Thus, in order to examine the trade-offs between productivity, efficiency and costs of complex biogas production plants, this study details a multi-objective optimization of a system converting biogas derived from swine manure into electricity by using solid oxide fuel cells. The analysis shows that the proposed system is able to achieve a levelized cost of electricity of 0.13-0.20 USD_{2019}/kWh and an exergy efficiency between 17.7-19.8%. Since the anaerobic reactor and fuel cell systems comprises 65-74% of total equipment costs, the hydraulic retention time of organic wastes and the average current density of fuel cells play a major role in minimizing costs without compromising conversion efficiencies.

7.1 Context

Biomass conversion by anaerobic digestion is a remarkable alternative to provide renewable energy with relatively low energy consumption. Besides the potential to upgrade organic residues, this process can also reduce greenhouse gas emissions in waste management and produce an alternative fertilizer from the digestate [46]. In general, the main challenges of biomass digestion projects are the low energy density of organic wastes and the economic viability of biogas production. Moreover, in the small and distributed pro-

duction scale, the efficiency of conventional cogeneration systems may be still significantly limited. Thus, the development of techniques to improve productivity and economic return of products derived from biogas are essential to increase the renewable energy offer from biomass digestion.

In recent years, fuel cell systems have been promoted as an alternative to increase efficiency and revenues of biogas plants. For instance, Siefert and Litster [156] proposed a system of thermophilic anaerobic digestion combined with a solid oxide fuel cell (SOFC) and achieved positive investment return rates for wastewater treatment plants (WWTP). More recently, Gandiglio, et al. [155] reported energy efficiencies above 50% for an industrial-size SOFC system operating with WWTP biogas, demonstrating that this system concept could achieve remarkable performances. Furthermore, Curletti, et al. [153] observed that SOFC systems could theoretically achieve energy efficiency above 70% and positive net present values with mathematical optimization.

Although several studies have reported analysis for biogas systems, few were able to employ an optimization routine for the entire process of biogas production and utilization. In cases of biogas derived from agriculture wastes, for instance, the power generation can directly affect biogas production since heat is used to maintain the mesophilic conditions (35-40 °C) in the digester. Thus, the search for optimal design and operation solutions have to include a detailed model of those processes. In order to fulfill this knowledge gap, this study presents an optimization analysis including detailed models for anaerobic digestion and solid oxide fuel cells to discuss the impact of some design variables in costs and efficiency.

7.2 Process description

Figure 7.1 shows the biogas production and power generation processes analyzed in this study. The organic wastes from a pig farm with 4500 animals are used to produce biogas for a solid oxide fuel cell system, which cogenerates power and heat. In addition, the system is designed to endure an environmental temperature of 5 °C, which corresponds to a harsh winter climate for most cities in Brazil.

The digester is modelled as a continuously stirred reactor in steady-state and operating in the mesophilic temperature range (35 °C). The swine manure is mixed with a recycled portion of effluent and heated to temperatures slightly above 35 °C (max. 40 °C) to maintain the operational temperature in the anaerobic reactor. If the heat recovery from power generation is not able to supply enough energy for the digester heating, a heat pump system is dimensioned to match the energy demand. The anaerobic digestion effluent is stored and used in crops irrigation, while biogas is sent to a gas processing unit to remove

Figure 7.1: Biogas production and power generation flowsheet

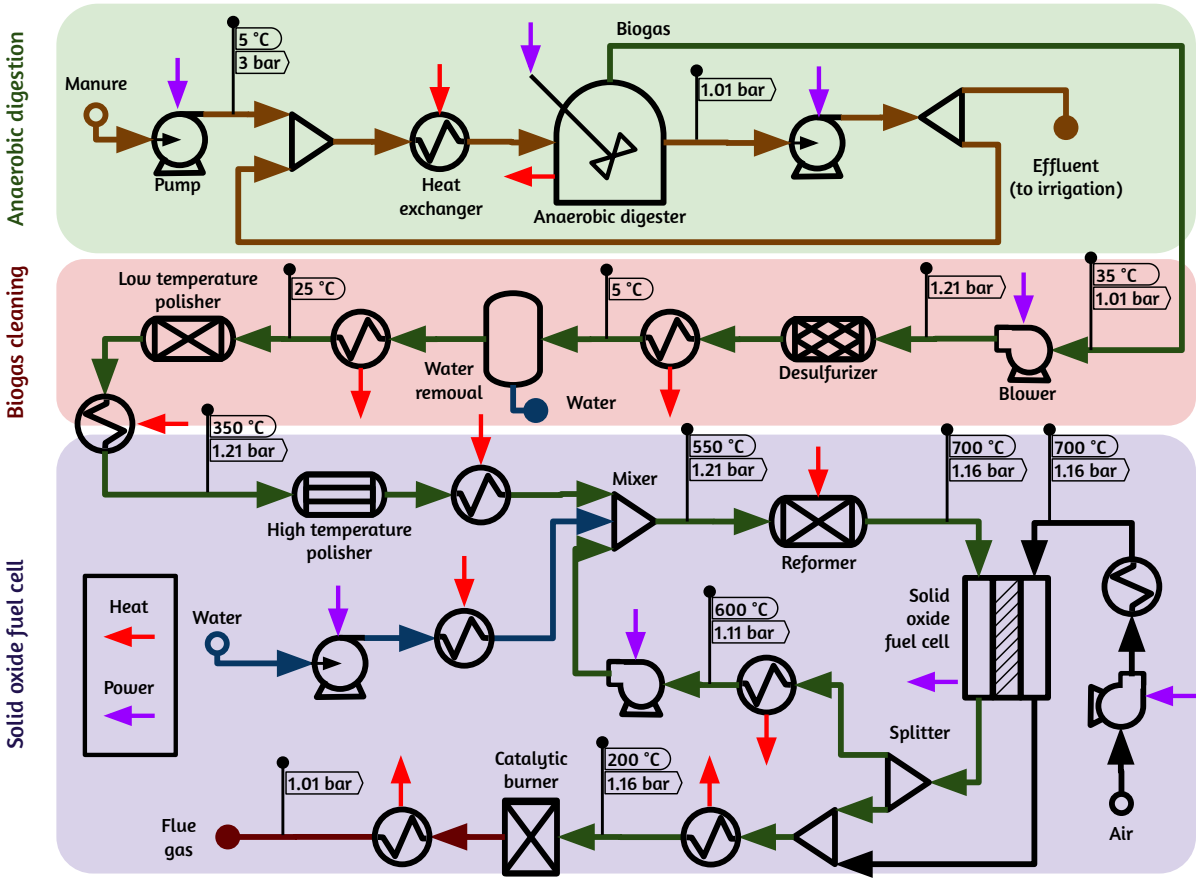

Source: [42]

major contaminants.

The gas processing unit aims to remove impurities which could potentially harm or reduce the efficiency of downstream equipment. The unit consists of three steps: desulfurization, dehumidification and a low temperature polisher [186]. The desulfurization uses an iron oxide media to react hydrogen sulfide into a stable metal sulfide. Next, water is condensed at low temperatures (5 °C) to improve the efficiency of the following carbon activated adsorption, which removes organic vapors and siloxanes. After the removal of main contaminants, clean biogas is sent to the fuel cell unit for power and heat cogeneration.

Since the concentration of hydrogen sulfide in biogas can have sudden spikes depending on the anaerobic digestion conditions, the proposed system has an additional high temperature polisher using activated carbon to work as a safe-bed for reactors and fuel cells. Steam is added to biogas in order to avoid carbon deposition and to convert methane into hydrogen through steam reforming. Also, a portion of the anode off-gas is recycled to reduce fuel losses and steam consumption. A small reformer is used to increase the hydrogen concentration at the fuel cell inlet and reduce drastic temperature drops caused

by the internal reforming of methane.

In order to simplify the thermodynamic model, the solid oxide fuel cells are assumed to be planar, anode supported and arranged in stacks with concurrent flow of fuel and air. The electricity produced by the fuel cells is converted into alternating current by a power inverter for the power grid. A high percent of theoretical air is employed to avoid an excessive temperature difference in the fuel cell stacks (>200 K) [152]. Since the fuel cell is unable to convert all hydrogen into electricity, a portion of the anode exhaust gas is reacted with the cathode off-gas in a catalytic burner to supply heat for other processes.

The main operational conditions and assumptions for the proposed system are presented in Table 7.1. It is important to highlight that the values for hydraulic retention time (HRT) of swine manure, the SOFC fuel utilization efficiency, current density (j), percent of theoretical air and steam to fuel ratio are varied in a multi-objective optimization. The heat exchanger network and utility systems (cooling tower and heat pump/refrigeration) are dimensioned by another optimization routine, based on the mixed-integer linear programming (MILP) problem proposed by Papoulias and Grossmann [76]. This approach of process synthesis is similar to the one proposed by Palazzi, et al. [150] for the optimization of fuel cell systems and aims to ensure more design flexibility for optimization.

Table 7.1: Main operational conditions and assumptions

Parameter	Value	Source
Environmental temperature (°C)	5	
Waste production (l/d-animal)	4.5	[28]
Total solids (TS) - swine manure (kg/m^3)	60	[27]
Power consumption for mixing (W/$m^3_{reactor}$)	6.5	[29]
Heat loss - SOFC (% fuel LHV)	2	[57]
Heat loss - Catalytic burner (% fuel LHV)	2	[57]
Pressure drop - SOFC and reactor (kPa)	5	[57]
Isentropic efficiency - pump and compressors (%)	70	
Isentropic efficiency - anode recycle compressor (%)	50	
Prereforming conversion (% inlet CH_4)	5	
Anode recycle ratio	0.5	
Power inverter efficiency (%)	95	
Minimal temperature for heat recovery (°C)	30 + $T_{\text{dew point}}$	
Global temperature approach (°C)	20	
Heat pump (R134a) temperatures (°C)	-15/60	
Heat pump (R134a) COP	2.5	

Source: [42]

7.3 Modelling details

This study uses the same methods presented in the previous chapter to model the thermodynamic, economic and optimization problems. The main difference of this analysis is the inclusion of a detailed anaerobic digestion model and the modification of optimization parameters, which are presented in Table 7.2.

Table 7.2: Optimization parameters

Parameter	Value
Hydraulic retention time of organic wastes (d)	25-35
Steam to fuel ratio (mol/mol)	1.0-2.0
Fuel utilization efficiency - SOFC	0.5-0.7
Average current density - SOFC (A/cm^2)	0.1 - 0.3
Percent of theoretical air - SOFC	200-300 %
Objective functions	η_{ex} and LCOE
Number of generations	30
Population size	50

Source: [42]

7.3.1 Anaerobic digestion model description

The Anaerobic Digestion Model N°1 (ADM1) is used to model the biogas production from swine manure using the calibrated parameters proposed by Jurado, et al. [197]. The ADM1 is a general kinetic model for anaerobic digestion that consists of several differential equations for the main substances in the process [25]. In general, the mathematical model assumes a continuously stirred reactor (CSTR) configuration and liquid-gas phase equilibrium, as described in Eqs. (7.1) to (7.3). Since solids retention is usually present in anaerobic reactors, a simple modification in the retention time (x1.5 HRT) of these components is included to reduce deviations in the model estimations, as proposed in the original ADM1 publication [25]. A detailed description of these parameters can be consulted in chapter 2 and the original ADM1 publication [25].

$$\frac{dZ_i}{dt} = (Z_{in,i} - Z_{liq,i})\frac{\dot{V}_{liq}}{V_{liq}} - Z_{gas,i}\frac{\dot{V}_{gas}}{V_{gas}} + \sum_j \nu_{i,j} r_j \tag{7.1}$$

$$\dot{V}_{gas} = \frac{RTV_{liq}}{P - P_{H_2O}}\left(\frac{\rho_{H_2}}{16} + \frac{\rho_{CH_4}}{64} + \rho_{CO_2}\right) \tag{7.2}$$

$$\rho_i = k_L a\left(Z_i - K_{H,i} Z_{gas,i} RT\right) \text{ for i } \in \{H_2, CH_4, CO_2\} \tag{7.3}$$

A constant value of pH (8.2) was assumed, based on the experimental data of Jurado, et al. [197], to simplify the charge balance and acid-base equilibrium, which can be major sources of instability in this type of model. Thus, the model assumes that the pH is ideally controlled in order to simplify solution of the ADM1 system of differential equations. Moreover, an average concentration of H_2S (400 ppm) based on the average values reported by Papadias, et al. [186] is assumed in this analysis, since the ADM1 [25] and Jurado et al. [197] studies have not included the effects of H_2S generation in their studies.

Table 7.3 presents a comparison between the results of the model with experimental data from Jurado et al. [197]. The results for biogas production and methane concentration are in fairly agreement with experimental data, therefore the model was considered as a valid representation of the process for a thermoeconomic study. However, the model employed in this study has some deviations compared with experimental data for organic acids, which are probably connected with the CSTR simplification. The main impact of these deviations is on the estimation of the exergy flow rate of digestate (outlet flow of anaerobic digestion). This impacts on the distribution of exergy destruction, in which part of the exergy destroyed actually in the anaerobic digestion may be attributed to the digester effluent in this analysis.

Table 7.3: Model validation using data reported by Jurado, et al. [197]

	Dataset 1		Dataset 2	
Parameter	Experiment	Model	Experiment	Model
Operational conditions				
Influent COD (gCOD/l)	71.1 ± 17.0	71.1	72.1 ± 17.0	72.1
Retention time (d)	26.0 ± 3.5	26.0	26.7 ± 1.9	26.7
Temperature (°C)	38	38	38	38
pH	8.2 ± 0.1	8.2	8.3 ± 0.1	8.3
Results				
Biogas production (l/d)	2.2 ± 0.1	2.3	2.2 ± 0.2	2.0
Methane (vol. %)	61.0 ± 0.6	55.5	63.2 ± 1.2	63.1
Acetic acid (mgCOD/l)	35 ± 14	367	28 ± 7	895
Propionic acid (mgCOD/l)	5 ± 2	22	3 ± 0.4	22
Butyric acid (mgCOD/l)	5 ± 3	14	5 ± 4	14

Source: [42]

Reactor size and heat losses

The anaerobic reactor size is determined by the hydraulic retention time of the organic wastes, which is a design variable in the optimization problem. In order to estimate the heat losses, average values for overall heat transfer coefficients (U) proposed by Tchobanoglous, et al. [29] are assumed to simplify the calculations. Table 7.4 shows a summary of the values adopted in this analysis to estimate the heat losses for the anaerobic reactor.

Table 7.4: Model assumptions for heat losses of the anaerobic reactor

Parameter	Value	Observation
U - Walls ($W/m^2.°C$)	0.7	Concrete (300 mm) with insulation [29]
U - Floor ($W/m^2.°C$)	2.85	Concrete (300 mm) in contact with moist earth [29]
U - Cover ($W/m^2.°C$)	0.95	Insulating board (25 mm) installed under roofing [29]
Environment temperature	5 °C	Brazilian winter climate
Diameter/Height ratio	1	Minimal surface area per volume

Source: [42]

7.3.2 Exergy analysis assumptions

In order to estimate the exergy flow rate of organic compounds in waste streams, the correlation between specific chemical exergy and chemical oxygen demand (COD) proposed by Nogueira Nakashima and Oliveira Junior [46] is employed in this study. Thus, the exergy efficiency of the overall system is defined based on the total exergy flow rate of organic wastes and water consumption, as presented in Eq. (7.4). In order to simplify the analysis, it is assumed that all water present in swine manure can be recovered in irrigation and, therefore, can be excluded from the exergy consumption.

$$\eta_{ex} = \frac{\dot{W}_{net}}{\dot{B}_{COD} + \sum \dot{B}_{\text{process water}}} \tag{7.4}$$

The multi-objective optimization is unconstrained, but technical limitations are indirectly enforced in the optimization by altering the price of equipment. For example, if the model calculates a high temperature change in the SOFC (> 200 K), the equipment cost is double to simulate a drastic reduction in the equipment lifetime. Moreover, the variables domain was tested and limited to avoid technical problems, for instance, fuel depletion, carbon formation and high concentration of volatile acids on anaerobic digestion.

7.4 Results and discussion

Figure 7.2 shows the results for the multi-objective optimization of exergy efficiency and LCOE for the proposed system. As it can be observed, the optimal values for the electricity costs are between 0.13-0.20 USD_{2019}/kWh, while the exergy efficiency varies from 17.7-19.8%. The results also indicate a clear trend of higher costs for more efficient systems, which can be explained by observing the differences between the opposing optimal points, as described in Table 7.5.

Figure 7.2: Multi-objective optimization results

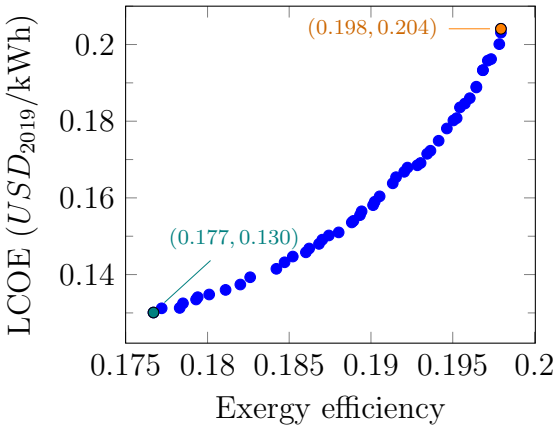

Source: [42]

The results presented in Table 7.5 and Fig. 7.3 indicate that the optimal variables mainly differ in the values for hydraulic retention time and current density. These parameters directly affect the anaerobic digestion and power generation processes, as it can be observed in the results for methane production and cell voltage. For these processes, a larger equipment is able to achieve better conversion efficiencies but this improvement has a thermodynamic limit. As the methane production and cell voltage get closer to their thermodynamic limits, the effective gains in these parameters are quite small compared with the increase in equipment costs. Thus, although the exergy efficiency can be increased in 17.9% compared with the minimal LCOE solution, this performance gain may not be justifiable since the total equipment costs are increased by a much higher factor (70%).

The results presented in Table 7.5 can also be compared with values reported by previous researchers. For instance, MosayebNezhad, et al. [154] estimated a levelized cost of electricity of 0.134-0.309 EUR_{2018}/kWh for a SOFC system annexed to a wastewater treatment plant (WWTP) for the year of 2018 and a short term scenario. Girona, et al. [198] also determined an average LCOE of 0.173 EUR_{2018}/kWh for a similar system, while Papadias, et al. [186] calculated a value of 0.105 USD_{2010}/kWh for a molten carbonate

Table 7.5: Multi-objective optimization results

Parameter	Max. η_{ex}	Min. LCOE
Variables		
Hydraulic retention time (d)	32.0	25.2
Percent of theoretical air (%)	202	202
Steam to fuel ratio (mol/mol)	1.0	1.0
Current density (A/cm^2)	0.1	0.3
Fuel use ratio (-)	0.7	0.7
Investment ($kUSD_{2019}$)		
Equipment	431	254
Total overnight cost	982	578
Overall system		
Net power (kW)	68	61
Exergy efficiency (%)	19.8	17.7
LCOE (USD_{2019}/kWh)	0.20	0.13
Anaerobic digestion		
CH_4 production (Nm^3/d)	334	320
CH_4 concentration (%)	42	43
Reactor volume (m^3)	649	509
Heat loss (kW)	41	39
Fuel cell		
Gross power (kW)	84	71
Voltage (per cell)	0.8	0.7
Total cell area (m^2)	107	36
Outlet temperature (°C)	788	840
Utilities		
Auxiliary heating (kW)	17	5.9
Refrigeration (kW)	0.3	0.3

Source: [42]

fuel cell (MCFC) using WWTP biogas. It is important to highlight that these previous works have not considered the costs of biogas production in their analysis, since several wastewater treatment plants are already working without an energy recovery system. Thus, if the costs of the anaerobic digestion system was attributed to the pig farming, the levelized costs could be significantly lower than those presented previously.

The minimal LCOE achieved by the proposed system is superior to the average electricity costs in Brazil (approx. 0.10-0.12 USD/kWh with taxes) [184] and other bioenergy

Figure 7.3: Hydraulic retention time (HRT) and current density (j) for the Pareto frontier

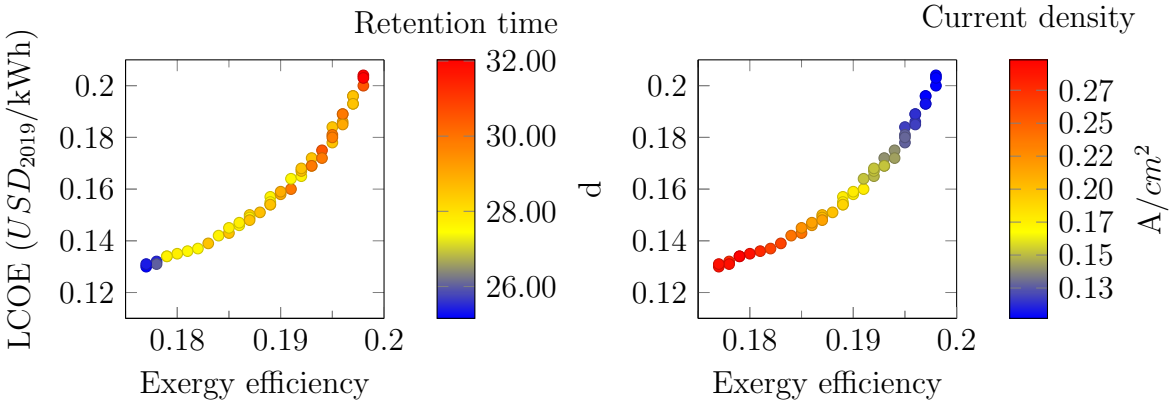

Source : Author

sources (approx. 0.07 USD/kWh) [188], therefore this system would not be economically viable without other financial incentives. A similar result has also been reported by other studies for power generation using swine manure mono-digestion [199, 200], in which the electricity costs were higher than selling prices. Other researchers have indicated that the economic feasibility of these systems could be improved for scenarios with large power plants (1MW) or by using a more concentrated feedstock [201, 156], but the amount of organic wastes readily available may not be sufficient to power these facilities.

The influence of the weighted average capital cost (WACC) on the levelized cost of electricity (LCOE) is depicted in Figure 7.4 for the minimum cost scenario. As it can be observed, the system can attain an interest ratio of return of 2%-6% if the average electricity costs are 0.10-0.12 USD/kWh.

Figure 7.4: Influence of WACC in the LCOE for the minimum cost scenario

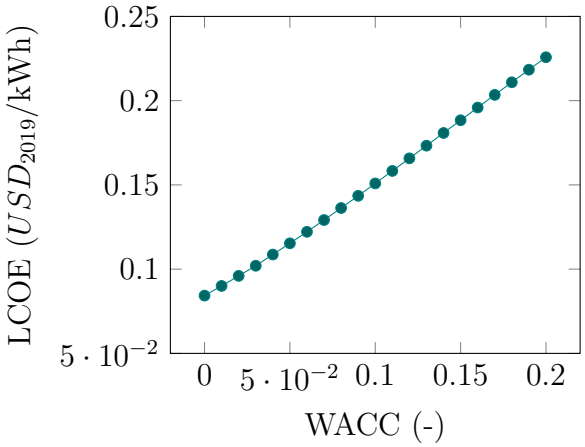

Source: Author

7.4.1 Equipment cost breakdown

Figure 7.5 shows a detailed distribution of equipment costs for the optimal solutions with maximum efficiency and minimal LCOE. As it can be observed, the anaerobic digester and SOFC system are the most expensive equipment, representing 65-74% of total equipment cost, due to their large size or high specific costs. Thus, the electricity cost may be significantly reduced if the swine manure could be supplied at higher concentration of solids (e.g., improving manure collection), since this would reduce the influent flow rate and, consequently, the reactor volume for a constant HRT. In fact, many biogas plants achieve a similar effect by mixing other organic waste (or energy crop) with manure in order to boost biogas production. Other remarkable contributions to the total equipment costs are the gas processing unit (11-17%) and heat exchanger network (9%).

Figure 7.5: Total equipment cost for selected optimal solutions

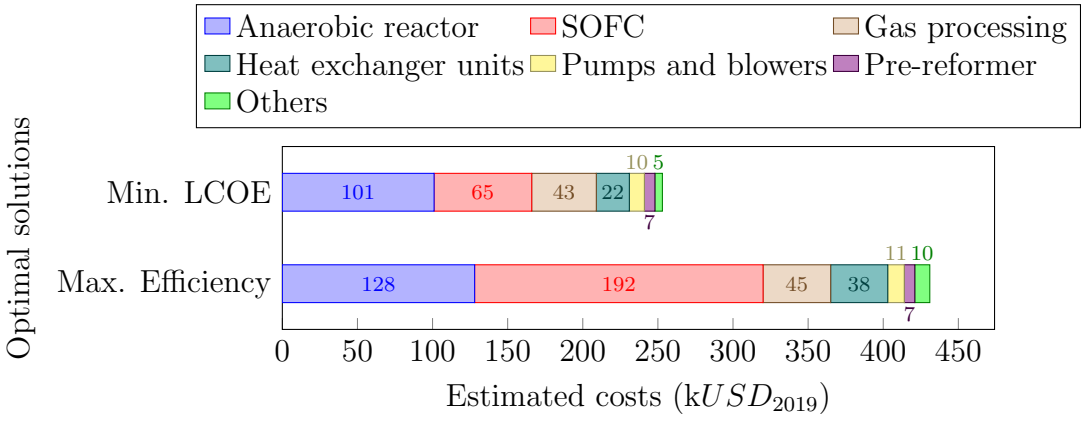

Source: [42]

7.4.2 Exergy assessment

The main source of exergy destruction rate for the selected optimal solutions is the exergy loss of organic matter that is not converted by the anaerobic digestion (70%), as it can be observed in Fig. 7.6. In general, anaerobic digestion can not convert complex organic substances (e.g., lignin) in a reasonable retention time due to limitations of the hydrolysis process. Thus, a significant portion of organic matter is considered as inert to the process and remains in the effluent (or sludge), which is usually discarded to the environment. Similar results were also reported by Nogueira Nakashima and Oliveira Junior for sugarcane vinasse [46], a massive effluent in ethanol distilleries, in which the inclusion of wastewater exergy indicates relative low exergy efficiencies for biogas plants (12.8%). Based on these results, it can be inferred that there is a significant potential to develop efficient technologies to convert organic wastes. For instance, the anaerobic sludge could

be separated and concentrated to produce fertilizers, energy or biofuels.

Figure 7.6: Exergy destroyed rate distribution for selected optimal solutions

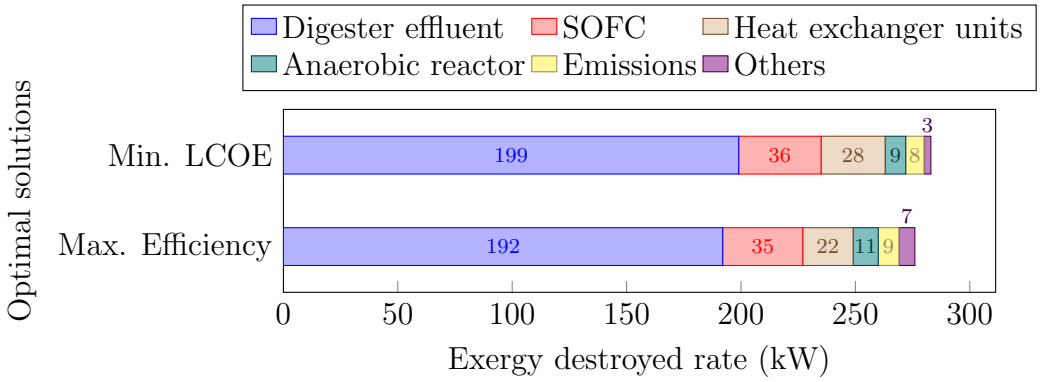

Source: [42]

7.5 Concluding remarks

In this study, a multi-optimization analysis for a system producing biogas from swine manure for power generation with solid oxide fuel cells is presented and discussed. Furthermore, a detailed modelling of the anaerobic digestion and fuel cell systems is employed to determine the impact of design variables in the electricity costs and system efficiency. The results indicate that the proposed system is able to achieve a minimal LCOE of 0.13 USD_{2019}/kWh and a maximum exergy efficiency of 19.8%. Moreover, these parameters are significantly affected by the hydraulic retention time of organic wastes and the average current density of the SOFC system. Since the anaerobic reactor and fuel cell system are responsible for 65-74% of the total equipment costs, the minimization of LCOE tries to reduce these equipment sizes without compromising the methane production or fuel conversion efficiency.

Nevertheless, the optimal solutions were not able to achieve competitive electricity costs compared with other energy sources (<0.10 USD/kWh). This can be partially attributed to the low concentration of organic wastes (6% TS) and the small scale of the system (<70 kW). The exergy analysis pinpoints a major unexplored potential in the anaerobic digestion effluent, which contains several organic substances that can not be converted by anaerobic digestion. Thus, the conversion of anaerobic digestion effluent/sludge into valuable products (e.g., fertilizer, solid fuels or energy) can have significant impacts in efficiency and, consequently, make biogas production more financially attractive.

8 Results overview

In order to compare the results of studies of this thesis, this chapter presents a summary of the main performance indicators for each plant configuration. Since each study of this research has its own particularities, some parameters were calculated based on the previous results or modified to allow a fair comparison between the numerical values. Tables 8.1 and 8.2 summarize a comparison between the exergy efficiency and gross profits of the different analysis of this thesis. Since some studies include the modelling of biogas/syngas production, while other studies focus only on the gas conversion into products, two efficiency types are presented in Table 8.1. The overall efficiency considers the organic wastes (e.g., vinasse, bagasse and swine manure) and includes the anaerobic digestion, gasification and utilities systems in the analysis. Thus, the overall efficiency is significantly lower than the values presented in other scenarios which assume biogas as the main input. (i.e., gas conversion efficiency).

Table 8.1: Summary of exergy efficiency results

Product	Input	Technology	Utility	Overall efficiency	Gas conversion efficiency[a]
Power generation systems					
Electricity	Vinasse & bagasse	Rankine	-	10.0	24.0
Electricity	Vinasse & bagasse	Combined cycle	-	18.0	38.1
Electricity	Swine manure	SOFC	-	17.7 - 19.8	45.2 - 48.5
Electricity	Biogas	SOFC	-	-	45.5 - 58.6
Electricity	Methane	SOFC	-	-	53.8
Biomethane production systems					
CH_4	Vinasse & bagasse	Selexol	Rankine	41.0	85.4

Continued on next page

Table 8.1 – *Continued from previous page*

Product	Input	Technology	Utility	Overall efficiency	Gas conversion efficiency[a]
CH_4	Vinasse & bagasse	Selexol	Combined cycle	44.0	81.4
Hydrogen production systems					
H_2	Vinasse & bagasse	Steam reforming	Rankine	32.0	62.2
H_2	Vinasse & bagasse	Steam reforming	Combined cycle	34.0	61.2
H_2	Biogas	Steam reforming	Power grid	-	63.0
Hybrid systems					
H_2 and electricity	Biogas	SOFC	-	-	58.7 - 60.2
H_2 and electricity	Biogas	Steam reforming & SOFC	-	-	64.5 - 65.6
H_2 and electricity	Methane	SOFC	-	-	68.6

[a]Excludes gas production and utilities systems.

Source: Author

Table 8.2: Summary of specific gross profits (USD/kWh_{fuel}) and equipment cost (USD/$kW_{product}$)

Product	Input	Technology	Utility	Specific gross profits[a] ($\frac{USD}{kWh_{fuel}}$)	Specific equipment cost ($\frac{kUSD}{kW_{prod.}}$)
Power generation systems					
Electricity	Biogas & syngas	Rankine	-	0.019	
Electricity	Biogas & syngas	Combined cycle	-	0.033	
Electricity[b]	Swine manure	SOFC	-	0.043	6.34

Continued on next page

Table 8.2 – *Continued from previous page*

Product	Input	Technology	Utility	Specific gross profits[a] ($\frac{USD}{kWh_{fuel}}$)	Specific equipment cost ($\frac{kUSD}{kW_{prod.}}$)
Electricity[b]	Biogas	SOFC	-	0.054	1.33
Electricity	Methane	SOFC	-	0.054	
Biomethane production systems					
CH_4	Biogas & syngas	Selexol	Rankine	0.037	
CH_4	Biogas & syngas	Selexol	Combined cycle	0.040	
Hydrogen production systems					
H_2	Vinasse & bagasse	Steam reforming	Rankine	0.053	
H_2	Vinasse & bagasse	Steam reforming	Combined cycle	0.056	
H_2[b]	Biogas	Steam reforming	Power grid	0.054	1.03
Hybrid systems					
H_2 and electricity[b]	Biogas	SOFC	-	0.049	2.13
H_2 and electricity[b]	Biogas	Steam reforming & SOFC	-	0.059	1.08
H_2 and electricity	Methane	SOFC	-	0.065	

[a]Assuming the product prices of 0.1 USD/$kWh_{electricity}$, 0.05 USD/kWh_{CH4} and 0.09 USD/kWh_{H2}. [b] Scenarios of optimal maximum NPV or minimum product costs

Source: Author

In addition, the specific gross profits (p) and investment costs presented in Table 8.2 represent the expected gains ($\sum_i c_{p,i}\dot{B}_{p,i}$) minus the electricity costs ($c_e\dot{W}_{grid}$) per unit of exergy of fuel ($\sum_i \dot{B}_{f,i}$). The specific gross profit (p), defined in Eq. 8.1, is presented as a simple parameter for comparing all studies in a common basis, since not all analysis estimated the capital costs of the production plant. As it can be observed in Table 8.2, systems that integrate fuel cell technology can achieve higher specific gross profits since their efficiency can be improved compared with conventional conversion routes of electricity and hydrogen. However, the specific equipment costs may also be significantly

higher than conventional technologies, as exemplified by the system working with swine manure. It is important to highlight that the specific equipment costs for SOFC systems presented in Table 8.2 are significantly lower than previous estimates (Table 2.4). This difference can be partially attributed to detailed economic analysis and optimizations evaluated in this thesis.

$$p = \frac{\sum_i \left(c_{p,i} \dot{B}_{p,i} \right) - c_e \dot{W}_{\text{grid}}}{\sum_i \dot{B}_{f,i}} \tag{8.1}$$

Lastly, Tables 8.3 and 8.4 summarize the exergy costs and specific CO_2 emissions of each product and scenario. Since some studies extend the analysis to include biogas production and bagasse conversion, two additional costs values are presented to allow a comparison between the results of different systems. The first is the exergy costs of the biofuels produced only by the biogas conversion route and the second is the exergy costs of products assuming an average specific costs and emissions for biogas. A detailed description of the exergy costs and specific emissions is provided in the Appendix C.

Table 8.3: Summary of total and non-renewable exergy costs for the transformation stage

Product	Input	Technology	Utility	Total exergy cost	Non-renewable exergy cost
Electricity					
Electricity	Vinasse & bagasse	Rankine	-	10.26	0.68
Electricity[a]	Biogas	SOFC	-	2.21 (6.59[b])	0 (0.57[b])
Electricity (with CH_4)	Vinasse & bagasse	Rankine	-	5.48-7.12	0.31-0.4
Electricity (with H_2)	Vinasse & bagasse	Rankine	-	6.7-7.12	0.40-0.41
Electricity (with H_2)[a]	Biogas	Steam reforming & SOFC	-	2.13 (6.35[b])	0 (0.56[b])
Methane					
CH_4 (with power)	Vinasse & bagasse	Selexol	Rankine	2.88-2.91 (3.18-3.23[c])	0.19-0.20 (0.27[c])
Hydrogen					
H_2	Biogas	Steam reforming	Power grid	1.59 (4.63[b])	0 (0.42[b])

Continued on next page

Table 8.3 – *Continued from previous page*

Product	Input	Technology	Utility	Total exergy cost	Non-renewable exergy cost
H_2 (with power)	Vinasse & bagasse	Steam reforming	Rankine	3.49-3.54 (5.09[c])	0.24 (0.39[c])
H_2 (with power)[a]	Biogas	SOFC	-	1.73 (5.08[b])	0 (0.52[b])
H2 (with power)[a]	Biogas	Steam reforming & SOFC	-	1.50 (4.49[b])	0 (0.39[b])

[a]Assuming the product prices of 0.1 USD/$kWh_{electricity}$, 0.05 USD/kWh_{CH4} and 0.09 USD/kWh_{H2}. [b] Scenarios of optimal maximum NPV or minimum product costs
Source: Author

Table 8.4: Summary of specific CO_2 emissions for the transformation stage

Product	Input	Technology	Utility	Specific CO_2 emissions (gCO_2/MJ)
Electricity				
Electricity	Vinasse & bagasse	Rankine	-	45.14
Electricity[a]	Biogas	SOFC	-	0 (37.26[b])
Electricity (with CH_4)	Vinasse & bagasse	Rankine	-	20.81-26.56
Electricity (with H_2)	Vinasse & bagasse	Rankine	-	26.56-27.54
Electricity (with H_2)[a]	Biogas	Steam reforming & SOFC	-	0 (35.96[b])
Methane				
CH_4 (with power)	Vinasse & bagasse	Selexol	Rankine	12.8-13.17 (18[c])
Hydrogen				
H_2	Biogas	Steam reforming	Power grid	0 (30.89[b])

Continued on next page

Table 8.4 – *Continued from previous page*

Product	Input	Technology	Utility	Specific CO_2 emissions (gCO_2/MJ)
H_2 (with power)[a]	Vinasse & bagasse	Steam reforming	Rankine	15.63-15.82 (26[c])
H_2 (with power)[a]	Biogas	SOFC	-	0 (33.37[b])
H_2 (with power)[a]	Biogas	Steam reforming & SOFC	-	0 (25.39[b])

[a] Scenarios of optimal maximum NPV or minimum product costs

[b] Assuming $c_{T,biogas} = 3\ kJ/kJ$, $c_{NR,biogas} = 0.26\ kJ/kJ$, $c_{CO2,biogas} = 17\ g_{CO2}/MJ$, $c_{T,elec.} = 1.80\ kJ/kJ$, $c_{NR,elec.} = 0.33\ kJ/kJ$, $c_{CO2,elec.} = 62\ g_{CO2}/MJ$

[c] Product derived from biogas only

Source: Author

Tables 8.3 and 8.4 show that the exergy costs and specific emissions attributed to the products derived from vinasse are significantly higher than the average values including bagasse-derived products. This can be attributed to the high exergy costs and specific emissions of vinasse compared with bagasse, since vinasse is produced after several irreversible processes (e.g., juice concentration, fermentation, distillation). This effect can also be perceived for the fuel cell and hydrogen production systems when the costs of vinasse-derived biogas and electricity [45, 89]. As it can be expected, systems with higher efficiencies have products with lower exergy costs and specific emissions. For instance, the system based on a steam reforming process with a downstream solid oxide fuel cell (H2-SOFC) is able to achieve lower exergy costs and specific emissions of products compared with other systems.

It is important to notice that the analyses presented in this study have some limitations which may influence some of the results presented.

- The results for the exergy unit costs and specific emissions of transportation service are dependent on the assumed efficiencies for the distribution and use of each fuel. Biofuels and electricity can have different end-uses and be converted by different technologies, therefore, the results presented in this study does not take these variabilities into account.

- Sugar is produced alongside with ethanol in all macro analysis in this study. Although this represents a common Brazilian context, the production of sugar affects the exergy cost formation and specific emissions attributed to fuels. Since the production of sugar may alter along the year, the results presented in the macro-analysis represent only a general scenario.

- The gasification model used to convert sugarcane bagasse uses empirical correlations calibrated for wood. Thus, the model results are an extrapolation and it is possible that deviations exist when compared with experimental data for sugarcane bagasse gasification.

- The anaerobic digestion model employed in this study presents some deviations for the concentration of organic acids in the treated effluent. This directly affects the exergy flow rate estimated for the digestate and, consequently, the exergy destruction in the anaerobic digestion. Thus, the exergy potential attributed to the digestate may be overestimated.

- The assumption of a constant overall heat transfer coefficient greatly simplifies the estimation of the heat exchanger area, but it may only be acceptable for sorting optimal designs solutions. A rigorous design of each heat exchanger may lead to different cost values.

- The SOFC model is solved assuming an average current density that is constant along the active cell area. A more accurate condition would be to assume a constant voltage and determine iteratively the local current density. However, this would significantly increase the computational time required to solve the problem and, consequently, compromise the optimization studies.

- The analysis presented in this study assumes constant costs of resources, products and replacing equipment. These values can alter along the years of operation of the biogas plant, which impacts the profitability and cost of products.

9 Conclusions

In this thesis, the conversion of organic wastes into biofuels and electricity throughout anaerobic digestion was investigated at different scenarios by using a systematic framework. At first, the impact of anaerobic digestion and gasification in the Brazilian sugarcane industry was evaluated using exergy analysis, pinch technology and modern optimization routines. Vinasse biodigestion and bagasse gasification can produce an additional 17.8 MW of electricity for a standard sized sugarcane mill (500 ton/h, divided equally into sugar and ethanol production). In the best scenario analyzed, an additional 58.6 MW of exergy can be recovered from sugarcane wastes if synthetic natural gas is produced. In addition, hydrogen production has the highest value for revenues estimated based on the production costs and selling prices of products.

Anaerobic digestion has limitations to convert organic substances into methane (e.g. lignin) which leads to significant amount of exergy losses linked with vinasse disposal. For instance, the effluent of anaerobic digestion can represent an exergy loss of 48% of the exergy consumed by a biomethane production unit converting sugarcane vinasse. Possible solutions include the use of vinasse concentration and/or incineration. Significant improvement of efficiency can also be obtained by reducing the electricity consumption of biomethane production using vinasse, since the power generation utilities are also a great source of irreversibilities. The fist study demonstrated that, among the proposed products for waste conversion, methane is the most efficient option while hydrogen may be the most financially attractive.

In a subsequent stage, the analysis of waste conversion into biofuels and electricity was extended to include the whole life-cycle of the products, from farming to transportation. It was possible to observed that, besides improving the operational revenues (as demonstrated in the previous work), the co-production of hydrogen and electricity can also increase the transportation service delivered to society. One of the main reasons for that is the impact of the end-use efficiency in the transportation service. Although methane can be efficiently produced from wastes using anaerobic digestion and gasification, its distribution and use in vehicles still has several inefficiencies that reduce the effective amount of transportation achieved from this fuel. On the other hand, electricity has efficient distribution and vehicles, but may have several losses in production if there

is not a good purpose for the energy associated with heat. In addition, electricity may not be very financially attractive, since the electricity price is influenced by several energy sources.

In this scenario, the study observed that hydrogen may be an interesting solution for this energy dilemma. Hydrogen production requires a significant amount of steam and heat, which may be combined with a power generation unit to efficiently deliver hydrogen and power. Since hydrogen has a high efficiency of conversion in the end-use stage, the transportation service obtained from a sugarcane ethanol plant are maximized when wastes are converted into hydrogen and electricity. In addition, the operational revenues are also maximized because hydrogen has a market price similar to electricity (in energy basis), but it is easily produced from anaerobic digestion and gasification. Thus, the conversion of wastes into hydrogen and electricity may be interesting for energy producers due to the higher revenues, while for energy buyers (society) this choice maximizes the use of natural resources for transportation services. Moreover, the methane and hydrogen produced from wastes have significantly less emissions than their fossil derivatives counterparts, but the exergy cost of production is also significantly higher due to the irreversibilities in conversion.

Based on theses results, the next research works focused in the development and evaluation of advanced system for producing hydrogen and electricity using solid oxide fuel cells. The research proposed a simplified model for solid oxide fuel cells which was valid for different mixtures of methane, water and carbon dioxide, the main components of steam reformed biogas. Differently from previous works, this model also considered the temperature and composition changes along the fuel cell, which influence the performance and reforming reactions. The analysis have shown that the system may achieve 57-69% of exergy efficiency, 12-28% more than only power generation using fuel cells, depending on the methane concentration and modelling assumptions. This drastic performance improvement is possible since hydrogen separation reduces the amount of fuel that has to be combusted due to incomplete conversion in the fuel cell. However, this solution also depletes the potential for heat cogeneration, which may be an undesirable feature for biogas plants that require heat for anaerobic digestion. In addition, the results are very sensitive to uncertainties in the hydrogen separation unit, such as efficiency and minimal concentration of hydrogen in the inlet.

This thesis also included the economic analysis and multi-objective optimization of the proposed designs for biogas conversion using fuel cells. Differently from previous works, this analysis also included an automated design of the heat transfer network based on the minimization of heat transfer units. The research observed that hydrogen production is much more profitable and efficient than electricity generation for the assumptions adopted

in the analysis. In addition, the usual design for hydrogen and electricity co-production proved to be not economic viable although it can reach higher exergy efficiencies compared with a common solid oxide fuel cell. However, the study also proposes a different approach for hydrogen and electricity co-production using the purge gas of hydrogen separation to power a solid oxide fuel cell. Since biogas has significant concentration of carbon dioxide, the hydrogen separation is less efficient and lead to significant losses in the combustion of purge gases. The fuel cell partially converts the purge gas into electricity and reduces this major source of inefficiency, which leads to higher efficiencies and economic profitability. The study estimates that this modification can improve the net present value of hydrogen production systems in 23%.

Lastly, this research also investigated the energy integration of solid oxide fuel cells in small biogas plants, considering the Brazilian context. In this work, the anaerobic digestion of pig manure was modelled using the Anaerobic Digestion Model N°1, which allows the optimization of the problem to evaluate the impact of operational parameters in anaerobic digestion. The analysis observed that the levelized cost of electricity is estimated to be between 0.13-0.20 USD/kWh, a value that is relatively low compared with previous works and very close to economic viability in Brazil. The hydraulic retention time of wastes and the current density of the solid oxide fuel cell were the variables with most influence in the trade-off between efficiency and electricity costs. A number of technical improvements can be foreseen to improve the technical and economic viability of fuel cells in small biogas plants. For example, improve the concentration of organic substances in the wastes, commercialize the digestate as fertilizer, increase the size of the plant or produce hydrogen as a by-product.

Suggestions for future works

- Evaluate the biogas production efficiency along a complete year, discussing how seasonal changes affect the biogas production unit. Devise novel processes of sugar production that reduce the concentration of sulfur in vinasse, reducing losses and consumptions in biogas production and purification;

- Compare the performance of second generation ethanol (2G ethanol) with the results for bagasse gasification and conversion into methane/hydrogen;

- Design and optimize multi-technology units to recover and reduce solid municipal wastes;

- Evaluate the possibility to replace gas turbines for solid oxide fuel cells in oxycombustion systems;

- Evaluate the use of biogas dry reforming to produce hydrogen and power fuel cells.

References

[1] IEA. Renewables Information: Overview. Technical report, IEA, Paris, 2020.

[2] IEA. Outlook for biogas and biomethane: Prospects for organic growth. Technical report, IEA, Paris, 2020.

[3] CIBIOGÁS. Panorama do Biogás no Brasil 2020. Technical 001/2021, Centro Internacional de Energias Renováveis - CIBiogás, Foz do Iguaçu, March 2021.

[4] CIBIOGÁS. Panorama do Biogás no Brasil 2019. Technical 002/2020, Centro Internacional de Energias Renováveis - CIBiogás, April 2020.

[5] ANEEL (Brazilian Electricity Regulatory Agency). Dados abertos - Geração, 2021.

[6] ANEEL (Brazilian Electricity Regulatory Agency). RESOLUÇÃO NORMATIVA Nº 482,, April 2012.

[7] ANEEL (Brazilian Electricity Regulatory Agency). RESOLUÇÃO NORMATIVA Nº 687,, November 2015.

[8] ANEEL (Brazilian Electricity Regulatory Agency). Dados abertos - Tarifas, 2021.

[9] MAN Engines. POWER: Gas engines for Power Generation, 2020.

[10] Capstone Turbine Corporation. PRODUCTS: the ideal solution for today's distributed generation needs, 2020.

[11] Ansaldo Energia. AE-T100 Biogas Micro Turbine, 2020.

[12] MTU. Biogas generation sets, 2020.

[13] Gruppo AB. Catálogo, 2020.

[14] EPE (Brazilian Energy Research Office). SIEnergia - Sistema de Informação para Energia, resíduos agropecuários e urbanos, 2021.

[15] EPE (Brazilian Energy Research Office). Plano Nacional de Energia 2050. Technical report, Ministry of Mines and Energy, Brasília, Brazil, 2020.

[16] MCTIC (Brazilian Ministry of Science, Technology, Innovation and Communication). Plano de ciência, tecnologia e inovação para energias renováveis e biocombustíveis. Technical report, MCTIC, Brasília, 2018.

[17] Antonio Carlos Mendes Thame. Marco regulatório do gás, 2020.

[18] ABIOGÁS. O que a Lei do Gás representa para o biogás, 2021.

[19] ANP (Brazillian National Agency of Oil, Natural gas and Biofuels). Certificados da Produção ou Importação Eficiente de Biocombustíveis Válidos, 2021.

[20] ANEEL (Brazilian Electricity Regulatory Agency). Sistema de Informações de Geração da ANEEL - SIGA, 2021.

[21] EPE (Brazilian Energy Research Office). Brazillian Energetic Balance (BEN) 2020: year 2019. Technical report, EPE, Rio de Janeiro, Brazil, 2020.

[22] IEA. The Future of Hydrogen. Technical report, IEA, Paris, 2019.

[23] Maria Wellisch, Jennifer Green, Bernadette McCabe, Saija Rasi, Wouter Siemens, Jonas Ammenberg, Jan Liebetrau, Guenther Bochmann, and Jerry D. Murphy. Drivers for sucessful and sustainable biogas projects. Technical report, IEA Task 37, 2020.

[24] Carlos Augustos de Lemos Chernicharo. *Anaerobic reactors*, volume 4 of *Biological Wastewater Treatment*. IWA publishing, London, 2007.

[25] D. J. Batstone and International Water Association, editors. *Anaerobic digestion model no. 1: (ADM1)*. Number 13 in Scientific & technical report. IWA Publ, London, 2002. OCLC: 248361874.

[26] Ernesto L. Barrera, Henri Spanjers, Kimberly Solon, Youri Amerlinck, Ingmar Nopens, and Jo Dewulf. Modeling the anaerobic digestion of cane-molasses vinasse: Extension of the Anaerobic Digestion Model No. 1 (ADM1) with sulfate reduction for a very high strength and sulfate rich wastewater. *Water Research*, 71:42–54, March 2015.

[27] Fachagentur Nachwachsende Rohstoffe e. V (FNR). *Practical guide of biogas: generation and use (In portuguese)*. FNR, Gülzow, 5 th edition, 2010.

[28] Dieter Deublein and Angelika Steinhauser. *Biogas from Waste and Renewable Resources*. Wiley-VCH Verlag GmbH & Co. KGaA, Weinheim, Germany, February 2008.

[29] George Tchobanoglous, H. David Stensel, Ryujiro Tsuchihashi, Franklin L. Burton, Mohammad Abu-Orf, Gregory Bowden, William Pfrang, and Metcalf & Eddy, editors. *Wastewater engineering: treatment and resource recovery*. McGraw-Hill Education, New York, NY, fifth edition edition, 2014. OCLC: ocn858915999.

[30] James R. Baker, Mark W. Milke, and James R. Mihelcic. Relationship between chemical and theoretical oxygen demand for specific classes of organic chemicals. *Water Research*, 33(2):327–334, February 1999.

[31] Oliver Jende, Christoph Platzer, Carolina Cabral, Heike Hoffmann, Sebastian Rosenfeldt, Luis Colturato, Thilo Burkard, Carsten Linnenberg, Walter Stinner, Frank Zörner, and Enga Schröder. *Relevant technologies of anaerobic digestion for Brazil: feedstock, reactors and uses of biogas (In Portuguese)*. Probiogas. Ministry of Cities, Brasília, January 2015.

[32] Rafael Nogueira Nakashima and Silvio de Oliveira Junior. Exergy analysis of biogas production in ethanol distilleries. In *Proceedings of the 24th ABCM International Congress of Mechanical Engineering*. ABCM, 2017.

[33] Teodorita Al Seadi Biosantech, Dominik Rutz, Rainer Janssen, and Bernhard Drosg. Biomass resources for biogas production. In *The Biogas Handbook*, pages 19–51. Elsevier, 2013.

[34] Lili Dong, Guangli Cao, Xianzhang Guo, Tianshu Liu, Jiwen Wu, and Nanqi Ren. Efficient biogas production from cattle manure in a plug flow reactor: A large scale long term study. *Bioresource Technology*, 278:450–455, 2019.

[35] Veronica Moset, Morten Poulsen, Radziah Wahid, Ole Højberg, and Henrik Bjarne Møller. Mesophilic versus thermophilic anaerobic digestion of cattle manure: methane productivity and microbial ecology. *Microbial Biotechnology*, 8(5):787–800, 2015.

[36] Linas Jurgutis, Alvyra Slepetiene, Jonas Volungevicius, and Kristina Amaleviciute-Volunge. Biogas production from chicken manure at different organic loading rates in a mesophilic full scale anaerobic digestion plant. *Biomass and Bioenergy*, 141:105693, October 2020.

[37] Baoning Zhu, Ruihong Zhang, Petros Gikas, Joshua Rapport, Bryan Jenkins, and Xiujin Li. Biogas production from municipal solid wastes using an integrated rotary drum and anaerobic-phased solids digester system. *Bioresource Technology*, 101(16):6374–6380, August 2010.

[38] Edmond-Jacques Nyns, Marcell Nikolausz, and Jan Liebetrau. Biogas. In *Ullmann's Encyclopedia of Industrial Chemistry*, pages 1–14. Wiley-VCH, Germany, 2014.

[39] Christian Rosen and Ulf Jeppsson. Aspects on ADM1 Implementation within the BSM2 Framework. Technical report, Lund University, Lund, Sweden, November 2006.

[40] M. H. Zwietering, J. T. de Koos, B. E. Hasenack, J. C. de Witt, and K. van't Riet. Modeling of bacterial growth as a function of temperature. *Applied and Environmental Microbiology*, 57(4):1094–1101, 1991.

[41] Rafael Nogueira Nakashima. Exergy assessment of biogas generation and usage in the sugarcane industry (In portuguese). Master's thesis, University of São Paulo, São Paulo, September 2018.

[42] Rafael Nogueira Nakashima and Silvio de Oliveira Junior. Trade-offs between productivity, efficiency and costs of biogas plants for agriculture wastes. In *Proceedings of the 34rd International Conference on Efficiency, Cost, Optimization, Simulation and Environmental Impact of Energy Systems*, Taormina, Italy, 2021.

[43] R. N. Nakashima, Daniel Flórez-Orrego, and S. De Oliveira Junior. Integrated anaerobic digestion and gasification processes for upgrade of ethanol biorefinery residues. *Journal of Power Technologies*, 99(2):104–114, 2019.

[44] EPA (United States Environmental Protection Agency). Project Development Handbook: A Handbook for Developing Anaerobic Digestion/Biogas Systems on Farms in the United States. Technical Report 430-B-20-001, EPA, Washington, DC, U.S., 2020.

[45] Rafael Nogueira Nakashima, Daniel Flórez-Orrego, Hector Ivan Velásquez, and Silvio De Oliveira Junior. Sugarcane bagasse and vinasse conversion to electricity and biofuels: an exergoeconomic and environmental assessment. *International Journal of Exergy*, 33(1):44, 2020.

[46] R.N. Nakashima and S. de Oliveira Junior. Comparative exergy assessment of vinasse disposal alternatives: Concentration, anaerobic digestion and fertirrigation. *Renewable Energy*, 147:1969–1978, March 2020.

[47] Anneli Petersson. Biogas cleaning. In *The Biogas Handbook*, pages 329–341. Elsevier, 2013.

[48] Rodrigo Marcelo Leme and Joaquim E.A. Seabra. Technical-economic assessment of different biogas upgrading routes from vinasse anaerobic digestion in the Brazilian bioethanol industry. *Energy*, 119:754–766, January 2017.

[49] Sara Giarola, Ornella Forte, Andrea Lanzini, Marta Gandiglio, Massimo Santarelli, and Adam Hawkes. Techno-economic assessment of biogas-fed solid oxide fuel cell combined heat and power system at industrial scale. *Applied Energy*, 211:689–704, February 2018.

[50] Prasad Kaparaju and Jukka Rintala. Generation of heat and power from biogas for stationary applications: boilers, gas engines and turbines, combined heat and power (CHP) plants and fuel cells. In *The Biogas Handbook*, pages 404–427. Elsevier, 2013.

[51] US Energy Information Administration. Distributed Generation and Combined Heat & Power System Characteristics and Costs in the Buildings Sector. Technical Report DC 20585, U.S. Department of Energy, Washington, DC, U.S., 2017.

[52] U. S. Department of Energy. Fuel Cell Technologies Office Multi-Year Research, Development, and Demonstration Plan - Section 3.4 Fuel Cells. Technical report, U.S. Department of Energy, United States of America, 2017.

[53] Natural gas and Biofuels) ANP (Brazilian National Agency of Oil. Resolução ANP N 685, de 29.6.2017 - DOU 30.6.2017. Technical report, ANP, Brasília, Brazil, 2017.

[54] Qie Sun, Hailong Li, Jinying Yan, Longcheng Liu, Zhixin Yu, and Xinhai Yu. Selection of appropriate biogas upgrading technology-a review of biogas cleaning, upgrading and utilisation. *Renewable and Sustainable Energy Reviews*, 51:521–532, November 2015.

[55] Michael Beil and Wiebke Beyrich. Biogas upgrading to biomethane. In *The Biogas Handbook*, pages 342–377. Elsevier, 2013.

[56] Fredric Bauer, Tobias Persson, Christian Hulteberg, and Daniel Tamm. Biogas upgrading - technology overview, comparison and perspectives for the future. *Biofuels, Bioproducts and Biorefining*, 7(5):499–511, September 2013.

[57] W.L. Becker, R.J. Braun, M. Penev, and M. Melaina. Design and technoeconomic performance analysis of a 1MW solid oxide fuel cell polygeneration system for combined production of heat, hydrogen, and power. *Journal of Power Sources*, 200:34–44, February 2012.

[58] Peter Häussinger, Reiner Lohmüller, and Allan M. Watson. Hydrogen, 2. Production. In Wiley-VCH Verlag GmbH & Co. KGaA, editor, *Ullmann's Encyclopedia of Industrial Chemistry*, page o13_o03. Wiley-VCH Verlag GmbH & Co. KGaA, Weinheim, Germany, October 2011.

[59] Joan M. Ogden. Review of small stationary reformers for hydrogen production. Technical Report IEA/H2/TR-02/002, International Energy Agency, Princeton, NJ, 2002.

[60] Rainer Reimert, Friedemann Marschner, Hans-Joachim Renner, Walter Boll, Emil Supp, Miron Brejc, Waldemar Liebner, and Georg Schaub. Gas Production, 2. Processes. In Wiley-VCH Verlag GmbH & Co. KGaA, editor, *Ullmann's Encyclopedia of Industrial Chemistry*, page o12_o01. Wiley-VCH Verlag GmbH & Co. KGaA, Weinheim, Germany, October 2011.

[61] K. Sasaki and Y. Teraoka. Equilibria in Fuel Cell Gases. *Journal of The Electrochemical Society*, 150(7):A878, 2003.

[62] J.R. Rostrup-Nielsen and J. Bøgild Hansen. Steam Reforming for Fuel Cells. In *Fuel Cells: Technologies for Fuel Processing*, pages 49–71. Elsevier, 2011.

[63] A Simpson and A Lutz. Exergy analysis of hydrogen production via steam methane reforming. *International Journal of Hydrogen Energy*, 32(18):4811–4820, December 2007.

[64] Air liquide. Air liquide technology handbook: November 2019, 2019.

[65] Walter Boll, Gerhard Hochgesand, Christopher Higman, Emil Supp, Peter Kalteier, Wolf-Dieter Müller, Manfred Kriebel, Holger Schlichting, and Heiner Tanz. Gas Production, 3. Gas Treating. In Wiley-VCH Verlag GmbH & Co. KGaA, editor, *Ullmann's Encyclopedia of Industrial Chemistry*, page o12_o02. Wiley-VCH Verlag GmbH & Co. KGaA, Weinheim, Germany, October 2011.

[66] Ryan O'Hayre, Suk-Won Cha, Whitney Colella, and Fritz B. Prinz. *Fuel Cell Fundamentals*. John Wiley & Sons, Inc, Hoboken, NJ, USA, May 2016.

[67] James Larminie and Andrew Dicks. *Fuel Cell Systems Explained*. John Wiley & Sons, Ltd,., West Sussex, England, February 2003.

[68] Cheng Bao, Ying Wang, Daili Feng, Zeyi Jiang, and Xinxin Zhang. Macroscopic modeling of solid oxide fuel cell (SOFC) and model-based control of SOFC and gas turbine hybrid system. *Progress in Energy and Combustion Science*, 66:83–140, May 2018.

[69] P. Aguiar, C.S. Adjiman, and N.P. Brandon. Anode-supported intermediate temperature direct internal reforming solid oxide fuel cell. I: model-based steady-state performance. *Journal of Power Sources*, 138(1-2):120–136, November 2004.

[70] Angelika Heinzel, Marcella Cappadonia, Ulrich Stimming, Karl V. Kordesch, and Julio Cesar Tambasco Oliveira. Fuel Cells. In *Ullmann's Encyclopedia of Industrial Chemistry*, pages 1–24. Wiley-VCH Verlag GmbH & Co. KGaA, Weinheim, Germany, May 2018.

[71] R. Nogueira Nakashima and S. Oliveira Junior. Multi-objective optimization of biogas systems producing hydrogen and electricity with solid oxide fuel cells. *International Journal of Hydrogen Energy*, page S036031992103442X, September 2021.

[72] E. Fontell, T. Kivisaari, N. Christiansen, J.-B. Hansen, and J. Pålsson. Conceptual study of a 250kW planar SOFC system for CHP application. *Journal of Power Sources*, 131(1-2):49–56, May 2004.

[73] F. Calise, M. Dentice d' Accadia, L. Vanoli, and Michael R. von Spakovsky. Full load synthesis/design optimization of a hybrid SOFC–GT power plant. *Energy*, 32(4):446–458, April 2007.

[74] Ian C. Kemp. *Pinch Analysis and Process Integration*. Elsevier, 2006.

[75] L. E. Grimes. The synthesis and evaluation of networks of heat exchanger that feature the minimum number of units. Master's thesis, Carnegie-Melon, Pittsburgh, 1980.

[76] Soterios A. Papoulias and Ignacio E. Grossmann. A structural optimization approach in process synthesis—II. *Computers & Chemical Engineering*, 7(6):707–721, January 1983.

[77] F. Maréchal and B. Kalitventzeff. Effect modelling and optimization, a new methodology for combined energy and environment synthesis of industrial processes. *Applied Thermal Engineering*, 17(8-10):981–992, August 1997.

[78] Yang Chen, Ignacio E. Grossmann, and David C. Miller. Computational strategies for large-scale MILP transshipment models for heat exchanger network synthesis. *Computers & Chemical Engineering*, 82:68–83, November 2015.

[79] Lothar Riekert. The efficiency of energy-utilization in chemical processes. *Chemical Engineering Science*, 29(7):1613–1620, July 1974.

[80] J Szargut, D. R. Morris, and F. R. Steward. *Exergy analysis of thermal, chemical, and metallurgical processes*. Hemisphere, 1987.

[81] Jan Szargut. *Exergy method: technical and ecological applications*. Number 18 in International series on developments in heat transfer. WIT Press, Southampton ; Boston, 2005. OCLC: ocm56874184.

[82] T.J. Kotas. *The Exergy Method of Thermal Plant Analysis*. Elsevier, 1985.

[83] Silvio de Oliveira Junior. *Exergy: Production, Cost and Renewability*. Green Energy and Technology. Springer London, London, 2013.

[84] Shingo Tai, Kazuo Matsushige, and Takeshi Goda. Chemical exergy of organic matter in wastewater. *International Journal of Environmental Studies*, 27(3-4):301–315, October 1986.

[85] Adrian Bejan, G. Tsatsaronis, and Michael J. Moran. *Thermal design and optimization*. Wiley, New York, 1996.

[86] Daniel Flórez-Orrego and Silvio de Oliveira Junior. Modeling and optimization of an industrial ammonia synthesis unit: An exergy approach. *Energy*, 137:234–250, October 2017.

[87] Andrea Lazzaretto and George Tsatsaronis. SPECO: A systematic and general methodology for calculating efficiencies and costs in thermal systems. *Energy*, 31(8-9):1257–1289, July 2006.

[88] J.A.M. Silva and S. Oliveira. An exergy-based approach to determine production cost and CO2 allocation in refineries. *Energy*, 67:607–616, April 2014.

[89] Daniel Flórez-Orrego, Julio A.M. Silva, and Silvio de Oliveira Jr. Renewable and non-renewable exergy cost and specific CO2 emission of electricity generation: The Brazilian case. *Energy Conversion and Management*, 85:619–629, September 2014.

[90] Chemical Engineering magazine. The chemical engineering plant cost index, 2021.

[91] Kalyanmoy Deb, Samir Agrawal, Amrit Pratap, and T Meyarivan. A Fast Elitist Non-dominated Sorting Genetic Algorithm for Multi-objective Optimization: NSGA-II. In G. Goos, J. Hartmanis, J. van Leeuwen, Marc Schoenauer, Kalyanmoy Deb, Günther Rudolph, Xin Yao, Evelyne Lutton, Juan Julian Merelo, and Hans-Paul Schwefel, editors, *Parallel Problem Solving from Nature PPSN VI*, volume 1917, pages 849–858. Springer Berlin Heidelberg, Berlin, Heidelberg, 2000. Series Title: Lecture Notes in Computer Science.

[92] International Energy Agency. *CO2 Emissions From Fuel Combustion 2018: Overview*. International Energy Agency (IEA), 2018.

[93] Empresa de Pesquisa Energética. *Brazilian energy balance - Summary report: year base 2017*. Empresa de Pesquisa Energética (EPE), 2018.

[94] International Energy Agency. *World Energy Outlook 2018: Executive summary*. International Energy Agency (IEA), 2018.

[95] International Energy Agency (IEA). *Renewables information: Overview 2017*. IEA Statistics, 2017.

[96] Brazilian Energy Research Company (EPE). *Brazilian Energy Balance: year 2016*. EPE, Rio de Janeiro, RJ, Brazil, 2017.

[97] National Water Agency of Brazil (ANA). *Handbook of water conservation and reuse in the sugarcane industry (In portuguese)*. ANA; FIESP; UNICA; CTC, 2009.

[98] R N Nakashima and S de Oliveira Junior. Exergy assessment of vinasse disposal alternatives : concentration , anaerobic digestion and fertirrigation. In *31st International Conference on Efficiency, Cost, Optimization, Simulation and Environmental Impact on Energy Systems ECOS*, page 15, 2018.

[99] Luiz Felipe Pellegrini and Silvio de Oliveira. Exergy analysis of sugarcane bagasse gasification. *Energy*, 32(4):314–327, 2007.

[100] Wojciech M Budzianowski. Low-carbon power generation cycles: the feasibility of co2 capture and opportunities for integration. *Journal of Power Technologies*, 91(1):6–13, 2011.

[101] Reynaldo Palacios-Bereche, Klever Joao Mosqueira-Salazar, Marcelo Modesto, Adriano V. Ensinas, Silvia A. Nebra, Luis M. Serra, and Miguel-Angel Lozano. Exergetic analysis of the integrated first- and second-generation ethanol production from sugarcane. *Energy*, 62:46–61, December 2013.

[102] Giulio Allesina, Simone Pedrazzi, Luca Guidetti, and Paolo Tartarini. Modeling of coupling gasification and anaerobic digestion processes for maize bioenergy conversion. *Biomass and Bioenergy*, 81:444–451, 2015.

[103] Jorge Vinicius da Silva Neto, Waldyr L. R. Gallo, and Edson Aparecido Abdul Nour. Production and use of biogas from vinasse: Implications for the energy balance and GHG emissions of sugar cane ethanol in the brazilian context. *Environmental Progress & Sustainable Energy*, 39(1):13226, January 2020.

[104] Martin Gassner and François Maréchal. Thermo-economic process model for thermochemical production of Synthetic Natural Gas (SNG) from lignocellulosic biomass. *Biomass and Bioenergy*, 33(11):1587–1604, November 2009.

[105] Laurence Tock and François Maréchal. Co-production of hydrogen and electricity from lignocellulosic biomass: Process design and thermo-economic optimization. *Energy*, 45(1):339–349, sep 2012.

[106] Wodzisław Piekarczyk, Lucyna Czarnowska, Krzysztof Ptasiński, and Wojciech Stanek. Thermodynamic evaluation of biomass-to-biofuels production systems. *Energy*, 62:95–104, 2013.

[107] Daniel Flórez-Orrego, Julio A M da Silva, Héctor Velásquez, and Silvio de Oliveira. Renewable and non-renewable exergy costs and CO2 emissions in the production of fuels for Brazilian transportation sector. *Energy*, 88:18–36, 2015.

[108] Daniel Flórez-Orrego, Julio A M Silva, and Silvio De Oliveira. Exergy and environmental comparison of the end use of vehicle fuels: The Brazilian case. *Energy Conversion and Management*, 100:220–231, 2015.

[109] Adriano V. Ensinas, Silvia A. Nebra, Miguel A. Lozano, and Luis M. Serra. Analysis of process steam demand reduction and electricity generation in sugar and ethanol production from sugarcane. *Energy Conversion and Management*, 48(11):2978 – 2987, 2007. 19th International Conference on Efficiency, Cost, Optimization, Simulation and Environmental Impact of Energy Systems.

[110] Ernesto L Barrera, Henri Spanjers, Osvaldo Romero, Elena Rosa, and Jo Dewulf. Characterization of the sulfate reduction process in the anaerobic digestion of a very high strength and sulfate rich vinasse. *Chemical Engineering Journal*, 248:383–393, 2014.

[111] Ann C. Wilkie, Kelly J. Riedesel, and John M. Owens. Stillage characterization and anaerobic treatment of ethanol stillage from conventional and cellulosic feedstocks. *Biomass and Bioenergy*, 19(2):63–102, aug 2000.

[112] A. Carrara, A. Perdichizzi, and G. Barigozzi. Simulation of an hydrogen production steam reforming industrial plant for energetic performance prediction. *International Journal of Hydrogen Energy*, 35(8):3499–3508, apr 2010.

[113] Daniel Flórez-Orrego and Silvio de Oliveira Junior. On the efficiency, exergy costs and CO2 emission cost allocation for an integrated syngas and ammonia production plant. *Energy*, 117:341–360, dec 2016.

[114] Prabir Basu. *Biomass Gasification and Pyrolysis*. Elsevier, 2010.

[115] Jim Andersson and Joakim Lundgren. Techno-economic analysis of ammonia production via integrated biomass gasification. *Applied Energy*, 130:484–490, oct 2014.

[116] Yurany Camacho Ardila, Jaiver Efren Jaimes Figueroa, Betânia Hoss Lunelli, Rubens Maciel Filho, and Maria Regina Wolf Maciel. Syngas production from sugar cane bagasse in a circulating fluidized bed gasifier using Aspen Plus™: Modelling and Simulation. *Computer Aided Chemical Engineering*, 30:1093–1097, jan 2012.

[117] C M Kinchin and R L Bain. Hydrogen Production from Biomass via Indirect Gasification : The Impact of NREL Process Development Unit Gasifier Correlations, 2009.

[118] Haldor Topsøe. From solid fuels to substitute natural gas (SNG) using TREMP Topsøe Recycle Energy-efficient Methanation Process. `www.topsoe.com`, 2009.

[119] Sheng Li, Xiaozhou Ji, Xiaosong Zhang, Lin Gao, and Hongguang Jin. Coal to SNG: Technical progress, modeling and system optimization through exergy analysis. *Applied Energy*, 136:98–109, dec 2014.

[120] Sanford A Klein and FL Alvarado. *Engineering Equation Solver (EES)*. F-Chart Software, Madison, WI, 2002.

[121] AspenTech. *Aspen Plus (Version 8.8) [Computer software]*, 2015.

[122] Ernesto L. Barrera, Henri Spanjers, Kimberly Solon, Youri Amerlinck, Ingmar Nopens, and Jo Dewulf. Modeling the anaerobic digestion of cane-molasses vinasse: Extension of the Anaerobic Digestion Model No. 1 (ADM1) with sulfate reduction for a very high strength and sulfate rich wastewater. *Water Research*, 71:42–54, 2015.

[123] Mathworks. *Matlab (Version R2015a) [Computer software]*, 2015.

[124] Min-Jung Yoo, Lindsay Lessard, Maziar Kermani, and François Maréchal. Osmoselua – an integrated approach to energy systems integration with lcia and gis. In Krist V. Gernaey, Jakob K. Huusom, and Rafiqul Gani, editors, *12th International Symposium on Process Systems Engineering and 25th European Symposium on Computer Aided Process Engineering*, volume 37 of *Computer Aided Chemical Engineering*, pages 587 – 592. Elsevier, 2015.

[125] M. A. Lozano and A. Valero. Theory of the exergetic cost. *Energy*, 18(9):939–954, 1993.

[126] Wojciech Stanek and Lucyna Czarnowska. Thermo-ecological cost - Szargut's proposal on exergy and ecology connection. *Energy*, 165:1050–1059, 2018.

[127] S.A. Nebra and Maria Fernandez Parra. The exergy of sucrose-water solutions: proposal of a calculation method. In *18th International Conference on Efficiency, Cost, Optimization, Simulation and Environmental Impact on Energy Systems ECOS*, pages 385–392, 06 2005.

[128] Randall P. Field and Robert Brasington. Baseline flowsheet model for IGCC with carbon capture. *Industrial and Engineering Chemistry Research*, 50(19):11306–11312, 2011.

[129] Metcalf & Eddy, Franklin L Burton, H David Stensel, and George Tchobanoglous. *Wastewater engineering: treatment and reuse*. McGraw Hill, 2003.

[130] Isaias De Carvalho Macedo, Manoel Regis Lima Verde Leal, and João Eduardo Azevedo Ramos Silva. *Greenhouse gases emissions of the ethanol use in Brazil (In portuguese)*. Deparment of Environment, São Paulo State Government, 2004.

[131] Aspen Plus. *Rate-based model of the CO2 capture process by NaOH using Aspen Plus*. Aspen Tecnology, Inc., Bedford, MA, USA, 2013.

[132] Hamadi Cherif, Christophe Coquelet, Paolo Stringari, Denis Clodic, Laura Pellegrini, Stefania Moioli, and Stefano Langé. Experimental and Simulation Results for the Removal of H2S from Biogas by Means of Sodium Hydroxide in Structured Packed Columns. In *ICBST 2016: 18th International Conference on Biogas Science and Technology*, page 9, 2016.

[133] Maria Puig-Arnavat, Juan Carlos Bruno, and Alberto Coronas. Modified Thermodynamic Equilibrium Model for Biomass Gasification: A Study of the Influence of Operating Conditions. *Energy & Fuels*, 26(2):1385–1394, feb 2012.

[134] Alexis Duret, Claude Friedli, and François Maréchal. Process design of Synthetic Natural Gas (SNG) production using wood gasification. *Journal of Cleaner Production*, 13(15):1434–1446, dec 2005.

[135] Daniel Flórez-orrego. Thermodynamics and environmental comparison (co2 emissions) of production and end use routes of vehicle fuels, derived from petroleum, natural gas, biofuels, hydrogen and electricity (electric vehicles) (in portuguese). Master's thesis, University of São Paulo, 2014.

[136] Daniel Flórez-Orrego, S. Sharma, Silvio De Oliveira, and F. Marechal. Combined Exergy Analysis and Energy Integration for Design Optimization of Nitrogen Fertilizer Plants. In *30th International Conference on Efficiency, Cost, Optimization, Simulation and Environmental Impact of Energy Systems, ECOS 2017*, San Diego, CA, USA, 2017.

[137] V.E.N. Santos, R.N. Ely, A.S. Szklo, and A. Magrini. Chemicals, electricity and fuels from biorefineries processing Brazil's sugarcane bagasse: Production recipes and minimum selling prices. *Renewable and Sustainable Energy Reviews*, 53:1443–1458, jan 2016.

[138] D. Hotza and J.C. Diniz da Costa. Fuel cells development and hydrogen production from renewable resources in Brazil. *International Journal of Hydrogen Energy*, 33(19):4915–4935, oct 2008.

[139] S A Channiwala and P P Parikh. A unified correlation for estimating HHV of solid, liquid and gaseous fuels. *Fuel*, 81(8):1051–1063, 2002.

[140] Luiz Felipe Pellegrini and Silvio de Oliveira Junior. Combined production of sugar, ethanol and electricity: Thermoeconomic and environmental analysis and optimization. *Energy*, 36(6):3704 – 3715, 2011.

[141] Marina O.S. Dias, Tassia L. Junqueira, Otávio Cavalett, Marcelo P. Cunha, Charles D.F. Jesus, Carlos E.V. Rossell, Rubens Maciel Filho, and Antonio Bonomi. Integrated versus stand-alone second generation ethanol production from sugarcane bagasse and trash. *Bioresource Technology*, 103(1):152–161, 2012.

[142] Pablo A. Silva Ortiz, Rubens Maciel Filho, and John Posada. Mass and heat integration in ethanol production mills for enhanced process efficiency and exergy-based renewability performance. *Processes*, 7(10), 2019.

[143] Pablo A. Silva Ortiz, Daniel Flórez-Orrego, Silvio de Oliveira Junior, François Maréchal, and Rubens Maciel Filho. Exergetic, environmental and economic assessment of sugarcane first-generation biorefineries. *Journal of Power of Technologies*, 99(2):67–81, 2019.

[144] Milagros Cecilia Palacios-Bereche, Reynaldo Palacios-Bereche, and Silvia Azucena Nebra. Comparison through energy, exergy and economic analyses of two alternatives for the energy exploitation of vinasse. *Energy*, 197:117231, April 2020.

[145] Pablo A. Silva Ortiz, François Maréchal, and Silvio de Oliveira Junior. Exergy assessment and techno-economic optimization of bioethanol production routes. *Fuel*, 279:118327, November 2020.

[146] Tuong-Van Nguyen and Lasse Røngaard Clausen. Techno-economic analysis of polygeneration systems based on catalytic hydropyrolysis for the production of bio-oil and fuels. *Energy Conversion and Management*, 184:539–558, March 2019.

[147] Emanuela Peduzzi, Laurence Tock, Guillaume Boissonnet, and François Maréchal. Thermo-economic evaluation and optimization of the thermo-chemical conversion of biomass into methanol. *Energy*, 58:9–16, September 2013.

[148] Meire Ellen Gorete Ribeiro Domingos, Daniel Flórez Orrego, Moisés Teles Dos Santos, Hector Ivan Velásquez, and Silvio De Oliveira Junior. Exergy and environmental analysis of black liquor upgrading gasification in an integrated kraft pulp and ammonia production plant. *International Journal of Exergy*, 35(1):35, 2021.

[149] Daniel Flórez-Orrego, François Maréchal, and Silvio de Oliveira Junior. Comparative exergy and economic assessment of fossil and biomass-based routes for ammonia production. *Energy Conversion and Management*, 194:22–36, August 2019.

[150] Francesca Palazzi, Nordahl Autissier, François M.A. Marechal, and Daniel Favrat. A methodology for thermo-economic modeling and optimization of solid oxide fuel cell systems. *Applied Thermal Engineering*, 27(16):2703–2712, November 2007.

[151] M. Pérez-Fortes, A. Mian, S. Srikanth, L. Wang, S. Diethelm, E. Varkaraki, I. Mirabelli, R. Makkus, R. Schoon, F. Maréchal, and J. Van herle. Design of a Pilot SOFC System for the Combined Production of Hydrogen and Electricity under Refueling Station Requirements. *Fuel Cells*, 19(4):389–407, May 2019.

[152] J Van herle, F Maréchal, S Leuenberger, Y Membrez, O Bucheli, and D Favrat. Process flow model of solid oxide fuel cell system supplied with sewage biogas. *Journal of Power Sources*, 131(1-2):127–141, May 2004.

[153] F. Curletti, M. Gandiglio, A. Lanzini, M. Santarelli, and F. Maréchal. Large size biogas-fed Solid Oxide Fuel Cell power plants with carbon dioxide management: Technical and economic optimization. *Journal of Power Sources*, 294:669–690, October 2015.

[154] M. MosayebNezhad, A.S. Mehr, M. Gandiglio, A. Lanzini, and M. Santarelli. Techno-economic assessment of biogas-fed CHP hybrid systems in a real wastewater treatment plant. *Applied Thermal Engineering*, 129:1263–1280, January 2018.

[155] Marta Gandiglio, Andrea Lanzini, Massimo Santarelli, Marco Acri, Tuomas Hakala, and Markus Rautanen. Results from an industrial size biogas-fed SOFC plant (the DEMOSOFC project). *International Journal of Hydrogen Energy*, 45(8):5449–5464, February 2020.

[156] Nicholas S. Siefert and Shawn Litster. Exergy & economic analysis of biogas fueled solid oxide fuel cell systems. *Journal of Power Sources*, 272:386–397, December 2014.

[157] Gioele Marcoberardino, Dario Vitali, Francesco Spinelli, Marco Binotti, and Giampaolo Manzolini. Green Hydrogen Production from Raw Biogas: A Techno-Economic Investigation of Conventional Processes Using Pressure Swing Adsorption Unit. *Processes*, 6(3):19, February 2018.

[158] David Peterson and Eric Miller. Hydrogen Production Cost from Solid Oxide Electrolysis. DOE Hydrogen and Fuel Cells Program Record 16014, Department of Energy - USA, 2016.

[159] Mariagiovanna Minutillo, Alessandra Perna, and Alessandro Sorce. Green hydrogen production plants via biogas steam and autothermal reforming processes: energy and exergy analyses. *Applied Energy*, 277:115452, November 2020.

[160] Rafael Nogueira Nakashima and Silvio de Oliveira Junior. Thermodynamic evaluation of solid oxide fuel cells co-producing hydrogen and power from biogas. In *33th International Conference on Efficiency, Cost, Optimization, Simulation and Environmental Impact of Energy Systems, ECOS 2020*, pages 1052–1066, Osaka, Japan, 2020.

[161] Yi Jiang and Anil V. Virkar. Fuel Composition and Diluent Effect on Gas Transport and Performance of Anode-Supported SOFCs. *Journal of The Electrochemical Society*, 150(7):A942, 2003.

[162] Dennis D. Papadias, Shabbir Ahmed, Romesh Kumar, and Fred Joseck. Hydrogen quality for fuel cell vehicles – A modeling study of the sensitivity of impurity content in hydrogen to the process variables in the SMR–PSA pathway. *International Journal of Hydrogen Energy*, 34(15):6021–6035, August 2009.

[163] National Renewable Energy Laboratory (NREL). H2A Current Distributed Hydrogen Production Model, 2018.

[164] Christopher Rackauckas and Qing Nie. Differentialequations.jl–a performant and feature-rich ecosystem for solving differential equations in julia. *Journal of Open Research Software*, 5(1), 2017. Publisher: Ubiquity Press.

[165] Ian H. Bell, Jorrit Wronski, Sylvain Quoilin, and Vincent Lemort. Pure and Pseudo-pure Fluid Thermophysical Property Evaluation and the Open-Source Thermophysical Property Library CoolProp. *Industrial & Engineering Chemistry Research*, 53(6):2498–2508, February 2014.

[166] Bonnie J. McBride, Michael J. Zehe, and Sanford Gordon. NASA Glenn Coefficients for Calculating Thermodynamic Properties of Individual Species. Technical Report NASA/TP-2002-211556, NASA Glenn Research Center, Cleveland, OH United States, 2002.

[167] Edward N. Fuller, Paul D. Schettler, and J. Calvin Giddings. New method for prediction of binary gas-phase diffusion coefficients. *Industrial & Engineering Chemistry*, 58(5):18–27, May 1966.

[168] Edward N. Fuller, Keith Ensley, and J. Calvin Giddings. Diffusion of halogenated hydrocarbons in helium. The effect of structure on collision cross sections. *The Journal of Physical Chemistry*, 73(11):3679–3685, November 1969.

[169] Bruce E. Poling, J. M. Prausnitz, and John P. O'Connell. *The properties of gases and liquids*. McGraw-Hill, New York, 5th ed edition, 2001.

[170] Iain Dunning, Joey Huchette, and Miles Lubin. JuMP: A Modeling Language for Mathematical Optimization. *SIAM Review*, 59(2):295–320, 2017.

[171] Andrew Makhorin. GLPK (GNU Linear Programming Kit), 2012.

[172] Cheng Bao, Zeyi Jiang, and Xinxin Zhang. Modeling mass transfer in solid oxide fuel cell anode: I. Comparison between Fickian, Stefan-Maxwell and dusty-gas models. *Journal of Power Sources*, 310:32–40, April 2016.

[173] R. Nogueira Nakashima and S. Oliveira Junior. Thermodynamic Evaluation Of Solid Oxide Fuel Cells Converting Biogas Into Hydrogen And Electricity (In press). *International Journal of Thermodynamics*, In press, 2021.

[174] Robert Byron Bird, Warren E. Stewart, and Edwin N. Lightfoot. *Transport phenomena*. Wiley, New York, rev. 2. ed edition, 2007. OCLC: 255914840.

[175] B.A. Haberman and J.B. Young. Three-dimensional simulation of chemically reacting gas flows in the porous support structure of an integrated-planar solid oxide

fuel cell. *International Journal of Heat and Mass Transfer*, 47(17-18):3617–3629, August 2004.

[176] E. Achenbach and E. Riensche. Methane/steam reforming kinetics for solid oxide fuel cells. *Journal of Power Sources*, 52(2):283–288, December 1994.

[177] Cheng Bao, Zeyi Jiang, and Xinxin Zhang. Modeling mass transfer in solid oxide fuel cell anode: II. H2/CO co-oxidation and surface diffusion in synthesis-gas operation. *Journal of Power Sources*, 324:261–271, August 2016.

[178] Q. Fu, P. Freundt, J. Bomhard, and F. Hauler. SOFC Stacks Operating under Direct Internal Steam Reforming of Methane. *Fuel Cells*, 17(2):151–156, April 2017.

[179] F. Marechal, F. Palazzi, J. Godat, and D. Favrat. Thermo-Economic Modelling and Optimisation of Fuel Cell Systems. *Fuel Cells*, 5(1):5–24, February 2005.

[180] Bodo Linnhoff, David R. Mason, and Ian Wardle. Understanding heat exchanger networks. *Computers & Chemical Engineering*, 3(1-4):295–302, January 1979.

[181] Ian C Kemp. Data extraction and energy targeting. In *Pinch Analysis and Process Integration*, pages 41–98. Elsevier, 2007.

[182] Brazilian Energy Research Office (EPE). Equipment cost correlations: Natural gas industry (In portuguese). Technical report, Brazilian Ministry of Mines and Energy, Brasília, Brazil, 2018.

[183] Joel Theis. Cost Estimation Methodology for NETL Assessments of Power Plant Performance. Technical Report NETL-PUB-22580, National Energy Technology Laboratory, United States of America, 2019.

[184] ANEEL (Brazilian National Agency of Electricity). Open data: Electricity costs (In Portuguese), 2020.

[185] Warren D. Seider, Daniel R. Lewin, J. D. Seader, Soemantri Widagdo, R. Gani, and Ka Ming Ng. *Product and process design principles: synthesis, analysis and evaluation.* Wiley, New York, fourth edition edition, 2017.

[186] Dionissios D. Papadias, Shabbir Ahmed, and Romesh Kumar. Fuel quality issues with biogas energy – An economic analysis for a stationary fuel cell system. *Energy*, 44(1):257–277, August 2012.

[187] Oliveira Junior. *Exergy Production, Cost and Renewability.* Green Energy and Technology. Springer, 2013. OCLC: 1184485089.

[188] IRENA. Renewable Power Generation Costs in 2019. Technical report, International Renewable Energy Agency, Abu Dhabi, 2020.

[189] Jingang Yao, Michael Kraussler, Florian Benedikt, and Hermann Hofbauer. Techno-economic assessment of hydrogen production based on dual fluidized bed biomass steam gasification, biogas steam reforming, and alkaline water electrolysis processes. *Energy Conversion and Management*, 145:278–292, August 2017.

[190] Javier A. Francesconi, Miguel C. Mussati, and Pio A. Aguirre. Analysis of design variables for water-gas-shift reactors by model-based optimization. *Journal of Power Sources*, 173(1):467–477, November 2007.

[191] Max Stone Peters, Klaus D. Timmerhaus, and Ronald E. West. *Plant design and economics for chemical engineers*. McGraw-Hill chemical engineering series. McGraw-Hill, New York, 5th ed edition, 2003.

[192] R.-U. Dietrich, J. Oelze, A. Lindermeir, C. Spieker, C. Spitta, and M. Steffen. Power Generation from Biogas using SOFC - Results for a 1 kW $_{e}$ Demonstration Unit. *Fuel Cells*, 14(2):239–250, April 2014.

[193] Kai W. Bedringås, Ivar S. Ertesvåg, Ståle Byggstøyl, and Bjørn F. Magnussen. Exergy analysis of solid-oxide fuel-cell (SOFC) systems. *Energy*, 22(4):403–412, April 1997.

[194] S.H Chan, C.F Low, and O.L Ding. Energy and exergy analysis of simple solid-oxide fuel-cell power systems. *Journal of Power Sources*, 103(2):188–200, January 2002.

[195] Young Duk Lee, Kook Young Ahn, Tatiana Morosuk, and George Tsatsaronis. Exergetic and exergoeconomic evaluation of a solid-oxide fuel-cell-based combined heat and power generation system. *Energy Conversion and Management*, 85:154–164, September 2014.

[196] Vinod M. Janardhanan, Vincent Heuveline, and Olaf Deutschmann. Performance analysis of a SOFC under direct internal reforming conditions. *Journal of Power Sources*, 172(1):296–307, October 2007.

[197] E. Jurado, G. Antonopoulou, G. Lyberatos, H.N. Gavala, and I.V. Skiadas. Continuous anaerobic digestion of swine manure: ADM1-based modelling and effect of addition of swine manure fibers pretreated with aqueous ammonia soaking. *Applied Energy*, 172:190–198, June 2016.

[198] K. Girona, J. Laurencin, J. Fouletier, and F. Lefebvre-Joud. Carbon deposition in CH4/CO2 operated SOFC: Simulation and experimentation studies. *Journal of Power Sources*, 210:381–391, July 2012.

[199] C. Dennehy, P.G. Lawlor, G.E. Gardiner, Y. Jiang, L. Shalloo, and X. Zhan. Stochastic modelling of the economic viability of on-farm co-digestion of pig manure and food waste in Ireland. *Applied Energy*, 205:1528–1537, November 2017.

[200] Angelica Buzinaro Avaci, Samuel Nelson Melegari de Souza, Ivan Werncke, and Luiz Inácio Chaves. Financial economic scenario for the microgeneration of electric energy from swine culture-originated biogas. *Renewable and Sustainable Energy Reviews*, 25:272–276, September 2013.

[201] Jean Agustin Velásquez Piñas, Osvaldo José Venturini, Electo Eduardo Silva Lora, Oscar Almazan del Olmo, and Orly Denisse Calle Roalcaba. An economic holistic feasibility assessment of centralized and decentralized biogas plants with mono-digestion and co-digestion systems. *Renewable Energy*, 139:40–51, August 2019.

[202] Jiří Klemeš, Olga Arsenyeva, Petro Kapustenko, and Leonid Tovazhnyanskyy. *Compact heat exchangers for energy transfer intensification: Low grade heat and fouling mitigation*. CRC Press, 2017. OCLC: 1003588466.

[203] Richard Turton, editor. *Analysis, synthesis, and design of chemical processes*. Prentice Hall, Upper Saddle River, NJ, 4th ed edition, 2012.

[204] M. Penev, G. Saur, C. Hunter, and J. Zuboy. H2A Hydrogen Production Model: Version 3.2018 User Guide (DRAFT). User Guide i, U.S. Department of Energy, United States of America, 2018.

[205] Battelle Memorial Institute. Manufacturing Cost Analysis of 1, 5, 10 and 25 kW. Technical Report DE-EE0005250, U.S. Department of Energy, United States of America, 2017.

[206] XE. XE Currency Charts: EUR to USD, 2020.

Appendix A - Unit exergy costs and specific CO_2 emissions for macro analysis

A detailed description of the exergy flow rates, unit exergy costs and specific CO_2 emissions for the waste upgrade cases in Figures 9.1, 9.2 and 9.3 is shown in Tables A1, A2 and A3, respectively.

Figure 9.1: Waste upgrade plant for power generation (only)

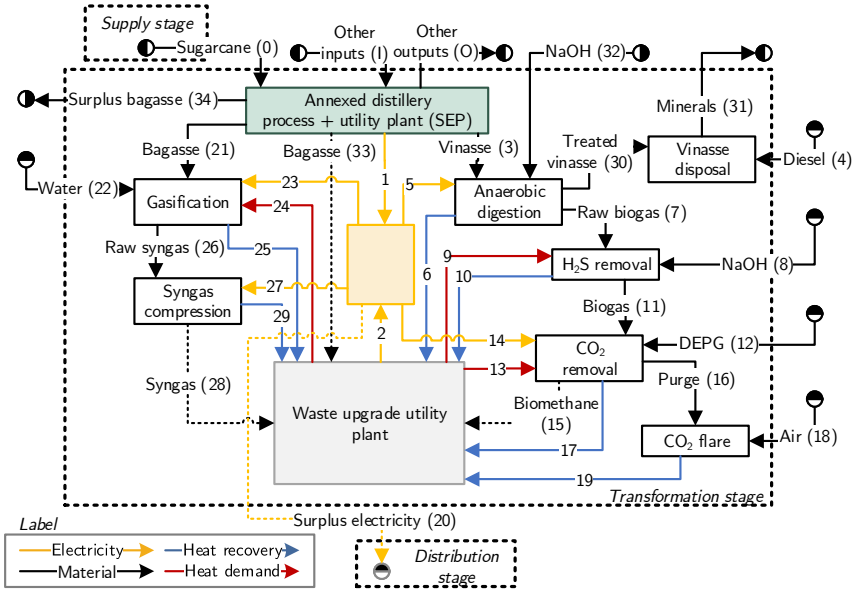

Source: [45]

Table A1: Case E - Exergy flow rates, unit exergy costs and specific CO_2 emissions

N°	Description	$\dot{B}$ (kW)	c_T (kJ/kJ)	c_{NR} (kJ/kJ)	c_{co2} (gCO2/kJ)
1	SEP electricity	4,225.0	7.124	0.402	0.027
2	WUP electricity	19,362.0	10.940	0.738	0.049
3	Vinasse	43,813.0	2.545	0.152	0.011

Continued on next page

Table A1 – *Continued from previous page*

N°	Description	$\dot{B}$ (kW)	c_T (kJ/kJ)	c_{NR} (kJ/kJ)	c_{co2} (gCO2/kJ)
4	Diesel	505.3	1.038	1.038	0.003
5	Electricity	164.0	10.260	0.678	0.045
6	Heat	983.8	2.771	0.167	0.012
7	Raw biogas	20,832.0	2.771	0.167	0.012
8	NaOH	783.5	3.717	2.193	0.137
9	Heat	10.8	10.940	0.738	0.049
10	Heat	0.5	3.040	0.260	0.017
11	Biogas	19,987.0	3.040	0.260	0.017
12	DEPG	0.7	1.000	1.000	0.000
13	Heat	41.5	10.940	0.738	0.049
14	Electricity	981.3	10.260	0.678	0.045
15	Biomethane	19,170.0	3.517	0.291	0.020
16	Purge	884.2	3.517	0.291	0.020
17	Heat	212.8	3.517	0.291	0.020
18	Air	0.9	0.000	0.000	0.000
19	Heat	205.0	15.170	1.254	0.084
20	Surplus electricity	17,766.0	10.260	0.678	0.045
21	Bagasse	72,335.0	1.249	0.071	0.005
22	Water	118.4	1.000	0.000	0.000
23	Electricity	2,170.0	10.260	0.678	0.045
24	Heat	4,598.0	10.940	0.738	0.049
25	Heat	8,333.0	2.910	0.178	0.012
26	Raw syngas	47,700.0	2.910	0.178	0.012
27	Electricity	2,506.0	10.260	0.678	0.045
28	Syngas	47,622.0	3.419	0.212	0.014
29	Heat	495.3	3.419	0.212	0.014
30	Treated vinasse	20,737.0	2.545	0.152	0.011
31	Minerals	187.0	285.100	19.620	1.180
32	NaOH	10.7	3.717	2.193	0.137
33	Bagasse	0.0	0.000	0.000	0.000
34	Surplus bagasse	0.0	0.000	0.000	0.000

Source: [45]

Figure 9.2: Waste upgrade plant for biomethane production and surplus electricity (if applicable)

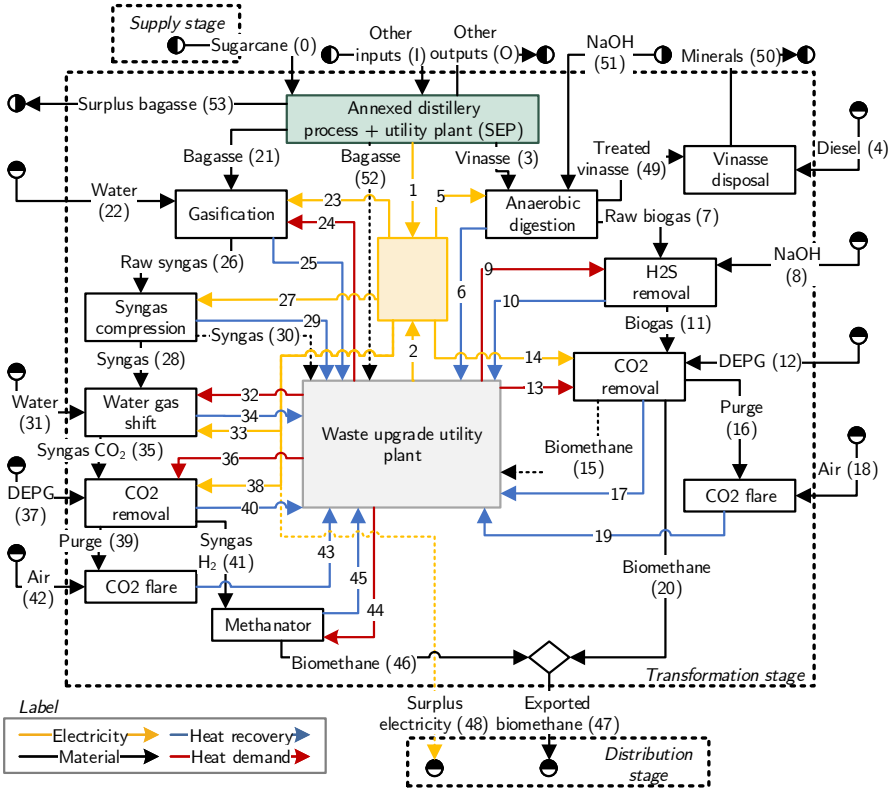

Source: [45]

Table A2: Case M1 - Exergy flow rates, unit exergy costs and specific CO_2 emissions

N°	Description	$\dot{B}$ (kW)	c_T (kJ/kJ)	c_{NR} (kJ/kJ)	c_{co2} (gCO2/kJ)
1	SEP electricity	0.0	7.124	0.402	0.027
2	WUP electricity	6,081.0	4.622	0.271	0.018
3	Vinasse	43,813.0	2.545	0.152	0.011
4	Diesel	505.3	1.038	1.038	0.003
5	Electricity	164.0	4.622	0.271	0.018
6	Heat	983.8	2.729	0.164	0.011
7	Raw biogas	20,832.0	2.729	0.164	0.011
8	NaOH	783.5	3.717	2.193	0.137
9	Heat	10.8	4.622	0.271	0.018
10	Heat	0.5	2.992	0.257	0.017
11	Biogas	19,987.0	2.992	0.257	0.017
12	DEPG	0.7	1.000	1.000	0.000

Continued on next page

Table A2 – *Continued from previous page*

N°	Description	$\dot{B}$ (kW)	c_T (kJ/kJ)	c_{NR} (kJ/kJ)	c_{co2} (gCO2/kJ)
13	Heat	41.5	4.622	0.271	0.018
14	Electricity	981.3	4.622	0.271	0.018
15	Biomethane	0.0	3.184	0.267	0.018
16	Purge	884.2	3.184	0.267	0.018
17	Heat	212.8	3.184	0.267	0.018
18	Air	0.9	0.000	0.000	0.000
19	Heat	205.0	13.730	1.150	0.077
20	Biomethane	19,170.0	3.184	0.267	0.018
21	Bagasse	72,335.0	1.249	0.071	0.005
22	Water	118.4	1.000	0.000	0.000
23	Electricity	2,170.0	4.622	0.271	0.018
24	Heat	4,598.0	4.622	0.271	0.018
25	Heat	8,333.0	2.173	0.124	0.008
26	Raw syngas	47,700.0	2.173	0.124	0.008
27	Electricity	2,506.0	4.622	0.271	0.018
28	Syngas	40,098.0	2.395	0.137	0.009
29	Heat	495.3	2.395	0.137	0.009
30	Syngas	7,524.0	2.395	0.137	0.009
31	Water	103.4	1.000	0.000	0.000
32	Heat	3,243.0	4.622	0.271	0.018
33	Electricity	10.1	4.622	0.271	0.018
34	Heat	2,985.0	2.600	0.149	0.010
35	Syngas CO_2	39,770.0	2.600	0.149	0.010
36	Heat	39.9	4.622	0.271	0.018
37	DEPG	1.3	1.000	1.000	0.000
38	Electricity	250.1	4.622	0.271	0.018
39	Purge	763.7	2.645	0.152	0.010
40	Heat	17.0	2.645	0.152	0.010
41	Syngas H_2	38,824.0	2.645	0.152	0.010
42	Air	0.1	0.000	0.000	0.000
43	Heat	6.1	329.500	18.910	1.251
44	Heat	460.3	4.622	0.271	0.018
45	Heat	4,946.0	2.747	0.158	0.010
46	Biomethane	33,203.0	2.747	0.158	0.010

Continued on next page

Table A2 – *Continued from previous page*

N°	Description	$\dot{B}$ (kW)	c_T (kJ/kJ)	c_{NR} (kJ/kJ)	c_{co2} (gCO2/kJ)
47	Exported biomethane	52,374.0	2.907	0.198	0.013
48	Surplus electricity	0.0	4.622	0.271	0.018
49	Treated vinasse	20,737.0	2.545	0.152	0.011
50	Minerals	187.0	285.100	19.620	1.180
51	NaOH	10.7	3.717	2.193	0.137
52	Bagasse	0.0	0.000	0.000	0.000
53	Surplus bagasse	0.0	0.000	0.000	0.000

Source: [45]

Table A3: Case M2 - Exergy flow rates, unit exergy costs and specific CO_2 emissions

N°	Description	$\dot{B}$ (kW)	c_T (kJ/kJ)	c_{NR} (kJ/kJ)	c_{co2} (gCO2/kJ)
1	SEP electricity	4,225.0	7.124	0.402	0.027
2	WUP electricity	4,405.0	3.907	0.230	0.015
3	Vinasse	43,813.0	2.545	0.152	0.011
4	Diesel	505.3	1.038	1.038	0.003
5	Electricity	164.0	5.482	0.315	0.021
6	Heat	983.8	2.735	0.164	0.011
7	Raw biogas	20,832.0	2.735	0.164	0.011
8	NaOH	783.5	3.717	2.193	0.137
9	Heat	10.8	3.907	0.230	0.015
10	Heat	0.5	2.999	0.257	0.017
11	Biogas	19,987.0	2.999	0.257	0.017
12	DEPG	0.7	1.000	1.000	0.000
13	Heat	41.5	3.907	0.230	0.015
14	Electricity	981.3	5.482	0.315	0.021
15	Biomethane	0.0	3.231	0.269	0.018
16	Purge	884.2	3.231	0.269	0.018
17	Heat	212.8	3.231	0.269	0.018
18	Air	0.9	0.000	0.000	0.000
19	Heat	205.0	13.930	1.160	0.078
20	Biomethane	19,170.0	3.231	0.269	0.018
21	Bagasse	72,335.0	1.249	0.071	0.005
22	Water	118.4	1.000	0.000	0.000

Continued on next page

Table A3 – *Continued from previous page*

N°	Description	$\dot{B}$ (kW)	c_T (kJ/kJ)	c_{NR} (kJ/kJ)	c_{co2} (gCO2/kJ)
23	Electricity	2,170.0	5.482	0.315	0.021
24	Heat	4,598.0	3.907	0.230	0.015
25	Heat	8,333.0	2.148	0.122	0.008
26	Raw syngas	47,700.0	2.148	0.122	0.008
27	Electricity	2,506.0	5.482	0.315	0.021
28	Syngas	47,622.0	2.414	0.138	0.009
29	Heat	495.3	2.414	0.138	0.009
30	Syngas	0.0	2.414	0.138	0.009
31	Water	122.7	1.000	0.000	0.000
32	Heat	3,851.0	3.907	0.230	0.015
33	Electricity	12.0	5.482	0.315	0.021
34	Heat	3,545.0	2.564	0.147	0.010
35	Syngas CO_2	47,232.0	2.564	0.147	0.010
36	Heat	47.3	3.907	0.230	0.015
37	DEPG	1.6	1.000	1.000	0.000
38	Electricity	297.0	5.482	0.315	0.021
39	Purge	907.0	2.614	0.149	0.010
40	Heat	20.2	2.614	0.149	0.010
41	Syngas H_2	46,109.0	2.614	0.149	0.010
42	Air	0.1	0.000	0.000	0.000
43	Heat	7.3	325.600	18.610	1.231
44	Heat	546.7	3.907	0.230	0.015
45	Heat	5,874.0	2.707	0.155	0.010
46	Biomethane	39,434.0	2.707	0.155	0.010
47	Exported biomethane	58,604.0	2.878	0.192	0.013
48	Surplus electricity	2,499.0	5.482	0.315	0.021
49	Treated vinasse	20,737.0	2.545	0.152	0.011
50	Minerals	187.0	285.100	19.620	1.180
51	NaOH	10.7	3.717	2.193	0.137
52	Bagasse	0.0	0.000	0.000	0.000
53	Surplus bagasse	0.0	0.000	0.000	0.000

Source: [45]

Figure 9.3: Waste upgrade plant for hydrogen production and surplus electricity (if applicable)

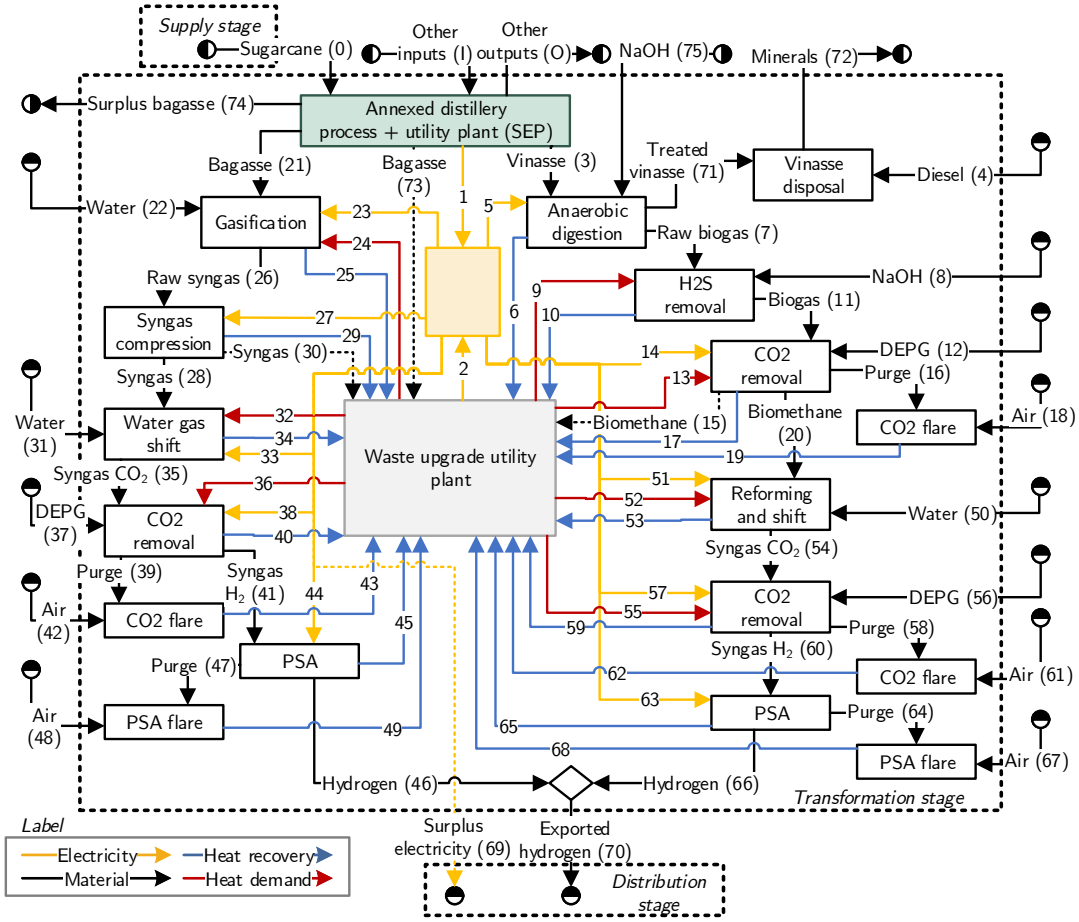

Source: [45]

Table A4: Case H1 - Exergy flow rates, unit exergy costs and specific CO_2 emissions

N°	Description	$\dot{B}$ (kW)	c_T (kJ/kJ)	c_{NR} (kJ/kJ)	c_{co2} (gCO2/kJ)
1	SEP electricity	0.0	7.124	0.402	0.027
2	WUP electricity	7,195.0	6.329	0.424	0.028
3	Vinasse	43,813.0	2.545	0.152	0.011
4	Diesel	505.3	1.038	1.038	0.003
5	Electricity	164.0	6.329	0.424	0.028
6	Heat	983.8	2.742	0.165	0.011
7	Raw biogas	20,832.0	2.742	0.165	0.011
8	NaOH	783.5	3.717	2.193	0.137
9	Heat	10.8	6.329	0.424	0.028

Continued on next page

Table A4 – *Continued from previous page*

N°	Description	$\dot{B}$ (kW)	c_T (kJ/kJ)	c_{NR} (kJ/kJ)	c_{co2} (gCO2/kJ)
10	Heat	0.5	3.007	0.258	0.017
11	Biogas	19,987.0	3.007	0.258	0.017
12	DEPG	0.7	1.000	1.000	0.000
13	Heat	41.5	6.329	0.424	0.028
14	Electricity	981.3	6.329	0.424	0.028
15	Biomethane	0.0	3.285	0.276	0.019
16	Purge	884.2	3.285	0.276	0.019
17	Heat	212.8	3.285	0.276	0.019
18	Air	0.9	0.000	0.000	0.000
19	Heat	205.0	14.160	1.189	0.080
20	Biomethane	19,170.0	3.285	0.276	0.019
21	Bagasse	62,495.0	1.249	0.071	0.005
22	Water	102.3	1.000	0.000	0.000
23	Electricity	1,875.0	6.329	0.424	0.028
24	Heat	3,972.0	6.329	0.424	0.028
25	Heat	7,200.0	2.379	0.142	0.009
26	Raw syngas	41,211.0	2.379	0.142	0.009
27	Electricity	2,165.0	6.329	0.424	0.028
28	Syngas	41,144.0	2.688	0.163	0.011
29	Heat	427.9	2.688	0.163	0.011
30	Syngas	0.0	2.688	0.163	0.011
31	Water	106.0	1.000	0.000	0.000
32	Heat	3,327.0	6.329	0.424	0.028
33	Electricity	10.4	6.329	0.424	0.028
34	Heat	3,063.0	3.005	0.185	0.012
35	Syngas CO_2	40,807.0	3.005	0.185	0.012
36	Heat	63.8	6.329	0.424	0.028
37	DEPG	2.4	1.000	1.000	0.000
38	Electricity	350.8	6.329	0.424	0.028
39	Purge	1,384.0	3.089	0.191	0.013
40	Heat	17.6	3.089	0.191	0.013
41	Syngas H_2	39,144.0	3.089	0.191	0.013
42	Air	0.2	0.000	0.000	0.000
43	Heat	18.3	233.900	14.460	0.960

Continued on next page

Table A4 – *Continued from previous page*

N°	Description	$\dot{B}$ (kW)	c_T (kJ/kJ)	c_{NR} (kJ/kJ)	c_{co2} (gCO2/kJ)
44	Electricity	682.5	6.329	0.424	0.028
45	Heat	81.4	3.177	0.197	0.013
46	Hydrogen	28,587.0	3.177	0.197	0.013
47	Purge	10,750.0	3.177	0.197	0.013
48	Air	16.9	0.000	0.000	0.000
49	Heat	7,126.0	4.793	0.297	0.020
50	Water	49.0	1.000	0.000	0.000
51	Electricity	2.0	6.329	0.424	0.028
52	Heat	5,331.0	6.329	0.424	0.028
53	Heat	2,277.0	4.825	0.376	0.025
54	Syngas CO_2	17,779.0	4.825	0.376	0.025
55	Heat	40.0	6.329	0.424	0.028
56	DEPG	0.5	1.000	1.000	0.000
57	Electricity	579.0	6.329	0.424	0.028
58	Purge	329.8	4.992	0.387	0.026
59	Heat	91.0	4.992	0.387	0.026
60	Syngas H_2	17,549.0	4.992	0.387	0.026
61	Air	0.0	0.000	0.000	0.000
62	Heat	28.0	58.790	4.557	0.305
63	Electricity	385.0	6.329	0.424	0.028
64	Purge	5,833.0	5.088	0.393	0.026
65	Heat	51.0	5.088	0.393	0.026
66	Hydrogen	11,813.0	5.088	0.393	0.026
67	Air	9.7	0.000	0.000	0.000
68	Heat	4,731.0	6.273	0.485	0.032
69	Surplus electricity	0.0	6.329	0.424	0.028
70	Exported hydrogen	40,399.0	3.736	0.254	0.017
71	Treated vinasse	20,737.0	2.545	0.152	0.011
72	Minerals	187.0	285.100	19.620	1.180
73	Bagasse	8,736.0	1.249	0.071	0.005
74	Surplus bagasse	1,104.0	1.249	0.071	0.005
75	NaOH	10.7	3.717	2.193	0.137

Source: [45]

Table A5: Case H2 - Exergy flow rates, unit exergy costs and specific CO_2 emissions

N°	Description	$\dot{B}$ (kW)	c_T (kJ/kJ)	c_{NR} (kJ/kJ)	c_{co2} (gCO2/kJ)
1	SEP electricity	0.0	7.124	0.402	0.027
2	WUP electricity	7,195.0	6.329	0.424	0.028
3	Vinasse	43,813.0	2.545	0.152	0.011
4	Diesel	505.3	1.038	1.038	0.003
5	Electricity	164.0	6.329	0.424	0.028
6	Heat	983.8	2.742	0.165	0.011
7	Raw biogas	20,832.0	2.742	0.165	0.011
8	NaOH	783.5	3.717	2.193	0.137
9	Heat	10.8	6.329	0.424	0.028
10	Heat	0.5	3.007	0.258	0.017
11	Biogas	19,987.0	3.007	0.258	0.017
12	DEPG	0.7	1.000	1.000	0.000
13	Heat	41.5	6.329	0.424	0.028
14	Electricity	981.3	6.329	0.424	0.028
15	Biomethane	0.0	3.285	0.276	0.019
16	Purge	884.2	3.285	0.276	0.019
17	Heat	212.8	3.285	0.276	0.019
18	Air	0.9	0.000	0.000	0.000
19	Heat	205.0	14.160	1.189	0.080
20	Biomethane	19,170.0	3.285	0.276	0.019
21	Bagasse	62,495.0	1.249	0.071	0.005
22	Water	102.3	1.000	0.000	0.000
23	Electricity	1,875.0	6.329	0.424	0.028
24	Heat	3,972.0	6.329	0.424	0.028
25	Heat	7,200.0	2.379	0.142	0.009
26	Raw syngas	41,211.0	2.379	0.142	0.009
27	Electricity	2,165.0	6.329	0.424	0.028
28	Syngas	41,144.0	2.688	0.163	0.011
29	Heat	427.9	2.688	0.163	0.011
30	Syngas	0.0	2.688	0.163	0.011
31	Water	106.0	1.000	0.000	0.000
32	Heat	3,327.0	6.329	0.424	0.028
33	Electricity	10.4	6.329	0.424	0.028

Continued on next page

Table A5 – *Continued from previous page*

N°	Description	$\dot{B}$ (kW)	c_T (kJ/kJ)	c_{NR} (kJ/kJ)	c_{co2} (gCO2/kJ)
34	Heat	3,063.0	3.005	0.185	0.012
35	Syngas CO_2	40,807.0	3.005	0.185	0.012
36	Heat	63.8	6.329	0.424	0.028
37	DEPG	2.4	1.000	1.000	0.000
38	Electricity	350.8	6.329	0.424	0.028
39	Purge	1,384.0	3.089	0.191	0.013
40	Heat	17.6	3.089	0.191	0.013
41	Syngas H_2	39,144.0	3.089	0.191	0.013
42	Air	0.2	0.000	0.000	0.000
43	Heat	18.3	233.900	14.460	0.960
44	Electricity	682.5	6.329	0.424	0.028
45	Heat	81.4	3.177	0.197	0.013
46	Hydrogen	28,587.0	3.177	0.197	0.013
47	Purge	10,750.0	3.177	0.197	0.013
48	Air	16.9	0.000	0.000	0.000
49	Heat	7,126.0	4.793	0.297	0.020
50	Water	49.0	1.000	0.000	0.000
51	Electricity	2.0	6.329	0.424	0.028
52	Heat	5,331.0	6.329	0.424	0.028
53	Heat	2,277.0	4.825	0.376	0.025
54	Syngas CO_2	17,779.0	4.825	0.376	0.025
55	Heat	40.0	6.329	0.424	0.028
56	DEPG	0.5	1.000	1.000	0.000
57	Electricity	579.0	6.329	0.424	0.028
58	Purge	329.8	4.992	0.387	0.026
59	Heat	91.0	4.992	0.387	0.026
60	Syngas H_2	17,549.0	4.992	0.387	0.026
61	Air	0.0	0.000	0.000	0.000
62	Heat	28.0	58.790	4.557	0.305
63	Electricity	385.0	6.329	0.424	0.028
64	Purge	5,833.0	5.088	0.393	0.026
65	Heat	51.0	5.088	0.393	0.026
66	Hydrogen	11,813.0	5.088	0.393	0.026
67	Air	9.7	0.000	0.000	0.000

Continued on next page

Table A5 – *Continued from previous page*

N°	Description	$\dot{B}$ (kW)	c_T (kJ/kJ)	c_{NR} (kJ/kJ)	c_{co2} (gCO2/kJ)
68	Heat	4,731.0	6.273	0.485	0.032
69	Surplus electricity	0.0	6.329	0.424	0.028
70	Exported hydrogen	40,399.0	3.736	0.254	0.017
71	Treated vinasse	20,737.0	2.545	0.152	0.011
72	Minerals	187.0	285.100	19.620	1.180
73	Bagasse	8,736.0	1.249	0.071	0.005
74	Surplus bagasse	1104.0	1.249	0.071	0.005
75	NaOH	10.7	3.717	2.193	0.137

Source: [45]

Appendix B - Equipment cost functions

The correlations used to estimate the main equipment costs are described in Table B1, while other auxiliary functions are described in Table B2. Moreover, all purchase equipment costs are corrected to 2019 US dollars by using the CEPCI cost index [182, 90]. In most cases, the costs are estimated based on some operational variable or design feature derived from the thermodynamic model results. However, the purchase cost estimations for the chemical reactors and flash drum require some additional assumptions to be evaluated.

Table B1: Equipment cost correlations in USD

Equipment	Function	Unit	Year	Source
Anaerobic reactor	$200 V_{reactor} f_{usd/eur}$	m^3	2017	[199]
Blower	$\exp\left(7.0187 + 0.79 \ln(W_{blower})\right)$	hp	2013	[185]
Catalytic burner	$11816.2 \dot{m} F_T$	$\frac{kg}{s}$	2005	[179]
Compressor	$245410 \dot{V}^{0.86}$	$\frac{m^3}{s}$	2002	[191]
Desulfurizer	$27500 \left(\frac{\dot{V}_{biogas}}{2570}\right)^{0.6}$	$\frac{Nm^3}{d}$	2012	[186]
Desulfurizer media	$2.926 \dot{V}_{biogas}$	$\frac{Nm^3}{d}$	2012	[186]
Flash drum	$\exp\left(F_W\right)$	-	2013	[185]
H_2 compressor	$568094 \dot{V}^{0.63}$	$\frac{m^3}{s}$	2002	[191]
Heat exchanger (plate)	$\begin{cases} 540 A^{0.8} F_m f_{usd/eur} & A \leq 5.8 \\ 805 A^{0.8} F_m f_{usd/eur} & A > 5.8 \end{cases}$	m^2	2012	[202]
Heat exchanger (double tube)	$3.29 \left(10^{3.3444 + 0.2745 log(A) - 0.0472 log(A)^2}\right)$	m^2	2001	[203]
High temperature polisher vessel	$12800 \left(\frac{\dot{V}_{biogas}}{2570}\right)^{0.6}$	$\frac{Nm^3}{d}$	2012	[186]
High temperature polisher media	$0.058 \dot{V}_{biogas}$	$\frac{Nm^3}{d}$	2012	[186]
Low temperature polisher	$48800 \left(\frac{\dot{V}_{biogas}}{2570}\right)^{0.6}$	$\frac{Nm^3}{d}$	2012	[186]

Continued on next page

Table B1 – *Continued from previous page*

Equipment	Function	Unit	Year	Source
Low temperature polisher media	$2.926\dot{V}_{biogas}$	$\frac{Nm^3}{d}$	2012	[186]
Pump (Centrifugal)	$\exp\left(0.3826ln(\dot{V}_{H_2O}) + 9.8185\right)$	$\frac{m^3}{s}$	2002	[191]
Pump (Diaphragm)	$\exp\left(0.441ln(\dot{V}_{H_2O}) + 11.29\right)$	$\frac{m^3}{s}$	2002	[182, 191]
PSA	$54750\left(\frac{\dot{m}_{H_2}}{115}\right)^{0.4}$	$\frac{kg}{d}$	2007	[204]
SMR vessel	$21936\left(\frac{V_{vessel}}{0.0167}\right)^{0.7} F_k$	m^3	2005	[179]
SMR catalyst	$10^5 V_{cat}$	m^3	2005	[179]
SOFC module	$1668A_{sofc}$	m^2	2017	[205]
SOFC stack	$588A_{sofc}$	m^2	2017	[205]
WGS vessel	$5774\left(\frac{V_{vessel}}{0.104}\right)^{0.7} F_k$	m^3	2005	[179]
WGS catalyst	$1.68 \times 10^7 V_{cat}$	m^3	2005	[179]

Source: [42]

Table B2: Auxiliary cost equations

Parameter	Function or observation	Unit	Source
F_W	$5.6336 + 0.4599\|ln(W)\| + 0.0582\|ln(W)\|^2$	lb	[185]
F_T	$(1 + \exp(0.0954T_{burner} - 179.71))$	K	[179]
V_{vessel}	$\begin{cases} 1.36V_{cat} & \text{if steam reforming} \\ 1.17V_{cat} & \text{if water gas shift} \end{cases}$	m^3	[179]
F_k	$1.62+1.47F_mF_p$	-	[179]
F_P	$\frac{5146+6838log(P)+235(log(P))^6+20(log(P))^8}{10^4}$	barg	[179]
F_m	$\begin{cases} 1 & \text{if carbon steel} \\ 2.8 & \text{if stainless steel} \end{cases}$	-	[203]
$f_{usd/eur}$	1.2	-	[206]

Source: [173]

The catalyst volume (V_{cat}) is determined by integrating the reaction rate along the reactor volume as proposed by Marechal et al. [179]. Moreover, a linear distribution of temperature across the reactor length is assumed for the steam reforming reactor [58]. This additional assumption is included to avoid underestimating the temperature effect in the reaction rate, but requires an additional iteration step. On the other hand, the flash drum weight (W) is estimated based on the method proposed by Seider et al. [185].

Appendix C - Exergy costs and specific emissions for system analysis

Figure C1: Flowsheet of the SOFC system

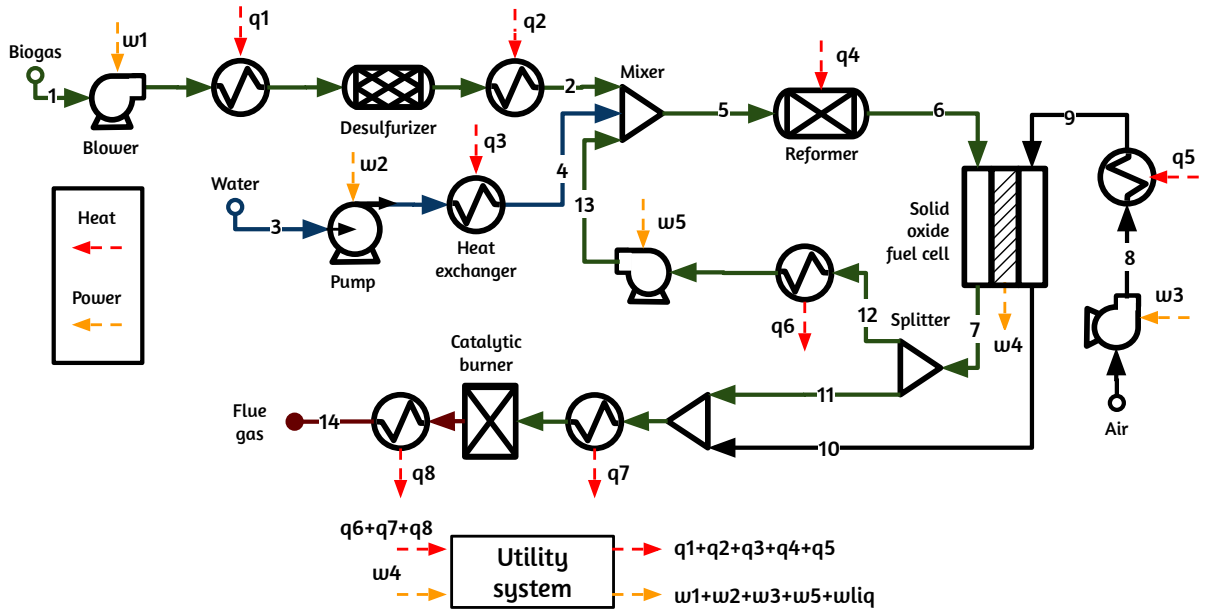

Source: Author

Table C1: Exergy costs and specific emissions for the SOFC system[a]

Stream	$\dot{B}$ (kW)	c_T (kJ/kJ)	c_{NR} (kJ/kJ)	c_{co2} (gCO2/kJ)
1	626.02	1.00 (3.00)	0 (0.26)	0 (17.00)
2	636.05	1.02 (3.06)	0 (0.26)	0 (17.33)
3	2.05	1 (1)	0 (0)	0 (0)
4	35.67	2.14 (6.26)	0 (0.54)	0 (35.08)
5	913.22	1.14 (3.41)	0 (0.29)	0 (19.34)
6	954.71	1.19 (3.57)	0 (0.31)	0 (20.19)
7	549.28	1.24 (3.72)	0 (0.32)	0 (21.07)
8	0.0	1 (1)	0 (0)	0 (0)

Continued on next page

Table C1 – *Continued from previous page*

Stream	$\dot{B}$ (kW)	c_T (kJ/kJ)	c_{NR} (kJ/kJ)	c_{co2} (gCO_2/MJ
9	226.31	2.23 (6.26)	0 (0.57)	0 (37.49)
10	259.32	2.23 (6.64)	0 (0.57)	0 (37.49)
11	274.64	1.24 (3.72)	0 (0.32)	0 (21.07)
12	274.64	1.24 (3.72)	0 (0.32)	0 (21.07)
13	250.42	1.27 (3.80)	0 (0.32)	0 (21.51)
14	31.86	0.0 (0.0)	0 (0)	0 (0)
w1	0.82	2.21 (6.59)	0 (0.57)	0 (37.26)
w2	0.001	2.21 (6.59)	0 (0.57)	0 (37.26)
w3	14.23	2.21 (6.59)	0 (0.57)	0 (37.26)
w4	306.95	1.24 (3.72)	0 (0.32)	0 (21.07)
w5	6.27	2.21 (6.59)	0 (0.57)	0 (37.26)
wliq	285.63	2.21 (6.59)	0 (0.57)	0 (37.26)
q1	5.75	2.21 (6.59)	0 (0.57)	0 (37.26)
q2	3.57	2.21 (6.59)	0 (0.57)	0 (37.26)
q3	33.58	2.21 (6.59)	0 (0.57)	0 (37.26)
q4	43.43	2.21 (6.59)	0 (0.57)	0 (37.26)
q5	213.51	2.21 (6.59)	0 (0.57)	0 (37.26)
q6	29.44	1.27 (3.80)	0 (0.33)	0 (21.51)
q7	265.42	2.22 (6.63)	0 (0.57)	0 (37.44)
q8	148.75	2.22 (6.63)	0 (0.57)	0 (37.44)

[a] Values in parenthesis assume $c_{T,biogas} = 3\ kJ/kJ$, $c_{NR,biogas} = 0.26\ kJ/kJ$, $c_{CO2,biogas} = 17\ g_{CO2}/MJ$, $c_{T,elec.} = 1.80\ kJ/kJ$, $c_{NR,elec.} = 0.33\ kJ/kJ$, $c_{CO2,elec.} = 62\ g_{CO2}/MJ$

Source: Author

Figure C2: Flowsheet of the SOFC-H2 system

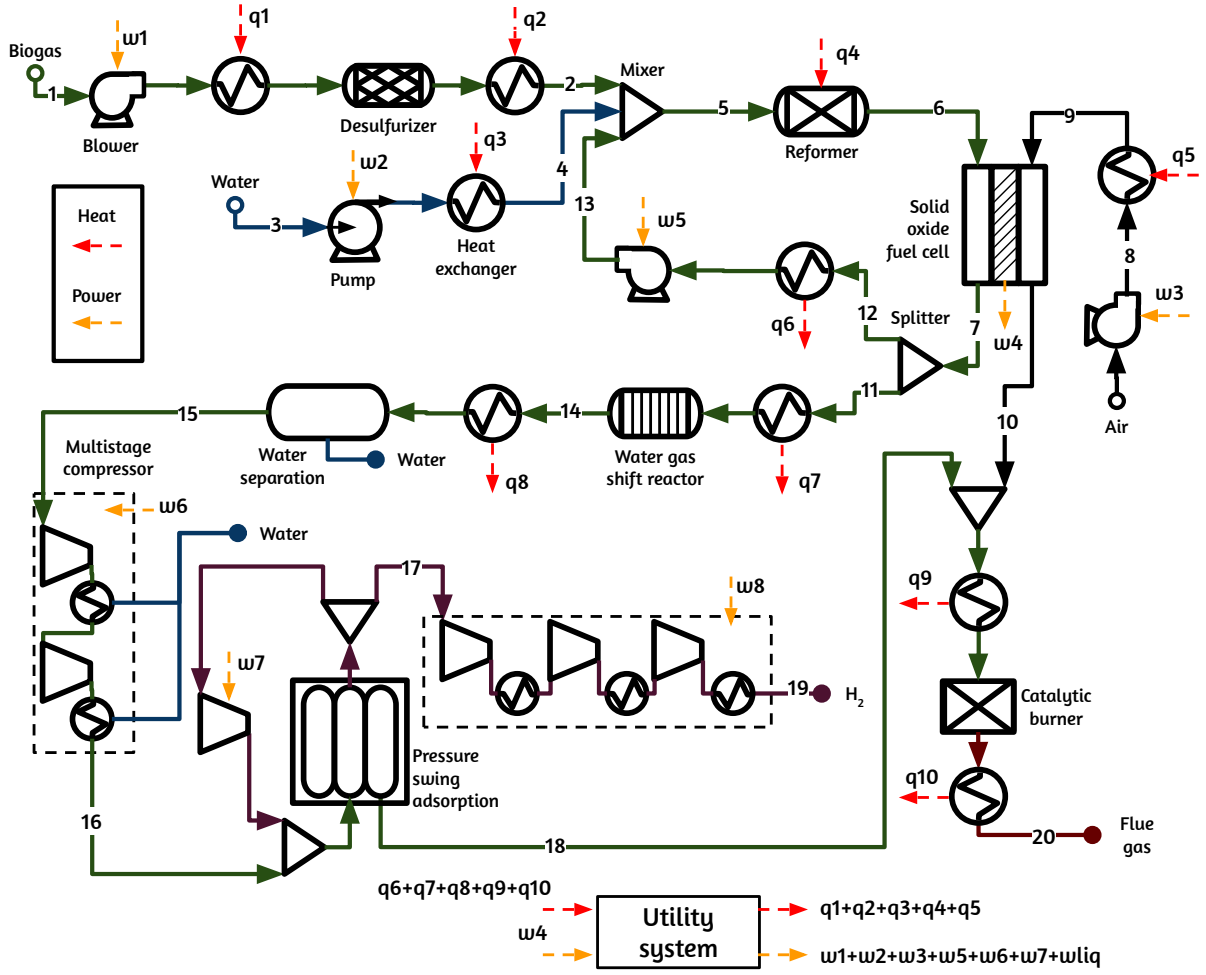

Table C2: Exergy costs and specific emissions for the SOFC-H2 system[a]

Stream	$\dot{B}$ (kW)	c_T (kJ/kJ)	c_{NR} (kJ/kJ)	c_{co2} (gCO2/kJ)
1	626.02	1.00 (3.00)	0 (0.26)	0 (17.00)
2	640.64	1.04 (3.11)	0 (0.27)	0 (17.90)
3	2.40	1 (1)	0 (0)	0 (0)
4	48.18	2.58 (7.42)	0 (0.90)	0 (54.37)
5	682.77	1.16 (3.44)	0 (0.32)	0 (20.63)
6	796.01	1.41 (4.16)	0 (0.41)	0 (26.61)
7	736.82	1.42 (4.17)	0 (0.41)	0 (26.62)
8	0.0	1 (1)	0 (0)	0 (0)
9	89.98	2.68 (7.70)	0 (0.90)	0 (56.66)
10	96.27	2.68 (7.70)	0 (0.90)	0 (56.66)
11	736.82	1.42 (4.17)	0 (0.41)	0 (26.62)
12	0.0	0 (0)	0 (0)	0 (26.62)

Continued on next page

Table C2 – *Continued from previous page*

Stream	$\dot{B}$ (kW)	c_T (kJ/kJ)	c_{NR} (kJ/kJ)	c_{co2} (gCO_2/MJ
13	0.0	0 (0)	0 (0)	0 (26.62)
14	661.19	1.42 (4.18)	0 (0.41)	0 (26.69)
15	653.55	1.43 (4.22)	0 (0.42)	0 (26.95)
16	678.64	1.60 (4.70)	0 (0.48)	0 (30.59)
17	372.77	1.66 (4.87)	0 (0.49)	0 (31.74)
18	292.44	1.60 (4.70)	0 (0.48)	0 (30.60)
19	382.13	1.73 (5.08)	0 (0.52)	0 (33.37)
20	20.113	0 (0)	0 (0)	0 (0)
w1	0.82	2.66 (7.65)	0 (0.88)	0 (56.30)
w2	0.001	2.66 (7.65)	0 (0.88)	0 (56.30)
w3	5.66	2.66 (7.65)	0 (0.88)	0 (56.30)
w4	45.37	1.42 (4.17)	0 (0.41)	0 (26.62)
w5	56.28	2.66 (7.65)	0 (0.88)	0 (56.30)
w6	0.24	2.66 (7.65)	0 (0.88)	0 (56.30)
w7	16.37	2.66 (7.65)	0 (0.88)	0 (56.30)
grid	34.00	2.66 (1.80)	0 (0.88)	0 (62.00)
q1	5.75	2.66 (7.65)	0 (0.88)	0 (56.30)
q2	8.07	2.66 (7.65)	0 (0.88)	0 (56.30)
q3	45.66	2.66 (7.65)	0 (0.88)	0 (56.30)
q4	126.98	2.66 (7.65)	0 (0.88)	0 (56.30)
q5	84.89	2.66 (7.65)	0 (0.88)	0 (56.30)
q6	0	0 (0)	0 (0)	0 (0)
q7	43.64	1.42 (4.18)	0 (0.41)	0 (26.69)
q8	30.18	1.42 (4.18)	0 (0.41)	0 (26.69)
q9	33.89	2.53 (7.35)	0 (0.78)	0 (50.07)
q10	253.78	2.53 (7.35)	0 (0.78)	0 (50.07)

[a] Values in parenthesis assume $c_{T,biogas} = 3\ kJ/kJ$, $c_{NR,biogas} = 0.26\ kJ/kJ$, $c_{CO2,biogas} = 17\ g_{CO2}/MJ$, $c_{T,elec.} = 1.80\ kJ/kJ$, $c_{NR,elec.} = 0.33\ kJ/kJ$, $c_{CO2,elec.} = 62\ g_{CO2}/MJ$

Source: Author

Figure C3: Flowsheet of the H2 system

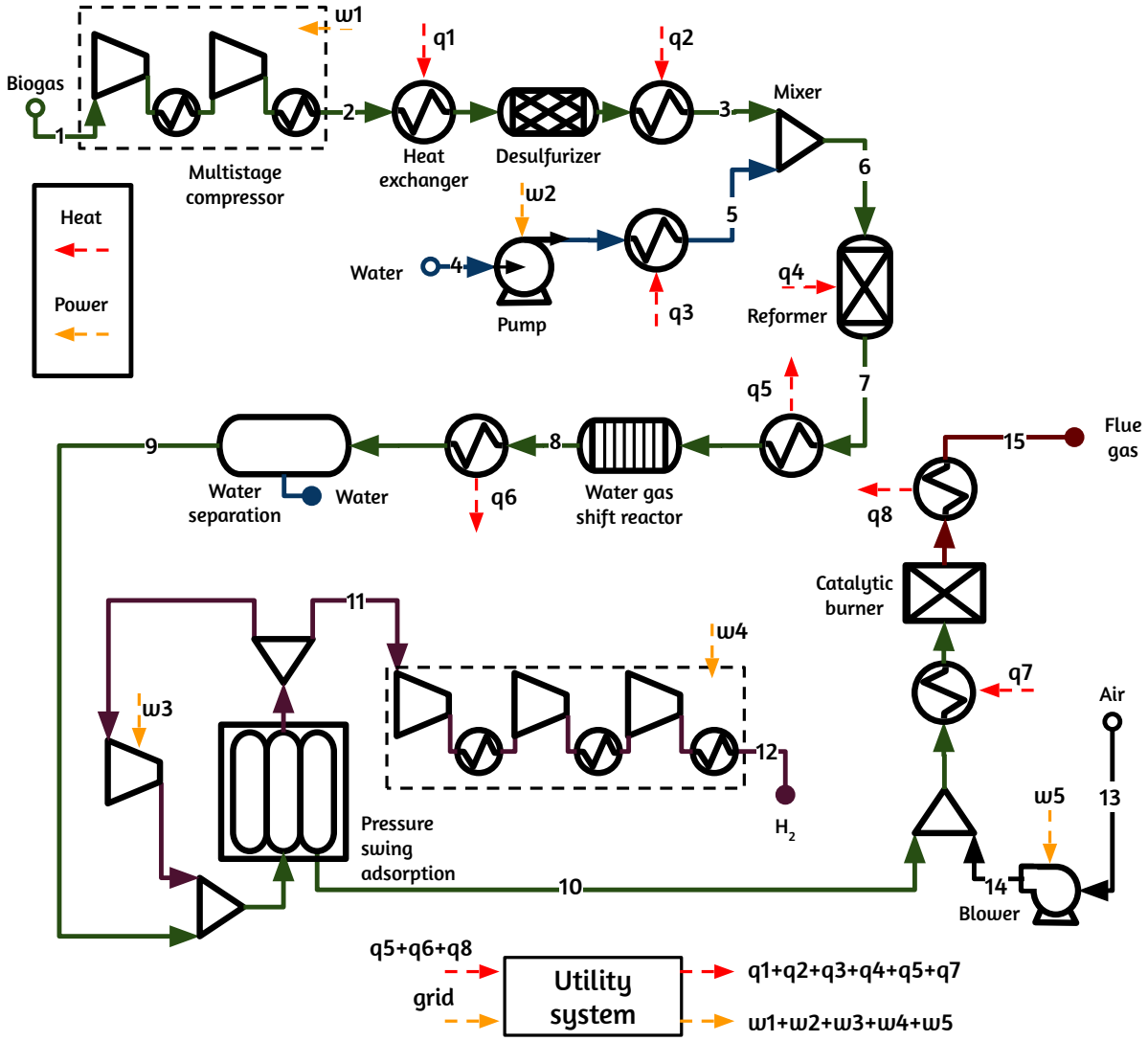

Table C3: Exergy costs and specific emissions for the H2 system[a]

Stream	$\dot{B}$ (kW)	c_T (kJ/kJ)	c_{NR} (kJ/kJ)	c_{co2} (gCO2/kJ)
1	626.02	1.00 (3.00)	0 (0.26)	0 (17.00)
2	635.18	1.01 (3.00)	0 (0.27)	0 (18.34)
3	649.26	1.04 (3.10)	0 (0.27)	0 (18.94)
4	3.20	1.00 (1.00)	0 (0)	0 (0)
5	88.24	2.47 (7.19)	0 (0.63)	0 (45.09)
6	730.72	1.22 (3.62)	0 (0.32)	0 (22.27)
7	878.25	1.47 (4.34)	0 (0.38)	0 (26.9)
8	778.46	1.53 (4.50)	0 (0.40)	0 (27.89)
9	742.54	1.53 (4.52)	0 (0.40)	0 (28.03)

Continued on next page

Table C3 – *Continued from previous page*

Stream	$\dot{B}$ (kW)	c_T (kJ/kJ)	c_{NR} (kJ/kJ)	c_{co2} (gCO_2/MJ
10	321.10	1.53 (4.52)	0 (0.40)	0 (28.03)
11	408.59	1.58 (4.67)	0 (0.41)	0 (28.94)
12	418.84	1.59 (4.63)	0 (0.42)	0 (30.89)
13	0.57	1 (1)	0 (0)	0 (0)
14	3.12	1.32 (2.23)	0 (0.38)	0 (70.72)
15	23.97	0 (0)	0 (0)	0 (0)
w1	16.21	1 (1.80)	0 (0.33)	0 (62.00)
w2	0.18	1 (1.80)	0 (0.33)	0 (62.00)
w3	0.21	1 (1.80)	0 (0.33)	0 (62.00)
w4	17.95	1 (1.80)	0 (0.33)	0 (62.00)
w5	3.56	1 (1.80)	0 (0.33)	0 (62.00)
grid	38.11	1 (1.80)	0 (0.33)	0 (62.00)
q1	5.80	2.52 (7.42)	0 (0.66)	0 (46.67)
q2	8.09	2.52 (7.42)	0 (0.66)	0 (46.67)
q3	85.04	2.52 (7.42)	0 (0.66)	0 (46.67)
q4	157.48	2.52 (7.42)	0 (0.66)	0 (46.67)
q5	68.84	1.53 (4.50)	0 (0.40)	0 (27.88)
q6	29.49	1.53 (4.52)	0 (0.40)	0 (28.03)
q7	20.61	2.52 (7.42)	0 (0.66)	0 (46.67)
q8	246.01	2.23 (6.56)	0 (0.58)	0 (41.40)

[a] Values in parenthesis assume $c_{T,biogas} = 3\ kJ/kJ$, $c_{NR,biogas} = 0.26\ kJ/kJ$, $c_{CO2,biogas} = 17\ g_{CO2}/MJ$, $c_{T,elec.} = 1.80\ kJ/kJ$, $c_{NR,elec.} = 0.33\ kJ/kJ$, $c_{CO2,elec.} = 62\ g_{CO2}/MJ$

Source: Author

Figure C4: Flowsheet of the H2-SOFC system

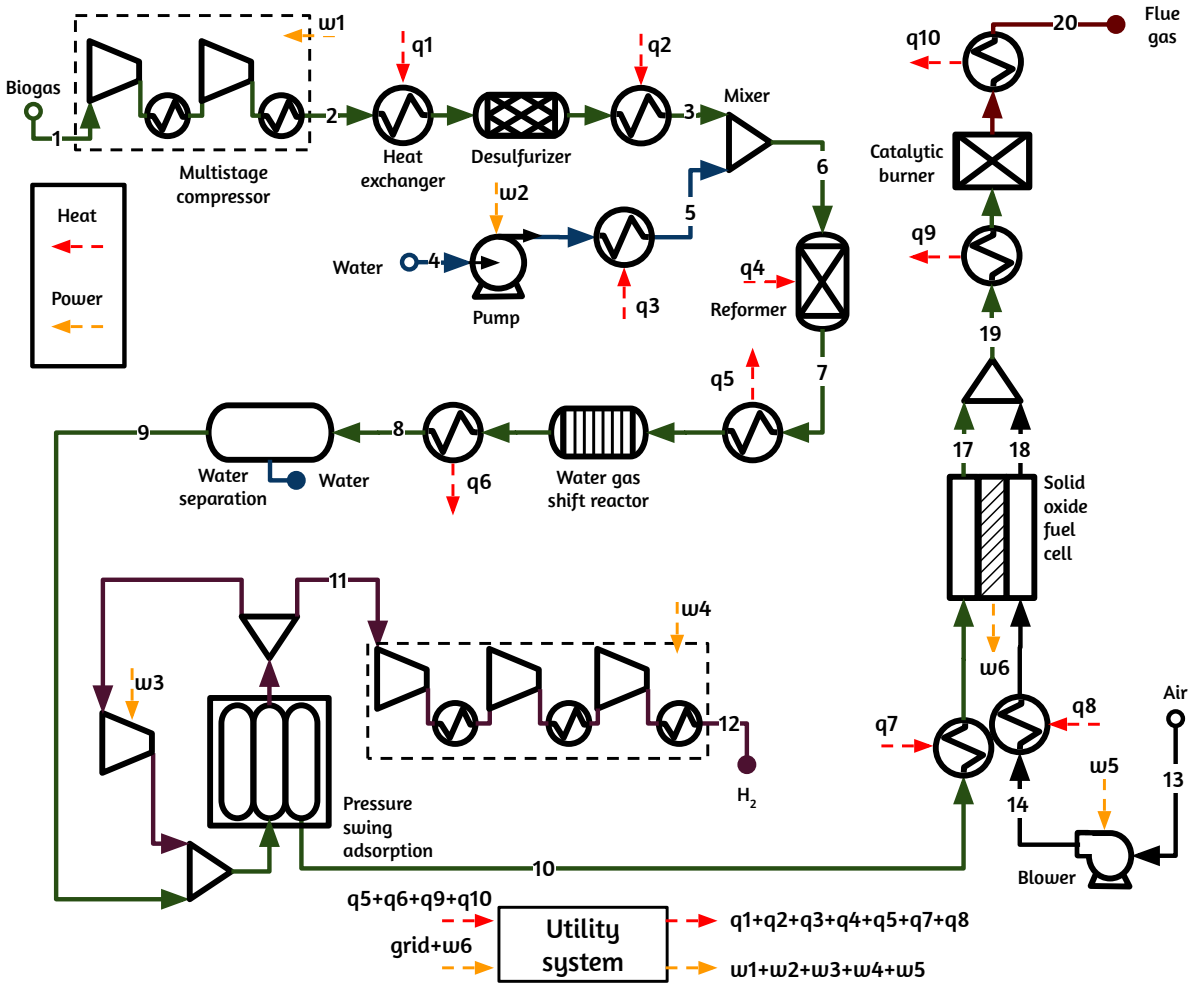

Table C4: Exergy costs and specific emissions for the H2-SOFC system[a]

Stream	$\dot{B}$ (kW)	c_T (kJ/kJ)	c_{NR} (kJ/kJ)	c_{co2} (gCO2/kJ)
1	626.02	1.00 (3.00)	0 (0.26)	0 (17.00)
2	635.18	1.04 (3.12)	0 (0.27)	0 (17.67)
3	649.26	1.06 (3.19)	0 (0.28)	0 (18.06)
4	2.51	1.00 (1.00)	0 (0)	0 (0)
5	69.18	2.09 (6.17)	0 (0.58)	0 (34.76)
6	712.29	1.17 (3.51)	0 (0.31)	0 (19.84)
7	850.97	1.35 (4.04)	0 (0.35)	0 (22.84)
8	790.37	1.35 (4.04)	0 (0.36)	0 (22.88)
9	737.92	1.39 (4.17)	0 (0.37)	0 (23.59)
10	357.20	1.39 (4.17)	0 (0.37)	0 (23.59)
11	367.72	1.44 (4.32)	0 (0.38)	0 (24.45)

Continued on next page

Table C4 – *Continued from previous page*

Stream	$\dot{B}$ (kW)	c_T (kJ/kJ)	c_{NR} (kJ/kJ)	c_{co2} (gCO_2/MJ
12	373.94	1.50 (4.49)	0 (0.39)	0 (25.39)
13	0.50	1 (1)	0 (0)	0 (0)
14	2.74	2.61 (7.24)	0 (0.64)	0 (41.01)
15	384.80	1.44 (4.32)	0 (0.38)	0 (24.42)
16	50.140	2.13 (6.35)	0 (0.56)	0 (35.83)
17	305.68	1.49 (4.44)	0 (0.39)	0 (25.14)
18	52.56	2.13 (6.35)	0 (0.56)	0 (35.96)
19	347.36	1.63 (4.87)	0 (0.43)	0 (27.55)
20	24.34	0 (0)	0 (0)	0 (0)
w1	16.21	2.13 (6.35)	0 (0.56)	0 (35.96)
w2	0.14	2.13 (6.35)	0 (0.56)	0 (35.96)
w3	0.24	2.13 (6.35)	0 (0.56)	0 (35.96)
w4	16.15	2.13 (6.35)	0 (0.56)	0 (35.96)
w5	3.12	2.13 (6.35)	0 (0.56)	0 (35.96)
w6	64.65	1.49 (4.44)	0 (0.39)	0 (25.39)
wliq	28.79	2.13 (6.35)	0 (0.56)	0 (35.96)
q1	5.80	2.13 (6.35)	0 (0.56)	0 (35.96)
q2	8.09	2.13 (6.35)	0 (0.56)	0 (35.96)
q3	66.67	2.13 (6.35)	0 (0.56)	0 (35.96)
q4	147.59	2.13 (6.35)	0 (0.56)	0 (35.96)
q5	59.23	1.35 (4.04)	0 (0.36)	0 (22.88)
q6	26.95	1.39 (4.17)	0 (0.37)	0 (23.59)
q7	27.03	2.13 (6.35)	0 (0.56)	0 (35.96)
q8	46.84	2.13 (6.35)	0 (0.56)	0 (35.96)
q9	57.32	2.03 (6.08)	0 (0.53)	0 (34.40)
q10	220.89	2.03 (6.08)	0 (0.53)	0 (34.40)

[a] Values in parenthesis assume $c_{T,biogas} = 3\ kJ/kJ$, $c_{NR,biogas} = 0.26\ kJ/kJ$, $c_{CO2,biogas} = 17\ g_{CO2}/MJ$, $c_{T,elec.} = 1.80\ kJ/kJ$, $c_{NR,elec.} = 0.33\ kJ/kJ$, $c_{CO2,elec.} = 62\ g_{CO2}/MJ$

Source: Author